Substrate Recognition and Activation by Two Flavoenzymes Involved in Pyrimidine Metabolism: Flavin-Dependent Thymidylate Synthase and tRNA-Dihydrouridine Synthase

by

Frederick W. Stull

A dissertation submitted in partial fulfillment
of the requirements for the degree of
Doctor of Philosophy
(Chemical Biology)
in the University of Michigan
2014

Doctoral Committee:

Associate Professor Bruce A. Palfey, Chair
Professor George A. Garcia
Associate Professor Patrick J. O'Brien
Professor Erik R. P. Zuiderweg

Acknowledgements

I would first and foremost like to thank my advisor, Bruce Palfey. I am grateful for the freedom he gave me to work on a number of projects, while still providing advice when I needed it. I feel that I have learned a great deal about science while working for him.

I would also like to thank both the past and present members of my thesis committee – George Garcia, Hashim Al-Hashimi, Pat O'Brien, and Erik Zuiderweg. They always showed genuine interest in the work I was doing and provided many helpful suggestions along the way. I'd also like to thank Ray Trievel for allowing me to use his MicroCal VP-ITC and Stephen Ragsdale for letting me use his anaerobic chambers.

In addition, I would like to acknowledge some of the collaborators that contributed to the work in this thesis. Erik Zuiderweg helped me collect the NMR spectra presented in Chapter 2. Steffen Bernard solved the structures of the FDTS variants in Chapter 2; it was great being able to work with my best man. Robin Teufel and Bradley Moore spearheaded the study in the Appendix describing the discovery of a novel enzymatic flavin-N5-oxide; it took a lot of work to figure out what that enzyme was doing, but it was worth it.

Finally, I would like to thank my friends and family for all of the support and encouragement they provided me over the past five years. I must also thank my wife, Christine. Thank you for giving me a reason to come home from lab every day.

Table of Contents

List of Figures

List of Tables

List of Appendices

Abstract

Pyrimidines are essential components of nucleic acids. In biology, they undergo a number of redox reactions catalyzed by flavin-dependent enzymes. This thesis investigates the mechanism of substrate recognition and activation of two flavin-dependent enzymes with pyrimidine-containing substrates: flavin-dependent thymidylate synthase (FDTS) and tRNA-dihydrouridine synthase (DUS). FDTS catalyzes the reductive methylation of the uracil moiety of 2'-deoxyuridine-5'-monophosphate (dUMP) into thymine, whereas DUS reduces specific uracils in tRNA to dihydrouracil.

NMR data indicate that FDTS ionizes N3 of the uracil in dUMP using an active-site arginine, which is proposed to initiate catalysis by enhancing the nucleophilicity of C5 of the uracil. Biochemical data on dUMP analogs suggests that the phosphate of dUMP acts as the base that removes the proton from C5 of dUMP during the FDTS-catalyzed reaction. Notably, both ionization of N3 and acid-base catalysis by the phosphate of dUMP are not implicated in the mechanism used by human thymidylate synthase.

Several equilibrium and kinetic methods were used to study the mechanism of deoxynucleotide recognition by *Thermotoga maritima* FDTS. FDTS binds deoxynucleotides with ~200-fold weaker affinity when the flavin is reduced relative to when it is oxidized, and the differences in affinity are largely due to differences in the dissociation rate constant. There is also a temperature-dependent effect on the

mechanism by which FDTS binds deoxynucleotides – below 45°C the FDTS homotetramer behaves as a dimer-of-dimers with deoxynucleotide binding while at temperatures above 45°C the four subunits of FDTS bind deoxynucleotides identically. *T. maritima* normally lives at 80°C, so this behavior likely results from studying the enzyme at non-physiological temperatures.

tRNAs contain a number of nucleobase and ribose modifications – including dihydrouracil – at different positions of the tRNA. Previous work has shown that yeast $tRNA^{Leu}$-CAA reacts poorly with yeast DUS2 unless it contains other modifications, suggesting that tRNA modifications are ordered. The reactivity of yeast DUS2 with other unmodified tRNAs was investigated; unmodified yeast $tRNA^{Asp}$, $tRNA^{Ala}$, and $tRNA^{His2}$ all reacted rapidly with yeast DUS2, indicating that not all tRNAs require prior modifications to react rapidly with yeast DUS2. Native gel electrophoresis showed that unmodified $tRNA^{Leu}$-CAA misfolds, explaining its poor reactivity with yeast DUS2.

Chapter 1

Introduction

Background

Pyrimidines are important biological molecules. They are major components of DNA and RNA – three three types of nucleobases are derived from pyrimidines (cytosine, uracil, and thymine), which are crucial components that constitute the alphabet of the genetic code. Pyrimidines are also precursors of activated sugars and activated lipids that are critical for synthesizing glycoproteins and cell membranes.[1]

Pyrimidines are subjected to a variety of redox reactions during cellular metabolism that are catalyzed by flavin-dependent enzymes. Flavins are derived from vitamin B2 (riboflavin), which contains the redox-active isoalloxazine moiety (Figure 1 - 1). Two derivatives of riboflavin are typically used by flavin-dependent enzymes: flavin mononucleotide (FMN), which has a phosphate at the end of the ribityl tail of riboflavin, and flavin adenine dinucleotide (FAD), which has an adenosine diphosphate group at the end of the ribityl tail. Flavoenzymes usually use FMN or FAD as a prosthetic group through extensive noncovalent interactions with the non-isoalloxazine portion of the flavin.

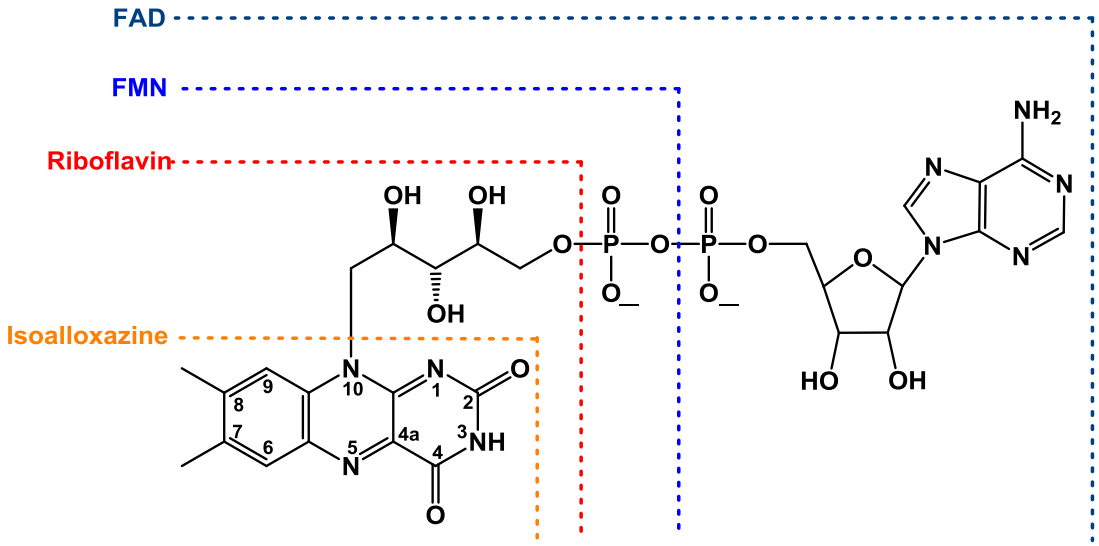

Figure 1 - 1. Flavin structures.

Flavins are capable of performing a wide range of chemistry, which is tightly controlled by the active sites of flavoenzymes.[2] One of the most common reactions is hydride transfer to or from N5 of the isoalloxazine. The two enzymes studied in this thesis are proposed to use flavin-dependent hydride transfers as part of their mechanisms. Flavoenzymes can also stabilize flavin semiquinones, allowing flavins to perform 1-electron transfers. In addition, flavins can undergo nucleophilic or electrophilic attack at N5 or C4a of the isoalloxazine, depending on the redox state of the flavin. Reduced flavin can react with molecular oxygen at the C4a position to make a flavin hydroperoxide intermediate – the hydroperoxide intermediate can then either eliminate hydrogen peroxide or be used to oxygenate other substrates.

Flavoenzymes often use ping-pong kinetic mechanisms, where one substrate donates electrons to oxidized flavin and a second substrate takes the electrons from reduced flavin. As a result, the catalytic cycle of most flavoenzymes can be broken up into half-reactions (Figure 1 - 2). In the reductive half-reaction, an electron-rich substrate

donates its electrons to oxidized flavin, making reduced flavin. In the oxidative half-reaction, the reduced flavin donates the electrons to an electron-poor substrate. The reductive and oxidative half-reactions can be studied independently, simplifying the number of steps being investigated and avoiding the complications of turnover.

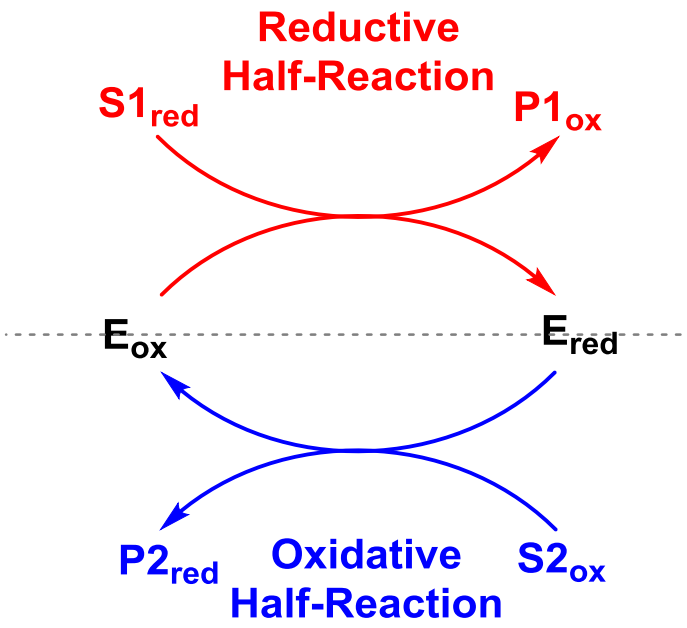

Figure 1 - 2. General catalytic cycle of most flavoenzymes. In the reductive half-reaction, the reducing substrate donates its electrons to oxidized flavin. The now-reduced flavin donates the electrons to the oxidizing substrate in the oxidative half-reaction.

The flavin prosthetic group is also a chromophore/fluorophore with unique spectra for each redox state of the flavin (Figure 1 - 3). Oxidized flavin is bright yellow, with absorbance peaks around 450 and 370 nm, and is usually fluorescent. 2-electron reduced flavin is pale yellow, with a relatively featureless absorbance spectrum, and is usually non-fluorescent. The flavin semiquinone has a distinct absorbance spectrum that depends on the protonation state of the semiquinone – anionic semiquinone has a high-extinction peak around 370 nm and a second peak around 480 nm whereas the neutral semiquinone has a broad absorbance spectrum that extends past 650 nm. The

various flavin adducts also have characteristic absorbance spectra that aid their identification. The different spectral signals enable the monitoring of electron transfer to and from the flavin during each half-reaction, so that detailed information on the number and nature of chemical steps can be determined. The oxidized and reduced flavin chromophores/fluorophores are also often sensitive to changes in the local environment of the flavin. As a result, ligand binding can often be monitored through perturbations to the absorbance/fluorescence spectrum of the flavin.

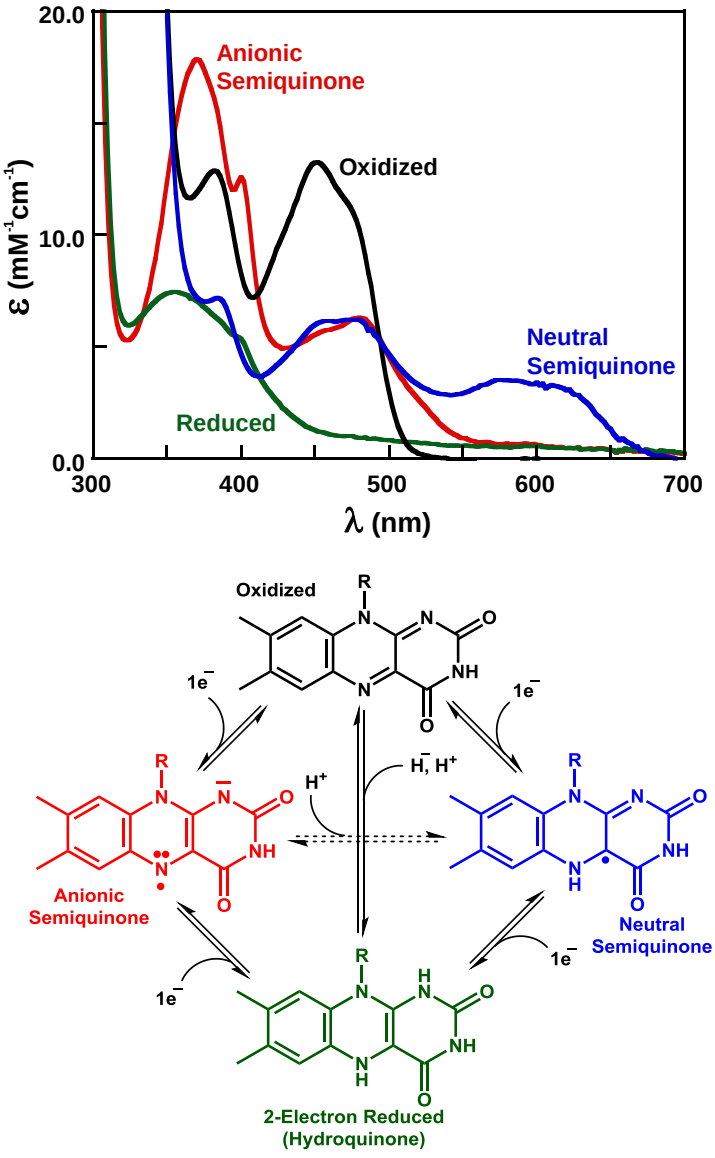

Figure 1 - 3. UV/visible absorbance spectra and structures of the different flavin redox states.

This thesis focuses on the mechanism of substrate recognition and activation by two flavoenzymes with pyrimidine-containing substrates – flavin-dependent thymidylate synthase and tRNA-dihydrouridine synthase. The following provides an overview of five enzymes that catalyze flavin-dependent hydride transfers to pyrimidine moieties, with greater emphasis placed on flavin-dependent thymidylate synthase and tRNA-dihydrouridine synthase.

Dihydropyrimidine Dehydrogenase

Dihydropyrimidine dehydrogenase (DPDH) catalyzes the NADPH-dependent conversion of uracil or thymine to the corresponding 5, 6-dihydropyrimidine, which is the first step in the degradation of pyrimidines (Figure 1 - 4).[3] One of the final products in the degradation pathway for pyrimidines is β-alanine, which is a neurotransmitter.[4] Accordingly, defects in DPDH activity in humans are associated with a number of neurological pathologies.[5,6]

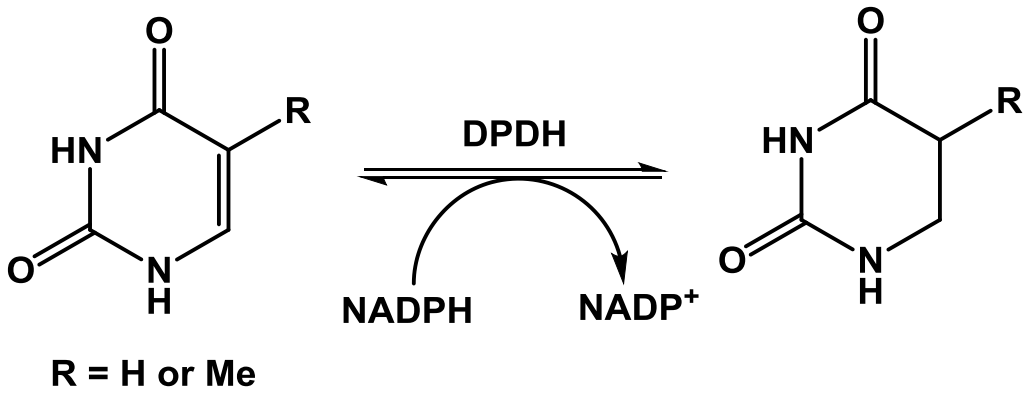

Figure 1 - 4. Reaction catalyzed by dihydropyrimidine dehydrogenase.

The pyrimidine degradation pathway initiated by DPDH is also the primary mechanism by which the cancer therapeutic, 5-fluorouracil (5FU), is degraded in cancer

patients.[7] This necessitates very high doses of 5FU in order for the drug to be an effective treatment option. In addition, the degradation of 5FU leads to fluorinated products that cause a number of side effects to the nervous system.[8] Therefore, inhibition of DPDH could be used to increase the efficiency of 5FU as a cancer treatment while also decreasing side effects of 5FU treatment.

Structures

The only DPDH structure solved to date is of the enzyme from pig liver.[9] The enzyme is a homodimer, with each dimer containing one FMN, one FAD, and four iron sulfur (Fe-S) clusters (Figure 1 - 5). Each monomer is composed of five domains – an FAD-containing domain, an FMN/pyrimidine-binding TIM-barrel domain, an NADPH-binding domain, an N-terminal Fe-S cluster domain, and a C-terminal Fe-S cluster domain. The two flavins are located on opposite ends of the protein, and are connected by four Fe-S clusters. The chain of Fe-S clusters connecting the FMN and FAD of the homodimer are arranged such that the Fe-S clusters in the C-terminal domain of one monomer are used to connect the FMN and FAD/N-terminal Fe-S clusters of the other monomer, indicating that DPDH is only active as a dimer.

Structures of DPDH with pyrimidine analogs bound in the FMN/pyrimidine-binding domain have also been determined.[9,10] A comparison of the ligand-free and pyrimidine-bound structures shows that an active site loop closes over the pyrimidine binding site when a pyrimidine binds to the enzyme. The pyrimidine binds on the *si*-face of the flavin, parallel to the isoalloxazine of the FMN. Several conserved asparagines and a threonine hydrogen bond to the pyrimidine. A conserved active-site cysteine is

positioned perpendicular to the plane of the pyrimidine, on the opposite face of the pyrimidine from the flavin. The cysteine is proposed to protonate C5 of the pyrimidine upon hydride transfer from reduced FMN to C6 of the pyrimidine.[3]

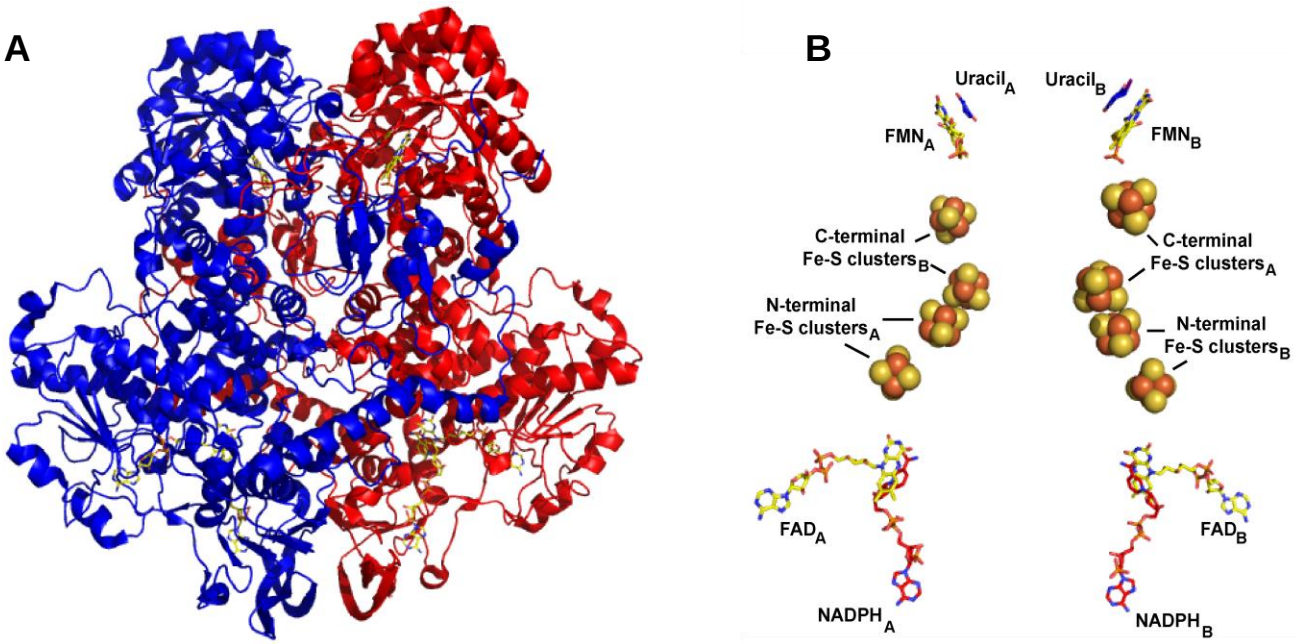

Figure 1 - 5. Structure of pig liver DPDH. (A) Cartoon structure of the DPDH homodimer (PDB code 1GTH). Monomer A is depicted in blue and monomer B is depicted in red. (B) The redox centers and substrates in the DPDH homodimer. The C-terminal Fe-S cluster of one monomer is used to connect the redox centers of the other monomer. The subscripts denote which monomer the redox centers belong to. Figure based on ref. 3.

The FAD binding domain is positioned adjacent to the NADPH-binding domain, on the opposite end of the protein from the FMN/pyrimidine binding domain. NADPH binds in an extended conformation in the NADPH-binding domain, with the reactive nicotinamide stacked against the *re*-face of the isoalloxazine of the FAD, poised for hydride transfer.[10] Only small, local rearrangements accompany NADPH binding to the NADPH-binding domain.

Mechanism

The catalytic cycle of DPDH can be broken up into half-reactions (Figure 1 - 6). In the reductive half-reaction, NADPH binds to the NADPH-binding domain and reduces the FAD of the FAD-binding domain. Using stereospecifically deuterated NADPH, it was shown that the pro-S hydrogen of NADPH is transferred to N5 of the isoalloxazine of the FAD, consistent with the structure of the NADPH-DPDH complex.[11] The electrons must then be transferred to the FMN on the opposite end of the protein, presumably using the Fe-S clusters. However, titrations of DPDH with NADPH only reduced one of the flavins of each DPDH monomer – reduction of the Fe-S clusters or transfer of electrons to the second flavin of the monomer was not observed in NADPH titrations.[12] In addition, the reduction potentials of two of the four Fe-S clusters has been estimated as ~-400 mV,[13] which is far lower than the reduction potential of the NADP/NADPH couple (-320 mV at pH 7, 25°C) and the potential of free flavins (-207 mV at pH 7, 25°C). Regardless, electrons must be transferred between the two flavins of DPDH for catalysis to occur.

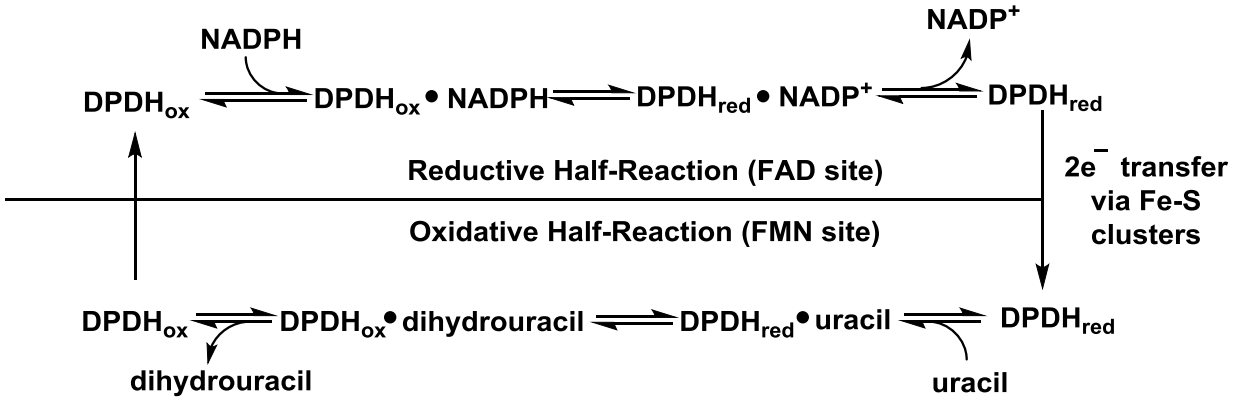

Figure 1 - 6. Catalytic cycle of dihydropyrimidine dehydrogenase.

In the oxidative half-reaction, DPDH transfers the hydride from reduced FMN in the FMN/pyrimidine-binding domain to C6 of the pyrimidine, and C5 of the pyrimidine is protonated by an active site acid. The structures showed that a conserved cysteine is properly positioned to act as the acid that protonates C5 of the pyrimidine. Mutation of this cysteine to alanine in the pig liver DPDH caused a dramatic loss of activity, with the mutant enzyme having ~1% of the activity of the wild-type enzyme.[12] 5-iodouracil is also a mechanism-based inhibitor of DPDH that acts by alkylating the active site cysteine.[14] Secondary tritium and solvent deuterium isotope effects have also suggested that hydride transfer to C6 and protonation of C5 of the pyrimidine occurs in a stepwise manner, as opposed to the concerted manner used by some other enzymes.[15]

tRNA-Dihydrouridine Synthase

tRNAs contain numerous modifications to the four RNA nucleobases.[16] One of the most abundant tRNA modifications is dihydrouridine, which is found primarily in the D-loop of tRNAs (for which the D-loop gets its name).[17] It is formed by the reduction of the carbon-carbon double bond of specific uracils by tRNA-dihydrouridine synthases (DUSs) (Figure 1 - 7).[18] The biological role of dihydrouridine is currently unknown. NMR studies have shown that dihydrouridine increases the conformational flexibility of tRNA,[19] suggesting that dihydrouridine might facilitate the conformational changes of tRNAs required when interacting with the ribosome or other binding partners. Supporting this idea, cold-loving organisms in general have more dihydrouridine whereas thermophilic organisms have less.[20] Other studies have shown that tRNA lacking dihydrouridine is more susceptible to degradation *in vivo*.[21] Dihydrouridine might therefore help protect tRNAs from degradation.

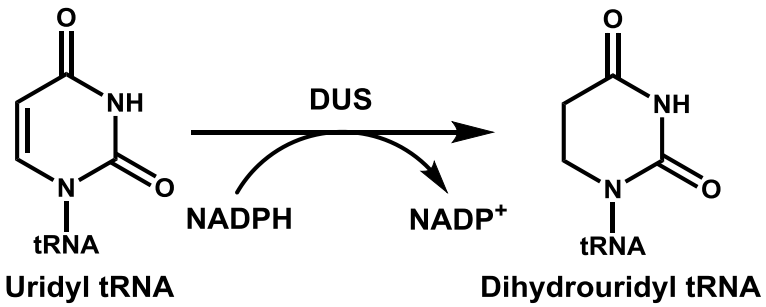

Figure 1 - 7. The reaction catalyzed by tRNA-dihydrouridine synthase.

Increased levels of dihydrouridine are found in a number of cancers.[22] Human DUS2 has been shown to be responsible for the increased dihydrouridine levels in pulmonary carcinogenesis[23] and repression of DUS2 inhibited the growth of the cancerous tissues. Inhibition of DUS2 activity therefore might be useful in the treatment of cancer.

Generally, several isoforms of DUS are present in most organisms, which selectively reduce uracils at different positions in tRNAs. In the budding yeast, *Saccharomyces cerevisiae*, there are four isoforms of DUS.[24] DUS1 modifies U16 and U17, DUS2 modifies U20, DUS3 modifies U47, and DUS4 modifies U20A and U20B (Figure 1 - 8). A sequence alignment of the four yeast DUS isoforms indicates that DUS1, DUS2, and DUS4 are similar in size and have a similar fold, whereas DUS3 is much larger and has additional motifs beyond those found in DUSs 1, 2 and 4. It is unclear how the different isoforms of DUS recognize their appropriate sites, especially considering that yeast DUS2 and DUS4 recognize neighboring sites in tRNA. However, for DUS1, 2 and 4, when a uracil is present at a recognized site it gets converted into dihydrouridine.[17] DUS3, on the other hand, does not modify all tRNA uracils at position

47, suggesting that it has a more complex method of recognizing tRNAs than the other yeast DUSs.

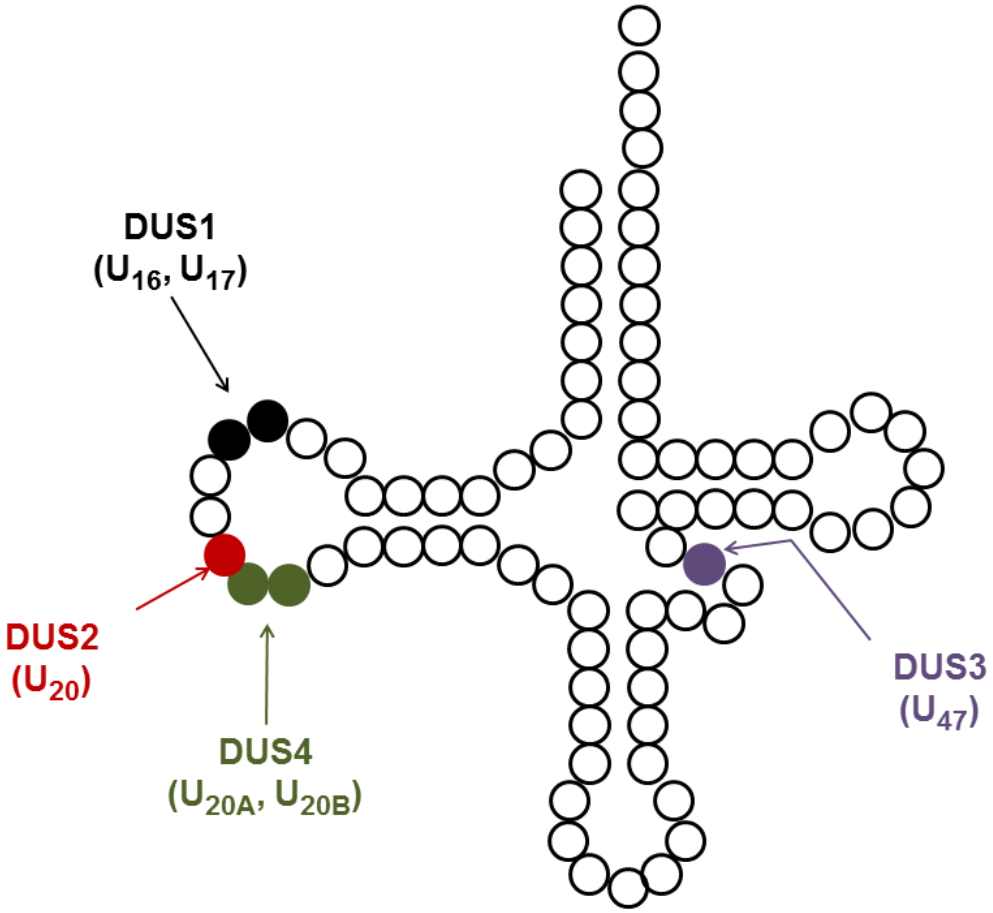

Figure 1 - 8. Sites of tRNA modification by the four yeast dihydrouridine synthases.

Structures

Three structures of DUSs have been solved to date.[25,26] All show similar architecture and domain organization. DUS has a TIM-barrel domain where the active-site containing the redox-active FMN is located. In addition to the TIM-barrel is a C-terminal helix bundle that might aid in tRNA recognition.

The co-crystal structure of DUS from *Thermus thermophilus* in complex with tRNA was recently solved.[26] In the structure, the tRNA largely retains its L-shape and binds in the positively charged groove between the TIM-barrel and helix-bundle domains (Figure 1 - 9). DUS forms multiple contacts with the D- T- and anticodon arms of the tRNA. The reactive uracil is flipped ~180° into the active site of the enzyme, stacking against the isoalloxazine of the FMN. Surprisingly, an active-site cysteine was covalently attached to C6 of the substrate uracil in the structure. This was proposed to be an artifact due to heterologous expression of the enzyme under non-native conditions in *Escherichia coli* – the environment inside *E. coli* is much different than *T. thermophilus* from which the enzyme originated. The covalent attachment between DUS and the tRNA likely facilitated the determination of the structure.

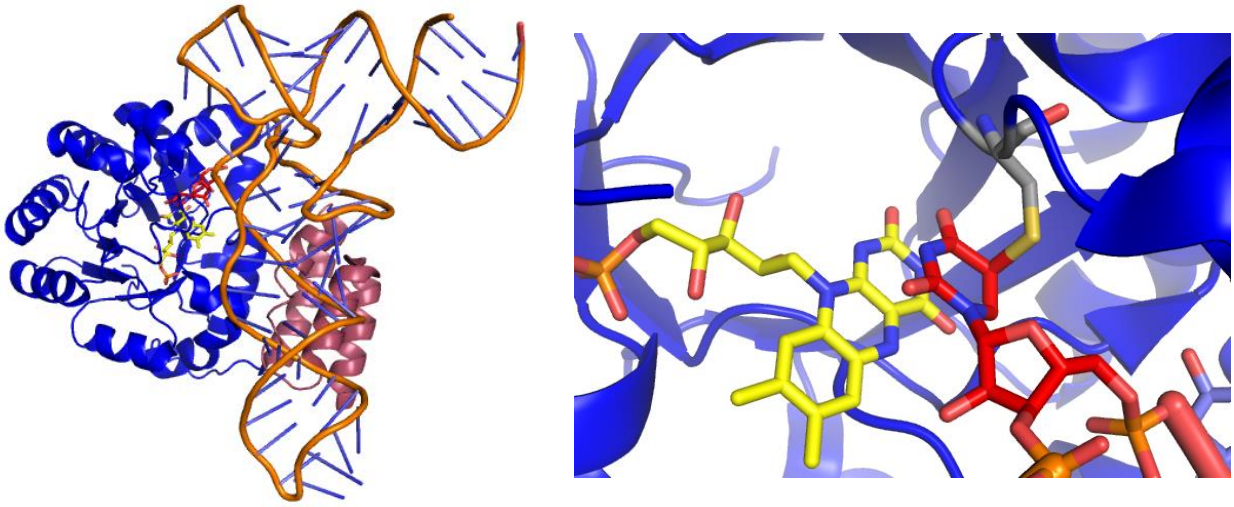

Figure 1 - 9. Structure of *T. thermophilus* DUS in complex with tRNA (PDB 3B0U). Left panel, overall structure; right panel, active site. The TIM-barrel domain is shown in blue, the helix-bundle domain is shown in pink, the FMN is shown in yellow, the substrate uracil of the tRNA is shown in red, and the cysteine is shown in gray.

Curiously, some well-defined electron-density of unknown origin was present in the DUS-tRNA structure in the space between the substrate uracil and the inner wall of the active site. Yu, et al. attributed this density to an unknown cofactor that originated from E. coli.[26] The cofactor appears to be important for activity – mutation of the residues interacting with the cofactor abolished the activity of the enzyme.[26]

Mechanism

Yeast DUS2 is the only enzyme whose mechanism has been studied in detail.[27] The catalytic cycle of yeast DUS2 can be broken up into half-reactions (Figure 1 - 10). In the reductive half-reaction, NADPH – which has been reported to be the reducing substrate for DUSs – binds to the enzyme and reduces the flavin. The reductive half-reaction of yeast DUS2 is complex, with multiple phases – the largest of which corresponding to hydride transfer from NADPH to the flavin. A transient charge-transfer band developed with reduction of the flavin, indicating that the product, $NADP^+$, does not immediately dissociate from the enzyme. Using stereospecifically-deuterated NADPH, it was shown that yeast DUS2 transfers the pro-R hydrogen of NADPH.[27] Reductive half-reactions with pro-R-deuterated NADPH exhibited a kinetic isotope effect of 3.5, indicating that hydride transfer from NADPH to the flavin is at least partially rate-limiting.

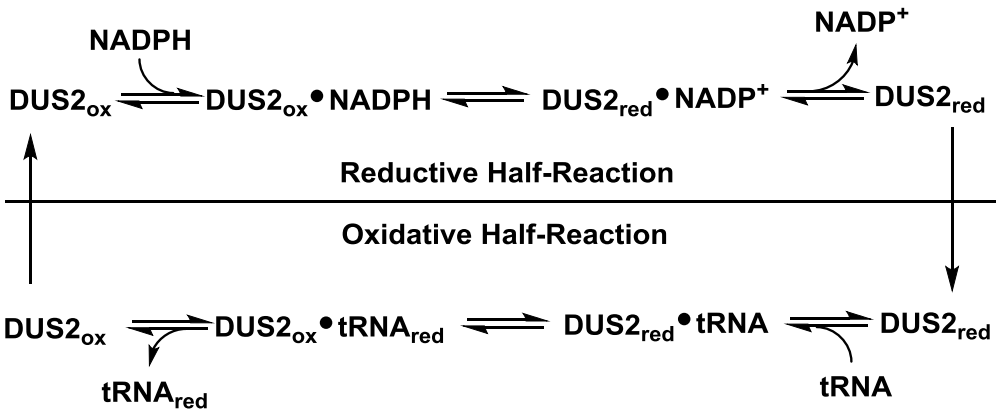

Figure 1 - 10. The catalytic cycle of tRNA-dihydrouridine synthase.

In the oxidative half-reaction, reduced DUS2 reacts with tRNA, reducing the carbon-carbon double bond of the tRNA uracil. A single phase has been observed when tRNA reacts with reduced DUS2 in the oxidative half-reaction.[27] Interestingly, yeast DUS2 reacts poorly in oxidative half-reactions with *in vitro*-transcribed $tRNA^{Leu}$-CAA. However, when $tRNA^{Leu}$-CAA isolated from a yeast DUS2 knockout strain was used instead, the rate constant was ~600-fold faster. This indicates that other, prior tRNA modifications are important for $tRNA^{Leu}$-CAA to adopt the correct structure to react rapidly with DUS2, and suggests that tRNA modifications might be ordered.

Subsequent to, or accompanying hydride transfer from reduced FMN to C6 of the uracil, C5 of the uracil needs to be protonated to form dihydrouridine. An active-site cysteine has been proposed to be the general acid that performs this role. Mutation of the active-site cysteine to alanine in yeast DUS2 resulted in a massive decrease in the reactivity of yeast DUS2 with tRNAs.[27]

Dihydroorotate Dehydrogenase

Dihydroorotate dehydrogenases (DHODs) are FMN-dependent enzymes that catalyze the oxidation of dihydroorotate (DHO) to orotate (OA) in the only redox step in the *de novo* biosynthesis of pyrimidines (Figure 1 - 11).[1] DHODs can be grouped into two classes based on sequence similarity. Class 1 enzymes are cytosolic, and have been further divided into two subsclasses: Class 1A DHODs are homodimers that are oxidized by fumarate;[28] Class 1B DHODs are $\alpha_2\beta_2$ heterotetramers that contain a 2-iron-2-sulfur cluster (2Fe-2S) and an FAD in addition to FMN, which are reoxidized by NAD^+.[29] Class 2 DHODs are membrane-associated monomeric enzymes that are re-oxidized by membrane-bound ubiquinone.[30]

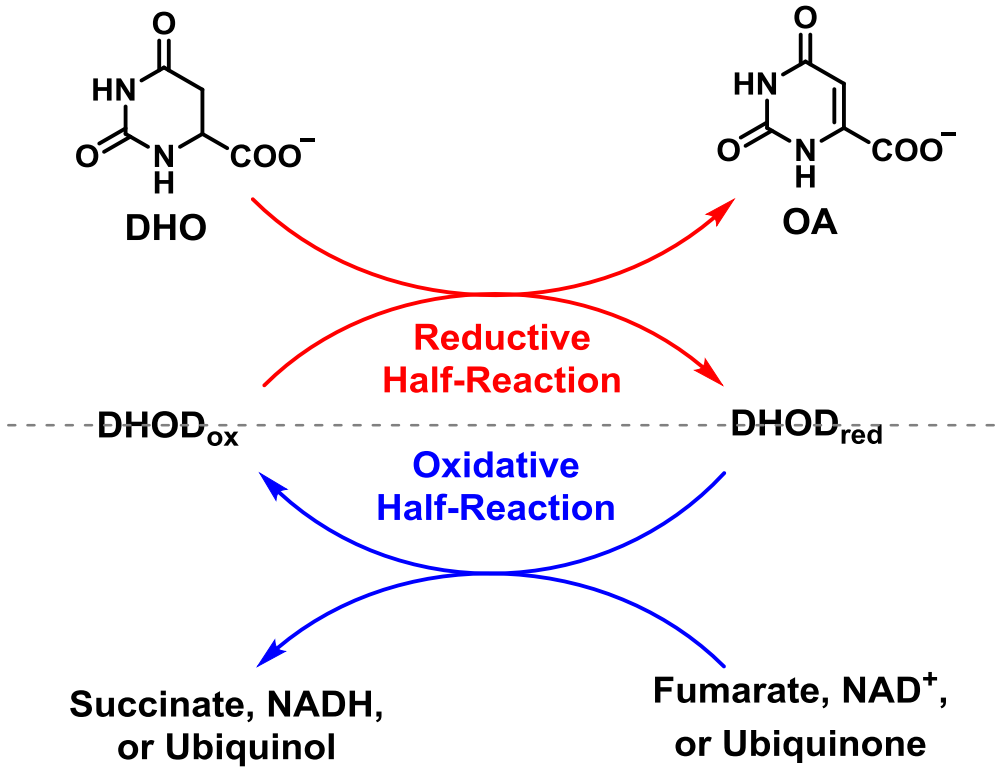

Figure 1 - 11. The catalytic cycle of dihydroorotate dehydrogenases.

Structures

Structures of all DHOD classes/subclasses have been solved. All DHODs contain a TIM-barrel domain where the FMN is located. Class 1A enzymes are homodimeric, with the TIM-barrel domains of each monomer associated through conserved salt bridges (Figure 1 - 12).[31–36] In Class 1A enzymes, an active site cysteine is used as the active site base, and is positioned above C5 of orotate in the orotate-bound complex. Co-crystal structures with fumarate indicate that the oxidizing substrate binds in the same pocket as DHO, with the unsaturated carbons of fumarate in close proximity to N5 of the flavin.

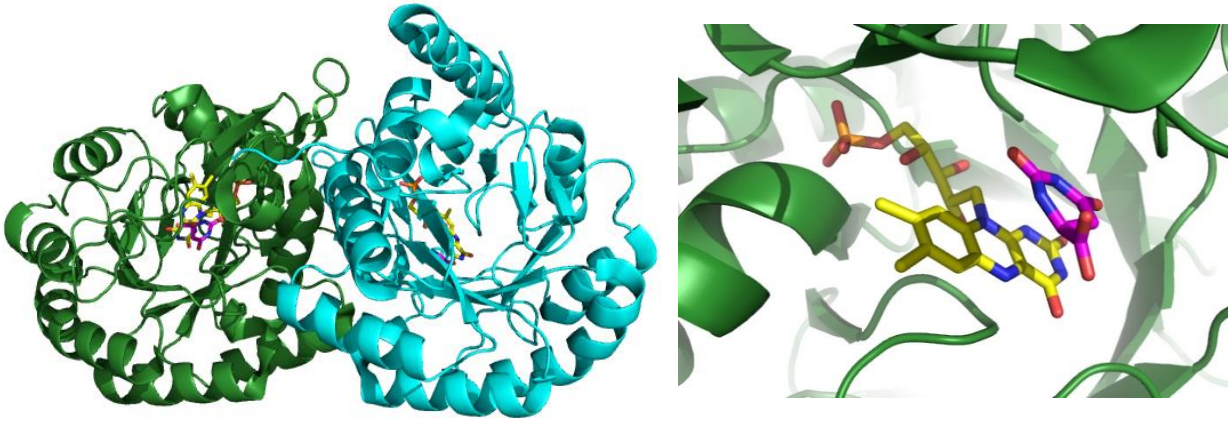

Figure 1 - 12. Structure of the homodimeric Class 1A DHOD from *Trypanosoma cruzi* (PDB 2E68). Left panel, overall structure of the homodimer; right panel, the active site. The FMN is shown in yellow and DHO is shown in magenta.

Class 1B enzymes are $\alpha_2\beta_2$ heterotretrameric enzymes. Each heterodimer of the $\alpha_2\beta_2$ heterotetramer is composed of a PyrDb subunit and a PyrK subunit (Figure 1 - 13).[37] The PyrDb subunit is a TIM-barrel and contains the FMN used to oxidize DHO. An active site cysteine is used as the active site base to remove the C5 proton of DHO. The PyrK subunit contains a 2Fe-2S cluster and an FAD. The 2Fe-2S cluster is

positioned between the FMN and FAD of the heterodimer. NAD+ is believed to bind with the nicotinamide near the isoalloxazine of the FAD to allow reduction of NAD^+ to NADH. The 2Fe-2S cluster is assumed to play a role in electron transfer between the two flavins.

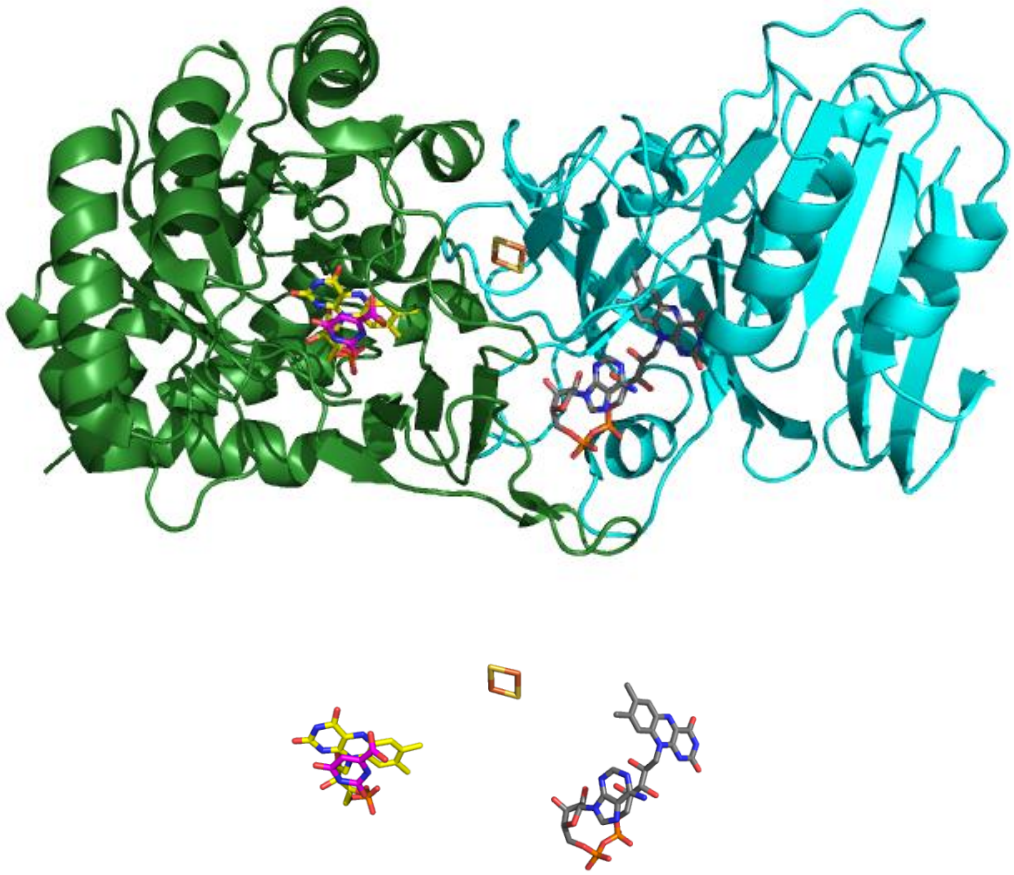

Figure 1 - 13. Structure of one heterodimer of the Class 1B DHOD from *Lactococcus lactis* (PDB 1EP2). Top panel, the overall structure of one heterodimer; bottom panel, the redox centers and OA in the heterodimer. The PyrDb subunit is shown in green; the PyrK subunit is shown in cyan; FMN is shown in yellow; OA is shown in magenta; FAD is shown in gray; the 2Fe-2S cluster is shown in orange.

Class 2 DHODs contain, in addition to the TIM-barrel, an N-terminal extension that is responsible for associating the protein with the membrane (Figure 1 - 14).[38–43] The N-terminal domain sits on top of the TIM-barrel domain and helps form a tunnel leading to the isoalloxazine of the flavin. This tunnel is proposed to be the ubiquinone binding site (ubiquinones are embedded in the membrane). An active site serine sits above the pyrimidine binding site, well-positioned to serve as the active site base. A hydrogen bonding network connects the active site serine to bulk solvent, which has been proposed to help activate the serine as a base.[44]

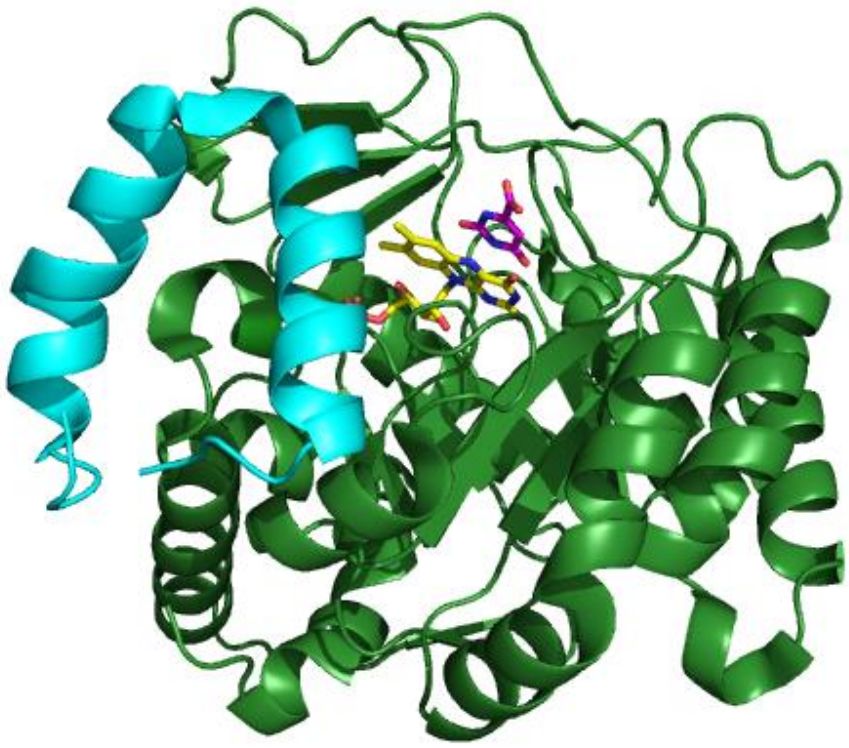

Figure 1 - 14. Structure of human Class 2 DHOD (PDB 1D3G). The TIM-barrel domain is shown in green; the N-terminal extension that associates with the membrane is shown in cyan; FMN is shown in yellow; OA is shown in magenta.

Mechanism

The catalytic cycle of DHODs can be broken up into half-reaction (Figure 1 - 11). In the reductive half-reaction, DHO reduces the FMN, with OA being made in the process. In the oxidative half-reaction, the electrons obtained from DHO are transferred to fumarate in Class 1A DHODs, NAD^+ in Class 1B DHODs, and ubiquinone in Class 2 DHODs.

Most of the mechanistic work on DHODs has focused on the reductive half-reaction. In the reductive half-reaction, two things must ultimately be accomplished – hydride transfer from C6 of DHO to N5 of oxidized FMN and removal of the proton from C5 of DHO. These two events can occur simultaneously (a concerted mechanism) or in a stepwise manner. Kinetic isotope effects have been used to probe the two possible mechanisms in the different classes of enzymes. Isotope effects on steady-state assays indicated that the Class 2 DHOD from bovine liver[45] and the Class 1B DHOD from *Clostridium oroticum*[46] use a concerted mechanism, while the Class 1A DHOD from *Crithidia fasciculata*[47] uses a stepwise mechanism. However, isotope effects on the reductive half-reaction indicated that a concerted mechanism is used by the Class 1A DHOD from *Lactococcus lactis*[48] and the Class 2 enzyme from humans and *Escherichia coli*[49] use either a stepwise mechanism or a concerted mechanism with tunneling. It is unclear why the conclusions from steady state and oxidative half-reaction experiments produced contradictory mechanisms. However, it could suggest that the mechanism of DHO oxidation by DHODs is not identical amongst enzymes of the same Class.

Little is known about the mechanism of the oxidative half-reaction of DHODs. The Class 1A DHODs use fumarate as the oxidizing substrate. A study on the Class 1A enzyme from *Enterococcus faecalis* showed that fumarate binds weakly to the reduced form of the enzyme, and flavin oxidation by fumarate is rate-determining for the entire catalytic cycle.[50] The Class 1B enzymes use NAD^+ as the oxidizing substrate. The oxidative half-reaction of Class 1B DHOD has not been studied in detail. Presumably, the electrons obtained from DHO get transferred to the FAD through the 2Fe-2S cluster, and then get transferred to NAD^+. The oxidative half-reaction of Class 2 DHODs is difficult to study due to the low solubility of ubiquinone. However, short-chain ubiquinone analogs have been shown to rapidly oxidize the reduced FMN of Class 2 DHODs.[51,52]

Flavin-Dependent Thymidylate Synthase

All organisms must replicate and maintain their DNA to survive. Thymidylate − an essential precursor for the biosynthesis of DNA − is formed by the reductive methylation of 2'-deoxyuridine-5'-monophosphate (dUMP) to form 2'-deoxythymidine-5'-monophosphate (dTMP) by thymidylate synthases. For decades, *de novo* biosynthesis of dTMP was thought to be catalyzed solely by the classical thymidylate synthases which do not use a prosthetic group. Classical thymidylate synthases are arguably one of the most thoroughly understood enzymes.[53]

Analysis of genomic databases showed that many organisms lacked the genes for classical thymidylate synthase, but were still capable of growing on dTMP-depleted media.[54,55] In 2002, a new class of enzymes was discovered in these organisms which synthesized dTMP with the help of a flavin adenine dinucleotide (FAD) prosthetic group;

these enzymes are called the flavin-dependent thymidylate synthases (FDTSs).[54,56] FDTSs are encoded by the *thyX* gene.

Since the discovery of FDTS, numerous studies have shown that FDTSs have a novel sequence, structure, and mechanism that is unrelated to classical thymidylate synthases. Classical thymidylate synthases are homodimers that use (*R*)-N^5,N^{10}-methylene-5,6,7,8-tetrahydrofolate (CH_2THF) as both the methylene donor and reductant in the conversion of dUMP to dTMP, making dihydrofolate (DHF) in the process (Figure 1 - 15).[57] The DHF is then converted back into CH_2THF by the enzymes dihydrofolate reductase and serine hydroxymethyltransferase. In contrast, FDTSs use CH_2THF only as the methylene donor and use reducing equivalents from an external reductant – widely assumed to be NADPH – to synthesize dTMP from dUMP, leaving the folate as tetrahydrofolate (THF).[57,58] The FAD prosthetic group of FDTS is used to shuttle electrons from the reductant to dTMP, cycling between oxidized (FAD) and reduced hydroquinone ($FADH_2$) redox states. Usually, organisms that rely on FDTS for dTMP biosynthesis also lack the gene for dihydrofolate reductase. DHF is generated only in dTMP biosynthesis, so the reductase is only needed in organisms that use the classical thymidylate synthase.[59]

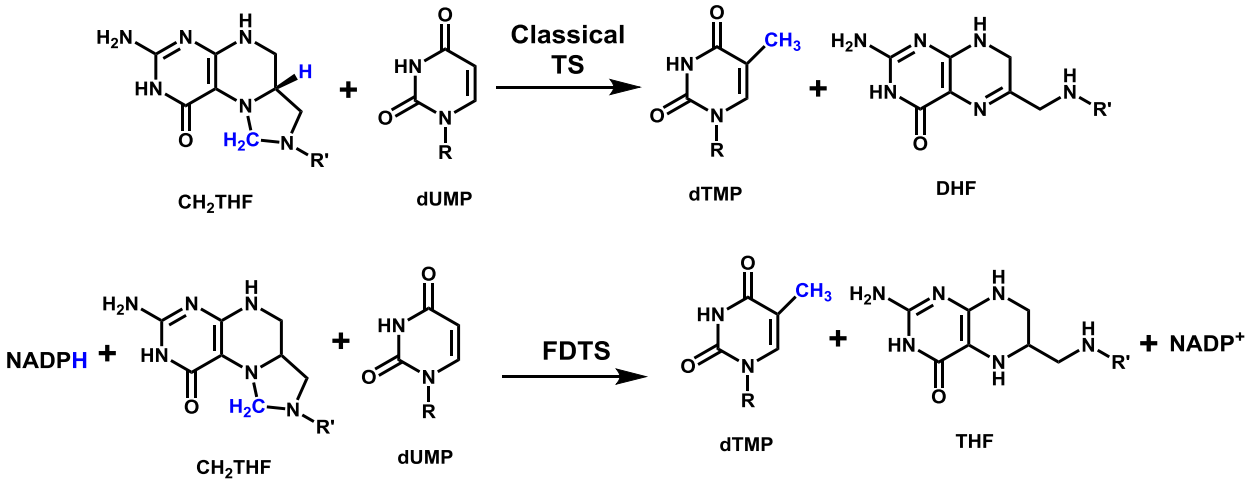

Figure 1 - 15. Overall reactions catalyzed by classical thymidylate synthase and flavin-dependent thymidylate synthase.

Classical thymidylate synthase and FDTS are generally mutually exclusive throughout nature; however some organisms contain genes for both enzymes.[60] It is unclear why some organisms contain genes for both thymidylate synthases. FDTS is only found in microorganisms and is overrepresented in hyperthermophilic, microaerophilic, and anaerobic microorganisms.[60] This could be due to the high NADPH-oxidase activity of FDTS,[61,62] which would wastefully consume NADPH in an aerobic environment. However, FDTS is present in several mesophilic and aerobic microorganisms as well, indicating that environmental factors alone do not explain the phylogenetic distribution of classical thymidylate synthase and FDTS. Escartin et al. showed that the use of FDTS limits the genome size of organisms compared to organisms that use classical thymidylate synthase due to the relatively low catalytic efficiency of FDTS,[63] suggesting an evolutionary need for the more prolific classical thymidylate synthase in higher organisms. Notably, a number of human pathogens (e.g., *Mycobacterium tuberculosis* and *Helicobacter pylori*) use FDTS to synthesize dTMP whereas humans use classical thymidylate synthase. Since dTMP biosynthesis is

essential for DNA replication, the unrelated structure and mechanism of FDTS relative to classical thymidylate synthase makes FDTS a promising candidate for the development of novel antibiotics. However, a thorough understanding of the mechanism and structure of FDTS is essential for the rational design of FDTS inhibitors.

Structures

The first structure of FDTS was solved by a structural genomics group about the same time its function was discovered.[56,64,65] FDTS is a tetramer with a unique fold, unrelated to classical thymidylate synthase or any other protein (Figure 1 - 16). The tetramer binds four FAD prosthetic groups that are oriented with the AMP moieties in the core of the protein and the isoalloxazines in solvent-exposed cavities near the surface of the tetramer. There are four active sites per tetramer, each of which consists of side chains provided by three of the four subunits as well as the isoalloxazine of an FAD. In the structure without bound ligands the positions of the isoalloxazines are not well defined and loop 86-97 (*T. maritima* FDTS numbering) is disordered. The active site becomes more ordered with dUMP (or one of its analogs) bound in an enclosed pocket partially composed of loop 86-97, with the uracil of dUMP stacked against the *re*-face of the isoalloxazine of FAD (Figure 1 - 17). Time-resolved fluorescence of FDTS from *T. maritima* showed that the isoalloxazine environment is much more dynamic when dUMP is not bound in the active site.[66]

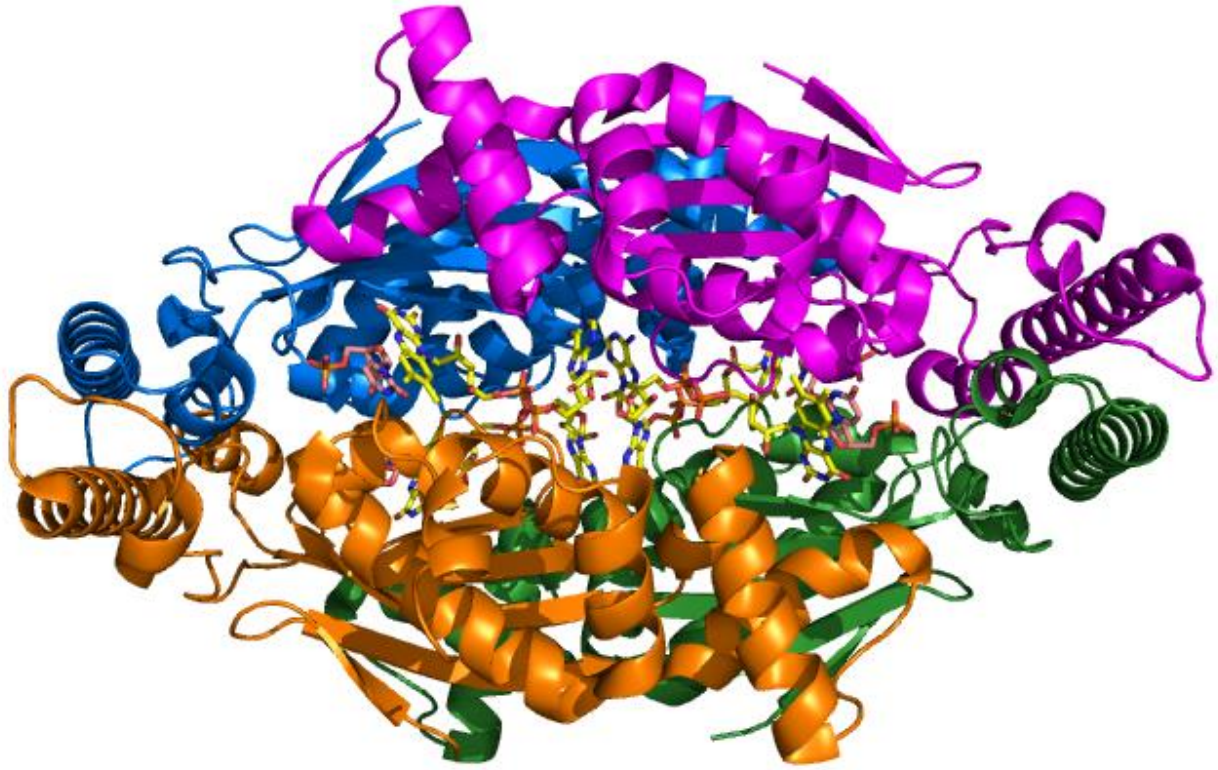

Figure 1 - 16. Quaternary structure of the FDTS homotetramer (PDB 1O26). Four FADs (yellow) lie in the groove between the four subunits.

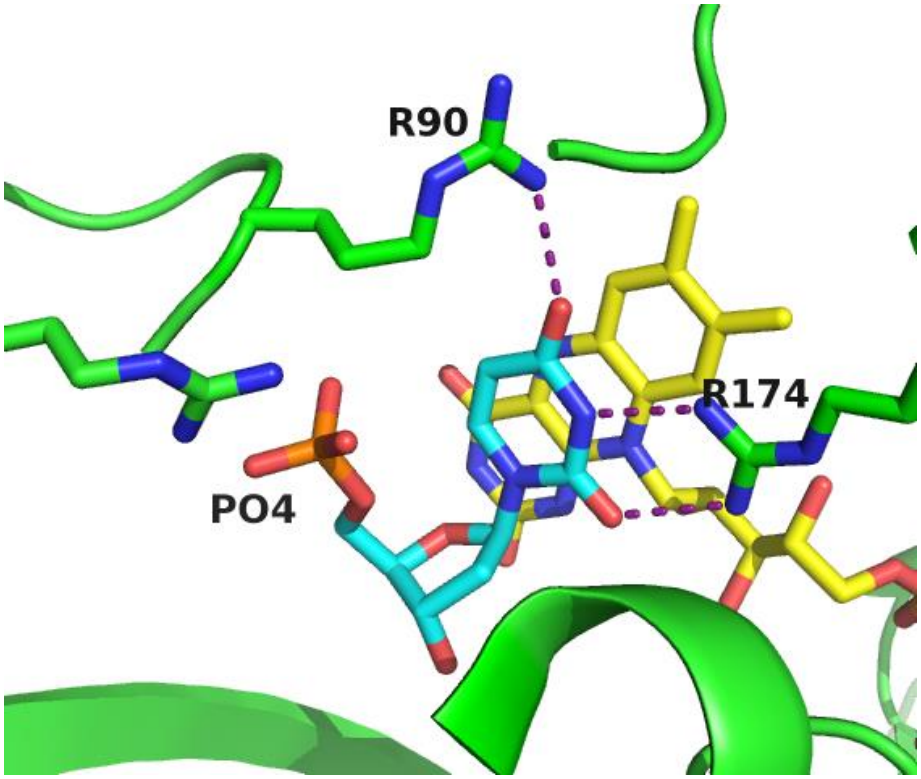

Figure 1 - 17. dUMP binding site of FDTS (PDB 1O26). dUMP is shown in cyan and the flavin is shown in yellow. In the mechanism proposed in Figure 1 - 20D, R90, R174, and the phosphate of dUMP stabilize the enolate resonance form of the uracil of dUMP.

An outstanding question from the available structural information is how the methylene gets transferred from CH_2THF to dUMP given how the isoalloxazine is stacked directly against the uracil of dUMP with no access for CH_2THF. Recently, several structures of *T. maritima* FDTS in complex with dUMP and CH_2THF or its analogues were solved.[67] In these structures the folates are bound on the *si*-face of the isoalloxazine, sandwiched between the isoalloxazine and a conserved active-site histidine (H53 in *T. maritima*) (Figure 1 - 18A) while the positions of dUMP and FAD are unperturbed compared to the structures without folates. Mutagenesis has confirmed the importance of this conserved histidine for FDTS activity.[67–69] The position of CH_2THF and its analogues in these structures conflicts with the required chemistry since dUMP and CH_2THF must come into contact with each other for methylene transfer, which

would be impossible because the isoalloxazine is in between the two substrates. A recent report on an enzyme catalyzing apparently related chemistry, FAD/Folate-dependent tRNA methyltransferase, indicated that the flavin of that enzyme transfers the methylene from CH_2THF to dUMP through an adduct with N5 of the reduced flavin.[70] It is unlikely that the flavin plays a similar role in FDTS, though, because enzyme containing 5-carba-5-deaza FAD is still active.[71] The structures of E144R and R174K *T. maritima* FDTS mutants and the structure of *Paramecium bursaria* chorella virus-1 (PBCV-1) FDTS[72] show the isoalloxazine in an alternate conformation, where the isoalloxazine is rotated and stacked against H53 (Figure 1 - 18B). Koehn and coworkers argued that this alternate conformation of the isoalloxazine would allow CH_2THF to bind in the crevice between the isoalloxazine and dUMP, facilitating methylene transfer from CH_2THF to dUMP.[67] They were able to model the iminium form of CH_2THF into the position vacated by the isoalloxazine when it moves to the alternate conformation. The iminium was then well-positioned to react with C5 of dUMP. However, to date no structures have been solved with CH_2THF productively bound on the *si*-face of the isoalloxazine, between the isoalloxazine and dUMP.

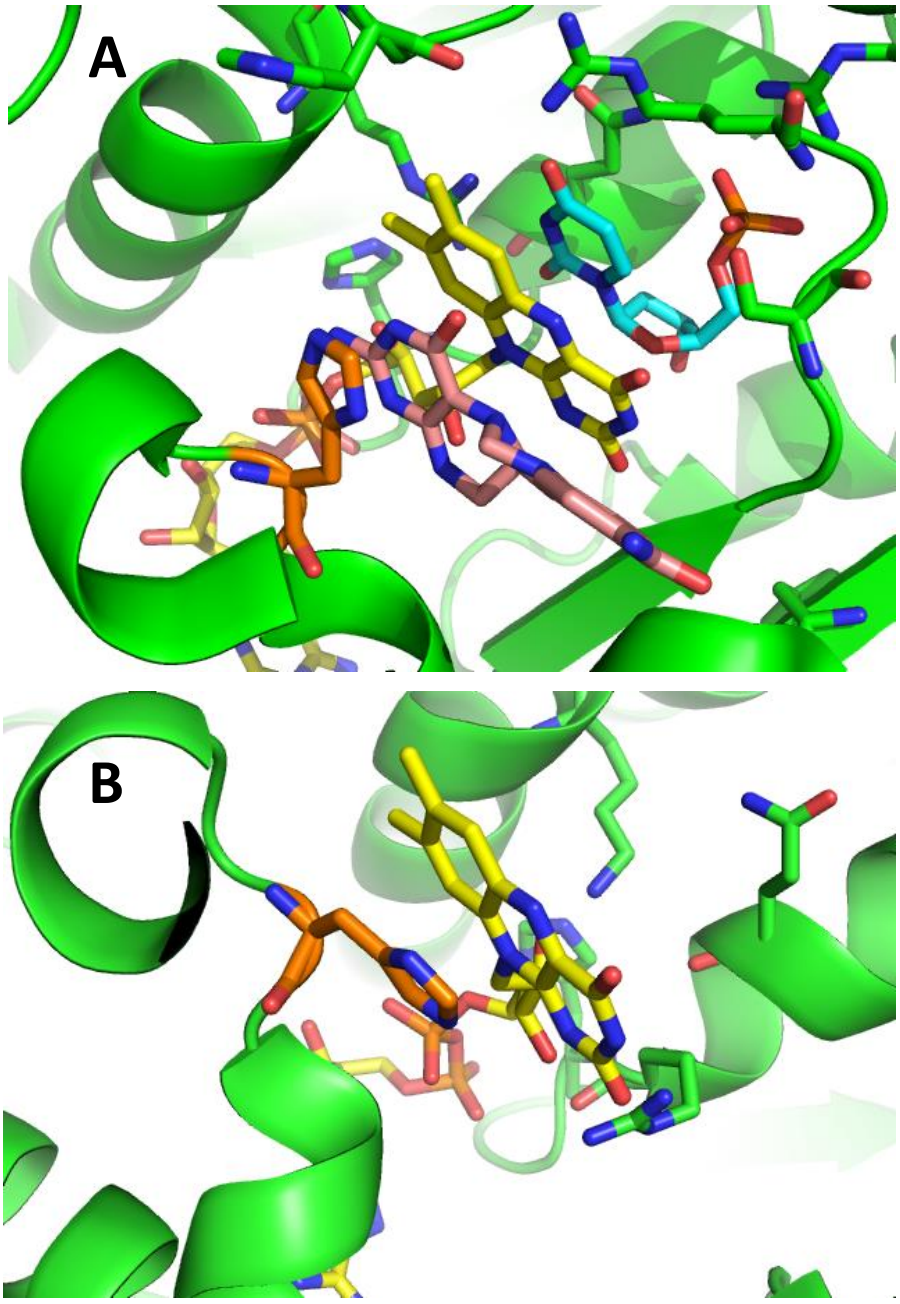

Figure 1 - 18. CH_2THF binding site and an alternative FAD conformation in *T. maritima* FDTS. (A) CH_2THF (salmon) has been shown to bind in the pocket between the isoalloxazine of FAD (yellow) and a conserved histidine (orange) (PDB 4GT9). This cannot be a reactive conformation since the isoalloxazine is between CH_2THF and dUMP (cyan). (B) In two mutant enzyme structures – E144R (PDB 4GTD) and R174K (PDB 4GTL) – the isoalloxazine (yellow) is in a different conformation, stacked against the conserved histidine (orange). In this conformation, CH_2THF could bind next to dUMP to allow methylene transfer.

Interestingly, a structure of PBCV-1 FDTS with a bound inhibitor, 2-hydroxy-3-(4-methoxybenzyl)-1,4-napthoquinone (C8-C1), has been solved where the inhibitor is bound on the *si*-face of the isoalloxazine.[73] The 1,4-napthoquinone moiety stacks against the isoalloxazine, partially overlapping with the putative dUMP binding pocket while the 4-methoxybenzyl moiety exits towards the surface of the protein. It is tempting to speculate that CH_2THF might bind in a similar orientation in the Michaelis complex since the pteridine and para-aminobenzoyl moieties of CH_2THF share structural similarities with the 1,4-napthoquinone and para-methoxybenzyl moieties of C8-C1, respectively.

The binding site for pyridine nucleotides is still unknown. The only structure with a pyridine nucleotide bound is an artifact – in the structure with NADP+ bound to *M. tuberculosis* FDTS, NADP+ displaced the FAD prosthetic group.[74] However, the nonproductive folate binding site may very well be the site for pyridine nucleotide binding. Kinetic studies have shown that NADPH and folates compete for the same binding site.[67] Pyridine nucleotides can also be easily accommodated in the folate binding site.

Chemical Mechanism

Like most flavoenzymes, the catalytic cycle of FDTS can be divided into half-reactions (Figure 1 - 19). In the reductive half-reaction, NADPH (or another reductant) reacts with the oxidized FAD of FDTS to reduce the flavin to the hydroquinone. In the oxidative half-reaction, the $FADH_2$ of FDTS reacts with dUMP and CH_2THF – flavin oxidation requires both substrates.[75] The methylene is transferred from CH_2THF to

dUMP and electrons are transferred from $FADH_2$ to make dTMP, THF, and oxidized FAD.

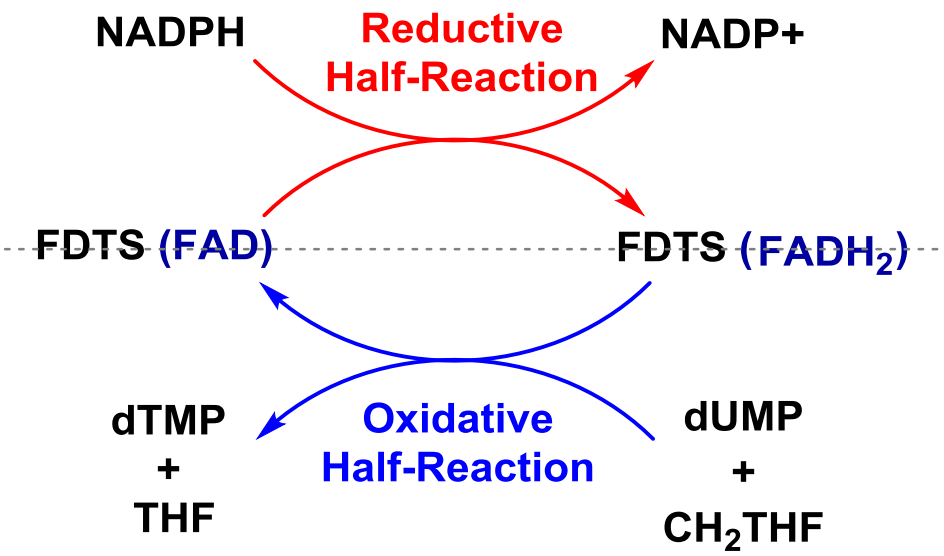

Figure 1 - 19. Catalytic cycle of FDTS. The catalytic cycle can be divided into half-reactions. In the reductive half-reaction, NADPH reduces the FAD prosthetic group of FDTS. In the oxidative half-reaction, the reduced FAD of FDTS reacts with dUMP and CH_2THF to make dTMP and THF.

Reductive Half-Reaction with NADPH

Reduced flavin is required to synthesize dTMP by FDTS.[54,64,75] When FDTSs were first discovered, it was shown that they strictly required NADPH/NADH for catalysis but had only a slight preference for NADPH over NADH.[54,64] Still, NADPH is widely assumed to be the physiological reductant that reduces the flavin. However, there are certain features of the reaction of NADPH with oxidized FDTS that are unusual, raising questions about its role as the physiological reductant. For one, the reaction of NADPH with *Campylobacter jejuni* FDTS under anaerobic conditions is extremely slow, taking nearly an hour to complete.[62] While the equivalent reaction of NADPH with *Thermotoga maritima* FDTS occurs quickly, taking seconds to complete, *T.*

maritima FDTS shows little preference for NADPH or NADH, which is unusual for flavoenzymes that use pyridine nucleotides as their physiological reductant.[62] Also, the K_d determined for NADPH binding to oxidized FDTS is ~1 mM − unusually weak binding for flavoenzymes that use pyridine nucleotides as reductants. *T. maritima* FDTS surprisingly exhibits lax stereochemistry in the hydride transfer from NADPH, abstracting 68% of the *proR* hydride when using [4*R*-^{2}H]NADPH and 8% of the *proS* hydride when using [4*S*-^{2}H]NADPH in the reductive half-reaction.[62] The hydride transfer reactions of pyridine nucleotides are always extremely stereospecific; there are no reports of other enzymes with lax stereochemistry in hydride transfer. Taking these points into consideration, it is conceivable that pyridine nucleotides are not the physiological reductant for FDTSs, but a better reductant has yet to be identified.

Oxidative Half-Reaction with dUMP and CH_2THF

Much of the work on FDTS has focused on the chemical mechanism for the formation of dTMP in the oxidative half-reaction. A number of mechanisms have been proposed (Figure 1 - 20). This section reviews the evidence supporting and contradicting each of these mechanisms.

Classical Thymidylate Synthase

When FDTSs were first discovered it was considered that they use a mechanism similar to classical thymidylate synthases, except that the reducing equivalents came from NADPH (via the flavin) instead of THF.[54] In classical thymidylate synthase, a conserved active-site cysteine covalently activates the uracil of dUMP by a Michael-like addition to C6 of the uracil ring (Figure 1 - 20A). The resulting enolate allows C5 of the

uracil to act as a nucleophile, which attacks the iminium form of CH_2THF, forming an adduct between the enzyme, dUMP, and CH_2THF. Upon deprotonation of C5, THF is eliminated, leaving an exocyclic methylene deoxynucleotide intermediate still covalently bound to the enzymatic cysteine. Finally, a hydride is transferred from THF to C7 of the intermediate, making DHF and eliminating the active-site cysteine, completing the catalytic cycle.

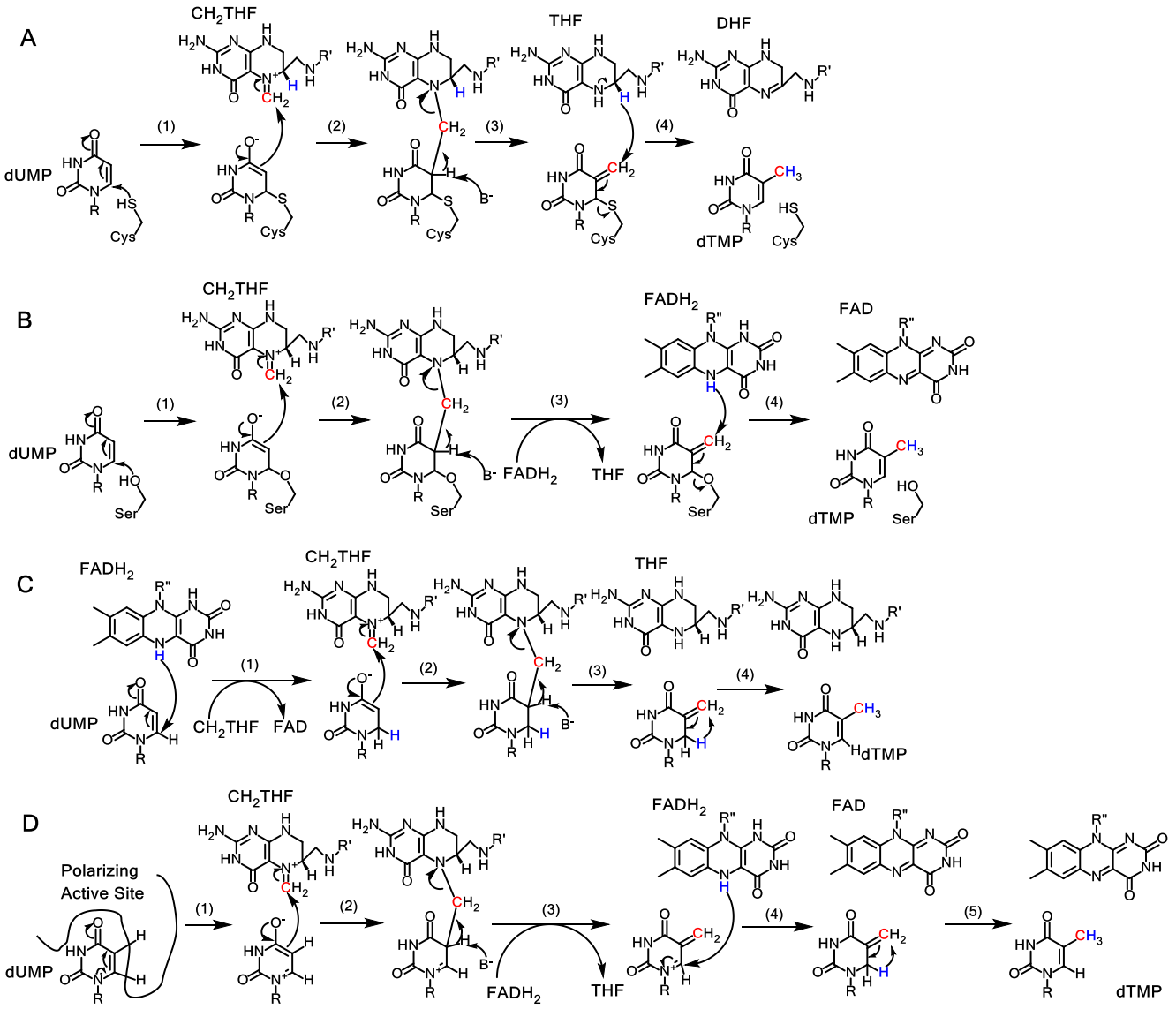

Figure 1 - 20. Thymidylate synthase chemical mechanisms. (A) The chemical mechanism of classical thymidylate synthase.[53] (B) A proposed mechanism for FDTS involving an active-site serine nucleophile.[68] (C) A proposed mechanism for FDTS where dUMP is activated by hydride transfer from reduced FAD.[71] (D) A proposed mechanism for FDTS where dUMP is activated by the electrostatically polarizing active site.[78]

Serine as the Activating Nucleophile?

The structure of FDTS showed that there is no active-site cysteine available to activate dUMP.[65] However, a conserved active-site serine was proposed to serve as the enzymatic nucleophile in place of cysteine. Mutagenesis studies on the FDTS from *H. pylori* showed that when the conserved active-site serine (S84; S88 in *T. maritima*) was mutated to alanine the enzymatic activity was diminished, but still present.[68] The authors argued that a neighboring serine (S85) was able to rescue the S84A mutant by serving as an alternative nucleophile to activate dUMP. Indeed, when a double-mutant S84A/S85A was used all activity was lost. In addition, they also detected a covalent adduct between dTMP and FDTS when an S84C mutant was used. Unlike in classical thymidylate synthase, this adduct did not contain the folate of CH_2THF. The authors claimed that these results suggest that FDTS uses a mechanism (Figure 1 - 20B) analogous to that of classical thymidylate synthase where an active-site serine covalently activates dUMP through Michael addition at C6. At the end, hydride transfer from reduced FAD instead of THF would make dTMP and eliminate the serine adduct, completing the catalytic cycle.

The use of a conserved active-site serine as the activating nucleophile was met with some skepticism since the proposed serine is poorly positioned for nucleophilic attack of dUMP in the crystal structures of FDTS – the serine is 4 Å away from C6 of dUMP and is parallel to the ring instead of perpendicular to it, which would be required for Michael-like addition. Also, no covalent complexes between 5-fluoro-dUMP and wild-type FDTS have been detected when using 5-fluoro-dUMP in place of dUMP during catalysis. A covalent adduct between 5-fluoro-dUMP, CH_2THF, and an active site

cysteine in classical thymidylate synthase was strong evidence supporting covalent activation.[76]

Koehn et al. performed mutagenesis studies on the FDTS from *T. maritima* similar to those done on the enzyme from *H. pylori*.[71] Surprisingly, the S88A mutant (S88 is the homologous putative nucleophile in *T. maritima* FDTS) retained significant activity and unlike in *H. pylori* FDTS, *T. maritima* FDTS does not have an adjacent serine, indicating that S88 does not activate dUMP.

Activation by Other Nucleophiles?

Since the active-site serine of FDTS was ruled out as a nucleophile, other groups have been considered. N5 of FAD is proposed to act as a nucleophile in the flavoenzymes UDP-galactopyranose mutase[77] and FAD/folate-dependent tRNA methyltransferase.[70] In the crystal structures of FDTS, N5 of FAD is positioned 3.5 Å away from C6 of dUMP, perpendicular to the plane of the uracil. Therefore, N5 of FAD could conceivably act as a nucleophile in FDTS. However, FDTS containing 5-carba-5-deaza FAD where the N5 nitrogen is replaced by a methylene was still oxidized by dUMP and CH_2THF, indicating that N5 of FAD cannot be the nucleophile.[71]

The only other potential nucleophiles in the crystal structure of FDTS are the phosphate oxygens of dUMP. dUMP is in an unusual conformation where the phosphate of dUMP is curled back towards the uracil moiety of dUMP (Fig. 1 - 17). This was also ruled out in stopped-flow studies showing that 2'-deoxyuridine 5'-monoposphorothioate (dUMP-S) reacts ~10-fold slower with FDTS than dUMP.[78] Since sulfur is more nucleophilic than oxygen, dUMP-S should be a better substrate than

dUMP if the phosphate oxygen serves as the nucleophile towards C6. Excluding the possibility of large conformational changes, no other groups in the active site could serve as a covalent activator of dUMP – indicating that there is no nucleophile in FDTS catalysis.

Activation by Hydride Transfer?

To probe the mechanism further, Koehn et al. followed the flow of hydrogens by monitoring the position of label incorporation using ^{1}H and ^{2}H NMR in multiple-turnover reactions in D_2O.[71] Since N5 of reduced FAD can exchange with solvent in FDTS, D_2O could be used to label dTMP.[58] dTMP was deuterated exclusively at position C7 when the reaction was carried out at 65°C (close to the physiological temperature of *T. maritima*). Surprisingly, when the reaction was performed at 37°C, deuterium was incorporated at both C6 (60%) and C7 (40%) of dTMP. The authors argued that the only way deuterium could be found at C6 would be from direct hydride transfer from reduced FAD to dUMP. These findings led them to suggest the mechanism shown in Figure 1 - 20C. In this mechanism, dUMP is initially activated by direct hydride transfer from reduced FAD. The resulting enolate attacks the iminium form of CH_2THF, forming an adduct between dUMP and CH_2THF. Upon deprotonation of C5, the adduct eliminates THF forming an exocyclic methylene tautomer of dTMP. This intermediate would then undergo an enzyme-catalyzed 1, 3-hydride shift where a hydride is transferred from C6 to C7, forming dTMP and explaining the distribution of deuterium between C6 and C7.

Several experiments show that hydride transfer does not occur until after activation of dUMP and transfer of the methylene from CH_2THF. 5-fluoro-dUMP and

CH_2THF do not oxidize reduced FDTS.[75] The fluoro substituent would not prevent hydride transfer from reduced flavin, but would prevent the breakdown of a nucleotide-folate adduct. The uncleavable C-F bond therefore must block the reaction sequence before redox chemistry takes place. Recent work directly monitoring the flavin chromophore in anaerobic stopped-flow experiments has shown that multiple steps occur prior to hydride transfer.[78] Also, chemical quenching experiments showed that dUMP is consumed prior to flavin oxidation and dTMP is formed concomitantly with the redox step. These results indicate that the reaction sequence of FDTS is not initiated by hydride transfer from reduced FAD to C6 of dUMP, so yet another mechanism was needed.

Activation by Polarization?

A mechanism was proposed that does not use a nucleophile to activate C6 of dUMP towards attacking CH_2THF.[78] Instead, dUMP is activated by an electrostatically polarizing active site that stabilizes a polarized resonance form of the uracil moiety (Figure 1 - 20D). A number of FDTS crystal structures with dUMP show that dUMP binds in a pocket where two conserved arginines are positioned in close proximity to O4 of dUMP (Figure 1 - 17). dUMP is also bound in an unusual curled conformation where two of the phosphate oxygens are positioned ~4.5 Å from N1 of dUMP. The positively charged arginines near O4 and the negatively charged phosphate oxygens near N1 favor the uracil pi electrons into the polarized resonance form (Figure 1 - 19D), increasing the nucleophilicity at C5. The now-nucleophilic C5 then attacks the iminium form of CH_2THF, forming an adduct. After deprotonation of C5 the adduct would eliminate THF, transferring the methylene to dUMP. A hydride would then be transferred

from reduced FAD to C6 of the intermediate. Finally, this intermediate would then undergo the 1,3-hydride shift to make dTMP.

The mechanism involving activation by polarization is consistent with most available data. It is additionally supported by mutagenesis studies. The reaction of dUMP and CH_2THF with reduced R90A and R174A FDTS mutants in anaerobic stopped-flow experiments is ~100-fold and ~400,000-fold slower than WT, respectively.[78] Also, deoxyuridine – which lacks the phosphate, but still binds to FDTS – cannot be processed by FDTS into deoxythymidine, indicating the importance of the phosphate in promoting catalysis by FDTS (Chapter 2). Indeed, the lower reactivity of dUMP-S relative to dUMP supports the role of phosphate as a polarizer since sulfur is less electronegative than oxygen and would, therefore, be less effective at polarizing dUMP. The activation of dUMP by polarization has never been proposed in pyrimidine enzymology. However, catalytically important polarization has been observed in unrelated enzymes using substrates containing α,β-unsaturated carbonyl moieties.[79]

Stopped-flow and acid quenching experiments indicated the presence of two transient intermediates during the reaction of reduced FDTS with dUMP and CH_2THF.[78] A separate set of acid quenching experiments using radioisotope labeling detected the presence of a single intermediate during the oxidative half-reaction. 5-hydroxymethyl-dUMP, identified by mass spectrometry, was recovered from the acid-quenched reaction mixtures.[80] This intermediate accumulated as dUMP was consumed and decayed with dTMP formation. The actual intermediate quenched by acid was proposed to be the exocyclic methylene tautomer in Figure 1 - 20C after step 3 of the hydride activation mechanism, which after an acid-catalyzed reaction with water and oxidation

by O_2, would make 5-hydroxymethyl-dUMP, the recovered product. More likely, the intermediate would be the one depicted in Figure 1 - 20D after step 3 which has not yet been reduced by $FADH_2$. This intermediate could undergo an acid-catalyzed reaction with water that would directly yield 5-hydroxymethyl-dUMP. Curiously, the timing of dUMP loss has different kinetics in the two sets of quenching experiments. Conrad et al. found that dUMP decayed after the first spectral intermediate formed while Mishanina et al. observed that dUMP decayed at the same time as the first detectable intermediate was formed.[78,80] It is unclear what caused this discrepancy since both experiments used 1 M HCl as the chemical quencher. Interestingly, the timing of 5-hydroxymethyl-dUMP detection observed by Mishanina et al. is consistent with the sum of the first and second intermediates detected by Conrad et al. The 5-hydroxymethyl-dUMP might therefore represent the acid-rearranged product of both the first and second intermediates detected by stopped-flow.

All mechanisms shown in Figure 1 - 20 predict that 5-fluoro-dUMP should form a covalent adduct with CH_2THF and perhaps an enzymatic side chain. However, such an adduct has never been detected. It is unclear why this is so. One possibility is that the adduct between 5-fluoro-dUMP and CH_2THF depicted in any of the mechanisms in Figure 1 - 20 is unstable when removed from the active-site environment of FDTS. It is also conceivable that the electronegative fluoro-substituent at C5 destabilizes the build-up of electron density at C5 in the polarized resonance form of dUMP, preventing a 5-fluoro-dUMP-CH_2THF adduct from occurring in the first place.

The mechanisms shown in Figure 1 - 20 all invoke a general base to remove the proton from C5 of the dUMP-CH_2THF adduct to facilitate methylene transfer and

eliminate THF. Deprotonation of C5 is clearly essential since C5 must be deprotonated in order to make dTMP. However, the identity of this general base is unknown. From the structures of dUMP complexes, the only potential base close enough is a phosphate oxygen of dUMP, which is 3.4 Å away from C5 (Figure 1 - 17). The phosphate oxygen is also on the correct face of the uracil moiety for deprotonation of C5 – opposite from the putative CH_2THF binding site. The phosphate oxygens could therefore conceivably serve a dual role in stabilizing the polarized resonance form of the uracil and in deprotonating C5 of the dUMP-CH_2THF adduct. Other active site groups cannot be ruled out, though, since conformational changes likely take place during dUMP-CH_2THF adduct formation that could bring other groups in close proximity to C5.

Kinetic Mechanism

While progress has been made on the chemical mechanism of FDTS, there are still many questions about the order of substrate binding and product release during the catalytic cycle. Several studies have attempted to elucidate the kinetic mechanism of FDTSs and have found different kinetic mechanisms for enzymes from different organisms – most of which use a ping-pong mechanism (Figure 1 - 21).[58,72,81–84] *T. maritima* FDTS has been shown to use a ping-pong mechanism and under multiple-turnover conditions the FAD remains oxidized, indicating that reduction of the flavin is rate-limiting.[58,61,83] PBCV-1 FDTS also uses a ping-pong mechanism for its substrates, with NADPH and CH_2THF competing for the same binding site.[72,82] Likely, NADPH first binds and reduces the flavin followed by $NADP^+$ dissociation and CH_2THF binding. A notable deviation from the sequential binding order seen in most FDTSs is the enzyme from *Chlamidya trachomatis* which exhibits ping-pong kinetics between dUMP and

CH_2THF.[81] Consistent with a ping-pong mechanism, THF was produced in reactions omitting dUMP. An active-site arginine (R477) was implicated in covalently transferring the methylene from CH_2THF to dUMP, producing the ping-pong kinetic patterns. However, this result could not be replicated by other groups.[67,85] A problem plaguing much of the published work on FDTS is the presence of O_2. The reduced flavin of FDTS, like most flavoenzymes, reacts with O_2 in a competing non-physiological side reaction, and the reaction of O_2 with FDTS is rapid enough to compete with thymidylate synthesis.[61,62,82,86] Unfortunately, the findings from a number of kinetic studies did not take into account the oxidase activity of FDTS, raising concerns about the validity of their findings.

Several studies have shown that the NADPH oxidase activity of FDTS is enhanced by the presence of dUMP, suggesting that dUMP binding enhances the hydride transfer step from NADPH to oxidized FAD [82,85,87]. This could be due to the ordering of the active-site observed in the dUMP-bound structures compared to the dUMP-free structures. Since dUMP stimulates the oxidation of NADPH by FDTS, it is likely that dUMP binds to the oxidized enzyme prior to FAD reduction by NADPH. Indeed, the binding affinity of FDTS for dUMP is ~200-fold higher for the oxidized enzyme compared to reduced enzyme (Chapter 3). Mason and co-workers originally argued that the enhanced NADPH oxidase activity by dUMP binding was due to an initial lag-phase in the reductive half-reaction of oxidized FDTS with NADPH that became shorter in duration with increasing dUMP concentration.[85] However, it was later shown that this initial lag phase was due to oxygen contamination which eventually became consumed in the original experiment.[83]

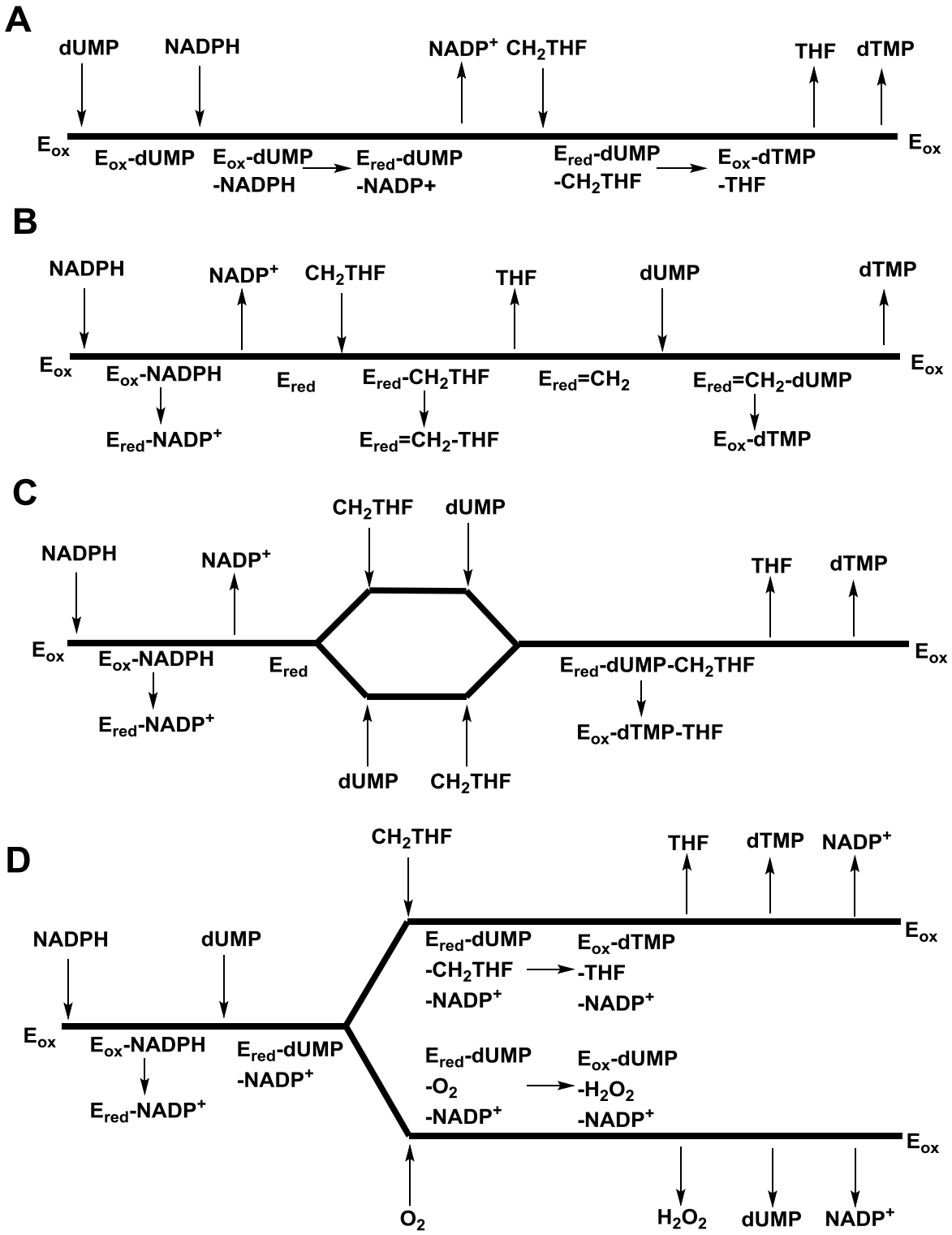

Figure 1 - 21. Proposed kinetic mechanisms for FDTS. Proposed kinetic mechanisms for FDTS from PBCV-1[72] (A), *C. trachomatis*[81] (B), *T. maritima*[58] (C), and *T. maritima*[83] (D).

Attempts have also been made to exploit the oxidase activity of FDTS to probe the kinetics of substrate binding and product release for some of the ligands involved in the FDTS-catalyzed reaction. In reductive half-reaction experiments, Wang and co-workers observed absorbance that developed upon FAD reduction which they attributed to a $FADH_2$-$NADP^+$ charge-transfer complex.[61] This complex decayed very slowly – with a rate constant of 0.00135 s^{-1} – which would indicate that $NADP^+$ does not dissociate from FDTS prior to reacting with dUMP and CH_2THF. However, the putative charge-transfer band is not consistent with typical reduced flavin-$NADP^+$ charge-transfer bands [88,89], and a charge transfer complex between reduced FDTS and $NADP^+$ has not been observed in reductive half-reactions or binding experiments.[90] More likely, the absorbance from 500-800 nm attributed to a charge-transfer complex was due to minor protein aggregation which settled out of solution over time. Indeed, given the crowded active-site seen in all FDTS structures to date, it is unlikely that FAD, $NADP^+$, dUMP, and CH_2THF could all be in the active-site at the same time. They also found that CH_2THF competitively inhibits the NADPH-oxidase activity of FDTS, which, they argued, meant CH_2THF and O_2 compete for the same site. More likely, CH_2THF competes with the NADPH used in their experiments which would cause the decreased the oxidase activity of FDTS in the presence of CH_2THF. Indeed, CH_2THF and NADPH have been shown to compete for the same binding site.[67]

Folate/FAD-Dependent tRNA Methyltransferase

In most tRNAs, the uracil at position 54 (U_{54}) in the T-loop is methylated to make ribothymidine (T_{54}). T_{54} interacts with another post-transcriptional modification, m^1A_{58}, to help stabilize the L-shape of tRNAs.[17] In most Gram-positive and some Gram-negative

bacteria, U_{54} is methylated by the recently discovered folate/FAD-dependent tRNA methyltransferase (TrmFO).[91] Unlike most RNA methyltransferases, which use S-adenosylmethionine as the methyl donor, TrmFO uses CH_2THF and 2-electron reduced FAD ($FADH^-$) to methylate U_{54} (Figure 1 - 22). The reducing equivalents required to reduce the flavin are believed to come from NADPH.

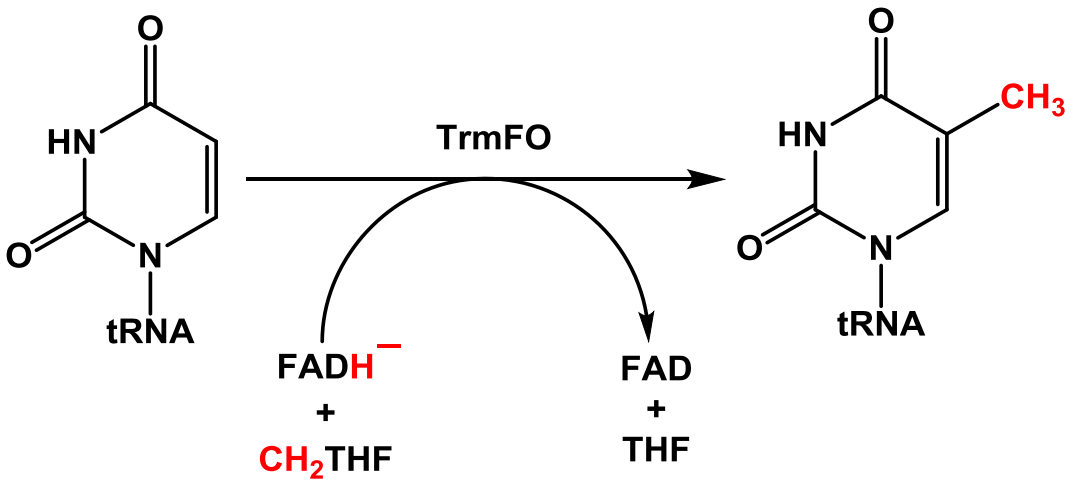

Figure 1 - 22. The reaction catalyzed by TrmFO.

Structures

The crystal structure of Thermus thermophilus TrmFO ($TrmFO_{TT}$) has been solved in the ligand-free form and in complex with THF (the folate product of the TrmFO reaction) or glutathione (Figure 1 - 23).[92] $TrmFO_{TT}$ is composed of two domains – an FAD-binding domain and an insertion domain. The FAD prosthetic group is bound with the adenosine moiety of the FAD buried deep in the FAD-binding domain and the isoalloxazine in a positively-charged cleft on the surface of the protein. THF binds next to the isoalloxazine of the FAD in the positively-charged cleft, with the pteridin moiety

sandwiched between the isoalloxazine and the imidazole of a conserved histidine residue. tRNA docking models with a tRNA T-arm analog indicated that tRNA can fit along the positively-charged cleft, with the substrate uracil near the isoalloxazine of the flavin. In the glutathione-bound structure, glutathione forms a disulfide bond with a conserved cysteine (C221 in $TrmFO_{TT}$) located on the opposite end of the protein from the flavin. It is unclear if glutathione plays a role in catalysis by TrmFO. However, biochemical data using a fluorouracil tRNA minihelix has suggested that the cysteine that forms a disulfide with glutathione is the nucleophile that initiates catalysis by attacking C6 of the reactive uracil moiety.[93]

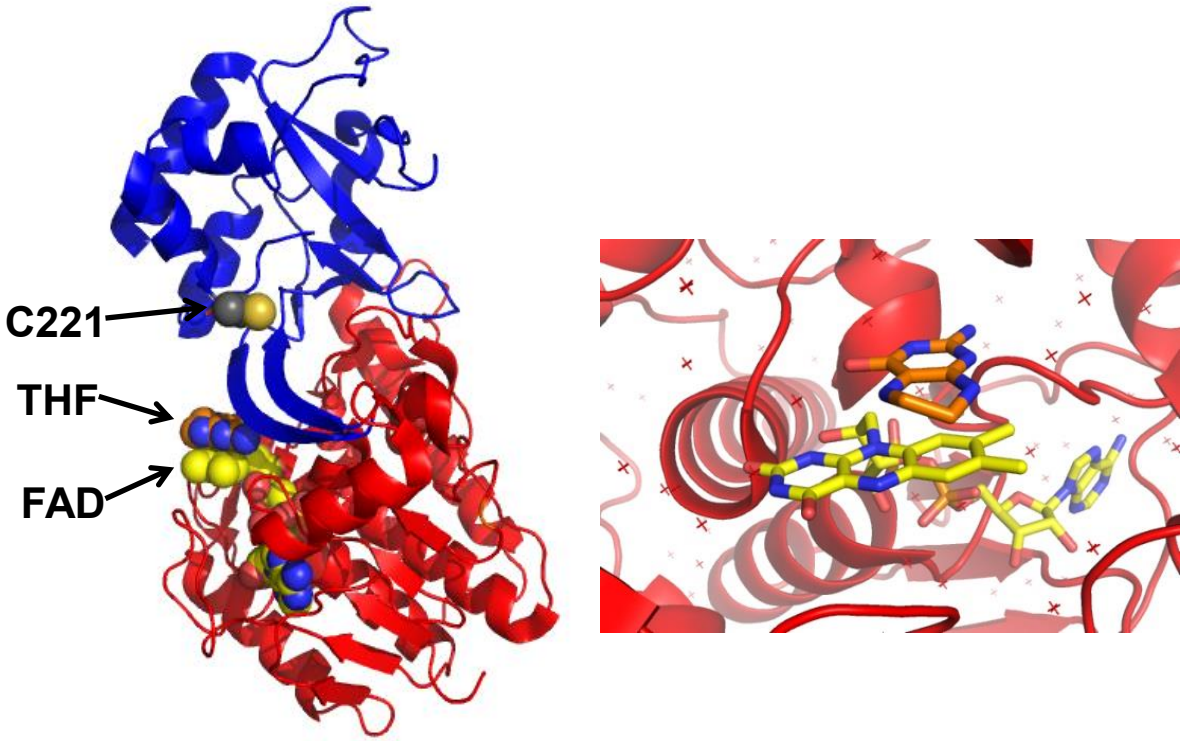

Figure 1 - 23. Structure of $TrmFO_{TT}$ (PDB 3G5R). Left panel, overall structure of $TrmFO_{TT}$; right panel, active site of $TrmFO_{TT}$. The FAD-binding domain is shown in red; the insertion domain is shown in blue; FAD is shown in yellow; THF is shown in orange; C221, which has been proposed to be the nucleophile that initiates catalysis with tRNA, is shown in gray.

Mechanism

Nearly all of the mechanistic work on TrmFO has focused on deciphering the chemical mechanism of the enzyme, and the majority of the biochemical work has been done on the *Bacillus subtilis* enzyme ($TrmFO_{BS}$). Reduced FAD is required for TrmFO to methylate U54 of tRNA. The physiological reductant has not been rigorously verified, but NADPH is at least capable of serving as the reductant.[91] Studies using tRNA containing 5-fluorouracil (5FU tRNA), a mechanism-based inhibitor of $TrmFO_{BS}$, found that C226 forms a covalent adduct with 5FU tRNA, suggesting that C226 is the nucleophile that initiates catalysis by forming a covalent adduct with C6 of the reactive uracil.[93] C226 (C221 in $TrmFO_{TT}$) is ~20 Å away from the isoalloxazine of the FAD, suggesting that large conformational changes must take place during TrmFO catalysis. Alternatively, TrmFO could dimerize when bound to tRNA, placing C226 of one monomer near the flavin of the other monomer. Curiously, recombinant $TrmFO_{BS}$ purifies with an air-stable flavin semiquinone.[94] $TrmFO_{BS}$ containing the air-stable flavin semiquinone was able to methylate ~1 mol equivalent of tRNA in the absence of CH_2THF and reductant, indicating that as-purified $TrmFO_{BS}$ co-purifies with the methylene and reducing equivalents as part of the enzyme. It was later shown that as-purified $TrmFO_{BS}$ contained an adduct between the flavin and the conserved C53, bridged by a methylene.[70] Mutation of C53 to alanine completely abolished activity of $TrmFO_{BS}$ and eliminated the air-stable semiquinone, indicating the importance of this residue in TrmFO activity. Based on the identification of a flavin-methylene-cysteine adduct, Hamdane et. al. proposed a chemical mechanism where the methylene of CH_2THF is first transferred to N5 of reduced flavin (Figure 1 - 24).[70] The thiol of C53

prevents the flavin-methylene intermediate from reacting with water until the tRNA uracil moiety is in the active site (Figure 1 - 24A). Once U_{54} is properly positioned in the active site, C53 can release the flavin-methylene intermediate to allow methylene and hydride transfer from $FADH^-$ to U_{54} to occur (Figure 1 - 24B).

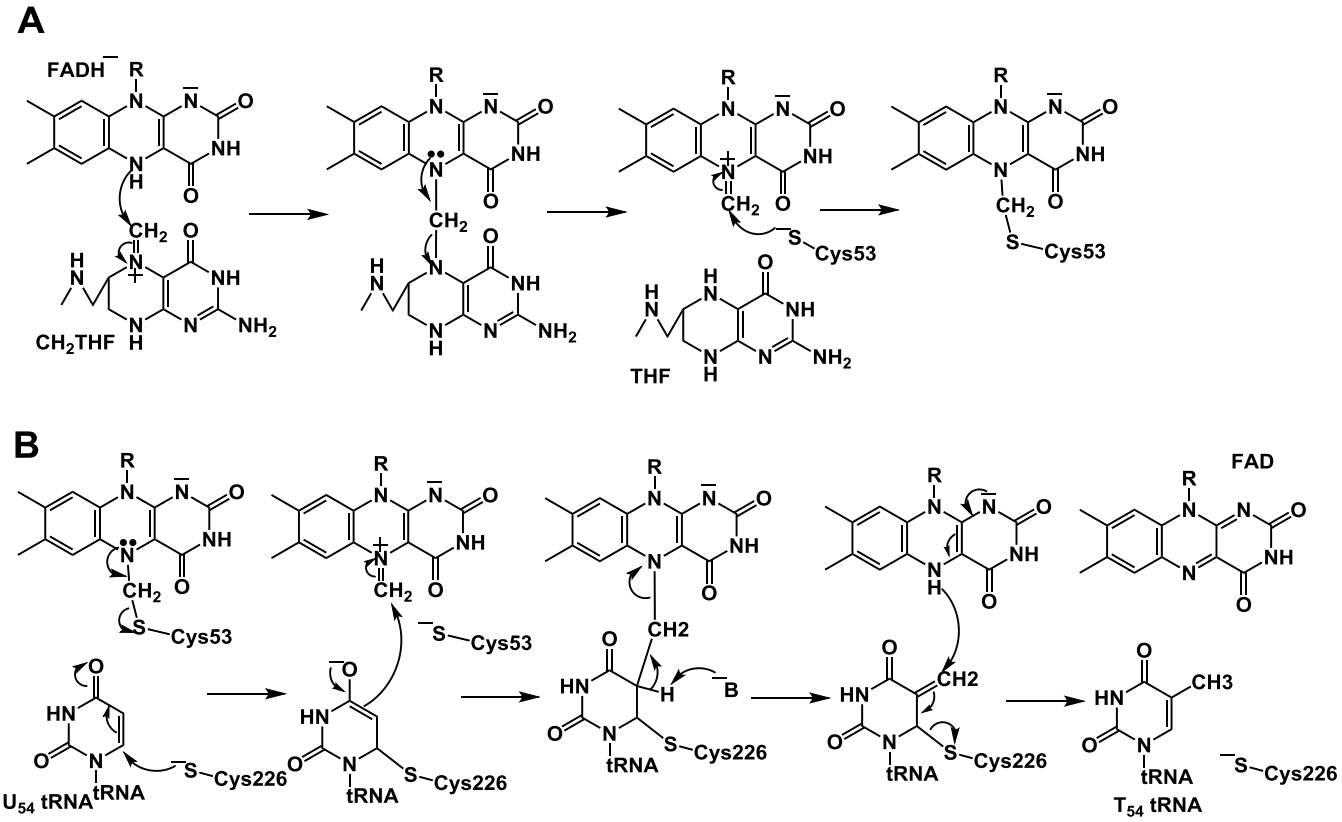

Figure 1 - 24. The chemical mechanism for tRNA methylation by $TrmFO_{BS}$ proposed in ref. 69. (A) The mechanism for the formation of the reduced FAD-methylene-cysteine adduct. (B) The mechanism for methylene and hydride transfer to U_{54} of tRNA.

Thesis Overview

The purpose of this thesis is to examine the mechanisms of substrate recognition and activation for flavin-dependent thymidylate synthase and tRNA-dihydrouridine synthase – two enzymes involving flavin-dependent hydride transfer to pyrimidines. In Chapter 2, I tested a recently proposed mechanism where dUMP is activated in FDTS by an electrostatically polarizing active site using ^{13}C-NMR. I find that FDTS does not merely stabilize a polarized resonance form of dUMP; instead, the enzyme ionizes N3 of dUMP using an active site arginine. A modified mechanism for dUMP activation is proposed based on this finding. In addition, I present evidence using substrate analogs that suggests that the phosphate of dUMP acts as the base that deprotonates C5 of the dUMP-CH_2THF adduct in the reaction catalyzed by FDTS. Chapter 3 looks at the binding of substrate and product nucleotides (dUMP and dTMP) to FDTS through a variety of equilibrium and kinetic methods. I show that FDTS binds nucleotides with ~200-fold weaker affinity when the flavin is reduced relative to when it is oxidized, and that the differences in affinity are largely due to differences in the dissociation rate constant for nucleotide binding. This finding suggests that the exchange between dTMP and dUMP occurs when the flavin of FDTS is reduced. I also find that there is a temperature-dependent effect on the mechanism by which FDTS binds nucleotides – below 45°C the FDTS homotetramer behaves as a dimer-of-dimers with nucleotide binding while at temperatures above 45°C the four subunits of FDTS bind nucleotides identically. Chapter 4 focuses on probing the mode of tRNA recognition by yeast tRNA-dihydrouridine synthase. In contrast with previous work on tRNA^{Leu}-CAA, I find that tRNA^{Asp}, tRNA^{Ala}, and tRNA^{His2} from yeast react quickly with DUS2 in the absence of

other tRNA modifications. Native gel electrophoresis shows that unmodified $tRNA^{Leu}$-CAA oligomerizes upon refolding while the other tRNAs (unmodified $tRNA^{Asp}$, $tRNA^{Ala}$, $tRNA^{His2}$, and modified $tRNA^{Leu}$-CAA) exist as monomers upon refolding, suggesting that $tRNA^{Leu}$-CAA requires other modifications to fold properly to react rapidly with DUS2.

References

(1) Evans, D. R., and Guy, H. I. (2004) Mammalian pyrimidine biosynthesis: fresh insights into an ancient pathway. *J. Biol. Chem. 279*, 33035–38.

(2) Fagan, R. L., and Palfey, B. A. (2010) Flavin-Dependent Enzymes, in *Comprehensive Natural Products Chemistry II, Vol 7: Cofactor Biosynthesis and Enzymology* (Begley, T. P., Ed.), pp 37–113. Elsevier Ltd.

(3) Schnackerz, K. D., Dobritzsch, D., Lindqvist, Y., and Cook, P. F. (2004) Dihydropyrimidine dehydrogenase: a flavoprotein with four iron-sulfur clusters. *Biochim. Biophys. Acta 1701*, 61–74.

(4) Tiedje, K. E., Stevens, K., Barnes, S., and Weaver, D. F. (2010) Beta-alanine as a small molecule neurotransmitter. *Neurochem. Int. 57*, 177–88.

(5) Fiumara, A., van Kuilenburg, Af. B. P., Caruso, U., Nocifora, C., Marzullo, E., Barone, R., Meli, C., and van Gennip, A. H. (2003) Dihydropyrimidine dehydrogenase deficiency and acute neurological presentation. *J. Inherit. Metab. Dis. 26*, 407–9.

(6) Al-Sanna'a, N. A., Van Kuilenburg, A. B. P., Atrak, T. M., Abdul-Jabbar, M. A., and Van Gennip, A. H. (2005) Dihydropyrimidine dehydrogenase deficiency presenting at birth. *J. Inherit. Metab. Dis. 28*, 793–6.

(7) Milano, G., and Etienne, M. C. (1994) Dihydropyrimidine dehydrogenase (DPD) and clinical pharmacology of 5-fluorouracil. *Anticancer Res. 14*, 2295–7.

(8) Hull, W. E., Port, R. E., Herrmann, R., Britsch, B., and Kunz, W. (1988) Metabolites of 5-Fluorouracil in Plasma and Urine , as Monitored by 19F Nuclear Magnetic Resonance Spectroscopy , for Patients Receiving Chemotherapy with or without Methotrexate Pretreatment. *Cancer Res. 48*, 1680–8.

(9) Dobritzsch, D., Schneider, G., Schnackerz, K. D., and Lindqvist, Y. (2001) Crystal structure of dihydropyrimidine dehydrogenase, a major determinant of the pharmacokinetics of the anti-cancer drug 5-fluorouracil. *EMBO J. 20*, 650–60.

(10) Dobritzsch, D., Ricagno, S., Schneider, G., Schnackerz, K. D., and Lindqvist, Y. (2002) Crystal structure of the productive ternary complex of dihydropyrimidine dehydrogenase with NADPH and 5-iodouracil: Implications for mechanism of inhibition and electron transfer. *J. Biol. Chem. 277*, 13155–66.

(11) Podschun, B. (1992) Stereochemistry of NADPH oxidation by dihydropyrimidine dehyrogenase from pig liver. *Biochem. Biophys. Res. Commun. 182*, 609–16.

(12) Rosenbaum, K., Jahnke, K., Curti, B., Hagen, W. R., Schnackerz, K. D., and Vanoni, M. a. (1998) Porcine recombinant dihydropyrimidine dehydrogenase: comparison of the spectroscopic and catalytic properties of the wild-type and C671A mutant enzymes. *Biochemistry 37*, 17598–609.

(13) Hagen, W. R., Vanoni, M. A., Rosenbaum, K., and Schnackerz, K. D. (2000) On the iron-sulfur clusters in the complex redox enzyme dihydropyrimidine dehydrogenase. *Eur. J. Biochem. 267*, 3640–6.

(14) Porter, D. J., Chestnut, W. G., Taylor, L. C., Merrill, B. M., and Spector, T. (1991) Inactivation of dihydropyrimidine dehydrogenase by 5-iodouracil. *J. Biol. Chem. 266*, 19988–94.

(15) Rosenbaum, K., Jahnke, K., Schnackerz, K. D., and Cook, P. F. (1998) Secondary tritium and solvent deuterium isotope effects as a probe of the reaction catalyzed by porcine recombinant dihydropyrimidine dehydrogenase. *Biochemistry 37*, 9156–9.

(16) Czerwoniec, A., Dunin-Horkawicz, S., Purta, E., Kaminska, K. H., Kasprzak, J. M., Bujnicki, J. M., Grosjean, H., and Rother, K. (2009) MODOMICS: a database of RNA modification pathways. 2008 update. *Nucleic Acids Res. 37*, D118–21.

(17) Jühling, F., Mörl, M., Hartmann, R. K., Sprinzl, M., Stadler, P. F., and Pütz, J. (2009) tRNAdb 2009: compilation of tRNA sequences and tRNA genes. *Nucleic Acids Res. 37*, D159–62.

(18) Xing, F., Martzen, M. R., and Phizicky, E. M. (2002) A conserved family of Saccharomyces cerevisiae synthases effects dihydrouridine modification of tRNA . A conserved family of Saccharomyces cerevisiae synthases effects dihydrouridine modification of tRNA. *RNA* 370–81.

(19) Dalluge, J. J., Hashizume, T., Sopchik, A. E., Mccloskey, J. A., and Davis, D. R. (1996) Conformational flexibility in RNA : the role of dihydrouridine. *Nucleic Acids Res. 24*, 1073–9.

(20) Noon, K. R., Guymon, R., Crain, P. F., Mccloskey, J. A., Thomm, M., Lim, J., and Cavicchioli, R. (2003) Influence of Temperature on tRNA Modification in Archaea : Methanococcoides burtonii (Optimum Growth Temperature [T opt], 23°C) and Stetteria hydrogenophila (T opt , 95°C). *J. Bacteriol. 185*, 5483–90.

(21) Alexandrov, A., Chernyakov, I., Gu, W., Hiley, S. L., Hughes, T. R., Grayhack, E. J., and Phizicky, E. M. (2006) Rapid tRNA decay can result from lack of nonessential modifications. *Mol. Cell 21*, 87–96.

(22) Kuchino, Y., and Borek, E. (1978) Tumour-specific phenylalanine tRNA contains two supernumerary methylated bases. *Nature 271*, 126–9.

(23) Kato, T., Daigo, Y., Hayama, S., Ishikawa, N., Yamabuki, T., Ito, T., Miyamoto, M., Kondo, S., and Nakamura, Y. (2005) A Novel Human tRNA-Dihydrouridine Synthase Involved in Pulmonary Carcinogenesis. *Cancer Res.* 4–6.

(24) Xing, F., Hiley, S. L., Hughes, T. R., and Phizicky, E. M. (2004) The Specificities of Four Yeast Dihydrouridine Synthases for Cytoplasmic tRNAs. *Biochemistry 279*, 17850 –60.

(25) Park, F., Gajiwala, K., Noland, B., Wu, L., He, D., Molinari, J., Loomis, K., Pagarigan, B., Kearins, P., Christopher, J., Peat, T., Badger, J., Hendle, J., Lin, J., and Buchanan, S. (2004) The 1.59 Å Resolution Crystal Structure of TM0096, a Flavin Mononucleotide Binding Protein From Thermotoga maritima. *Proteins 774*, 772–4.

(26) Yu, F., Tanaka, Y., Yamashita, K., Suzuki, T., Nakamura, A., Hirano, N., Suzuki, T., Yao, M., and Tanaka, I. (2011) Molecular basis of dihydrouridine formation on tRNA. *Proc. Natl. Acad. Sci. U. S. A. 108*, 19593–8.

(27) Rider, L. W., Ottosen, M. B., Gattis, S. G., and Palfey, B. A. (2009) Mechanism of Dihydrouridine Synthase 2 from Yeast and the Importance of Modifications for Efficient tRNA Reduction. *J. Biol. Chem. 284*, 10324 –33.

(28) Nagy, M., Lacroute, F., and Thomas, D. (1992) Divergent evolution of pyrimidine biosynthesis between anaerobic and aerobic yeasts. *Proc. Natl. Acad. Sci. U. S. A. 89*, 8966–70.

(29) Nielsen, F. S., Andersen, P. S., and Jensen, K. F. (1996) The B Form of Dihydroorotate Dehydrogenase from Lactococcus lactis Consists of Two Different Subunits, Encoded by the pyrDb and pyrK Genes, and Contains FMN, FAD, and [FeS] Redox Centers. *J. Biol. Chem. 271*, 29359–65.

(30) Jones, M. E. (1980) Pyrimidine nucleotide biosynthesis in animals: genes, enzymes, and regulation of UMP biosynthesis. *Annu. Rev. Biochem. 49*, 253–79.

(31) Rowland, P., Nielsen, F. S., Jensen, K. F., and Larsen, S. (1997) The crystal structure of the flavin containing enzyme dihydroorotate dehydrogenase A from Lactococcus lactis. *Structure 5*, 239–52.

(32) Rowland, P., Bjornberg, O., Nielsen, F. S., Jensen, K. F., and Larsen, S. (1998) The crystal structure of Lactococcus lactis dihydroorotate dehdrogenase A complexed

with the enzyme reaction product throws light on its enzymatic function. *Protein Sci. 7*, 1269–79.

(33) Nørager, S., Arent, S., Björnberg, O., Ottosen, M., Lo Leggio, L., Jensen, K. F., and Larsen, S. (2003) Lactococcus lactis dihydroorotate dehydrogenase A mutants reveal important facets of the enzymatic function. *J. Biol. Chem. 278*, 28812–22.

(34) Wolfe, A. E., Thymark, M., Gattis, S. G., Fagan, R. L., Hu, Y., Johansson, E., Arent, S., Larsen, S., and Palfey, B. a. (2007) Interaction of benzoate pyrimidine analogues with class 1A dihydroorotate dehydrogenase from Lactococcus lactis. *Biochemistry 46*, 5741–53.

(35) Inaoka, D. K., Sakamoto, K., Shimizu, H., Shiba, T., Kurisu, G., Nara, T., Aoki, T., Kita, K., and Harada, S. (2008) Structures of Trypanosoma cruzi dihydroorotate dehydrogenase complexed with substrates and products: atomic resolution insights into mechanisms of dihydroorotate oxidation and fumarate reduction. *Biochemistry 47*, 10881–91.

(36) Pinheiro, M. P., Iulek, J., and Cristina Nonato, M. (2008) Crystal structure of Trypanosoma cruzi dihydroorotate dehydrogenase from Y strain. *Biochem. Biophys. Res. Commun. 369*, 812–7.

(37) Rowland, P., Nørager, S., Jensen, K. F., and Larsen, S. (2000) Structure of dihydroorotate dehydrogenase B: electron transfer between two flavin groups bridged by an iron-sulphur cluster. *Structure 8*, 1227–38.

(38) Liu, S., Neidhardt, E. A., Grossman, T. H., Ocain, T., and Clardy, J. (2000) Structures of human dihydroorotate dehydrogenase in complex with antiproliferative agents. *Structure 8*, 25–33.

(39) Nørager, S., Jensen, K. F., Björnberg, O., and Larsen, S. (2002) E. coli dihydroorotate dehydrogenase reveals structural and functional distinctions between different classes of dihydroorotate dehydrogenases. *Structure 10*, 1211–23.

(40) Hansen, M., Nours, J. É. L. E., Johansson, E. V. A., Antal, T., Ullrich, A., and Löffler, M. (2004) Inhibitor binding in a class 2 dihydroorotate dehydrogenase causes variations in the membrane-associated N-terminal domain. *Protein Sci. 13*, 1031–42.

(41) Hurt, D. E., Widom, J., and Clardy, J. (2006) Structure of Plasmodium falciparum dihydroorotate dehydrogenase with a bound inhibitor. *Acta Crystallogr. D. Biol. Crystallogr. 62*, 312–23.

(42) Baumgartner, R., Walloschek, M., Kralik, M., Gotschlich, A., Tasler, S., Mies, J., and Leban, J. (2006) Dual binding mode of a novel series of DHODH inhibitors. *J. Med. Chem. 49*, 1239–47.

(43) Walse, B., Dufe, V. T., Svensson, B., Fritzson, I., Dahlberg, L., Khairoullina, A., Wellmar, U., and Al-Karadaghi, S. (2008) The structures of human dihydroorotate dehydrogenase with and without inhibitor reveal conformational flexibility in the inhibitor and substrate binding sites. *Biochemistry 47*, 8929–36.

(44) Kow, R. L., Whicher, J. R., McDonald, C. a, Palfey, B. a, and Fagan, R. L. (2009) Disruption of the proton relay network in the class 2 dihydroorotate dehydrogenase from Escherichia coli. *Biochemistry 48*, 9801–9.

(45) Hines, V., and Johnston, M. (1989) Mechanistic studies on the bovine liver mitochondrial dihydroorotate dehydrogenase using kinetic deuterium isotope effects. *Biochemistry 28*, 1227–34.

(46) Argyrou, A., Washabaugh, M. W., and Pickart, C. M. (2000) Dihydroorotate dehydrogenase from Clostridium oroticum is a class 1B enzyme and utilizes a concerted mechanism of catalysis. *Biochemistry 39*, 10373–84.

(47) Pascal, R. A., and Walsh, C. T. (1984) Mechanistic studies with deuterated dihydroorotates on the dihydroorotate oxidase from Crithidia fasciculata. *Biochemistry 23*, 2745–52.

(48) Fagan, R. L., Jensen, K. F., Björnberg, O., and Palfey, B. A. (2007) Mechanism of flavin reduction in the class 1A dihydroorotate dehydrogenase from Lactococcus lactis. *Biochemistry 46*, 4028–36.

(49) Fagan, R. L., Nelson, M. N., Pagano, P. M., and Palfey, B. A. (2006) Mechanism of flavin reduction in class 2 dihydroorotate dehydrogenases. *Biochemistry 45*, 14926–32.

(50) Rider, L. (2009) Flavoenzymes Involved in Pyrimidine Oxidation and Reduction. University of Michigan.

(51) Malmquist, N. A., Gujjar, R., Rathod, P. K., and Phillips, M. A. (2008) Analysis of Flavin Oxidation and Electron-Transfer Inhibition in Plasmodium Dihydroorotate Dehydrogenase. *Biochemistry 47*, 2466–75.

(52) Palfey, B. a, Björnberg, O., and Jensen, K. F. (2001) Insight into the chemistry of flavin reduction and oxidation in Escherichia coli dihydroorotate dehydrogenase obtained by rapid reaction studies. *Biochemistry 40*, 4381–90.

(53) Carreras, C. W., and Santi, D. V. (1995) The catalytic mechanism and structure of thymidylate synthase. *Annu. Rev. Biochem. 64*, 721–62.

(54) Myllykallio, H., Lipowski, G., Leduc, D., Filee, J., Forterre, P., and Liebl, U. (2002) An alternative flavin-dependent mechanism for thymidylate synthesis. *Science (80-.). 297*, 105–7.

(55) Giladi, M., Bitan-Banin, G., Mevarech, M., and Ortenberg, R. (2002) Genetic evidence for a novel thymidylate synthase in the halophilic archaeon Halobacterium salinarum and in Campylobacter jejuni. *FEMS Microbiol. Lett. 216*, 105–9.

(56) Lesley, S. a, Kuhn, P., Godzik, A., Deacon, A. M., Mathews, I., Kreusch, A., Spraggon, G., Klock, H. E., McMullan, D., Shin, T., Vincent, J., Robb, A., Brinen, L. S., Miller, M. D., McPhillips, T. M., Miller, M. a, Scheibe, D., Canaves, J. M., Guda, C., Jaroszewski, L., Selby, T. L., Elsliger, M.-A., Wooley, J., Taylor, S. S., Hodgson, K. O., Wilson, I. a, Schultz, P. G., and Stevens, R. C. (2002) Structural genomics of the Thermotoga maritima proteome implemented in a high-throughput structure determination pipeline. *Proc. Natl. Acad. Sci. U. S. A. 99*, 11664–9.

(57) Koehn, E. M., and Kohen, A. (2010) Flavin-dependent thymidylate synthase: a novel pathway towards thymine. *Arch. Biochem. Biophys. 493*, 96–102.

(58) Agrawal, N., Lesley, S. A., Kuhn, P., and Kohen, A. (2004) Mechanistic Studies of a Flavin-Dependent Thymidylate Synthase. *Biochemistry 43*, 10295–301.

(59) Myllykallio, H., Leduc, D., Filee, J., and Liebl, U. (2003) Life without dihydrofolate reductase FolA. *Trends Microbiol. 11*, 220–3.

(60) Leduc, D., Graziani, S., Meslet-Cladiere, L., Sodolescu, a, Liebl, U., and Myllykallio, H. (2004) Two distinct pathways for thymidylate (dTMP) synthesis in (hyper)thermophilic Bacteria and Archaea. *Biochem. Soc. Trans. 32*, 231–5.

(61) Wang, Z., Chernyshev, A., Koehn, E. M., Manuel, T. D., Lesley, S. A., and Kohen, A. (2009) Oxidase activity of a flavin-dependent thymidylate synthase. *FEBS J. 276*, 2801–10.

(62) Palfey, B. A., Ortiz-Maldonado, M., and Conrad, J. A. (2008) The Chemistry of Flavin-Dependent Thymidylate Synthesis. *Flavins Flavoproteins (Frago, S., Gomez-Moreno, C., Medina, M., Ed.) Prensas Univ. Zaragoza, Zaragoza, Spain*.

(63) Escartin, F., Skouloubris, S., Liebl, U., and Myllykallio, H. (2008) Flavin-dependent thymidylate synthase X limits chromosomal DNA replication. *Proc. Natl. Acad. Sci. U. S. A. 105*, 9948–52.

(64) Mathews, I., Deacon, A., Canaves, J., Mcmullan, D., Lesley, S., Agarwalla, S., and Kuhn, P. (2003) Functional Analysis of Substrate and Cofactor Complex Structures of a Thymidylate Synthase-Complementing Protein. *Structure 11*, 677–90.

(65) Kuhn, P., Lesley, S. A., Mathews, I. I., Canaves, J. M., Brinen, L. S., Dai, X., Deacon, A. M., Elsliger, M. A., Eshaghi, S., Floyd, R., Godzik, A., Grittini, C., Grzechnik, S. K., Guda, C., Hodgson, K. O., Jaroszewski, L., Karlak, C., Klock, H. E., Koesema, E., Kovarik, J. M., Kreusch, A. T., McMullan, D., McPhillips, T. M., Miller, M. A., Miller, M., Morse, A., Moy, K., Ouyang, J., Robb, A., Rodrigues, K., Selby, T. L., Spraggon, G.,

Stevens, R. C., Taylor, S. S., van den Bedem, H., Velasquez, J., Vincent, J., Wang, X., West, B., Wolf, G., Wooley, J., and Wilson, I. A. (2002) Crystal structure of thy1, a thymidylate synthase complementing protein from Thermotoga maritima at 2.25 Å resolution. *Proteins 49*, 142–5.

(66) Laptenok, S. P., Bouzhir-Sima, L., Lambry, J.-C., Myllykallio, H., Liebl, U., and Vos, M. H. (2013) Ultrafast real-time visualization of active site flexibility of flavoenzyme thymidylate synthase ThyX. *Proc. Natl. Acad. Sci. U. S. A. 110*, 8924–9.

(67) Koehn, E. M., Perissinotti, L. L., Moghram, S., Prabhakar, A., Lesley, S. A., and Mathews, I. I. (2012) Folate binding site of flavin-dependent thymidylate synthase. *Proc. Natl. Acad. Sci. U. S. A. 109*, 15722–7.

(68) Leduc, D., Graziani, S., Lipowski, G., Marchand, C., Le Maréchal, P., Liebl, U., and Myllykallio, H. (2004) Functional evidence for active site location of tetrameric thymidylate synthase X at the interphase of three monomers. *Proc. Natl. Acad. Sci. U. S. A. 101*, 7252–7.

(69) Ulmer, J. E., Boum, Y., Thouvenel, C. D., Myllykallio, H., and Sibley, C. H. (2008) Functional analysis of the Mycobacterium tuberculosis FAD-dependent thymidylate synthase, ThyX, reveals new amino acid residues contributing to an extended ThyX motif. *J. Bacteriol. 190*, 2056–64.

(70) Hamdane, D., Argentini, M., Cornu, D., Golinelli-Pimpaneau, B., and Fontecave, M. (2012) FAD/folate-dependent tRNA methyltransferase: flavin as a new methyl-transfer agent. *J. Am. Chem. Soc. 134*, 19739–45.

(71) Koehn, E. M., Fleischmann, T., Conrad, J. A., Palfey, B. A., Lesley, S. A., Mathews, I. I., and Kohen, A. (2009) An unusual mechanism of thymidylate biosynthesis in organisms containing the thyX gene. *Nature 458*, 919–23.

(72) Graziani, S., Bernauer, J., Skouloubris, S., Graille, M., Zhou, C.-Z., Marchand, C., Decottignies, P., van Tilbeurgh, H., Myllykallio, H., and Liebl, U. (2006) Catalytic mechanism and structure of viral flavin-dependent thymidylate synthase ThyX. *J. Biol. Chem. 281*, 24048–57.

(73) Basta, T., Boum, Y., Briffotaux, J., Becker, H. F., Lamarre-Jouenne, I., Lambry, J.-C., Skouloubris, S., Liebl, U., Graille, M., van Tilbeurgh, H., and Myllykallio, H. (2012) Mechanistic and structural basis for inhibition of thymidylate synthase ThyX. *Open Biol. 2*, 1–10.

(74) Sampathkumar, P., Turley, S., Sibley, C. H., and Hol, W. G. J. (2006) NADP+ expels both the co-factor and a substrate analog from the Mycobacterium tuberculosis ThyX active site: opportunities for anti-bacterial drug design. *J. Mol. Biol. 360*, 1–6.

(75) Gattis, S. G., and Palfey, B. A. (2005) Direct observation of the participation of flavin in product formation by thyX-encoded thymidylate synthase. *J. Am. Chem. Soc. 127*, 832–3.

(76) Matthews, D. A., Villafranca, J. E., Janson, C. A., Smith, W. W., Welsh, K., and Freer, S. (1990) Stereochemical Mechanism of Action for Thymidylate Synthase Based on the X-ray Structure of the Covalent Inhibitory Ternary Complex with. *J. Mol. Biol. 214*, 937–48.

(77) Soltero-Higgin, M., Carlson, E. E., Gruber, T. D., and Kiessling, L. L. (2004) A unique catalytic mechanism for UDP-galactopyranose mutase. *Nat. Struct. Mol. Biol. 11*, 539–43.

(78) Conrad, J. A., Ortiz-Maldonado, M., Hoppe, S. W., and Palfey, B. A. (2014) Detection of Intermediates in the Oxidative Half-Reaction of the FAD-Dependent Thymidylate Synthase from Thermotoga maritima: Carbon Transfer without Covalent Pyrimidine Activation. *Biochemistry 53*, 5199–207.

(79) D'Ordine, R. L., Pawlak, J., Bahnson, B. J., and Anderson, V. E. (2002) Polarization of cinnamoyl-CoA substrates bound to enoyl-CoA hydratase: correlation of (13)C NMR with quantum mechanical calculations and calculation of electronic strain energy. *Biochemistry 41*, 2630–40.

(80) Mishanina, T. V, Koehn, E. M., Conrad, J. A., Palfey, B. A., Lesley, S. A., and Kohen, A. (2012) Trapping of an intermediate in the reaction catalyzed by flavin-dependent thymidylate synthase. *J. Am. Chem. Soc. 134*, 4442–8.

(81) Griffin, J., Roshick, C., Iliffe-Lee, E., and McClarty, G. (2005) Catalytic mechanism of Chlamydia trachomatis flavin-dependent thymidylate synthase. *J. Biol. Chem. 280*, 5456–67.

(82) Graziani, S., Xia, Y., Gurnon, J. R., Van Etten, J. L., Leduc, D., Skouloubris, S., Myllykallio, H., and Liebl, U. (2004) Functional Analysis of FAD-dependent Thymidylate Synthase ThyX from Paramecium bursaria Chlorella Virus-1. *J. Biol. Chem. 279*, 54340–7.

(83) Chernyshev, A., Fleischmann, T., Koehn, E. M., Lesley, S. A., and Kohen, A. (2007) The relationships between oxidase and synthase activities of flavin dependent thymidylate synthase (FDTS). *Chem. Commun. (Camb).* 2861–3.

(84) Hunter, J. H., Gujjar, R., Pang, C. K. T., and Rathod, P. K. (2008) Kinetics and ligand-binding preferences of Mycobacterium tuberculosis thymidylate synthases, ThyA and ThyX. *PLoS One 3*, e2237.

(85) Mason, A., Agrawal, N., Washington, M. T., Lesley, S. a, and Kohen, A. (2006) A lag-phase in the reduction of flavin dependent thymidylate synthase (FDTS) revealed a mechanistic missing link. *Chem. Commun. (Camb).* 1781–3.

(86) Becker, H. F., Djaout, K., Lamarre, I., Ulmer, J. E., Schaming, D., Balland, V., Liebl, U., Myllykallio, H., and Vos, M. H. (2014) Substrate interaction dynamics and oxygen control in the active site of thymidylate synthase ThyX. *Biochem. J. 459*, 37–45.

(87) Bhattacharya, B., Giri, N., Mitra, M., and Gupta, S. K. Das. (2008) Cloning, characterization and expression analysis of nucleotide metabolism-related genes of mycobacteriophage L5. *FEMS Microbiol. Lett. 280*, 64–72.

(88) Massey, V., and Veeger, C. (1961) Studies on the reaction mechanism of lipoyl dehydrogenase. *Biochim. Biophys. Acta 48*, 33–47.

(89) Roitel, O., Scrutton, N. S., and Munro, A. W. (2003) Electron transfer in flavocytochrome P450 BM3: kinetics of flavin reduction and oxidation, the role of cysteine 999, and relationships with mammalian cytochrome P450 reductase. *Biochemistry 42*, 10809–21.

(90) Conrad, J. A. (2011) The Reactions of Flavin-Dependent Thymidylate Synthase from Thermotoga Maritima. University of Michigan.

(91) Urbonavicius, J., Skouloubris, S., Myllykallio, H., and Grosjean, H. (2005) Identification of a novel gene encoding a flavin-dependent tRNA:m5U methyltransferase in bacteria--evolutionary implications. *Nucleic Acids Res. 33*, 3955–64.

(92) Nishimasu, H., Ishitani, R., Yamashita, K., Iwashita, C., Hirata, A., Hori, H., and Nureki, O. (2009) Atomic structure of a folate/FAD-dependent tRNA T54 methyltransferase. *Proc. Natl. Acad. Sci. U. S. A. 106*, 8180–5.

(93) Hamdane, D., Argentini, M., Cornu, D., Myllykallio, H., Skouloubris, S., Hui-Bon-Hoa, G., and Golinelli-Pimpaneau, B. (2011) Insights into folate/FAD-dependent tRNA methyltransferase mechanism: role of two highly conserved cysteines in catalysis. *J. Biol. Chem. 286*, 36268–80.

(94) Hamdane, D., Guerineau, V., Un, S., and Golinelli-Pimpaneau, B. (2011) A catalytic intermediate and several flavin redox states stabilized by folate-dependent tRNA methyltransferase from Bacillus subtilis. *Biochemistry 50*, 5208–19.

Chapter 2

Deprotonations in the Reaction of Flavin-Dependent Thymidylate Synthase‡

‡The NMR spectra presented in this chapter were collected in collaboration with Erik Zuiderweg and the x-ray data collection and structure determination of the active site variants were performed by Steffen Bernard in the lab of Janet Smith.

2'-Deoxythymidine-5'-monophosphate (dTMP) − an essential precursor for the biosynthesis of DNA − is formed by the reductive methylation of 2'-deoxyuridine-5'-monophosphate (dUMP) to form dTMP by thymidylate synthases (TSs). There are currently two known classes of TSs. Classic TSs are homodimeric enzymes that use 5,10-methylenetetrahydrofolate (CH_2THF) as both the carbon-donor and reductant to form dTMP from dUMP without the use of a prosthetic group.[1] Flavin-dependent thymidylate synthases (FDTSs), on the other hand, are tetrameric enzymes that use a flavin adenine dinucleotide (FAD) prosthetic group to synthesize dTMP from dUMP, CH_2THF and NADPH.[2] Whereas the folate becomes dihydrofolate (DHF) in the classic TS reaction, the folate remains in the fully-reduced tetrahydrofolate (THF) state in the reaction catalyzed by FDTSs. The electrons required to form dTMP come from NADPH by way of the FAD prosthetic group in FDTSs instead of coming from the folate as in classic TSs.

Classic TS has been studied for decades and its chemical mechanism is well-understood (Figure 2 - 1A).[1] Classic TS first activates dUMP through a Michael-like

addition of an active-site cysteine to C6 of dUMP (step 1). The resulting enolate then attacks the iminium form of CH_2THF, forming a bridged intermediate between the cysteine, dUMP, and CH_2THF (step 2). Upon deprotonation at C5 of the pyrimidine, the adduct breaks down into THF and an exocyclic methylene intermediate still covalently attached to the active-site cysteine (step 3). Finally, a hydride is transferred from THF to the methylene of the intermediate to eliminate the cysteine, forming dTMP (step 4).

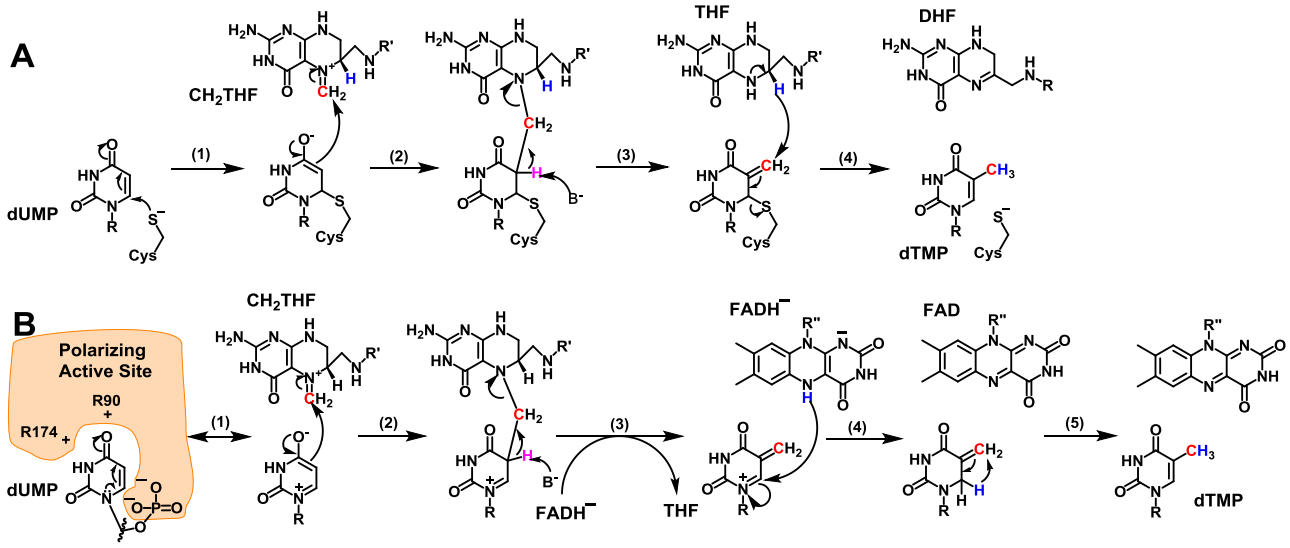

Figure 2 - 1. Thymidylate synthase chemical mechanisms. (A) the mechanism for classic TS using an enzymatic cysteine nucleophile.[1] (B) a proposed mechanism for FDTS using an electrostatically polarizing active site to activate dUMP.[5]

In contrast, the chemical mechanism of FDTS has not been fully determined. A major question is the mechanism of dUMP activation. Unlike classic TS, FDTS does not contain an active-site cysteine to activate dUMP through a Michael-like addition, and mutagenesis has ruled out all other potential enzymatic nucleophiles.[3] Hydride transfer from reduced FAD has been proposed to activate dUMP;[3] however, this is unlikely since 5-fluoro-2'-deoxyuridine-5'-monophosphate (5F-dUMP) cannot oxidize reduced FDTS in the presence of CH_2THF,[4] and stopped-flow experiments on the oxidative half-reaction

indicate multiple intermediates prior to flavin oxidation.[5] The electrostatically polarizing active site was recently proposed to activate dUMP.[5,6] In this mechanism, the arrangement of two arginines (R90 and R174 in *Thermotoga maritima* FDTS) near O4 of dUMP and the phosphate of dUMP near N1 stabilizes the resonance form of dUMP shown in Figure 2 - 1B (step 1). This resonance form contains an enolate with nucleophilicity at C5, which attacks CH_2THF, forming a bridged intermediate between dUMP and CH_2THF (step 2). Upon deprotonation at C5 by an unidentified base, the bridged intermediate breaks down into THF and an exocyclic methylene intermediate (step 3). A hydride is then transferred from reduced FAD to C6 of the intermediate (step 4).[3] The exocyclic methylene tautomer of dTMP then undergoes a 1, 3-hydride shift to form dTMP (step 5).

While the mechanism for dUMP activation presented in Figure 2 - 1B is consistent with most published data, it has not been completely verified. Here we used ^{13}C-NMR to test the hypothesis that dUMP is activated by an electrostatically polarizing active site. We show that polarization is more extreme than previously proposed (Figure 1B); the enzyme actually ionizes N3 of dUMP using an active site arginine. In addition, we present evidence suggesting that the phosphate of dUMP acts as the general base that deprotonates C5 of the dUMP-CH_2THF adduct in the reaction catalyzed by FDTS.

Experimental Procedures

Protein Preparations

Recombinant WT and mutant FDTSs from *T. maritima* were purified as previously reported,[5] followed by formation of apo-protein by treatment with concentrated sodium chloride[7] and reincorporation of exogenous FAD.

Synthesis of $^{13}C/^{15}N$-labeled dUMP and dU

5 mg commercially obtained $^{13}C/^{15}N$-labeled dCMP was deaminated by incubation with 1 M sodium nitrite in 1 mL aqueous 3 M ammonium acetate, pH 4 for 24 hours at 37 °C. Conversion of dCMP to dUMP was confirmed by a shift in the UV/Vis λ_{max} from 271 nm to 261 nm. The $^{13}C/^{15}N$-labeled dUMP was purified on a Shimadzu HPLC with a UV/Vis diode array detector at room temperature on a 5 µm, 25 cm x 4.6 mm Supelcosil LC-18-DB column using isocratic aqueous 10 mM ammonium acetate, pH 5 at 1 mL/min. The purified $^{13}C/^{15}N$-labeled dUMP was then lyophilized three times to remove the ammonium acetate. When needed, $^{13}C/^{15}N$-labeled dUMP was converted to dU using alkaline phosphatase and $^{13}C/^{15}N$-labeled dU was purified using the same HPLC method used for dUMP.

Synthesis of dUMS

The protocol for dUMS synthesis was adapted from a procedure for making sulfated guanosine.[8] 134 mg sulfur trioxide-dimethylformamide complex (0.88 mmol) was added to a solution of 200 mg deoxyuridine (0.88 mmol) in 10 mL dry dimethylformamide under argon at -10 °C with stirring. After two minutes, the reaction

was allowed to warm to room temperature where it remained for two hours with stirring under argon. The reaction was then placed on ice and 1 mL saturated aqueous potassium bicarbonate was added with stirring. After removing the solvent by lyophilization, the powder was dissolved in 1 mL water and dUMS was purified from dU-disulfate, dU-3'-monosulfate, and unreacted dU on a preparative 5 µm 250 mm x 21 mm NUCLEODUR®C18 Gravity HPLC column using isocratic 0.2 M ammonium acetate, pH 5 at 5 mL/min. The ammonium acetate was then removed from purified dUMS by five rounds of lyophilization. ^{1}H-NMR (400 MHz, D_2O, 298 K): δ 7.67 (d, 1H), 6.12 (t, 1H), 5.71 (d, 1H), 4.37 (m, 1H), 4.06 (m, 3H), 2,19 (m, 2H) ppm. ^{13}C-NMR (101 MHz, D_2O, 298 K): δ 166.1, 151.4, 141.5, 102.1, 85.5, 84.4, 70.7, 67.5, 38.8 ppm. MS (ESI, neg. mode): $[M-H]^-$ 307. Product ion scan fragments of 307[1^-]: 195, 111, 97. dUMS was also observed in the crystal structure of the FDTS-dUMS complex.

Spectrophotometric Titrations

Spectrophotometric titrations were performed on a Shimadzu UV-2501PC scanning spectrophotometer at 25 °C. ~16 µM enzyme in 0.1 M Tris-HCl pH 8 was titrated with ligand in the same buffer. Absorbance spectra were recorded after each addition. The change in flavin absorbance due to ligand binding was plotted against ligand concentration. For weak or moderate binding the data were fit to a square hyperbola in KaleidaGraph to determine the K_d. When binding was tight, data were fit to Eq. 1, where $\Delta\varepsilon_{max}$ is the maximum change in extinction coefficient, E_0 is the initial enzyme concentration, and L_0 is the ligand concentration.

$$\Delta A = \Delta\varepsilon_{max}\left[\frac{E_0 + L_0 + K_d - \sqrt{(E_0 + L_0 + K_d)^2 - 4E_0L_0}}{2}\right] \text{Eq. 1}$$

Reactions of dU and dUMS with FDTS

Experiments testing the reactivity of dU and dUMS with FDTS were performed in anaerobic cuvettes[9] and monitored in a scanning spectrophotometer. Cuvettes were made anaerobic by repeated cycles of vacuum and equilibration with anaerobic argon. ~80 µM FDTS in 0.1 M Tris-HCl pH 8 at 25 °C was anaerobically titrated with ~30 mM dithionite in the same buffer until the flavin was completely reduced. 200 µM CH_2THF (after mixing) was added, followed by addition of either 10 mM dU or 200 µM dUMS (after mixing). No oxidation of the flavin occurred over four hours with either dU or dUMS. The flavin could then be reoxidized by exposure to air.

After air exposure, the reduced FDTS-dUMS-CH_2THF sample was treated with 1 M HCl to denature the protein. The precipitated protein was removed by centrifugation and the pH of the supernatant was raised to ~5 by adding 10 mM ammonium acetate and titrating with 10 M NaOH. The supernatant was then analyzed by HPLC using a 5 µM, 25 cm x 4.6 mm Supelcosil LC-18-DB column with 1 mL/min flow rate. A 0 to 10 minute, 0 to 50% methanol gradient was used in 10 mM ammonium acetate, pH 5, followed by 15 minutes of isocratic 50% methanol in the same buffer. No new compounds were detected in the sample (i.e., only reactant or flavin-derived peaks were detected).

^{13}C-NMR Spectroscopy

All ^{13}C-NMR spectra of enzyme complexes were acquired on a Varian/Agilent 600 MHz NMR spectrometer equipped with a ^{1}H-^{15}N-^{13}C triple resosance cryo-probe and cryogenic ^{13}C preamplifier in 50 mM Tris-HCl, pH 8, 0.2 % sodium azide, 10 %

D_2O, at 45 °C using 5 mm NMR tubes. Protons were decoupled during data acquisition. Peak assignments were obtained from ^{13}C-^{1}H, ^{1}H-^{1}H ^{13}C-^{13}C and ^{15}N-^{13}C-^{1}H chemical shift correlation spectra of the unbound nucleotide. 500 µM $^{13}C/^{15}N$-labeled dUMP or dU and 1.5 mM enzyme were used for the WT and mutant FDTS-ligand complexes. Data were processed using MestReNova. The ^{13}C-NMR spectrum of the ^{12}C dUMP-FDTS complex was subtracted from the spectra of the ^{13}C-labeled complexes to remove the resonances associated with the protein. For the reduced FDTS-dUMP complex, the flavin was reduced by addition of 10 mM glucose-6-phosphate and catalytic amounts of glucose-6-phosphate dehydrogenase and NADPH in an anaerobic chamber. The sample was placed in an NMR tube, capped with an anaerobic septum, and removed from the anaerobic chamber for data collection. The sample was pale yellow throughout the data collection, indicating that the flavin remained reduced. Spectra for the uncomplexed ligands were acquired separately. The sample for unbound dUMP at pH 12 was acquired in 50 mM sodium phosphate buffer, 0.2 % sodium azide, 10% D_2O.

Crystallization and Structure Determination

Crystals of FDTS were grown under previously reported conditions using the sitting drop vapor diffusion method.[10] For the R90A FDTS-dUMP, R174A FDTS-dUMP, and WT FDTS-dU complexes, crystals were grown by mixing protein-ligand stock solution (10 mg/mL FTDS variant, 20 mM dU(MP)) in 10 mM Tris-HCl, pH 7.9 with 40-50 % PEG 200, 0-150 mM NaCl and 100 mM Tris-HCl, pH 8.0 at a 1:1 ratio. The R174A crystals were grown by streak seeding of WT FDTS-dUMP crystals with an eyelash into a pre-equilibrated drop containing R174A FDTS and dUMP in the crystallization solution. Crystals were flash frozen in liquid N_2 without additional

cryoprotection. Crystals of the FDTS-dUMS complex (stock solution containing 10 mg/mL FDTS and 5 mM dUMS in 10 mM Tris-HCl, pH 7.9) were grown in 7 % PEG 4K, 100 mM NaCl, 100 mM Na/K phosphate, pH 6.6. The crystals were serially transferred to solutions of increasing PEG 4K and glycerol to a final concentration of 24 % PEG 4K, 10% glycerol, 200 mM NaCl, 100 mM Na/K phosphate, pH 6.6 before being flash frozen in liquid N_2.

Diffraction data were collected at the General Medical Sciences and Cancer Institutes Structural Biology Facility at the Advanced Photon Source (GM/CA at APS) on beamline 23ID-D. The data were processed in HKL2000,[11] XDS[12] or MOSFLM[13] . A single chain of FTDS (PDB ID 4GT9) was used for molecular replacement in MolRep[14] and iterative rounds of model building in Coot[15] and refinement in Refmac[16] were used to generate the final model. TLS groups were identified using the TLSMD server.[17] Restraints for 2′-deoxyuridine-5′-monosufate were generated using the GRADE server.[18] An additional copy of FAD was observed near the active site in the FTDS-dUMS complex, the adenine portion is disordered and crosses a crystallographic 2-fold axis so riboflavin was built in place of FAD. The final models were validated with MolProbity.[19]

Results

The mutant enzymes studied here were selected because a mechanism was proposed where dUMP is activated as a nucleophile by three charged groups in the active site of FDTS oriented around polar ends of the uracil ring – R90, R174, and the phosphate of dUMP (Figure 2 - 2).[5] These groups enhance the contribution of the

enolate resonance form of the uracil ring, increasing nucleophilicity at C5 (Figure 2 - 1B). Mutagenesis supported this idea; the rate constants for flavin oxidation of the R90A mutant and the R174A mutant were 8-fold and 3000-fold smaller, respectively, than wild-type FDTS in oxidative half-reactions with dUMP and CH_2THF.

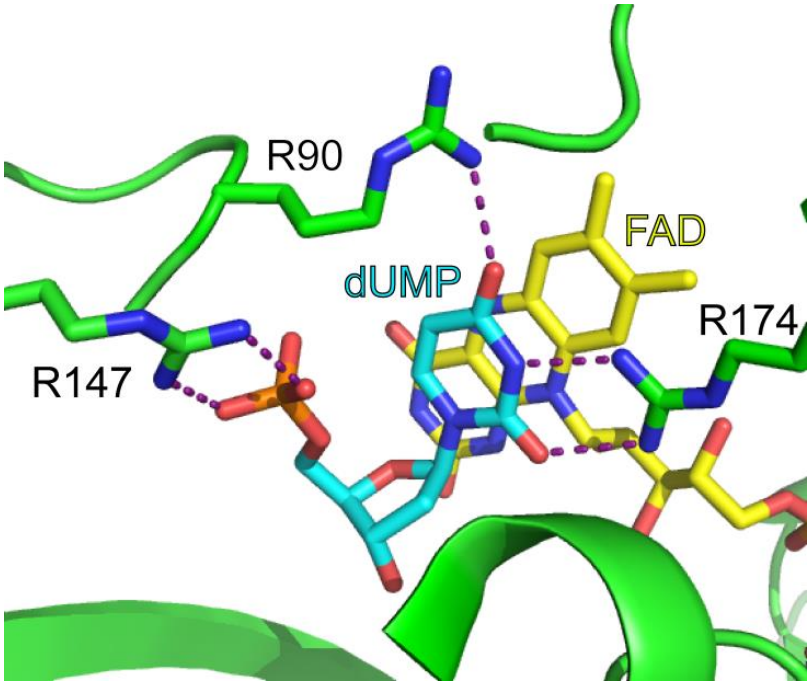

Figure 2 - 2. Active site of flavin-dependent thymidylate synthase (PDB code: 1O26). In the mechanism shown in Figure 2 - 1B, the arrangement of R90, R174, and the phosphate of dUMP (cyan) are proposed to stabilize an alternate resonance form of dUMP with enhanced nucleophilicity at C5. Also, note the close proximity of the phosphate oxygens to C5 of the uracil.

Binding

A large change in the flavin UV/visible absorbance spectrum of oxidized WT FDTS occurs upon binding of dUMP (Figure 2 - 3A) – the extinction coefficients for the peaks at 375 nm and 450 nm increase and decrease, respectively. This spectral change can be used to track dUMP binding in titrations, allowing the dissociation constant of

dUMP for FDTS to be determined. dUMP bound stoichiometrically to WT FDTS, providing only an estimate of the K_d of 30 nM (Table 2 - 1). 2'-deoxyuridine (dU) – which lacks the 5' phosphate group – induces a similar change as dUMP in the flavin absorbance spectrum of WT FDTS upon binding to the enzyme (Figure 2 - 3B). The dissociation constant for dU binding to oxidized WT FDTS was 78 µM (Table 2 - 1). The R90A mutant and the R174A mutant bound dUMP with dissociation constants of 14 µM and 110 µM, respectively (Table 2 - 1). The flavin spectral change upon binding of dUMP to the R90A mutant was similar to dUMP binding to WT FDTS (Figure 2 - 3C). However, the spectral change in the flavin of the R174A mutant was clearly different from the rest of the mutants tested (Figure 2 - 3D) – the 450 nm peak blue-shifted slightly and the extinction coefficient of the 450 nm peak decreased upon binding dUMP.

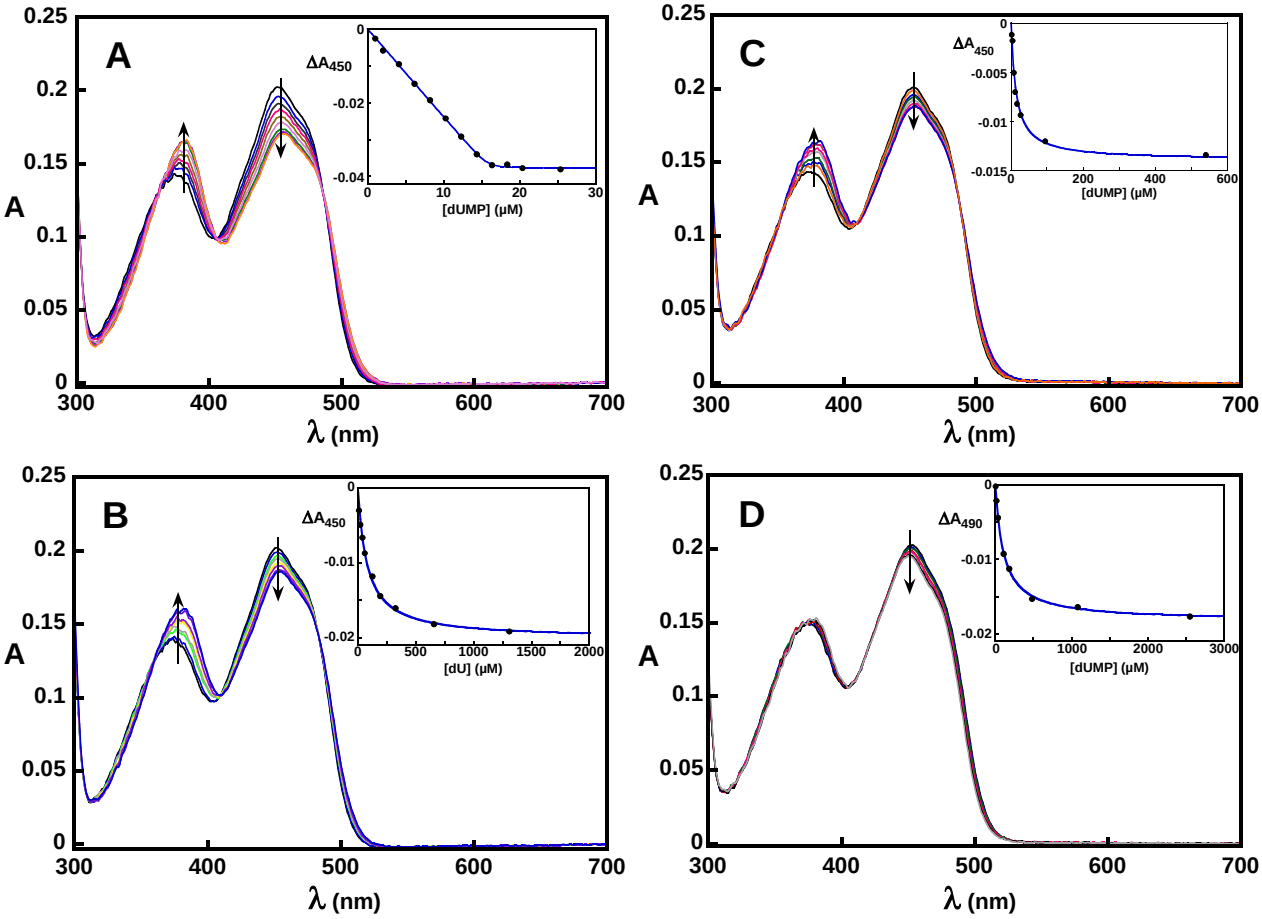

Figure 2 - 3. Spectrophotometric titrations of WT FDTS with dUMP (A) and dU (B) and R90A FDTS (C) and R174A FDTS (D) with dUMP in 0.1 M Tris-HCl, pH 8 at 25 °C. The insets show the change in absorbance as a function of ligand concentration. The spectral change for dUMP binding to R174A FDTS was noticeably different from other FDTS variants. Fitting to Eq. 1 gives a K_d of 30 nM for dUMP binding to WT FDTS. Fitting to a square hyperbola gives a K_d of 78 μM for dU binding to WT FDTS, and 14 μM and 110 μM for dUMP binding to R90A and R174A FDTS, respectively.

Table 2 - 1: Ligand Binding to WT and Mutant FDTSs

enzyme + ligand complex	K_d (μM)[a]
WT + dUMP	0.03 ± 0.02[b]
WT + dU	78 ± 5
R90A + dUMP	14 ± 2
R174A + dUMP	110 ± 10
WT + dUMS	0.17 ± 0.08[b]

[a]0.1 M Tris-HCl, pH 8 at 25 °C.
[b]Estimate from Fitting to Equation 1.

NMR

We probed polarization by comparing the ^{13}C-NMR spectra of ^{13}C/^{15}N-labeled dUMP in aqueous solution at pH 8 with ^{13}C/^{15}N-labeled dUMP bound to FDTS. Due to the size of the enzyme tetramer (110 kDa), we were unable to perform multinuclear NMR experiments on the complex. Instead, we collected 1-dimensional ^{13}C-NMR spectra of labeled dUMP bound to WT FDTS (Figure 2 - 4). Spectra were recorded at 45 °C to minimize peak broadening due to chemical shit anisotropy. We used an excess of FDTS over dUMP, well above the K_d of dUMP, to ensure that the signals resulted from dUMP bound to the enzyme. The resonances associated with the protein were subtracted from the ^{13}C-NMR spectra of the ^{13}C-labeled dUMP-FDTS complexes by using the spectrum of the unlabeled complex. The peaks associated with dUMP in the ligand-protein complex were substantially broadened, confirming binding.

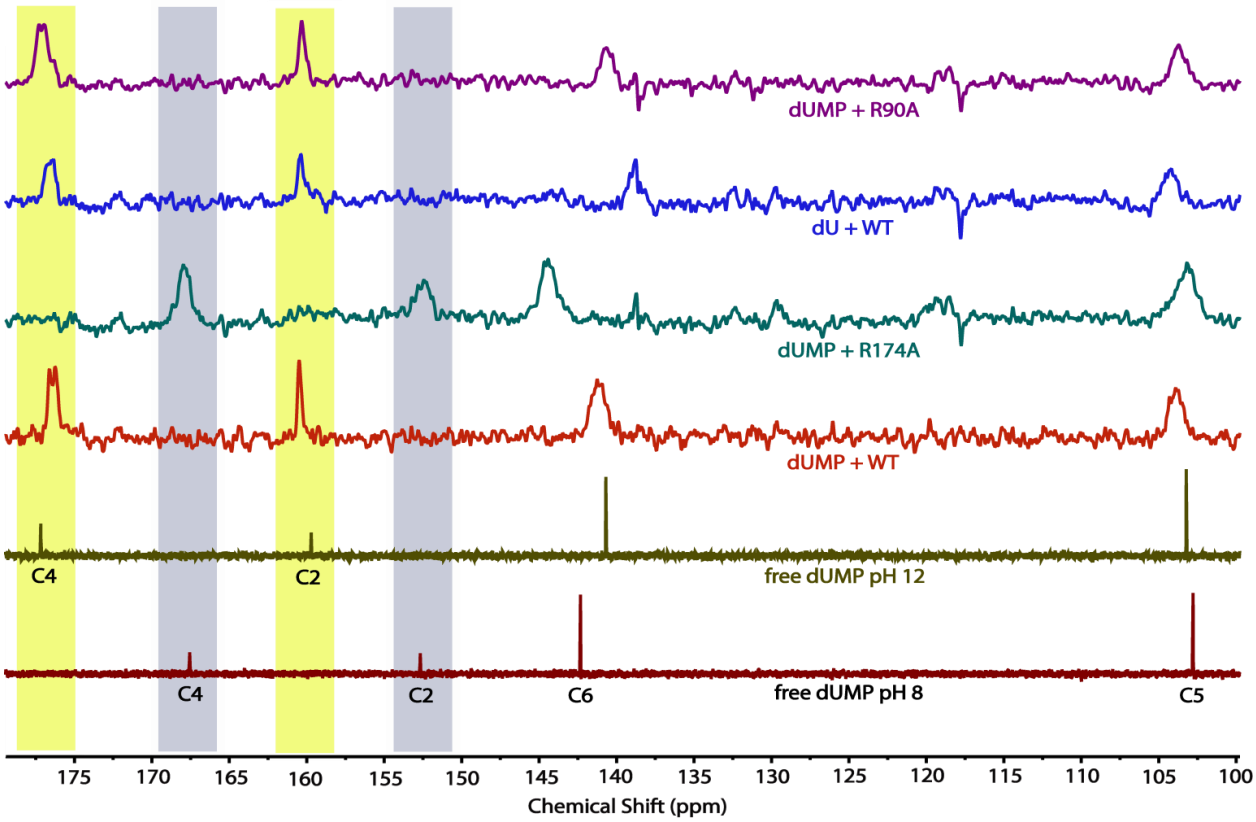

Figure 2 - 4. The ^{13}C-NMR spectra of uracil carbons of dUMP/dU free in solution or bound to WT and mutant FDTSs at 45°C. All of the ligand-FDTS complexes were at pH 8. The C4 andC2 signals for dUMP shifted upfield ~8 ppm when bound to WT FDTS, having nearly identical chemical shifts as free dUMP at pH 12. Mutation of R174 – which is 2.8 Å from N3 of dUMP in the dUMP-WT FDTS structure – to alanine eliminated the changes in chemical shifts of the dUMP-FDTS complex. In contrast, mutation of R90 to alanine or removal of the phosphate of dUMP had little effect on the ^{13}C-NMR spectrum of the uracil carbons in the complex. Highlighted in yellow and blue, respectively, are the chemical shifts of the carbonyl carbons of N3-ionized and N3-unionized uracil.

Table 2 - 2: Chemical Shifts for Uracil Carbons[a]

	C2 (ppm)	C4 (ppm)	C5 (ppm)	C6 (ppm)
unbound dUMP pH 8	152.7	167.6	102.8	142.3
unbound dUMP pH 12	159.7	177.2	103.2	140.7
dUMP + WT	160.5	176.4	103.9	141.2
dUMP + R174A	152.6	167.9	103.2	144.4
dUMP + R90A	160.3	177	103.7	140.7
dU + WT	160.4	176.6	104.3	138.8

[a]45°C, pH 8 unless stated otherwise.

Binding of dUMP to WT FDTS produced substantial changes in the ^{13}C chemical shifts of the uracil ring (Figure 2 - 4 and Table 2 - 2). Most notably, the ^{13}C-NMR signals of the two carbonyl carbons, C2 and C4, shifted downfield by approximately 8 ppm each. dUMP bound to WT FDTS had the same ^{13}C spectrum whether the flavin was in the oxidized form or the hydroquinone form, indicating that the redox state of the flavin does not affect the electrons of the uracil of dUMP.

We further tested the polarization hypothesis by individually removing the charged groups interacting with the uracil ring and obtained chemical shifts. To test the importance of the phosphate of dUMP, a ^{13}C-NMR spectrum was collected of dU bound to WT FDTS. The ^{13}C chemical shifts of the uracil in unbound dU are identical to the chemical shifts of the uracil in unbound dUMP. Surprisingly, the ^{13}C spectrum of dU bound to WT FDTS was nearly identical to the ^{13}C spectrum of dUMP bound to WT FDTS (Figure 2 - 4); the only notable difference was that the signal for C6 (which is 3.3 Å away from the phosphate of dUMP in the dUMP-FDTS structure) was ~2 ppm lower than the C6 resonance of the dUMP-FDTS complex. Likewise, dUMP bound to R90A FDTS also had ^{13}C chemical shifts that were similar to dUMP bound to WT FDTS. However, dUMP bound to R174A FDTS had chemical shift values that were similar to those of free dUMP at pH 8 (Figure 2 - 4). The peaks were still broadened in the complex, indicating that dUMP was bound to the R174A mutant.

The ^{13}C-NMR spectra at pH 8 of free dUMP and dUMP bound to WT FDTS and the various mutants show that R174 is largely responsible for producing the changes in the chemical shifts of the uracil of dUMP bound to FDTS. What might R174 be doing to cause these changes? The crystal structure of the dUMP-WT FDTS complex shows

that R174 is positioned 2.8 Å away from N3 of dUMP (Figure 2 - 2).[7] The pK_a of N3 is normally 9.3 in aqueous solutions.[20] We hypothesized that the close proximity of the positively charged guanidinium group of R174 to N3 lowers the pK_a of N3, ionizing it in the complex. To test this, we collected the ^{13}C-NMR spectrum of unbound dUMP at pH 12, well above the pK_a for N3 of dUMP. The ^{13}C chemical shift values of unbound dUMP at pH 12 were nearly identical to those of dUMP bound to WT FDTS, strongly suggesting that N3 of dUMP is ionized when bound to FDTS at pH 8 (Figure 2 - 4).

Structures

In order to confirm that dUMP and dU bind in a catalytically competent conformation in the active site variants of FDTS**,** we determined the crystal structures of dUMP bound complexes of the R90A and R174A FDTS variants and the structure of dU bound to WT FDTS (Table 2 - 3). In all three cases the nucleotide/nucleoside bound in the same position as in the WT FDTS-dUMP complex (Figure 2 - 5). Most of the protein residues were also in the same positions in all of the structures; one notable difference in the dU-FDTS structure was that R147 (which forms a salt bridge with the phosphate of dUMP) was flipped away from the phosphate binding site. We also observed a polyethylene glycol molecule in the dU-FDTS structure in the space occupied by the phosphate group and R147 in the dUMP-FTDS complex.

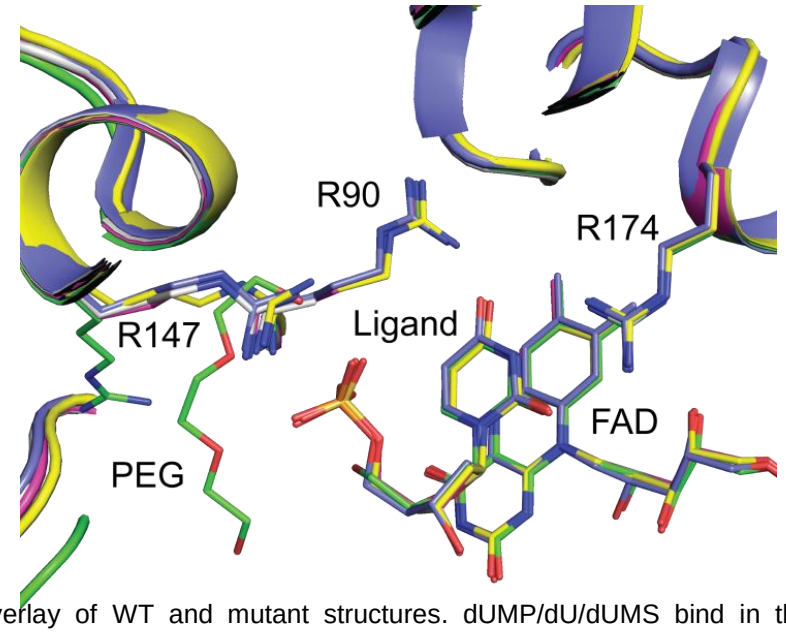

Figure 2 - 5. Overlay of WT and mutant structures. dUMP/dU/dUMS bind in the same position and orientation in all of the active site variants used in this study. dUMP + WT (PDB code: 1O26), blue; dU + WT, green; dUMP + R90A, gray; dUMP + R174A, magenta; dUMS + WT, yellow.

Table 2 - 3: Crystallographic Summary

Crystal Contents	FDTS R90A-FAD dUMP	FDTS R174A-FAD dUMP	FDTS-FAD dU	FDTS-FAD dUMS
Diffraction Data				
Space group	$P2_12_12_1$	$P2_12_12_1$	$P2_12_12_1$	$I4_122$
Cell (Å)	54.1 116.2 141.0	54.1 115.9 141.1	54.2 116.1 141.9	109.7 109.7 119.9
d_{min} (Å)	1.9 (1.97-1.90)[a]	2.00 (2.11-2.00)	1.93 (2.02- 1.93)	1.95 (2.06-1.95)
Average I/σ_I	22.9 (2.3)	8.7 (2.4)	22.8 (2.5)	20.4 (2.6)
R_{sym}	0.073 (0.856)	0.115 (0.682)	0.094 (0.897)	0.118 (1.096)
$CC_{1/2}$				99.9 (82.5)
Multiplicity	6.6 (5.9)	6.0 (6.1)	7.6 (6.8)	14.6 (14.2)
Completeness	99.5 (99.6)	90.7 (86.0)	98.1 (96.9)	99.7 (98.1)
No. of unique reflections	70476	54863	67137	27043
Refinement				
Data Range (Å)	89.68 -1.90	89.54 - 2.00	89.86 - 1.93	80.92-1.95
Reflections	66829	52046	62459	25671
R_{work}/ R_{free}	0.178 / 0.211	0.183 / 0.217	0.170 / 0.202	0.162 / 0.200
RMSD bonds (Å)	0.010	0.010	0.010	0.009
RMSD angles (°)	1.48	1.49	1.46	1.37
Ramachandran (%)				
Allowed	100	100	100	100
Outliers	0	0	0	0
Average B-factors (Å^2)				
Protein	37.1	34.8	39.3	22.8
Ligand	25.9	25.6	36.8	32.5
Water	38.0	37.3	40.4	37.8

[a]Values in parentheses refer to the outermost shell of data.

Lack of Reactivity of dUMP Analogs

In addition to the two arginine mutants, dU – which still binds to the WT enzyme – failed to support oxidation of WT FDTS containing reduced flavin in the presence of CH_2THF and could not be converted into 2'-deoxythymidine (dT), indicating that the phosphate of dUMP is important for catalysis by FDTS (Figure 2 - 6). However, the NMR data show that the phosphate of dUMP does not play a major role in ionizing the uracil ring of dUMP since dU was ionized when bound to FDTS. In addition, the crystal structure of the dU-FDTS complex showed that dU binds in a similar manner to dUMP. We therefore considered the possibility that the phosphate might be important in another step of the reaction catalyzed by FDTS.

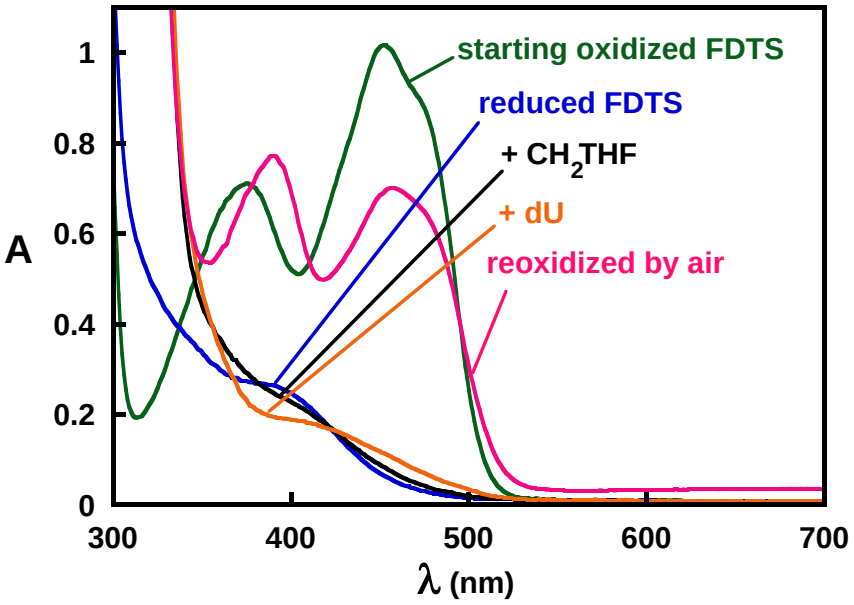

Figure 2 - 6. dU failed to oxidize reduced FDTS in the presence of CH_2THF. Anaerobic oxidized FDTS (green) in 0.1 M Tris-HCl, pH 8 at 25°C was titrated stoichiometrically with dithionite to reduce the flavin (blue). Anaerobic addition of CH_2THF perturbed the spectrum, indicating that it formed a complex with the enzyme (black). Anaerobic addition of dU to the reduced FDTS-CH_2THF complex also perturbed the spectrum but failed to oxidize the flavin (orange), indicating that the phosphate of dUMP plays an essential role in the FDTS-catalyzed reaction. The flavin could then be reoxidized by air (red).

Any mechanism for FDTS requires the involvement of a base to remove the proton at C5 of the dUMP-CH_2THF bridged intermediate. However, the base in the mechanism of FDTS is currently unknown. The base would have to be on the opposite face of the uracil ring from the side that reacts with CH_2THF; CH_2THF is proposed to react on the side of the uracil facing the flavin in Figure 2 - 2.[10] In the dUMP-WT FDTS structure no side-chains are properly positioned to act as a base. However, dUMP is bound in an unusual curled conformation where one of the phosphate oxygens of dUMP is 3.4 Å away from C5, close enough for the phosphate to act as a general base.

To test this possibility, we synthesized an analog of dUMP where the 5'-phosphate is replaced with sulfate – 2'-deoxyuridine-5'-monosulfate (dUMS). Sulfate is structurally similar to phosphate, but the pK_{a1} for sulfate is ~10 units lower than the pK_{a2} for phosphate,[21] making it a poor general base. dUMS bound to oxidized FDTS with an affinity similar to that of dUMP and produced a similar change in the flavin UV/visible absorbance spectrum upon binding to FDTS (Table 2 - 1, Figure 2 - 7A). The crystal structure of the dUMS-FDTS complex at 1.9 Å resolution showed that dUMS binds in the same position as dUMP (Figure 2 - 5), without affecting any protein residues. However, dUMS was unable to oxidize reduced FDTS in the presence of CH_2THF and no 2'-deoxythymidine-5'-monosulfate was detected (Figure 2 - 7B).

The reaction of dUMS with reduced FDTS and CH2THF should form a dUMS-CH2THF bridged intermediate, but should be unable to break down the intermediate since dUMS cannot remove the C5 proton of the intermediate. We attempted to detect the bridged intermediate from the reaction in Figure 2 - 7B by denaturing the enzyme using 1 M HCl and analyzing the supernatant by reverse-phase HPLC. No new species

were detected in the HPLC chromatogram (only dUMS, CH_2THF, FAD, and their decomposition products were detected), indicating that either the bridged intermediate is unstable when removed from the active site of FDTS or that the equilibrium constant for its formation lies to the left.

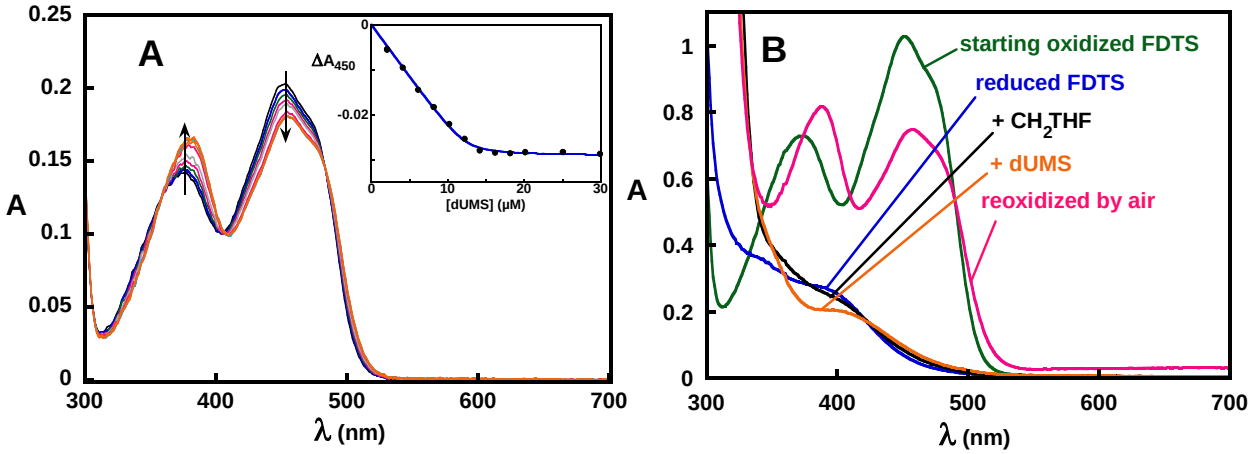

Figure 2 - 7. Binding and reactivity data for dUMS in 0.1 M Tris-HCl, pH 8 at 25°C. (A) spectrophotometric titration of WT FDTS with dUMS. dUMS produced a flavin spectral change similar to dUMP. Fitting to Eq. 1 gave a K_d of 170 nM. (B) dUMS failed to oxidize reduced FDTS in the presence of CH_2THF. Anaerobic oxidized FDTS (green) was titrated stoichiometrically with dithionite to reduce the flavin (blue). Anaerobic addition of CH_2THF perturbed the spectrum of the flavin (black), indicating that it formed a complex with the enzyme. Anaerobic addition of dUMS to the reduced FDTS-CH_2THF complex also perturbed the spectrum (orange), indicating binding, but it failed to oxidize the enzyme. The flavin was then reoxidized by exposure to air (red).

Discussion

Our data indicate that N3 of dUMP is ionized upon binding to FDTS. The ^{13}C chemical shift values for the uracil carbons of dUMP bound to FDTS at pH 8 are nearly identical to those of unbound dUMP at pH 12. R174 in *T. maritima* FDTS appears to be solely responsible for causing this ionization. When dUMP is bound to R174A FDTS the chemical shifts of the uracil carbons are nearly identical to those of unbound dUMP at pH 8. However, when the other active site groups that directly interact with dUMP are removed, the chemical shifts are nearly identical to dUMP bound to WT FDTS. The pK_a

for N3 of dUMP is 9.3 in water; the positively charged R174 therefore must lower the pK_a for N3 of dUMP by several units in the active site FDTS in order for it to be ionized at pH 8.

The large change in the flavin absorbance spectrum of WT FDTS upon binding dUMP is likely due to the N3-ionized form of the uracil stacking against the isoalloxazine of the flavin. Binding of dUMP to WT FDTS causes a large change in the UV/visible absorbance spectrum of the flavin. Binding of dU to WT FDTS and binding of dUMP to R90A FDTS also produce a similar change in the flavin absorbance spectrum; however, the absorbance spectral change upon binding dUMP by R174A FDTS is significantly different, indicating that the environment of the flavin is different in the dUMP-R174A FDTS complex.

The three charged groups in the dUMP binding site also play a significant role in the binding of dUMP by FDTS – removal of the phosphate and substitution of the two arginines with alanine each cause a substantial lowering of the binding affinity of FDTS for dUMP/dU. dU binds to WT FDTS 5300-fold weaker than dUMP, corresponding to a loss of ~5.2 kcal/mol of binding energy. The phosphate of dUMP forms a salt bridge with R147 and hydrogen bonds with S88 and Q75, all of which are lost with dU. dUMP binds to R90A FDTS 670-fold weaker than WT, corresponding to a loss of ~4.0 kcal/mol of binding energy. R90 would form a partial salt bridge with O4 due to resonance of the N3-ionized form of dUMP. Finally, dUMP binds to R174A FDTS 7300-fold weaker than WT FDTS, corresponding to a loss of ~5.4 kcal/mol of binding energy. R174 is positioned to form a salt bridge with N3 of the ionized form of dUMP – substitution of R174 with alanine removes this interaction.

We also found evidence consistent with the phosphate of dUMP acting as the base that deprotonates C5 of the dUMP-CH_2THF adduct during carbon transfer, explaining why dU does not support oxidation of the reduced flavin of FDTS in the presence of CH_2THF even though dU is ionized when bound to the enzyme. This finding also provides an explanation for the unusual conformation of dUMP bound to FDTS which, to our knowledge, is unique among nucleotide-binding proteins. Binding of dUMS to FDTS has similar affinity and produces similar spectral changes compared to binding of dUMP, indicating that the same interactions between the nucleotide and protein are intact with dUMS, including ionization of N3. In addition, the crystal structure of the dUMS-FDTS complex shows that dUMS binds in the same position as dUMP. However, dUMS is unable to support oxidation of the flavin in the presence of CH_2THF. While sulfate is structurally similar to phosphate, the pK_a for sulfate is many units lower than that of phosphate, making base catalysis normally performed by phosphate inaccessible to dUMS.

Our findings with dUMS are similar to those observed with 5F-dUMP,[4] which also blocks deprotonation of C5: 5F-dUMP produces a similar change in the UV/visible absorbance spectrum of the reduced FDTS-CH_2THF complex, but does not react. Curiously, we were unable to detect a dUMS-CH_2THF bridged intermediate by HPLC after acid-denaturing the enzyme from Figure 2 - 7B. However, past attempts to isolate an intermediate using 5F-dUMP were also unsuccessful,[3,22,23] indicating that the intermediate might be unstable when removed from the active site of the enzyme.

Ionization of N3 requires a modification of the mechanism shown in Figure 2 - 1B since the negative charge of the ionized nitrogen can be delocalized onto O2 and O4,

blocking the enolate-containing resonance structure from occurring (Figure 2 - 8A). We propose a new mechanism for dUMP activation based on ionization of N3. The C5-C6 pi-electrons cannot be delocalized onto the C4 carbonyl in the N3-ionized dUMP; this stabilizes the resonance structure with a formal negative charge on C5 in N3-ionized dUMP relative to unionized dUMP (Figure 2 - 8A). This resonance structure is highly nucleophilic at C5; we propose that the C5 carbanion directly attacks CH_2THF, initiating the oxidative half-reaction of FDTS (Figure 2 - 8B). Ionization of N3 is clearly important for chemistry. The rate constant for flavin oxidation in oxidative half-reaction experiments for the R174A mutant is 3000-fold slower than that of wild-type,[5] and our crystal structure shows this is not due to improper positioning of dUMP in the mutant. As a possible precedent for this mechanism of activation, dUMP can react with formaldehyde under basic conditions to make 5-hydroxymethyl dUMP.[24,25]

Following activation of dUMP and formation of the dUMP-CH_2THF bridged intermediate, the phosphate of dUMP abstracts the proton at C5 to break down the intermediate and eliminate THF (Figure 2 - 8B). dTMP is then formed by hydride transfer from reduced FAD and the rearrangement proposed previously (Figure 2 - 1B, steps 3-5).[3]

The findings presented here further establish that FDTS uses a novel mechanism to methylate a pyrimidine. Uracil activation by N3 ionization has never been reported, but may be used by other uracil-methylating enzymes. However, other mechanisms for the enzymatic deprotonation of uracil nitrogens have been identified: the immediate product of the reaction catalyzed by uracil DNA glycosylases is a uracil deprotonated at N1 that is stabilized by a strong hydrogen bond with O2.[26–29] In addition, the phosphate

of dUMP appears to be important for catalysis by FDTS, which is not the case with classic TS.

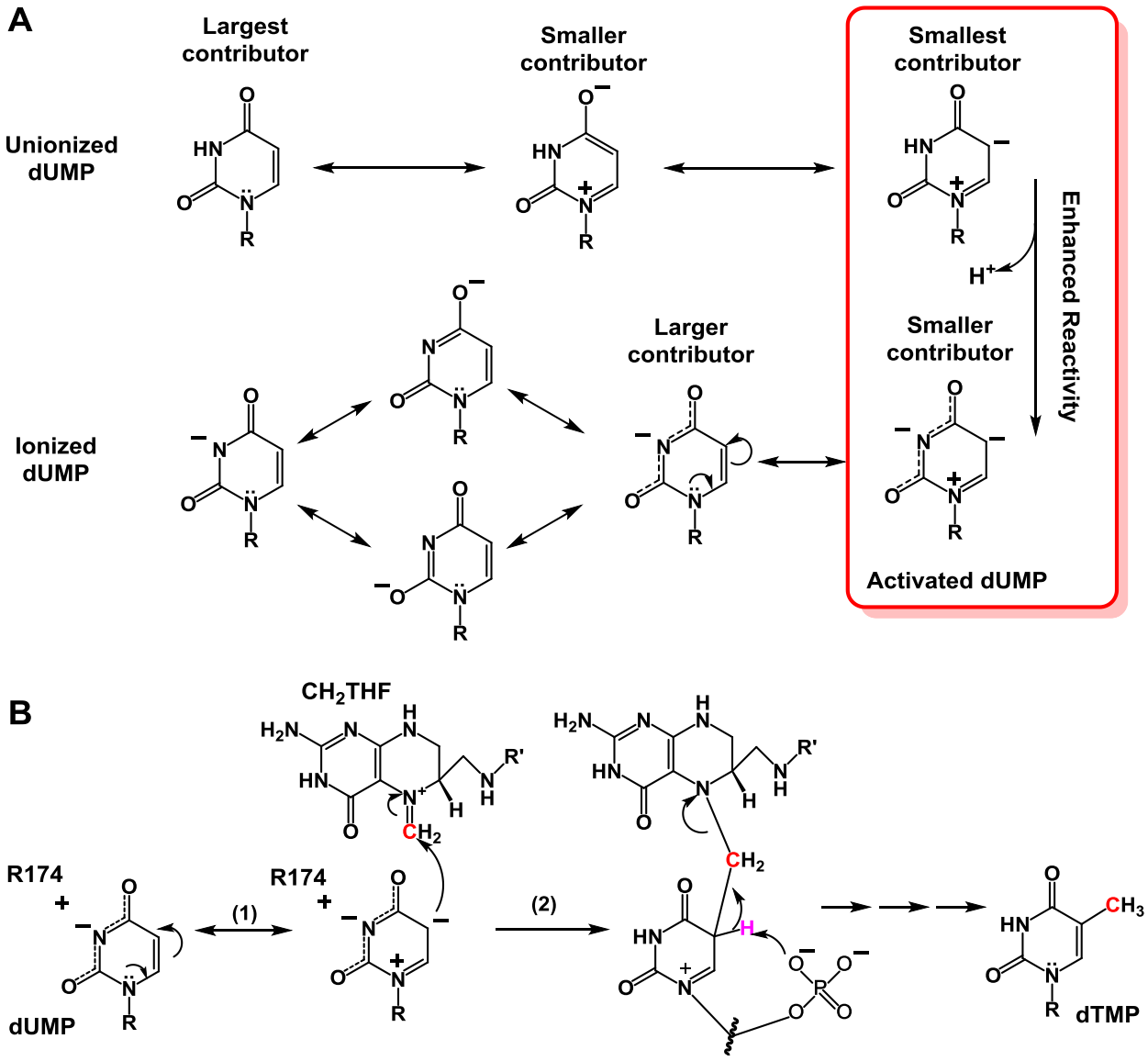

Figure 2 - 8. Proposed mechanism for the reaction of FDTS. (A) the proposed mechanism for activation of dUMP by ionization of N3. The negative charge of N3-ionized dUMP would be delocalized onto O4 and O2, preventing the enolate-containing resonance structure normally available with unionized dUMP. Destabilization of the enolate-containing resonance structure enhances the population of the resonance structure with a formal negative charge on C5 (red box), which is a good nucleophile. (B) the proposed mechanistic steps for the FDTS-catalyzed reaction following ionization of N3. Steps (3) – (5) in Figure 2 - 1B occur after removal of the C5 proton of the dUMP-CH_2THF adduct by the phosphate of dUMP.

Conclusions

FDTS ionizes N3 of dUMP, which is largely caused by an active site arginine, providing a new mechanism for dUMP activation. The phosphate of dUMP is crucial for flavin oxidation, suggesting that it acts as the base that deprotonates C5 of the dUMP-CH_2THF adduct. Notably, both ionization of N3 and acid-base catalysis by the phosphate of dUMP are not implicated in the mechanism used by classic TS.

References

(1) Carreras, C. W., and Santi, D. V. (1995) The catalytic mechanism and structure of thymidylate synthase. *Annu. Rev. Biochem. 64*, 721–62.

(2) Koehn, E. M., and Kohen, A. (2010) Flavin-dependent thymidylate synthase: a novel pathway towards thymine. *Arch. Biochem. Biophys. 493*, 96–102.

(3) Koehn, E. M., Fleischmann, T., Conrad, J. A., Palfey, B. A., Lesley, S. A., Mathews, I. I., and Kohen, A. (2009) An unusual mechanism of thymidylate biosynthesis in organisms containing the thyX gene. *Nature 458*, 919–23.

(4) Gattis, S. G., and Palfey, B. A. (2005) Direct observation of the participation of flavin in product formation by thyX-encoded thymidylate synthase. *J. Am. Chem. Soc. 127*, 832–3.

(5) Conrad, J. A., Ortiz-Maldonado, M., Hoppe, S. W., and Palfey, B. A. (2014) Detection of Intermediates in the Oxidative Half-Reaction of the FAD-Dependent Thymidylate Synthase from Thermotoga maritima: Carbon Transfer without Covalent Pyrimidine Activation. *Biochemistry 53*, 5199–207.

(6) Mishanina, T. V, Koehn, E. M., Conrad, J. A., Palfey, B. A., Lesley, S. A., and Kohen, A. (2012) Trapping of an intermediate in the reaction catalyzed by flavin-dependent thymidylate synthase. *J. Am. Chem. Soc. 134*, 4442–8.

(7) Mathews, I., Deacon, A., Canaves, J., Mcmullan, D., Lesley, S., Agarwalla, S., and Kuhn, P. (2003) Functional Analysis of Substrate and Cofactor Complex Structures of a Thymidylate Synthase-Complementing Protein. *Structure 11*, 677–90.

(8) Schroeder, F. C., Taggi, A. E., Gronquist, M., Malik, R. U., Grant, J. B., Eisner, T., and Meinwald, J. (2008) NMR-spectroscopic screening of spider venom reveals sulfated

nucleosides as major components for the brown recluse and related species. *Proc. Natl. Acad. Sci. U. S. A. 105*, 14283–7.

(9) Williams, C. H. J., Arscott, D. L., Matthews, R. G., Thorpe, C., and Wilkinson, K. D. (1979) Methodology Employed for Anaerobic Spectrophotometric Titrations and for Computer-Assisted Data Analysis. *Methods Enzymol. 62*, 185–98.

(10) Koehn, E. M., Perissinotti, L. L., Moghram, S., Prabhakar, A., Lesley, S. A., and Mathews, I. I. (2012) Folate binding site of flavin-dependent thymidylate synthase. *Proc. Natl. Acad. Sci. U. S. A. 109*, 15722–7.

(11) Otwinowski, Z., and Minor, W. (1997) Processing of X-Ray Diffraction Data Collected in Oscillation Mode. *Methods Enzym. 276*, 307–26.

(12) Kabsch, W. (2010) XDS. *Acta Crystallogr. D. Biol. Crystallogr. 66*, 125–32.

(13) Leslie, A. G. W., and Powell, H. R. (2007) Processing Diffraction Data with Mosflm, in *Evolving Methods for Macromolecular Crystallography* (Read, R. J., and Sussman, J. L., Eds.), pp 41–51.

(14) Vagin, A., and Teplyakov, A. (1997) MOLREP : an Automated Program for Molecular Replacement. *J. Appl. Crystallogr. 30*, 1022–5.

(15) Emsley, P., and Cowtan, K. (2004) Coot : model-building tools for molecular graphics. *Acta Crystallogr. Sect. D Biol. Crystallogr. 60*, 2126–32.

(16) Vagin, A. A., Steiner, R. A., Lebedev, A. A., Potterton, L., McNicholas, S., Long, F., and Murshudov, G. N. (2004) REFMAC5 dictionary: organization of prior chemical knowledge and guidelines for its use. *Acta Crystallogr. D. Biol. Crystallogr. 60*, 2184–95.

(17) Painter, J., and Merritt, E. A. (2006) TLSMD web server for the generation of multi-group TLS models. *J. Appl. Crystallogr. 39*, 109–11.

(18) Smart, O. S., Womack, T. O., Sharff, A., Flensburg, C., Keller, P., Paciorek, W., Vonrhein, C., and Bricogne, G. (2011) (2011) grade, version 1.1.1. Cambridge, United Kingdom, Global Phasing Ltd.,. *grade, version 1.1.1*.

(19) Chen, V. B., Arendall, W. B., Headd, J. J., Keedy, D. A., Immormino, R. M., Kapral, G. J., Murray, L. W., Richardson, J. S., and Richardson, D. C. (2010) MolProbity: all-atom structure validation for macromolecular crystallography. *Acta Crystallogr. D. Biol. Crystallogr. 66*, 12–21.

(20) Aylward, N. N. (1967) Thermodynamic Constants of the Ionisation of the Acid Imino-group of Uridine 5'-Monophosphate and Poly-uridylic Acid. *J. Chem. Soc. B Phys. Org.* 401–3.

(21) Jencks, W. P., and Regenstein, J. (2010) Ionization Constants of Acids and Bases, in *Handbook of Biochemistry and Molecular Biology, Fourth Edition* (Lundblad, R. L., and MacDonald, F. M., Eds.) 4th ed., pp 595–636.

(22) Leduc, D., Graziani, S., Lipowski, G., Marchand, C., Le Maréchal, P., Liebl, U., and Myllykallio, H. (2004) Functional evidence for active site location of tetrameric thymidylate synthase X at the interphase of three monomers. *Proc. Natl. Acad. Sci. U. S. A. 101*, 7252–7.

(23) Graziani, S., Xia, Y., Gurnon, J. R., Van Etten, J. L., Leduc, D., Skouloubris, S., Myllykallio, H., and Liebl, U. (2004) Functional Analysis of FAD-dependent Thymidylate Synthase ThyX from Paramecium bursaria Chlorella Virus-1. *J. Biol. Chem. 279*, 54340–7.

(24) Alegria, A. H. (1967) Hydroxymethylation of pyrimidine mononucleotides with formaldehyde. *Biochim. Biophys. Acta 149*, 317–24.

(25) Cline, R. E., Fink, R. M., and Fink, K. (1959) Synthesis of 5-Substituted Pyrimidines via Formaldehyde Addition. *J. Am. Chem. Soc 293*, 2521–7.

(26) Drohat, A. C., and Stivers, J. T. (2000) NMR Evidence for an Unusually Low N1 pKa for Uracil Bound to Uracil DNA Glycosylase : Implications for Catalysis. *J. Am. Chem. Soc. 122*, 1840–1.

(27) Drohat, A. C., and Stivers, J. T. (2000) Escherichia coli uracil DNA glycosylase: NMR characterization of the short hydrogen bond from His187 to uracil O2. *Biochemistry 39*, 11865–75.

(28) Dong, J., Drohat, A. C., Stivers, J. T., Pankiewicz, K. W., and Carey, P. R. (2000) Raman spectroscopy of uracil DNA glycosylase-DNA complexes: insights into DNA damage recognition and catalysis. *Biochemistry 39*, 13241–50.

(29) Werner, R. M., and Stivers, J. T. (2000) Kinetic isotope effect studies of the reaction catalyzed by uracil DNA glycosylase: evidence for an oxocarbenium ion-uracil anion intermediate. *Biochemistry 39*, 14054–64.

Chapter 3

Nucleotide Binding to Flavin-Dependent Thymidylate Synthase from *Thermotoga maritima*

Flavin-dependent thymidylate synthases (FDTSs) are tetrameric enzymes that use a flavin adenine dinucleotide (FAD) prosthetic group to synthesize the essential DNA precursor – 2'-deoxythymidine-5'-monophosphate (dTMP) – from 2'-deoxyuridine-5'-monophosphate (dUMP), 5, 10-methylenetetrahydrofolate (CH_2THF), and NADPH. A number of pathogenic microorganisms use FDTS to make dTMP whereas humans use classic thymidylate synthase (TS). FDTS has a structure that is unrelated to classic TS, and a very different mechanism, making FDTS a potential target for new antimicrobial drugs.[1–3] Whereas the electrons that reduce the methylene to form dTMP come from the reduced folate in classic TS, the electrons come from NADPH in FDTS. Structures of FDTS from several organisms have been solved, and all are very similar.[4–9] The majority of the structures with substrates or analogues bound are of the enzyme from *Thermotoga maritima*. FDTS is a homotetramer with four active sites per tetramer. Each active site contains the redox-active isoalloxazine of an FAD and is composed of residues from three of the four subunits. dUMP binds in a pocket enclosed by a loop (residues 89-94 in *T. maritima* FDTS), with the uracil stacked against the isoalloxazine. In the absence of dUMP, the loop is disordered and the active site is open. A crystal structure of FDTS with CH_2THF and dUMP showed that CH_2THF binds in a pocket on

the opposite face of the isoalloxazine from dUMP.[10] However, this binding mode was proposed to be non-catalytic since dUMP and CH_2THF must be adjacent to each other in order for methylene transfer to occur.

Details of the chemical mechanism of FDTS are beginning to be understood.[11–14] However, the timing of substrate binding and product release has not been fully characterized. The catalytic cycle of FDTS involves three substrates and three products, making for a complex catalytic cycle, and the active site of FDTS is not large enough to accommodate all three substrates at the same time. Most work suggests that NADPH and CH_2THF bind to the same site at different points in the catalytic cycle, and that dUMP binds in its own, independent site.[5,8,10,15] NADPH binds to oxidized FDTS and reduces the flavin in the reductive half-reaction. The resulting $NADP^+$ is then replaced by CH_2THF, allowing the reductive methylation of dUMP by CH_2THF and the reduced flavin, making dTMP in the oxidative half-reaction and completing the catalytic cycle. While there is some consensus on the timing of NADPH and CH_2THF binding and the release of their products, the timing of dUMP binding and dTMP release is less clear. The presence of dUMP has been shown to stimulate the reduction by NADPH for some FDTSs, suggesting that dUMP binds to oxidized FDTS prior to reduction of the flavin by NADPH.[16,17] However, another study has shown that dUMP does not enhance the reduction of oxidized FDTS by NADPH, suggesting that dUMP only participates in the oxidative half reaction.[18] No studies have directly compared the binding of dUMP or dTMP to oxidized and reduced FDTS.

Here we report that FDTS from *T. maritima* (TmFDTS) binds dUMP and dTMP significantly weaker when the flavin is reduced than when the flavin is oxidized, and the

difference in affinity is largely due to changes in the rate constant for deoxynucleotide dissociation. This finding suggests that the exchange between dTMP and dUMP in the catalytic cycle of TmFDTS occurs when the flavin is reduced. We also show that TmFDTS behaves as a dimer of dimers with regards to dUMP and dTMP binding at low temperatures.

Experimental Procedures

Protein Preparations

Recombinant TmFDTS was purified as previously reported,[19] followed by formation of apo-protein by treatment with concentrated sodium chloride[5] to remove dTMP bound to the protein. FAD was then added to the apo-protein and the excess FAD removed by desalting.

Instrumentation

UV/visible absorbance spectra were recorded on a Shimadzu UV-2501PC standard scanning spectrophotometer. Circular dichroism spectra were recorded on a Jasco J-810 spectropolarimeter equipped with a Jasco PFD-425S peltier temperature controller. Stopped-flow experiments were recorded using a Hi-Tech Scientific KinetAsyst SF-61 DX2 stopped-flow spectrophotometer.

Anaerobic Experiments

When necessary, enzyme solutions were made anaerobic in glass tonometers or anaerobic cuvettes[20] by repeated cycles of vacuum and equilibration with anaerobic

argon.[21] Ligand solutions were made anaerobic by bubbling in syringes with anaerobic argon.

Detection of Bound Nucleotides

TmFDTS was denatured by adding 1 M HCl and incubating at 70°C for one minute. The precipitated protein was removed by centrifugation. The pH of the supernatant was raised to ~5 by adding 10 mM ammonium acetate and titrating with 10 M NaOH. The supernatant was then analyzed on a Shimadzu HPLC with a UV/Vis diode array detector at room temperature on a 5 µm, 25 cm x 4.6 mm Supelcosil LC-18-DB column with 1 mL/min flow rate. A 0 to 10 minute, 0 to 50% methanol gradient was used in 10 mM ammonium acetate, pH 5, followed by 15 minutes of isocratic 50% methanol in 10 mM ammonium acetate, pH 5. The relative concentrations of bound nucleotides within each sample were determined using ε_{260} = 10000 $M^{-1}cm^{-1}$ for dUMP, ε_{267} = 9490 $M^{-1}cm^{-1}$ for dTMP, ε_{271} = 8860 $M^{-1}cm^{-1}$ for dCMP, and ε_{450} = 11300 $M^{-1}cm^{-1}$ for FAD.

Reduction Potentials

Reduction potentials were determined using the xanthine/xanthine oxidase method of Massey.[22] Experiments were performed in anaerobic cuvettes in 0.1 M Tris-HCl, pH 8 at 25°C and monitored in a standard scanning spectrophotometer. 1-hydroxyphenazine (E_m = -225 mV at pH 8, 25°C)[23] was used as the indicator dye for unbound TmFDTS. Phenosafranine (E_m = -274 mV at pH 8, 25°C)[23] was used as the indicator dye for dUMP- and dTMP-bound TmFDTS.

Spectrophotometric Titrations

Spectrophotometric titrations were performed on a scanning spectrophotometer. ~16 µM enzyme (active sites concentration) was used for titrations with oxidized TmFDTS; ~41 µM enzyme (active sites concentration) was used for titrations with reduced TmFDTS. Enzyme in 0.1 M Tris-HCl, pH 8 at 25 °C was titrated with ligand in the same buffer and absorbance spectra were recorded after each addition. The change in flavin absorbance due to ligand binding was plotted against ligand concentration.

Isothermal Titration Calorimetry

Isothermal titration calorimetry was performed using a MicroCal VP-ITC. Titrations were performed in 0.1 M Tris-HCl, pH 8 (pH determined at 25°C). 50 µM TmFDTS (tetramer concentration) was titrated with 2 mM dUMP or dTMP using 5 µL injections. Data were analyzed using the Origin software provided by MicroCal and fit to either a one site model or a two independent sites model (for more details, see Appendix 1). For a one-site model, the total heat content Q of the solution in the active cell volume V_o is

$$Q = \frac{nM_t \Delta H V_o}{2}\left[1 + \frac{L_t}{nM_t} + \frac{1}{nKM_t} - \sqrt{\left(1 + \frac{L_t}{nM_t} + \frac{1}{nKM_t}\right)^2 - \frac{4L_t}{nM_t}}\right] \qquad (1)$$

where n is the number of binding sites, M_t is the bulk concentration of macromolecule, ΔH is the molar heat of ligand binding, L_t is the bulk concentration of ligand, and K is the binding constant.

For two sets of independent binding sites

$$K_1 = \frac{\theta_1}{(1-\theta_1)[L]} \qquad K_2 = \frac{\theta_2}{(1-\theta_2)[L]} \tag{2}$$

where θ is the fraction of sites occupied by ligand L and [L] is the concentration of free ligand. Q in V_o for two independent binding sites is

$$Q = M_t V_o (n_1 \theta_1 \Delta H_1 + n_2 \theta_2 \Delta H_2) \tag{3}$$

The change in heat after the ith injection {ΔQ(i)} for the one or two-site model is

$$\Delta Q(i) = Q(i) + \frac{\Delta V_i}{V_o}\left[\frac{Q(i)+Q(i-1)}{2}\right] - Q(i-1) \tag{4}$$

where ΔV_i is the change in volume after the ith injection.

Binding Kinetics

The kinetics of binding dUMP or dTMP to oxidized TmFDTS was monitored in a stopped-flow spectrophotometer. Experiments were performed by mixing ~16 μM oxidized TmFDTS (active sites concentration) with 50-200 μM dUMP or dTMP (all concentrations are after mixing) in 0.1 M Tris-HCl, pH 8 at 25°C. Traces were monitored at 390 and 450 nm. Three traces were averaged for the two wavelengths at each nucleotide concentration. The averaged traces at 390 and 450 nm were fit simultaneously to a single exponential using PSI-Plot for each nucleotide concentration. The concentration dependence of the observed rate for dUMP or dTMP was fit to a line in KaleidaGraph, with the slope providing the association rate constant.

Competition with dCMP to Measure dUMP or dTMP Dissociation

The kinetics of dUMP or dTMP dissociation from TmFDTS through competition with dCMP was monitored in a stopped-flow spectrophotometer. Experiments were performed by mixing the preformed TmFDTS-dUMP or dTMP complex with a vast excess of dCMP (0.1-0.2 M after mixing) in 0.1 M Tris-HCl, pH 8 at 25°C. For experiments using oxidized enzyme, 21 µM of the TmFDTS-dUMP or dTMP complex were used (active sites after mixing); for experiments using reduced enzyme, 83 µM of the TmFDTS-dUMP or dTMP complex were used (active sites after mixing). Traces were monitored at 390 nm for the oxidized TmFDTS-dUMP complex, 480 nm for the oxidized TmFDTS-dTMP complex, and 370 nm for the reduced TmFDTS complexes. Traces were fit to sums of exponentials in KaleidaGraph. In all cases, the rate constant were the same for 0.1 M and 0.2 M dCMP, indicating that a sufficient amount of dCMP was used and that the observed rate constant corresponded to the dissociation rate constant for dUMP or dTMP binding to TmFDTS.

Global Fitting

The kinetic traces for nucleotide binding to TmFDTS and the competition experiments with dCMP were fit globally in Berkeley Madonna using the differential equations for the mechanism depicted in Figure 3 - 16 for each nucleotide and flavin redox state combination. The script used for the global fitting in Berekely Madonna can be found in Appendix 2. For the dUMP and oxidized TmFDTS global fitting, the return to baseline of the endothermic event observed by ITC was also included. For the reduced TmFDTS global fitting, it was assumed that the association rate constant was the same

as oxidized TmFDTS. The spectrophotometric titrations were simulated using the model obtained from the global fitting and the experimentally determined change in extinction coefficient upon nucleotide binding.

Results

Flavin-Dependent Thymidylate Synthase Co-Purifies with dTMP

For binding studies, it is important to ensure that the protein being used is free of bound ligands. FDTS binds deoxynucleotides tightly, so that the enzyme is purified with bound dTMP (Mishanina and Kohen, personal communication). We assessed the occupancy of TmFDTS purified with affinity chromatography by analyzing the acid-denatured enzyme using reverse-phase HPLC. Integration of the dTMP peak and the FAD peak showed that dTMP was present at approximately half the flavin concentration. Since TmFDTS is a tetramer, half of the active sites of TmFDTS likely co-purified with dTMP.

The co-purified dTMP and FAD were removed by making apo-protein using previously established methods.[5] FAD was then added to apo-TmFDTS to make holo-TmFDTS, and the excess FAD was removed by desalting. HPLC analysis of the resulting TmFDTS confirmed the absence of dTMP. TmFDTS treated in this way was able to bind dUMP or dTMP and could convert dUMP into dTMP in the presence of CH_2THF and reductant. The UV/visible absorbance spectrum of product-free TmFDTS had an A450/A375 ratio of 1.4, compared to TmFDTS containing half an equivalent of dTMP, which had an A450/A375 ratio of 1.25. The extinction coefficient at 450 nm (ε_{450})

of TmFDTS without bound dTMP was 12000 $M^{-1}cm^{-1}$. Product-free TmFDTS was used in all subsequent experiments in this study.

Reduction Potentials

The reduction potentials of the flavin in free TmFDTS and TmFDTS in complex with dUMP or dTMP at pH 8, 25 °C were determined using the xanthine/xanthine oxidase method of Massey.[22] The reduction potential of free TmFDTS was -201 mV using 1-hydroxyphenazine as the indicator dye (Figure 3 - 1A). The reduction potential of the TmFDTS-dUMP and TmFDTS-dTMP complexes were -262 mV and -264 mV, respectively, using phenosafranin as the indicator dye (Figures 3 - 1B and 3 - 1C). Nucleotide binding lowers the reduction potential of TmFDTS by ~60 mV. The change in reduction potential of TmFDTS upon binding nucleotides indicates that dUMP and dTMP bind to reduced FDTS 120- and 140-fold weaker, respectively, than to oxidized TmFDTS. The reduction potential for free TmFDTS and the nucleotide-TmFDTS complexes are higher than the potential of the $NADP^+$/NADPH couple (-354 mV at pH 8),[17] indicating that hydride transfer from NADPH to FDTS is favorable regardless of whether or not dUMP or dTMP are bound to the enzyme.

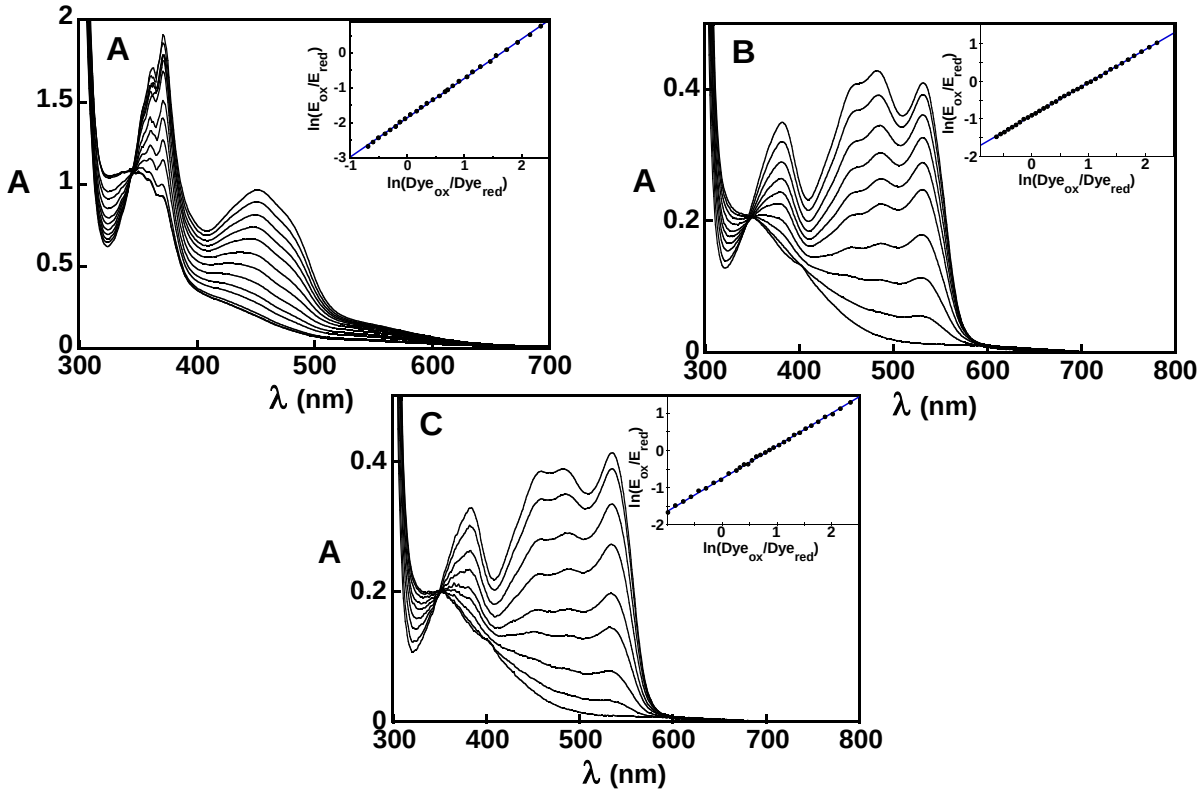

Figure 3 - 1. Determination of reduction potentials. Reduction potentials were determined using the xanthine/xanthine oxidase method of Massey in 0.1 M Tris-HCl, pH 8 at 25°C.[22] (A), the reduction potential of free TmFDTS determined using 1-hydroxyphenazine. (B) and (C), the reduction potential of the dUMP- and dTMPcomplexes, respectively, determined using phenosafranine. The insets show the Nernst plot for determining the potentials. The reduction potential of unbound TmFDTS was -201 mV. The reduction potentials of the dUMP- and dTMP- complexes were -262 mV and -264 mV, respectively.

Spectrophotometric Titrations

A large change in the UV/visible absorbance spectrum of oxidized TmFDTS occurs upon binding dUMP or dTMP. This spectral change can be used to track nucleotide binding in titration experiments. dUMP bound stoichiometrically to ~16 µM active sites oxidized TmFDTS, indicating that dUMP binds very tightly to oxidized TmFDTS (Chapter 2). We performed a similar titration with dTMP, and it also bound stoichiometrically to oxidized TmFDTS (Figure 3 - 2A). The point of saturation was equal to the concentration of active sites (based on flavin ε_{450}) in the sample. Binding of dUMP and dTMP to reduced TmFDTS also produces a change in the absorbance spectrum of the flavin, which can be used to monitor binding of either deoxynucleotide

to reduced TmFDTS (Figure 3 - 2B and 3 - 2C). dUMP and dTMP bound to ~41 μM reduced TmFDTS (active sites concentration) stoichiometrically, indicating that dUMP and dTMP also bind tightly to reduced TmFDTS.

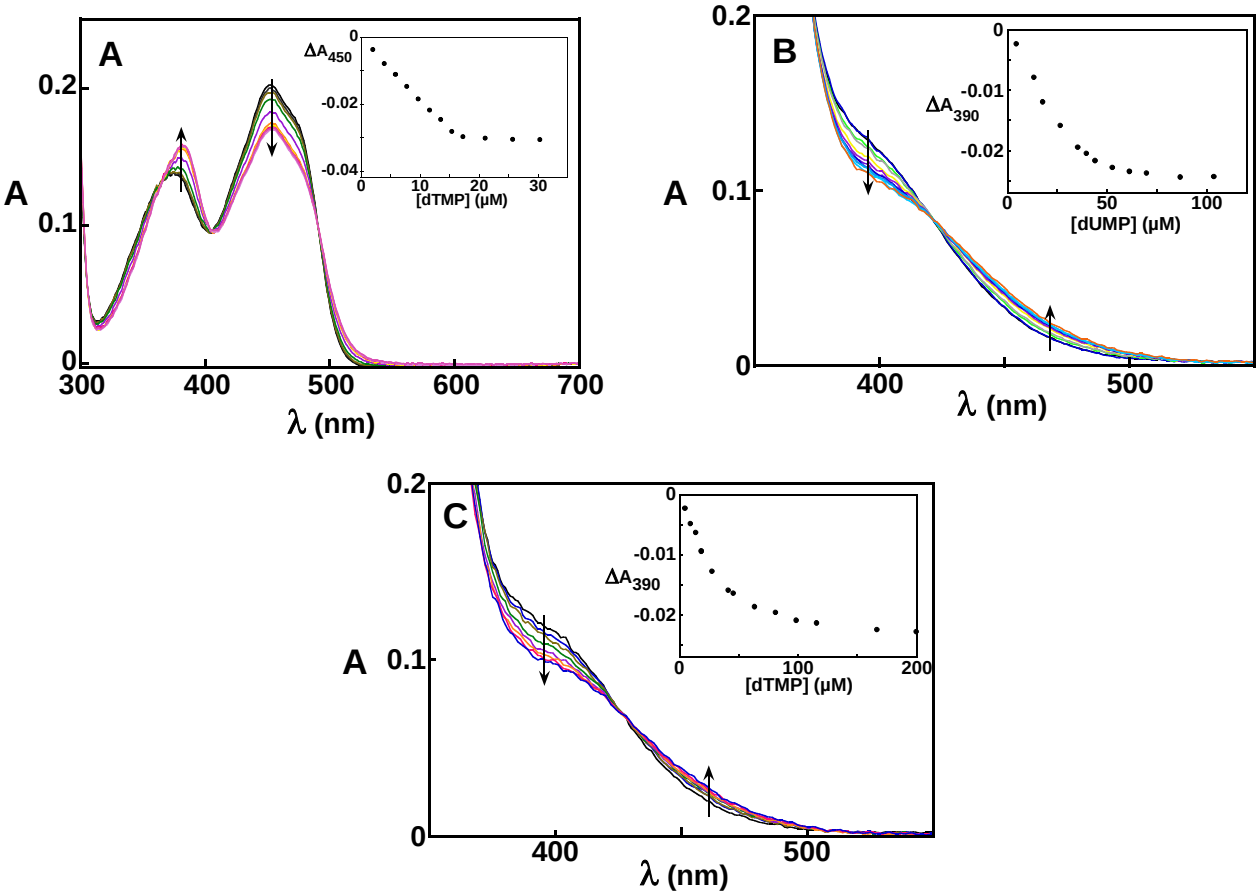

Figure 3 - 2. Absorbance binding titrations. (A), oxidized TmFDTS (~16 μM active sites) was titrated aerobically with dTMP. Reduced FDTS (~41 μM active sites) was titrated anaerobically with dUMP (B) or dTMP (C). The insets show the maximum change in absorbance due to dUMP or dTMP binding as a function of dUMP or dTMP concentration. dUMP or dTMP bound tightly to both oxidized and reduced TmFDTS.

Isothermal Titration Calorimetry

Binding of dUMP or dTMP to oxidized TmFDTS was additionally monitored by isothermal titration calorimetry (ITC). Interestingly, ITC thermograms at 25°C in 0.1 M Tris-HCl, pH 8 of dUMP or dTMP binding to oxidized TmFDTS indicated two sets of binding sites with different enthalpies and binding affinities (Figure 3 - 3A, 3 - 3B). Fitting of the binding isotherm to a two-site model (see Methods) using the concentration of TmFDTS tetramer (50 μM in the titration) showed that approximately two deoxynucleotide molecules bound to each of the two binding sites of the TmFDTS tetramer (Table 3 - 1). The higher affinity site bound dUMP or dTMP 17-18-fold tighter than the weaker affinity site. The site with lower affinity had ~3 kcal/mol more negative enthalpy of binding than the high affinity site for both dUMP and dTMP.

Table 3 - 1: Thermodynamic Parameters for Deoxynucleotide Binding to TmFDTS[a]

Nucleotide, Temperature	N1	K_d1 (nM)	ΔH1 (kcal/mol)	ΔS1 (cal/ molK)	N2	K_d2 (nM)	ΔH2 (kcal/mol)	ΔS2 (cal/ molK)
dUMP, 25°C	1.90 ± .03	1.4 ± .5	-2.73 ± .06	31.5	1.74 ± .03	25 ± 7	-5.56 ± .07	16
dUMP, 65°C	3.82 ± .01	83 ± 19	-16.1 ± .1	-15.1				
dTMP, 25°C	1.99 ± .02	12 ± 2	-0.02 ± .04	36.2	1.8 ± .02	220 ± 27	-3.6 ± .06	18.4
dTMP, 65°C	3.66 ± .01	490 ± 50	-14.9 ± .08	-15.3				

[a]0.1 M Tris-HCl, pH 8

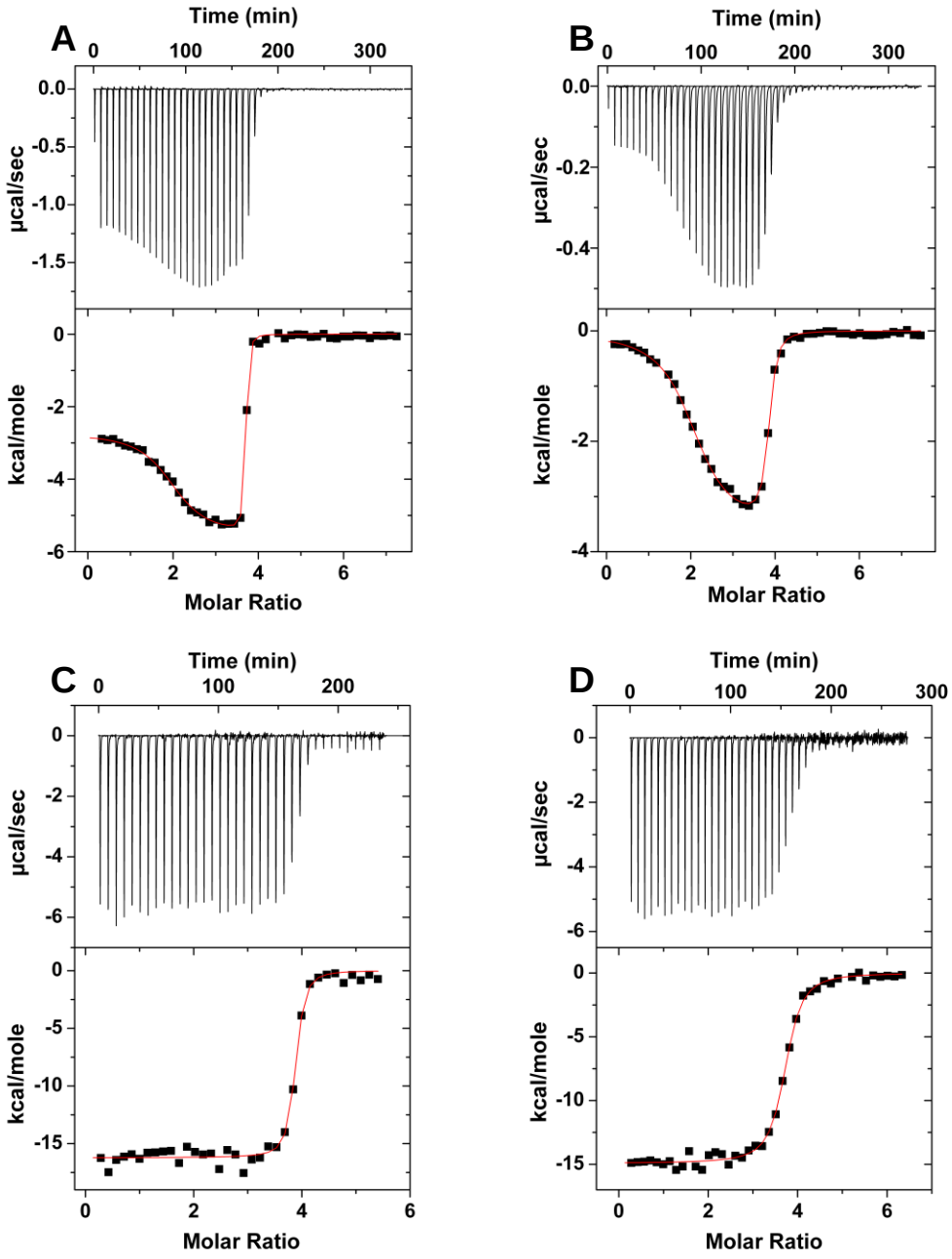

Figure 3 - 3. ITC data for the titration of oxidized TmFDTS with dUMP or dTMP at 25°C and 65°C in 0.1 M Tris-HCl, pH 8. 50 µM oxidized TmFDTS (tetramer) was titrated with either 2 mM dUMP at 25°C (A) or 65°C (C) or with 2 mM dTMP at 25°C (B) or 65°C (D). The red line is the best fit of the data using the two independent sites model for the titrations at 25°C or the one site model for the titrations at 65°C. The thermodynamic parameters from fitting the data can be found in Table 3 - 1.

TmFDTS is from a thermophilic organism whose physiological temperature is around 80°C, raising the possibility that the observation of asymmetry in the four active sites with deoxynucleotide binding might be a result of studying the enzyme at a low temperature. To test this, we performed the ITC titrations at 65°C (close to the physiological temperature of *T. maritima*). The ITC titration of dUMP or dTMP binding to oxidized TmFDTS at 65°C showed only a single binding event that corresponded to ~4 binding sites per enzyme (Figure 3 - 3C and 3 - 3D). One possible explanation for this behavior is the change in pH of the buffer caused by the change in temperature, which could protonate a group on the enzyme; the pH of Tris decreases by ~1 unit as the temperature is increased from 25 to 65°C. However, dUMP binding to oxidized TmFDTS at pH 7, 25°C still showed two sites, indicating that the transition between two sets of sites to one set when increasing the temperature is not due to changes in the pH (Figure 3 - 4). We expanded the temperature dependence by repeating titrations with dUMP over a range of temperatures between 5 and 65°C at 10° intervals (Figure 3 - 5 and Figure 3 - 6). The titrations showed that between 5 and 45°C, two sets of binding sites can be distinguished for dUMP binding to oxidized TmFDTS. However, at 55 and 65°C the titration curves fit to a single set of binding sites. The enthalpy and entropy of binding for both sets of sites decreased linearly with increasing temperature (Table 3 - 2 and Figure 3 - 7A and 3 - 7B). The heat capacity change (ΔC_p) of the binding interaction can be determined from the slope of the change in enthalpy with temperature. ΔC_p is -280 ± 30 cal/molK for the high affinity site and -250 ± 20 cal/molK for the low affinity site. Van't Hoff plots for dUMP binding to both sites were non-linear, which also indicates that ΔC_p is nonzero for the binding interaction (Figure 3 - 7C).[24] From the fits

of the titration curves, the affinity of the higher affinity site is ~18-fold higher than the lower affinity site for the experiments between 5 and 35°C, but is ~11-fold higher at 45°C (Table 3 - 2), suggesting that the transition between the TmFDTS tetramer behaving as a dimer-of-dimers or having four identical sites for deoxynucleotide binding occurs around 45°C. The binding affinities of the single site at 55°C and 65°C were similar to the lower affinity site in the titrations at lower temperatures.

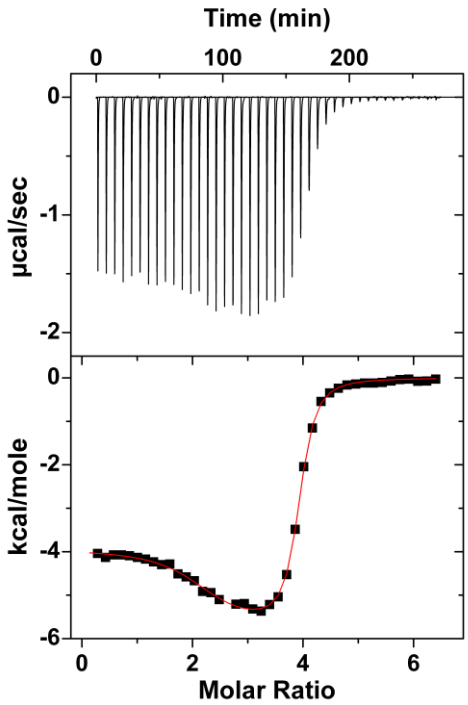

Figure 3 - 4. ITC data for the titration of oxidized TmFDTS with dUMP at 25°C in 0.1 M Tris-HCl, pH 7. The data were fit using the independent two-sites model. The fit gave N1 = 2.1, K_d1 = 32 nM, ΔH1 = -3.93 kcal/mol, ΔS1 = 21.1 cal/mol*K, N2 = 1.76, K_d2 = 530 nM, ΔH2 = -5.82 kcal/mol, ΔS2 = 9.19 cal/mol*K

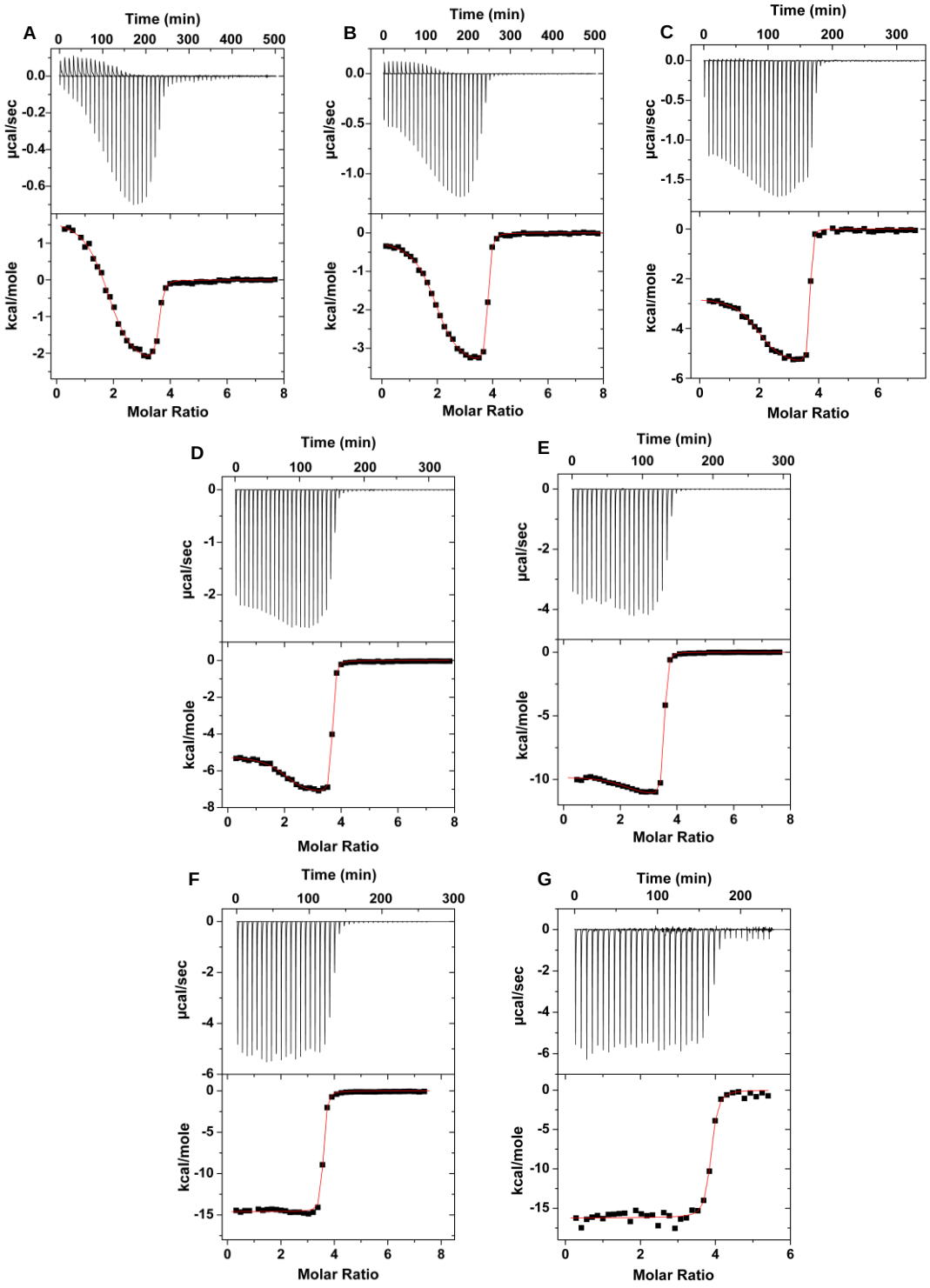

Figure 3 - 5. Temperature dependence of dUMP binding to TmFDTS by ITC in 0.1 M Tris-HCl, pH 8. Data for experiments at 5°C (A), 15°C (B), 25°C (C), 35°C (D), and 45°C (E) were fit using a two independent-sites model. Data for the experiment at 55°C (F) and 65°C (G) was fit using a one site model. In the experiments at 5°C, 15°C, and 25°C an exothermic signal followed by an endothermic signal occurred after each addition of dUMP until ~half of the active sites were filled. The thermodynamic parameters from fitting the data can be found in Table 3 - 2.

Table 3 - 2: Thermodynamic Parameters for dUMP Binding to Oxidized TmFDTS at Different Temperatures[a]

Temperature (°C)	N1	K_d1 (nM)	ΔH1 (kcal/mol)	ΔS1 (cal/mol*K)	N2	K_d2 (nM)	ΔH2 (kcal/mol)	ΔS2 (cal/mol*K)
5	1.74	8.3	1.73	43.2	1.80	140	-2.51	22.4
15	1.87	3.6	-0.13	38.2	1.89	71	-3.59	20.3
25	1.88	1.5	-2.67	31.5	1.75	25	-5.59	16
35	1.94	2.9	-5.19	22.2	1.68	53	-7.38	9.36
45	2.10	4.1	-9.77	7.68	1.38	49	-11.5	-2.67
55					3.51	35	-14.6	-10.4
65					3.82	83	-16.1	-15.1

[a]0.1 M Tris-HCl, pH 8

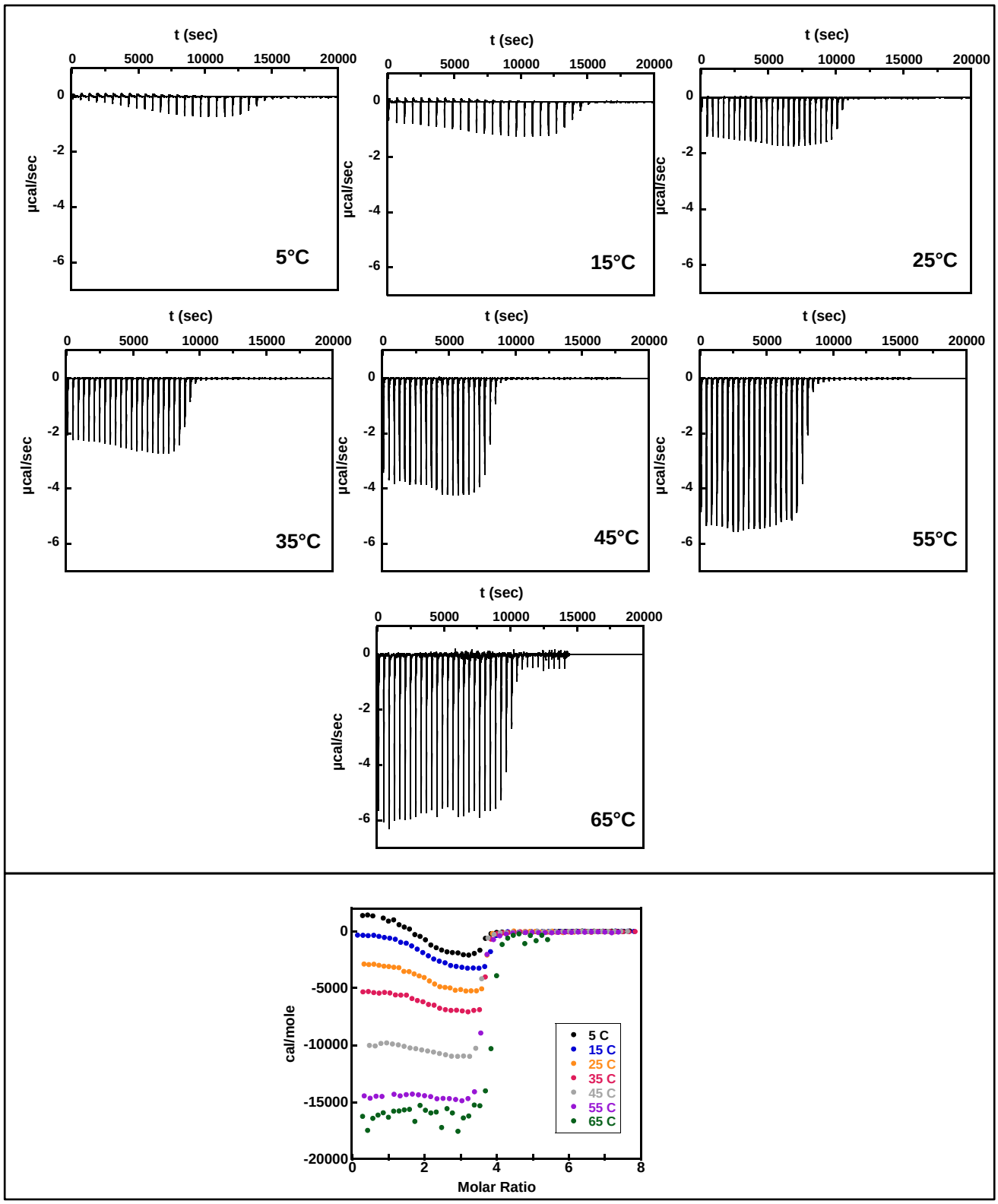

Figure 3 - 6. Overlay of temperature dependence of dUMP binding to TmFDTS by ITC in 0.1 M Tris-HCl, pH 8. Top panel, comparison of raw thermograms. Bottom panel, overlay of heats of injection for the different temperatures.

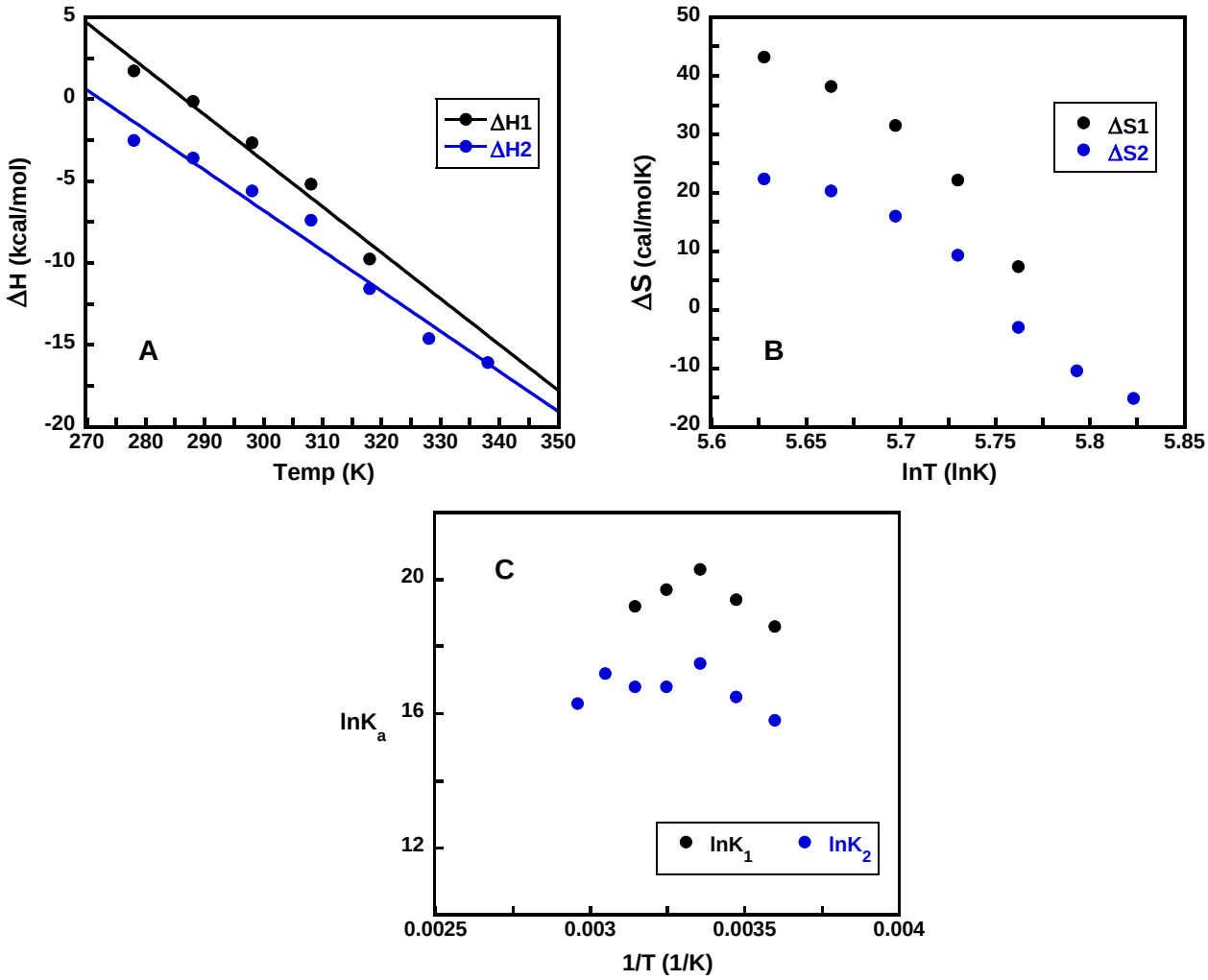

Figure 3 - 7. Temperature dependence of the thermodynamic parameters for dUMP binding to TmFDTS by ITC. (A) Enthalpy change with temperature. The slope provides the change in heat capacity (ΔC_p) of -280 ± 30 cal/molK for the high affinity site and -250 ± 20 cal/molK for the low affinity site. (B) Entropy change plotted against lnT in Kelvin. (C) Van't Hoff plot.

Curiously, in the ITC experiments between 5 and 25°C, addition of dUMP caused an exothermic signal which was followed by an endothermic signal; the amplitude of the endothermic signal became less prevalent throughout the course of the titration, disappearing when roughly half of the active sites were filled (Figure 3 - 5). The endothermic portion was attributed to a slower kinetic event that occurred during binding of dUMP to TmFDTS; it is unlikely that the endothermic portion is due to an instrument

artifact because it only occurred until half the active sites were filled, and the return to baseline from the endothermic event became slower as the temperature decreased. If the half time for a binding event in ITC is lower than the instrument recovery time (typically 10 – 20 seconds), the rate constant of the binding event dictates the exponential for the return to baseline.[25] Since the return to baseline from the endothermic process was very slow (taking several minutes to complete), and became slower as the temperature decreased, the exponential for the recovery from the endothermic process corresponds to the actual observed rate constant for that step. The amplitude for the recovery from the endothermic process was small at 25°C, making it difficult to accurately determine the rate constant for the return to baseline. To enhance the amplitude of the endothermic process, we performed the ITC titration at 25°C with larger injections that corresponded to half the number of binding sites (Figure 3 - 8). This experiment successfully increased the amplitude of the endothermic process; fitting that portion of the ITC thermogram to a single exponential gave an observed rate constant (k_{obs}) of 0.019 s^{-1}.

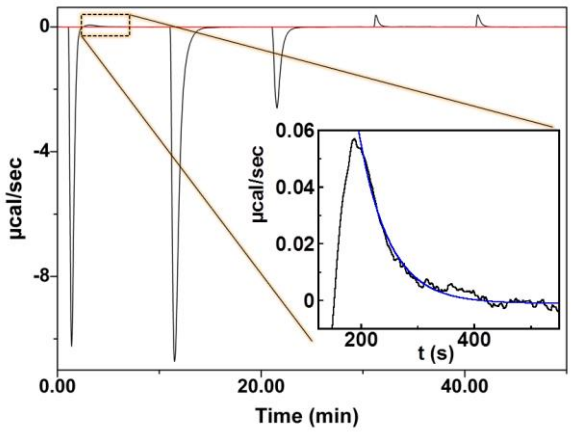

Figure 3 - 8. Kinetics of the return to baseline from the endothermic process detected by ITC when dUMP binds to oxidized TmFDTS. 50 µM oxidized TmFDTS (tetramer) was titrated with injections corresponding to 100 µM additions of dUMP in 0.1 M Tris-HCl, pH 8 at 25°C. The first injection gave an exothermic signal which overshot the baseline and peaked in the endothermic direction. The inset shows the decay from the endothermic signal back to baseline. Fitting the decay to a single exponential gives k_{obs} of 0.019 s^{-1}.

The structure of deoxynucleotide-free TmFDTS shows that histidine-53 (H53) exists in two different conformations in the four active sites of the TmFDTS tetramer (Figure 3 - 9A), indicating that H53 might be involved in producing the two sets of deoxynucleotide binding sites. To test this, an H53A mutant enzyme was titrated with dUMP by ITC at pH 8, 25°C (Figure 3 - 9B). The thermogram still showed two sets of binding sites; however, the binding affinities of the two sets of sites were very similar, such that the Origin software was unable to accurately fit the data to a two-site model (or a one-site model), suggesting that H53 is involved in producing the two sets of deoxynucleotide binding sites.

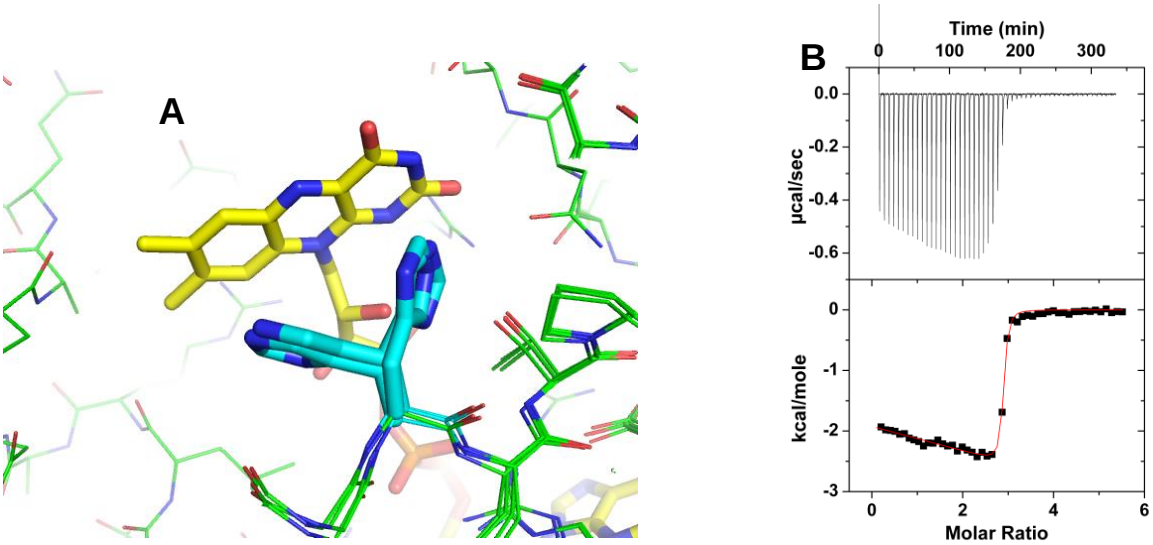

Figure 3 - 9. Involvement of H53 in the two sets of TmFDTS deoxynucleotide binding sites. (A) Overlay of the four active sites of deoxynucleotide-free TmFDTS (PDB code 1KQ4). H53 (cyan) is in two conformations in the four active sites of the TmFDTS homotetramer. Only one FAD (yellow) is shown for clarity. (B) dUMP binding to an H53A TmFDTS mutant enzyme by ITC in 0.1 M Tris-HCl, pH 8 at 25°C. The data could not be accurately fit to a two-site model, as indicated by the large error bars on the parameters of the fit – the fit parameters were N1 = 1.41 ± 1.4, K_d1 = 31 ± 105 nM, ΔH1 = 0.17 ± 5.2 kcal/mol, ΔS1 = 34.9 cal/molK, N2 = 1.44 ± 1.3, K_d2 = 40 ± 92 nM, ΔH2 = - 4.58 ± 5.23 kcal/mol, ΔS2 = 18.5 cal/molK.

The ITC titration at pH 8, 25°C was also performed in phosphate buffer and PIPES, which have different enthalpies of deprotonation than Tris in an attempt to quantify the number of protons released or taken up when dUMP binds to TmFDTS (Figure 3 - 10). The enthalpy of deprotonation for the pK_a values near 8 of phosphate buffer, PIPES, and Tris are 0.86 kcal/mol, 2.68 kcal/mol, and 11.34 kcal/mol, respectively.[26] If protons are released or absorbed upon ligand binding, the ΔH values from the titration should scale with the difference in ionization enthalpy between buffers multiplied by the number of protons released or taken up during ligand binding. The titrations in the different buffers all fit to a two-site model. The binding enthalpy values of the two sites were significantly more negative in Tris buffer than in phosphate buffer or PIPES, consistent with protons being released when dUMP binds to TmFDTS (Table 3 - 3). However, the binding enthalpy values for the two sites did not scale linearly with the ionization enthalpy of the different buffers; in fact, the binding enthalpy values in phosphate were more negative than in PIPES. The binding affinities for the two sites were nearly identical in Tris and PIPES; however, the affinities for the two sites in phosphate buffer were significantly higher (Table 3 - 3). This indicates that phosphate binds the dUMP binding site of TmFDTS, which would affect the binding enthalpies measured in phosphate buffer.

Figure 3 – 11 shows the dependence of the binding enthalpy for the two sites with the enthalpy of ionization for the two buffers that do not inhibit dUMP binding (Tris and PIPES). Linear regression of the data indicates that 0.25 and 0.43 protons are released by the complex when dUMP binds to the high affinity site and the low affinity site, respectively, with a sum of 0.68 protons released when dUMP binds to the entire

TmFDTS homotetramer. With these preliminary data (only two buffers examined), a fraction of a proton released suggests that an ionizable group is partially ionized in unbound dUMP and TmFDTS, in the TmFDTS-dUMP complex, or both; i.e., the pK_a of the ionizable group is near pH 8 in the complex or when free in solution. It also indicates that the pK_a of the ionizable group is lowered when dUMP binds to TmFDTS.

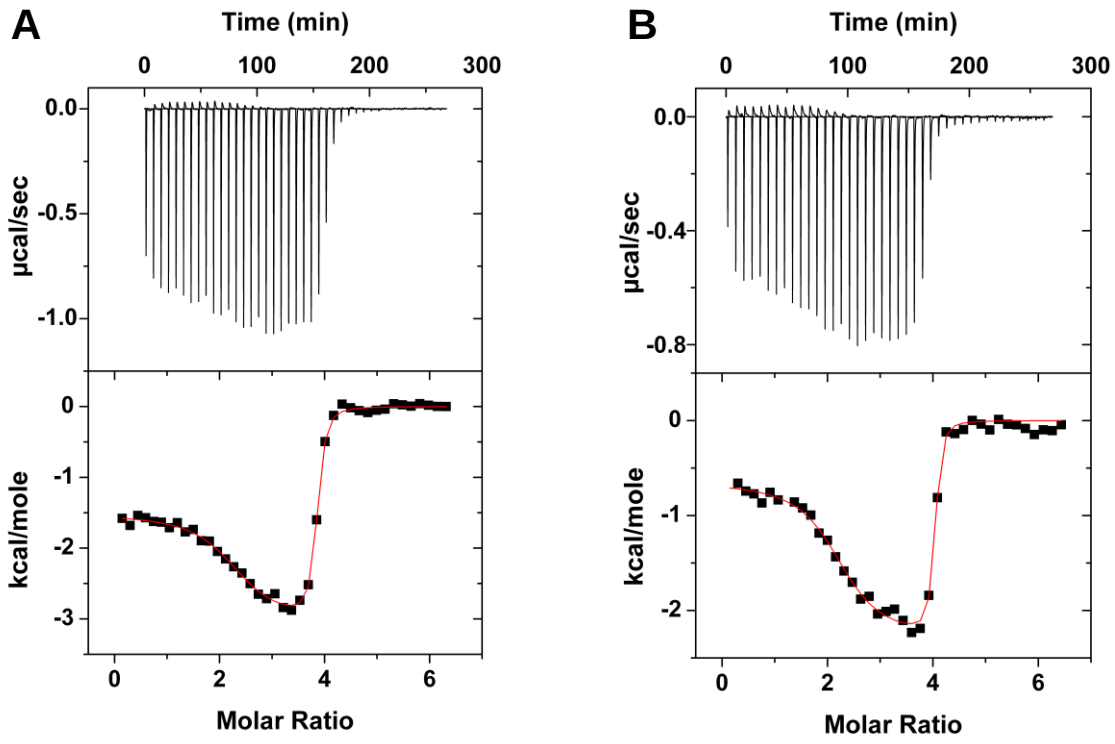

Figure 3 - 10. Titration of TmFDTS with dUMP in different buffers by ITC. TmFDTS was titrated with dUMP at pH 8, 25°C in 0.1 M sodium phosphate (A) or 0.1 M PIPES-Na (B). Both titrations fit to a two-site model. The thermodynamic parameters from the fit can be found in Table 3 - 3.

Table 3 - 3: Thermodynamic Parameters for dUMP Binding to TmFDTS in Different Buffers at pH8, 25°C[a]

Buffer	N1	K_d1 (nM)	ΔH1 (kcal/mol)	ΔS1 (cal/ molK)	N2	K_d2 (nM)	ΔH2 (kcal/mol)	ΔS2 (cal/ molK)
Tris	1.90 ± .03	1.4 ± .5	-2.73 ± .06	31.5	1.74 ± .03	25 ± 7	-5.56 ± .07	16.0
phosphate	2.18 ± .03	9.9 ± 2.1	-1.49 ± .03	31.6	1.60 ± .03	166 ± 18	-3.13 ± .05	20.5
PIPES	2.28 ± .03	1.4 ± .5	-0.60 ± .02	38.5	1.68 ± .03	35 ± 9	-1.83 ± .03	28.0

[a]0.1 M concentration

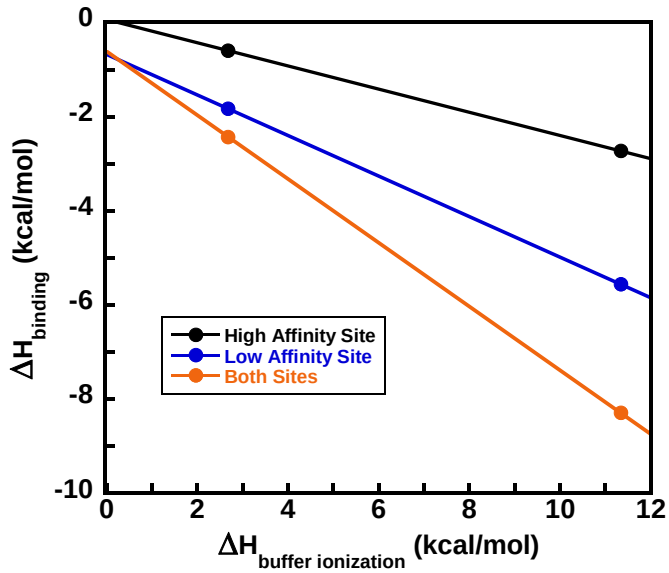

Figure 3 - 11. Binding enthalpy of the two sets of sites for dUMP binding to TmFDTS at pH 8, 25°C as a function of the ionization enthalpy of the reaction buffer. Two buffers were used: Tris (ionization enthalpy of 11.34 kcal/mol) and PIPES (ionization enthalpy of 2.68 kcal/mol). The slope of the linear regression gives the number of protons released from the complex when dUMP binds to TmFDTS. 0.25 protons are released when dUMP binds to the high affinity site, 0.43 when dUMP binds to the low affinity site, and 0.68 protons when all sites are bound.

Circular Dichroism

Enzyme-bound flavins generally have a detectable circular dichroism (CD) signal in the visible region that is sensitive to changes in the environment of the flavin. Oxidized TmFDTS (50 µM active sites concentration) was titrated with dUMP at 25°C and CD spectra were recorded between 300 and 500 nm after each addition. During the titration, two isodichroic points were present at different points in the titration – one at 365 nm that appeared when the first half of the active sites were filled (0-25 µM) and one at 372 nm that appeared when the second half of the active sites were filled (25-50 µM) (Figure 3 - 12A) – consistent with TmFDTS having two sets of sites with different affinities for binding of dUMP at 25°C. When the same titration was performed at 65°C, only a single isodichroic point at 365 nm was present and the signal change at 372 nm had a linear response until all of the active sites were filled (0-50 µM), consistent with all sites of the TmFDTS tetramer binding dUMP with the same affinity (Figure 3 - 12B).

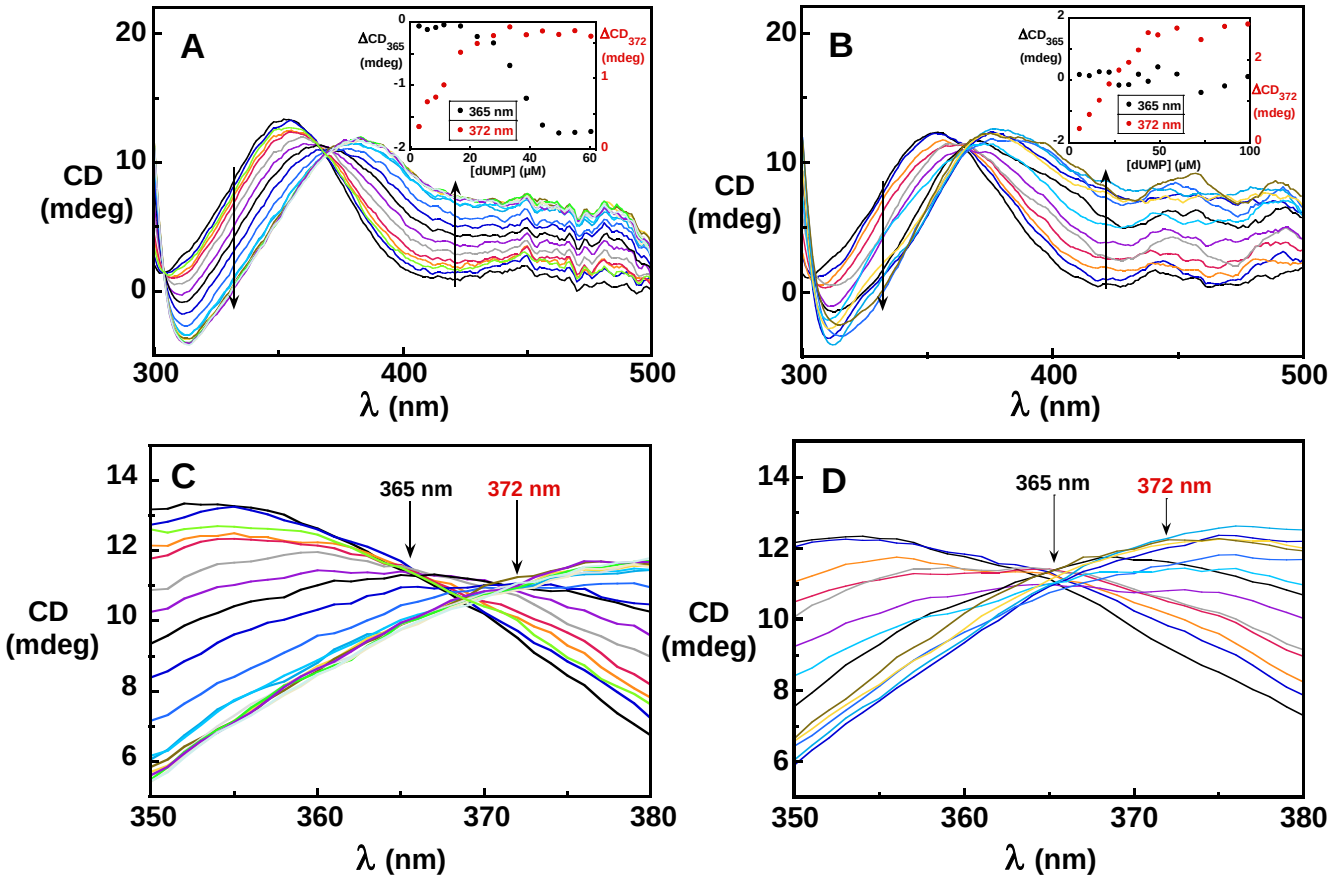

Figure 3 - 12. CD binding titrations. 50 μM oxidized TmFDTS (active sites) was titrated with dUMP at 25°C (A) or 65°C (B) in 0.1 M Tris-HCl, pH 8 while monitoring changes in the CD spectrum of the flavin. At 25°C, there were two isodichroic points at 365 nm and 372 nm that occurred during different portions of the titration. At 65°C, there was a single isodichroic point at 365 nm throughout the entire titration. The insets show the change in CD signal at 365 nm and 372 nm as a function of dUMP concentration. (C) and (D) zoom in on the isodichroic points for the titration at 25°C and 65°C, respectively.

Kinetics of Nucleotide Binding

Binding of dUMP or dTMP to oxidized TmFDTS causes a significant change in the absorbance spectrum of the flavin (Chapter 2 and Figure 3 - 2A). Binding of dUMP or dTMP to oxidized TmFDTS (16 µM active sites after mixing) was monitored at 25°C using a stopped-flow spectrophotometer. We were unable to perform the experiments at high temperatures due to limitations of the instrument. Traces at 390 and 450 nm for either deoxynucleotide fit to a single exponential at all concentrations of deoxynucleotide (Figures 3 - 13A to 3 - 13D). Traces at 390 nm and 450 nm were fit simultaneously using a single k_{obs} for each concentration of dUMP or dTMP. The observed rate constant for binding of either deoxynucleotide increased linearly with nucleotide concentration, consistent with a one-step bimolecular event (Figure 3 - 13E). The observation that only a single exponential is observed in the experiment at 25°C suggests that the two sets of sites detected by ITC and CD have similar association rate constant (k_{on}) values. The slope from the concentration dependence of the observed rate constant provides k_{on} for binding of the nucleotide to oxidized TmFDTS. k_{on} for binding of dUMP to oxidized TmFDTS was $4.4 \pm 0.1 \times 10^6$ $M^{-1}s^{-1}$ whereas k_{on} for binding of dTMP to oxidized TmFDTS was $3.5 \pm 0.1 \times 10^6$ $M^{-1}s^{-1}$. The y-intercept from the concentration dependence of the observed rate constant theoretically corresponds to the dissocation rate constant (k_{off}) for ligand binding in a simple one-step mechanism. However, the y-intercepts for binding of dUMP or dTMP to oxidized TmFDTS were too small to provide an accurate value for k_{off}, and the presence of two sets of sites complicates the interpretation of the y-intercept. We were unable to perform similar experiments for nucleotide binding to reduced TmFDTS because the spectral change

upon binding dUMP or dTMP to reduced TmFDTS was too small to observe by stopped-flow.

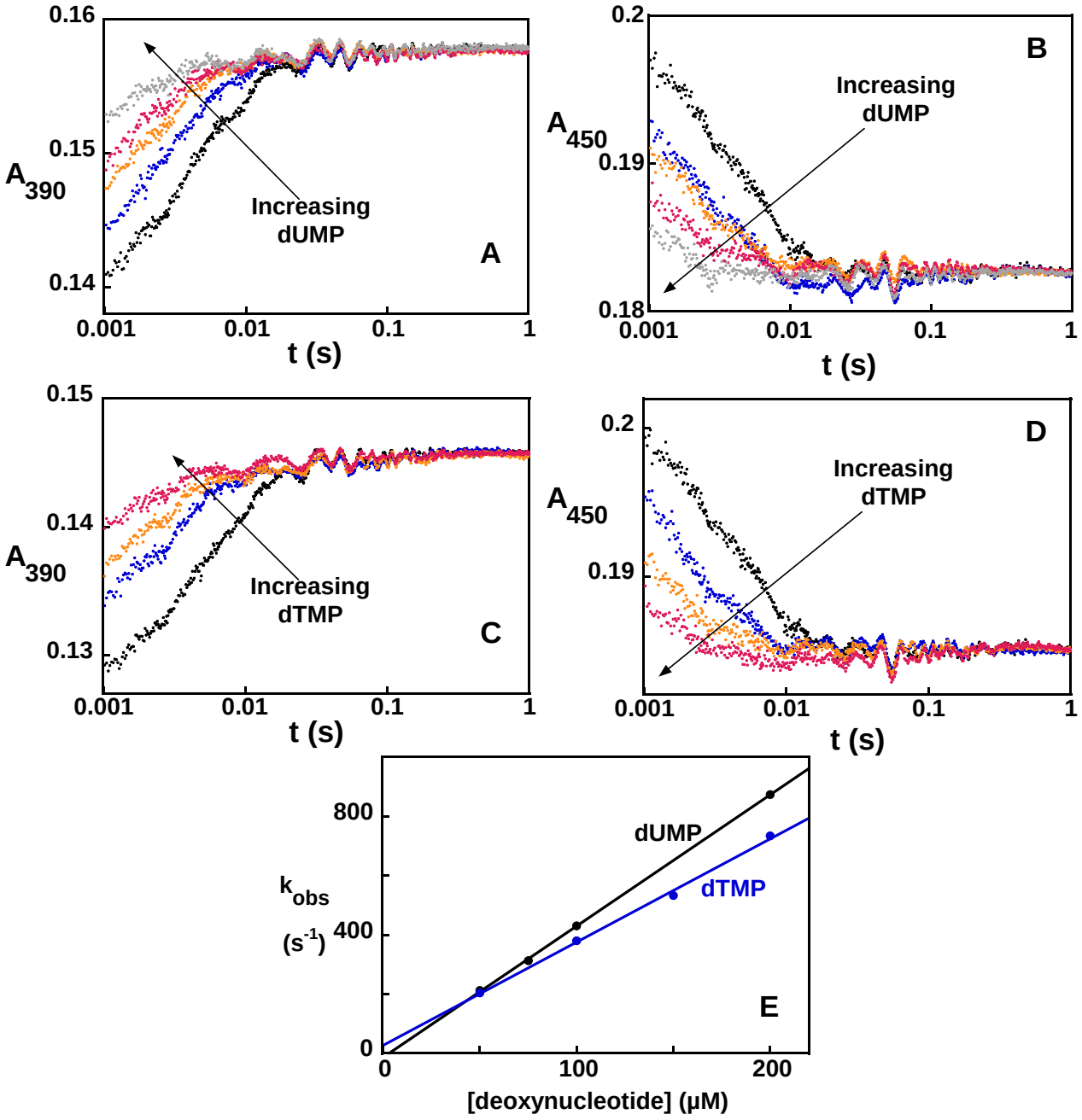

Figure 3 - 13. Deoxynucleotide binding kinetics. Binding was observed at 390 nm and 450 nm when ~16 μM oxidized TmFDTS (active sites after mixing) was mixed with 50 – 200 μM dUMP ((A) and (B)) or dTMP (((C) and (D)) (after mixing) in 0.1 M Tris-HCl, pH 8 at 25°C. Three traces were collected for each dUMP and dTMP concentration at each wavelength. Traces at all concentrations fit to a single exponential. (E) Dependence of the observed rate constant as a function of dUMP or dTMP concentration. The observed rate constant increased linearly with dUMP or dTMP concentration, giving association rate constants of 4.4 ± 0.1 x 10^6 $M^{-1}s^{-1}$ and 3.5 ± 0.1 x 10^6 $M^{-1}s^{-1}$, respectively, for dUMP and dTMP.

Competition with dCMP

We were unable to determine k_{off} for dUMP and dTMP from the intercepts in the binding kinetics studies. An alternative way to determine k_{off} is to use a competitor that has a different UV/visible absorbance spectrum when bound to the enzyme. 2'-Deoxycytidine-5'-monophosphate (dCMP) fulfills that requirement. The absorbance spectrum of the oxidized TmFDTS-dCMP complex is different from both the oxidized TmFDTS-dUMP and oxidized TmFDTS-dTMP complexes (Figure 3 - 14A). dCMP binds to oxidized TmFDTS with a K_d of 13 µM based on spectrophotometric titrations.

The dissociation of dTMP from the oxidized TmFDTS-dTMP complex was monitored in a stopped-flow spectrophotometer at 480 nm by mixing the pre-formed oxidized TmFDTS-dTMP complex against an excess concentration of dCMP. Traces fit to two exponentials that each contributed ~50% of the total absorbance change (Figure 3 - 14B). The observed rate constants for the first and second phase were 0.33 ± 0.06 s^{-1} and 0.060 ± 0.010 s^{-1}, respectively. The observed rate constants were identical for 100 mM dCMP and 200 mM dCMP (after mixing), indicating that the concentration of dCMP was high enough to make k_{off} rate-limiting. Two phases with similar amplitudes in the dissociation of dTMP from oxidized TmFDTS are consistent with two sets of binding sites with different affinities, as was observed by ITC and CD. However, only a single exponential was observed when dTMP binds to oxidized TmFDTS. This behavior suggests that the two binding sites have identical k_{on} values, but different k_{off} values. The two k_{off} values and the single k_{on} give K_d values of 17 ± 3 nM and 94 ± 16 nM for the two sites, which are similar to the K_d values for dTMP binding to oxidized TmFDTS obtained through the absorbance titration and ITC experiments (Table 3 - 4).

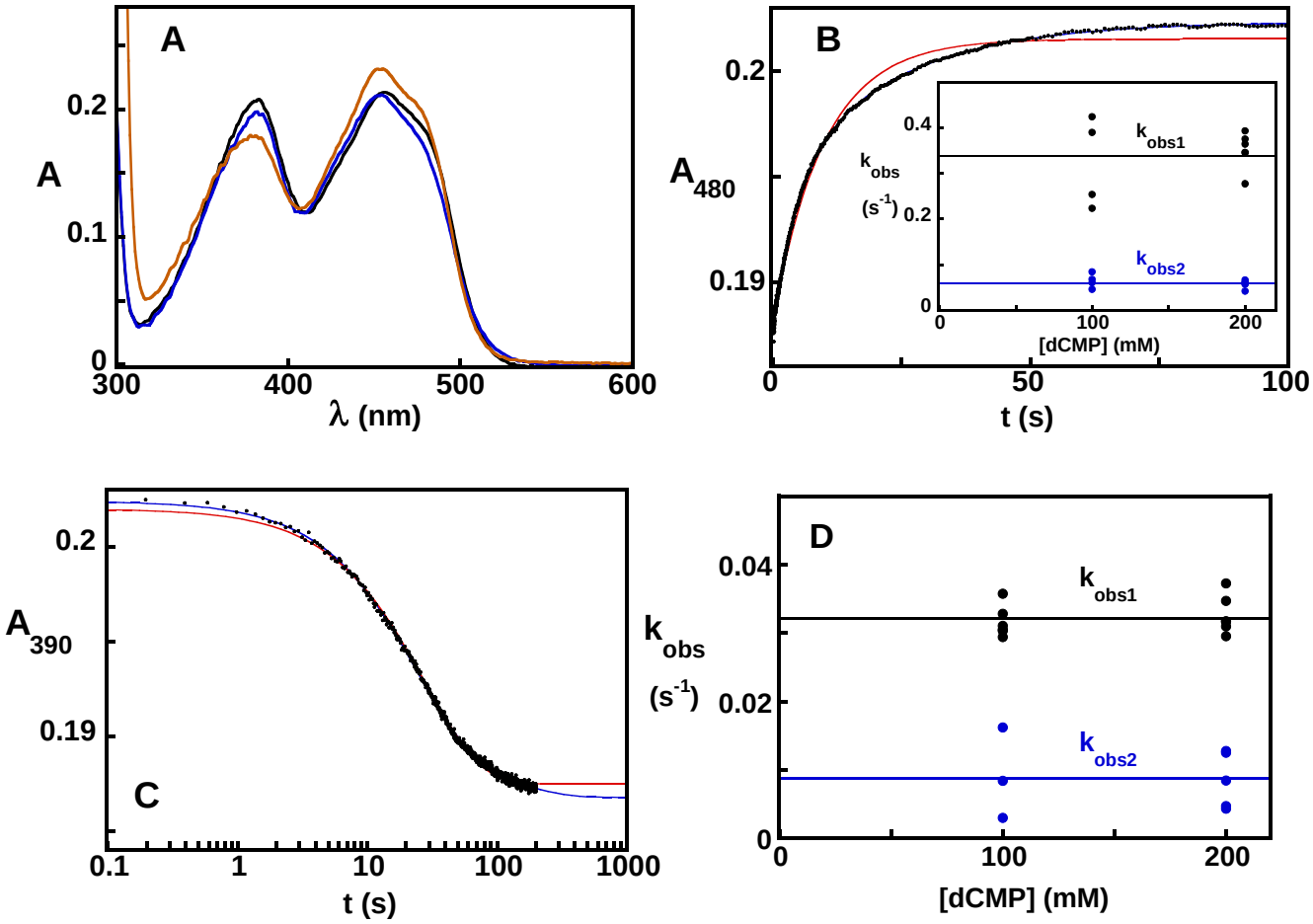

Figure 3 - 14. Competition of oxidized TmFDTS complexes with dCMP. (A) Absorbance spectra of oxidized TmFDTS in complex with saturating concentrations of different deoxynucleotides in 0.1 M Tris-HCl, pH 8 at 25°C. Black, dUMP; blue, dTMP; orange, dCMP. (B) Kinetic trace observed at 480 nm when 21 µM oxidized TmFDTS-dTMP complex (active sites after mixing) was mixed with 100 – 200 mM dCMP (after mixing). Traces were fit to two exponentials, with each exponential contributing ~50% of the total signal change. The red line is an attempt to fit the data to a single exponential, which poorly fits the data. The observed rate constants for the two phases did not vary between 100 and 200 mM dCMP (inset), indicating that saturating concentrations of dCMP were used and that the k_{obs} values correspond to the dissociation rate constants for the two sets of binding sites. The k_{off} values for dTMP dissociating from oxidized TmFDTS were 0.33 ± 0.06 s^{-1} and 0.06 ± 0.01 s^{-1}. (C) Kinetic trace observed at 390 nm when 21 µM oxidized TmFDTS-dUMP complex (active sites after mixing) was mixed with 100 – 200 mM dCMP (after mixing). Traces fit best to two exponentials (blue line) and did not fit as well to a single exponential (red line). A log scale is used for the x-axis to highlight the differences between fitting to one and two exponentials. (D) The k_{obs} values did not vary with dCMP concentration. The k_{off} values for dUMP dissociating from oxidized TmFDTS were 0.032 ± 0.002 s^{-1} and 0.009 ± 0.005 s^{-1}.

Table 3 - 4: Rate Constants and Dissociation Constants for Deoxynucleotide Binding to TmFDTS, pH 8 at 25 °C

Nucleotide	enzyme		k_{on} ($M^{-1}s^{-1}$)	k_{off} (s^{-1})	K_d from kinetics	K_d from ITC
dUMP	oxidized	site A	$4.4 \pm 0.1 \times 10^6$	0.009 ± 0.005	2 ± 1 nM	1.4 ± 0.5 nM
		site B		0.032 ± 0.002	7.3 ± 0.5 nM	25 ± 7 nM
	reduced	site A		1.2 ± 0.1	270 ± 20 nM[a]	
		site B		7.1 ± 0.6	1.6 ± 0.1 µM[a]	
dTMP	oxidized	site A	$3.5 \pm 0.1 \times 10^6$	0.06 ± 0.01	17 ± 3 nM	12 ± 2 nM
		site B		0.33 ± 0.06	94 ± 17 nM	220 ± 27 nM
	reduced	site A		14 ± 1	4 ± 0.3 µM[a]	
		site B		>80	> 23 µM[a]	

[a]Calculated using the k_{on} determined for oxidized TmFDTS

Analogous competition experiments were performed with the oxidized TmFDTS-dUMP complex to determine k_{off} for dUMP. Traces were monitored at 390 nm instead of 480 nm because the signal change between the oxidized TmFDTS-dUMP and the oxidized TmFDTS-dCMP complexes was larger at 390 nm compared to 480 nm. Traces were fit to two exponentials, with the first phase contributing ~85% of the total signal change (Figure 3 - 14C). The observed rate constants for the first and second exponentials were 0.032 ± 0.002 s^{-1} and 0.009 ± 0.005 s^{-1}, respectively, giving K_ds of 7.3 ± 0.5 nM and 2 ± 1 nM when combined with k_{on}, which again are similar to the values obtained through the absorbance titrations and ITC experiments (Table 3 - 4). After completion of the competition reaction with dCMP, the A450/A390 ratio in the UV/visible absorbance spectrum was 1.24 ± 0.01, which is not consistent with the spectrum of the oxidized TmFDTS-dCMP complex (A450/A390 = 1.41 ± 0.02) expected if all of the dUMP in the complex was replaced by dCMP (Figure 3 - 15A). Instead, the A450/A390 ratio was approximately half-way between that of the oxidized TmFDTS-dCMP complex and the oxidized TmFDTS-dUMP complex (A450/A390 = 1.10 ± 0.01), suggesting that dUMP in half the active sites of the oxidized TmFDTS-dUMP complex failed to dissociate when competed with excess dCMP, causing the amplitude for the second phase in the competition reaction to be relatively small. To test this, the unbound deoxynucleotides were removed from the enzyme after the competition reaction using a desalting column; the resulting enzyme was denatured with HCl to release the bound deoxynucleotides, which were then analyzed by HPLC. Integration of the HPLC peaks indicated the presence of dUMP at roughly half the concentration of flavin, consistent with dUMP not dissociating from half of the active sites in the

competition experiment (Figure 3 - 15B). The completed reaction from the TmFDTS-dTMP competition experiment was also desalted and analyzed for tightly bound deoxynucleotides; the A450/A390 ratio was 1.38 and only a trace amount of dTMP (10% of the flavin concentration) was detected by HPLC, consistent with the majority of dTMP dissociating from both populations of the enzyme (Figure 3 - 15C).

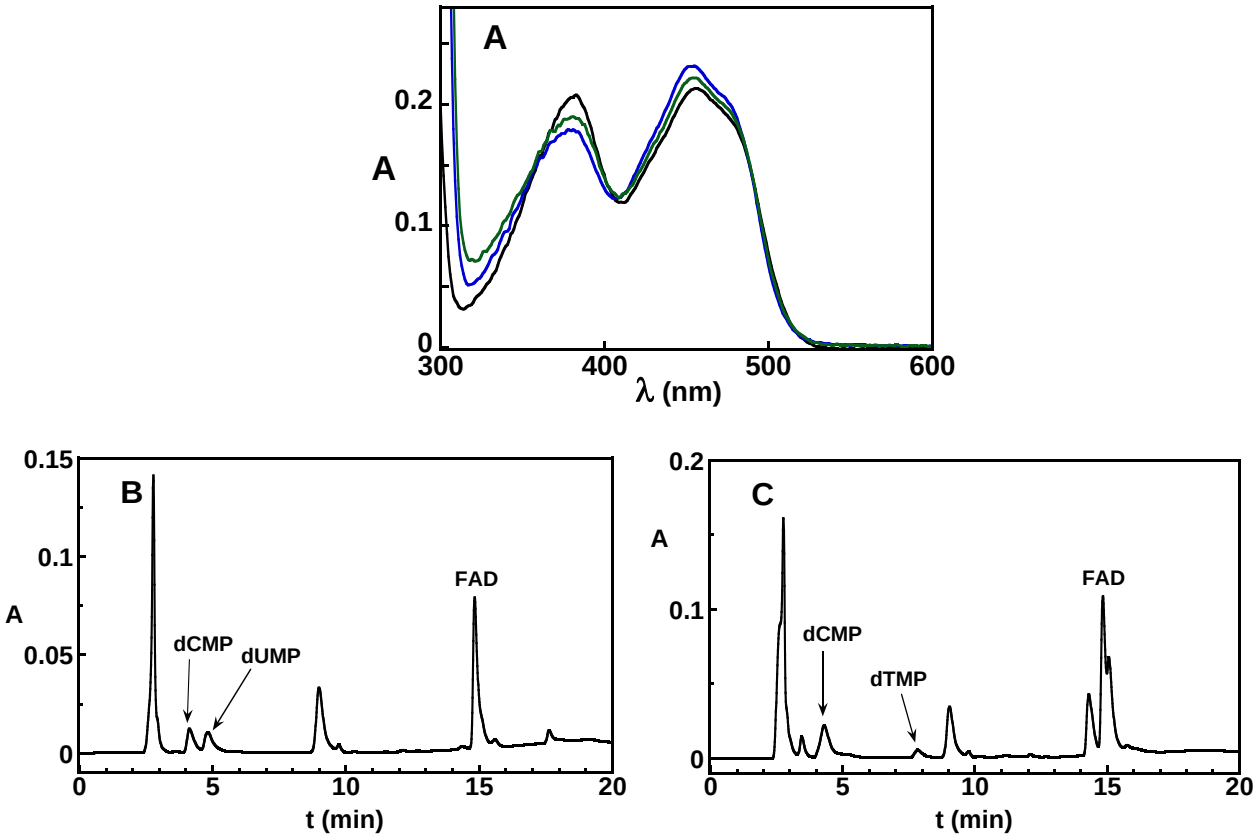

Figure 3 - 15. dUMP does not completely dissociate from oxidized TmFDTS in the competition experiments with dCMP. (A) the UV/visible absorbance spectrum of oxidized TmFDTS at the end of the competition experiment in Figure 8C (green) is halfway between the spectrum of the oxidized TmFDTS-dUMP complex (black) and the spectrum of the oxidized TmFDTS-dCMP complex (blue). (B) HPLC chromatogram of the compounds that were bound to TmFDTS at the end of the experiment in Figure 8C. The concentrations of dCMP (4 min) and dUMP (5 min) were ~half the concentration of flavin (15 min), indicating that dCMP failed to replace the dUMP in half of the active sites of oxidized TmFDTS. (C) HPLC chromatogram of the compounds that were bound to TmFDTS at the end of the experiment in Figure 8B. The concentration of dTMP (8 min) was ~10% of the concentration of flavin (15 min), indicating that most of the dTMP dissociated from oxidized TmFDTS. The concentration of dCMP (4 min) was ~70% of the concentration of flavin. The peak at 9 min in the chromatograms has the same UV/visible spectrum and retention time as adenosine-5'-monophosphate. It likely resulted from the hydrolysis of FAD when acid-denaturing the enzyme.

The UV/visible absorbance spectrum of the reduced TmFDTS-dCMP complex was also different from the reduced TmFDTS-dUMP and reduced TmFDTS-dTMP complexes (Figure 3 - 16A). Competition experiments were performed using excess dCMP with the reduced TmFDTS-dUMP and reduced TmFDTS-dTMP complexes to obtain k_{off} values for dUMP and dTMP bound to reduced TmFDTS. The UV/visible absorbance spectrum of the reduced TmFDTS-dUMP and reduced TmFDTS-dTMP complexes were identical. The dissociation of dUMP or dTMP from reduced TmFDTS was monitored at 370 nm using a stopped-flow spectrophotometer. Traces for the dissociation of dUMP fit to two exponentials, with each contributing half of the total signal change, again consistent with two binding sites (Figure 3 - 16B). k_{off} for the first phase was 7.1 ± 0.6 s^{-1} and k_{off} for the second phase was 1.2 ± 0.1 s^{-1} – the k_{off} values for the two sets of binding sites were ~200-fold faster with reduced TmFDTS than with oxidized TmFDTS (Table 3 - 4). For dissociation of dTMP, only one exponential was observed due to the speed of the reaction and the presence of a mixing artifact within the first 50 msec (Figure 3 - 16C and 3 - 16D). The mixing artifact was the result of the large viscosity difference between the enzyme solution and the 100-200 mM dCMP. k_{off} for the observable phase was 14 ± 1 s^{-1}. Extrapolation of the observable phase back to 0 seconds indicates that it accounted for only half of the total signal change between reduced TmFDTS-dTMP and reduced TmFDTS-dCMP. The rest of the signal change corresponds to a first, faster exponential that ended within the mixing artifact (50 msec). This provides a lower limit for k_{off} of ~80 s^{-1} for the first unobservable phase. The k_{off} values for both sets of dTMP binding sites were ~230-fold faster or more with reduced TmFDTS than with oxidized TmFDTS (Table 3 - 4).

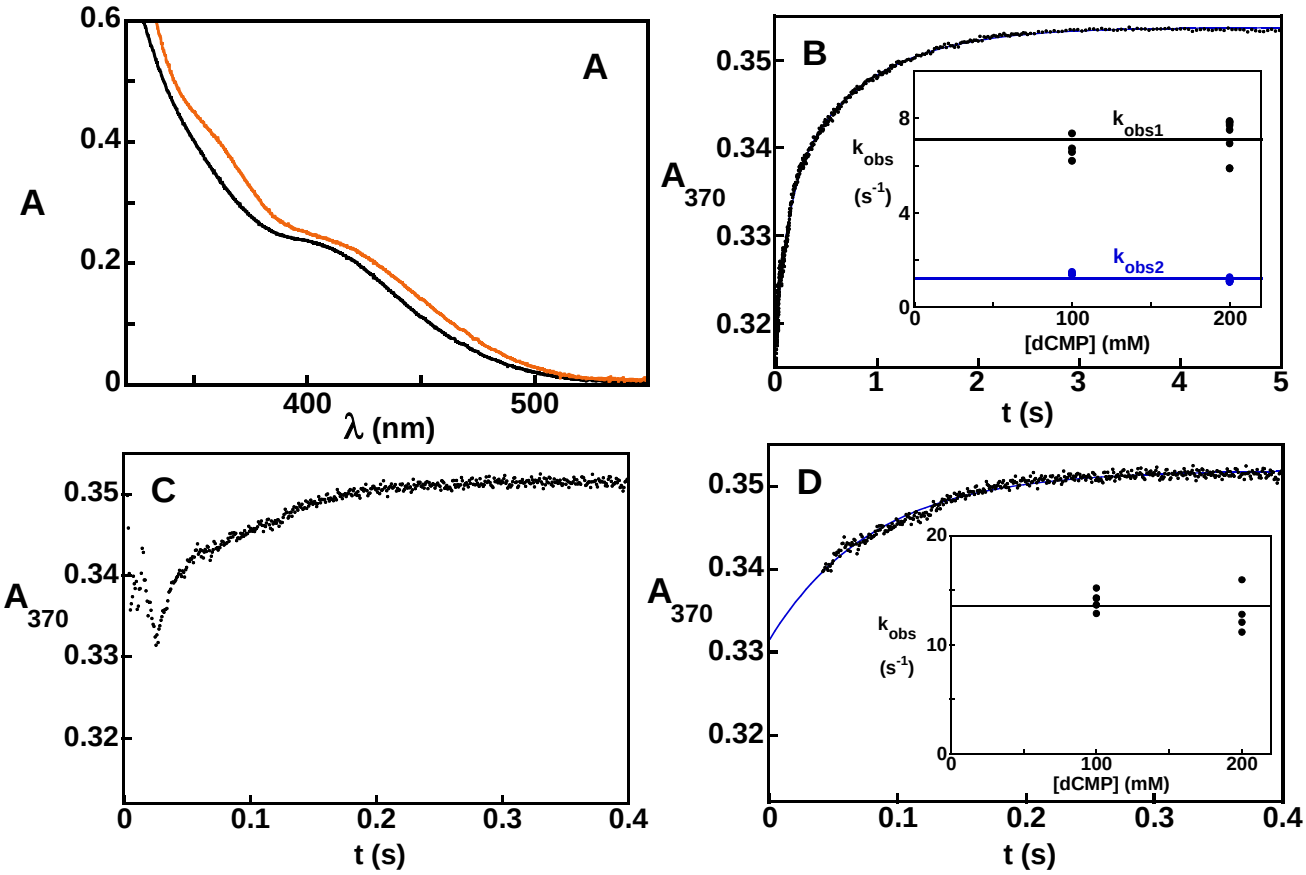

Figure 3 - 16. Competition of reduced TmFDTS complexes with dCMP. Absorbance spectra of reduced TmFDTS in complex with saturating concentrations of different deoxynucleotides in 0.1 M Tris-HCl, pH 8 at 25°C. Black, dUMP or dTMP; orange, dCMP. (B) Kinetic trace observed at 370 nm when 83 µM reduced TmFDTS-dUMP complex (active sites after mixing) was mixed with 100 – 200 mM dCMP (after mixing). Traces fit to two exponentials, with each exponential contributing ~50% of the total signal change. The k_{obs} values did not vary (inset), indicating that saturating concentrations of dCMP were used and that the k_{obs} values correspond to the k_{off} values for the two sets of binding sites. The k_{off} values for dUMP dissociating from reduced TmFDTS were 7.1 ± 0.6 s^{-1} and 1.2 ± 0.1 s^{-1} for the two sets of binding sites. (C) Kinetic trace observed at 370 nm when 83 µM reduced TmFDTS-dTMP complex (active sites after mixing) was mixed with 100 – 200 mM dCMP (after mixing). There was a reproducible mixing artifact within the first 50 msec due to the large viscosity difference between the two syringes. (D) The data after 50 msec fit to a single exponential with k_{obs} that did not vary between 100 mM and 200 mM dCMP, giving k_{off} of 14 ± 1 s^{-1}. Extrapolating the exponential to 0 sec indicated that the phase encompassed ~50% of the total absorbance change, suggesting that the rest of the absorbance change corresponds to a second exponential that occurred within the mixing artifact, with k_{off} > 80 s^{-1}.

Global Fitting

The kinetic and thermodynamic data at 25°C suggest that the TmFDTS homotetramer binds dUMP and dTMP with two independent sets of binding sites that have identical k_{on} values, but different k_{off} values (Figure 3 - 17). The kinetic data for deoxynucleotide binding (Figure 3 - 13) and the kinetics for deoxynucleotide dissociation from the competition with dCMP (Figures 3 - 14 and 3 - 16) for each deoxynucleotide and flavin redox state could be fit globally in Berkeley Madonna using the model in Figure 3 - 14 (Figures 3 - 18 to 3 – 21 and Appendix 2). For the global fitting with oxidized TmFDTS and dUMP or dTMP, four concentrations of deoxynucleotide binding data at 450 nm (50 - 200 μM dUMP or dTMP) and the two dCMP concentrations (0.1 and 0.2 M) for the competition experiments were used. The k_{on} values from the oxidized TmFDTS global fits were used for the global fitting of the reduced TmFDTS competition with dCMP data (Figures 3 - 20A and 3 - 21A). Since the absorbance titrations did not show two sets of sites, we forced the change in extinction coefficient upon binding dUMP or dTMP to each of the two sites to be identical in the global fitting. The refined microscopic rate constants from the global fitting were very similar to the rate constants from the primary analysis of the kinetic data, indicating that the data are consistent with the two independent binding sites model (Table 3 - 5). The absorbance titrations from Figure 3 - 2 were also simulated in Berkeley Madonna using the model in Figure 3 - 17 with the refined rate constants from the global fitting and the change in extinction coefficient upon deoxynucleotide binding from the experimental titrations. The simulated absorbance titrations showed good agreement with the experimental titrations (Figures 3 - 18 to 3 - 21). The experimental data from the ITC

titrations at 25°C could also be fit using the K_d values calculated from the refined global fitting models and identical N-values for the two sets of sites (Figures 3 - 18 to 3 - 21).

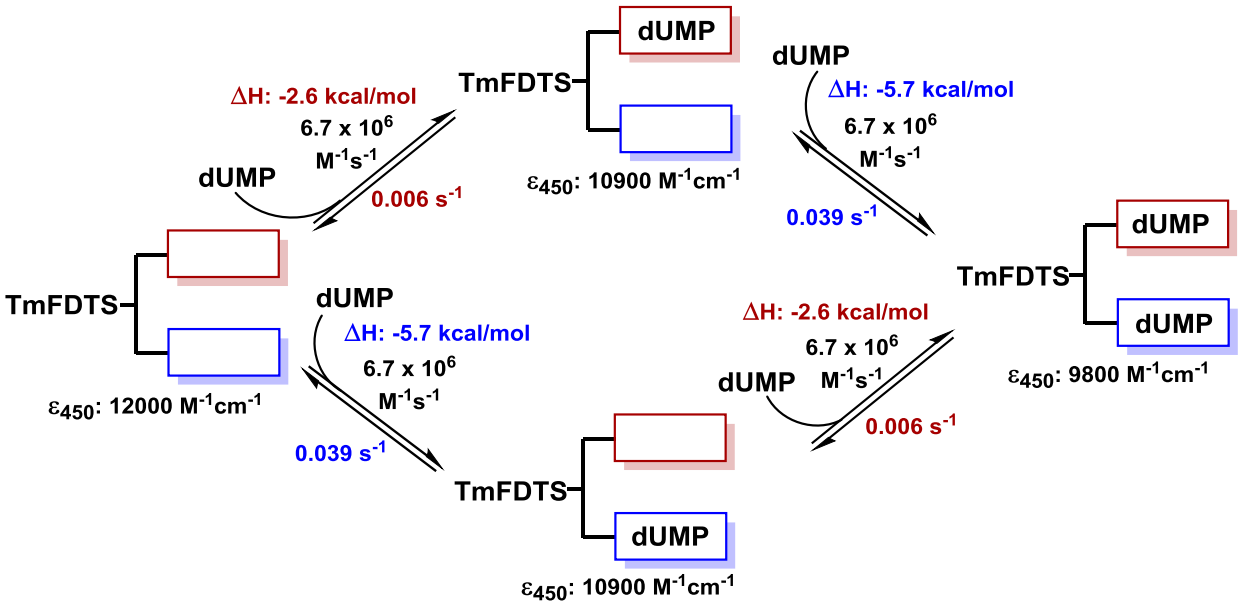

Figure 3 - 17. Two independent sites mechanism for deoxynucleotide binding to TmFDTS at low temperatures. The numbers shown in the figure are the refined numbers from the global fit for oxidized TmFDTS and dUMP at pH 8, 25°C. The values in red refer to the high affinity site; the values in blue refer to the low affinity site. The extinction coefficients shown refer to the concentration of the FAD prosthetic group.

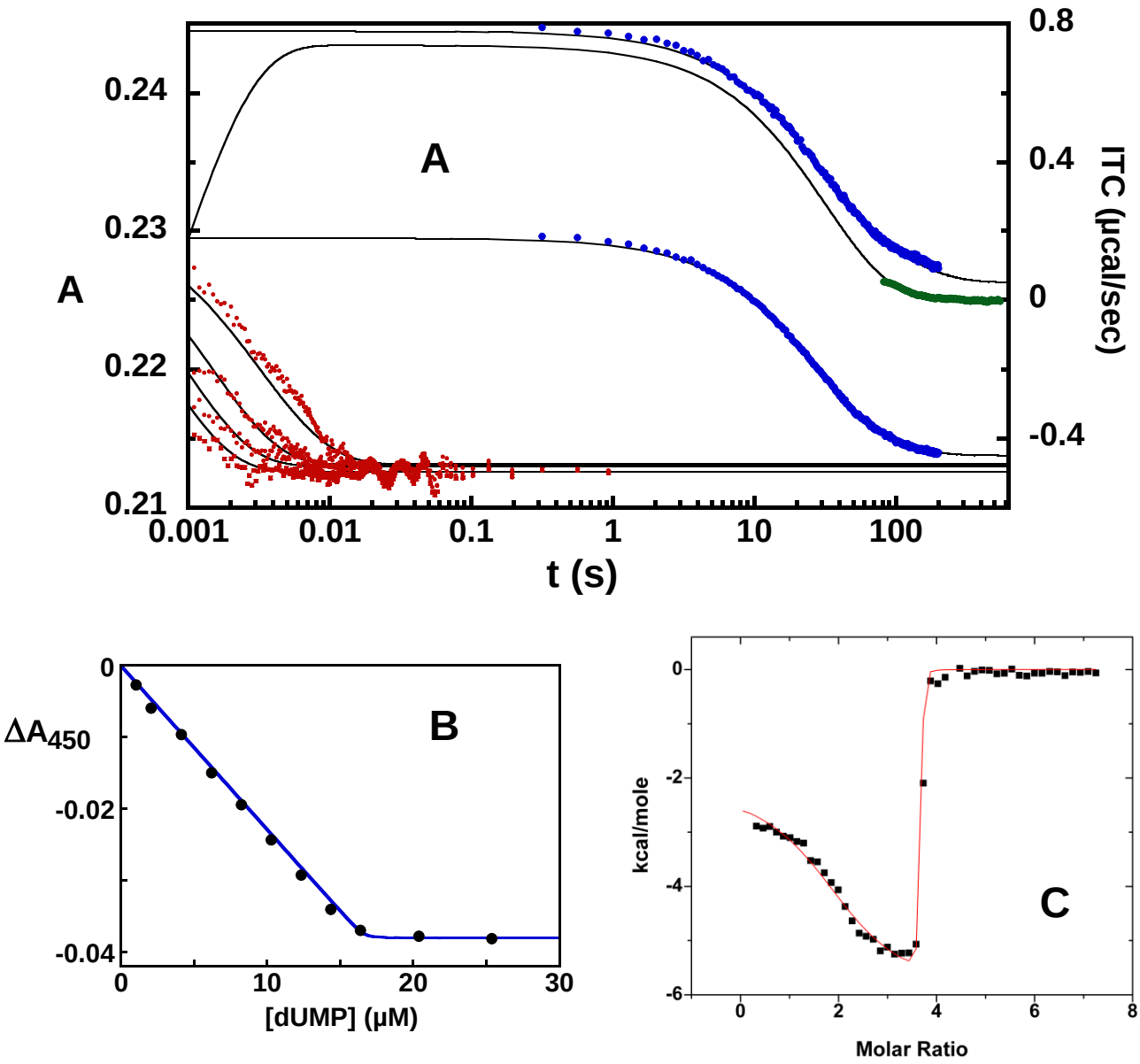

Figure 3 - 18. Global fitting of dUMP binding to oxidized TmFDTS data. (A) Stopped-flow absorbance data for dUMP binding to oxidized TmFDTS at 450 nm (red data), dissociation of dUMP from the oxidized TmFDTS-dUMP complex by competition with dCMP (blue data), and the return to baseline of the endothermic event by ITC (green data) could be fit globally in Berkeley Madonna to the two independent sites model shown in Figure 3 - 17. The black lines show the best fits obtained with Berkeley Madonna. The data for the kinetics of dUMP binding to oxidized TmFDTS were increased by 0.03 absorbance units for clarity. (B) The experimental absorbance titration from Chapter 2 (black data) with a simulated absorbance titration (blue line) made in Berkeley Madonna using the rate constants in Table 3 - 5. (C) The ITC titration (black data) fit using the K_d values from the global fitting and identical N-values for the two sets of binding sites (red trace).

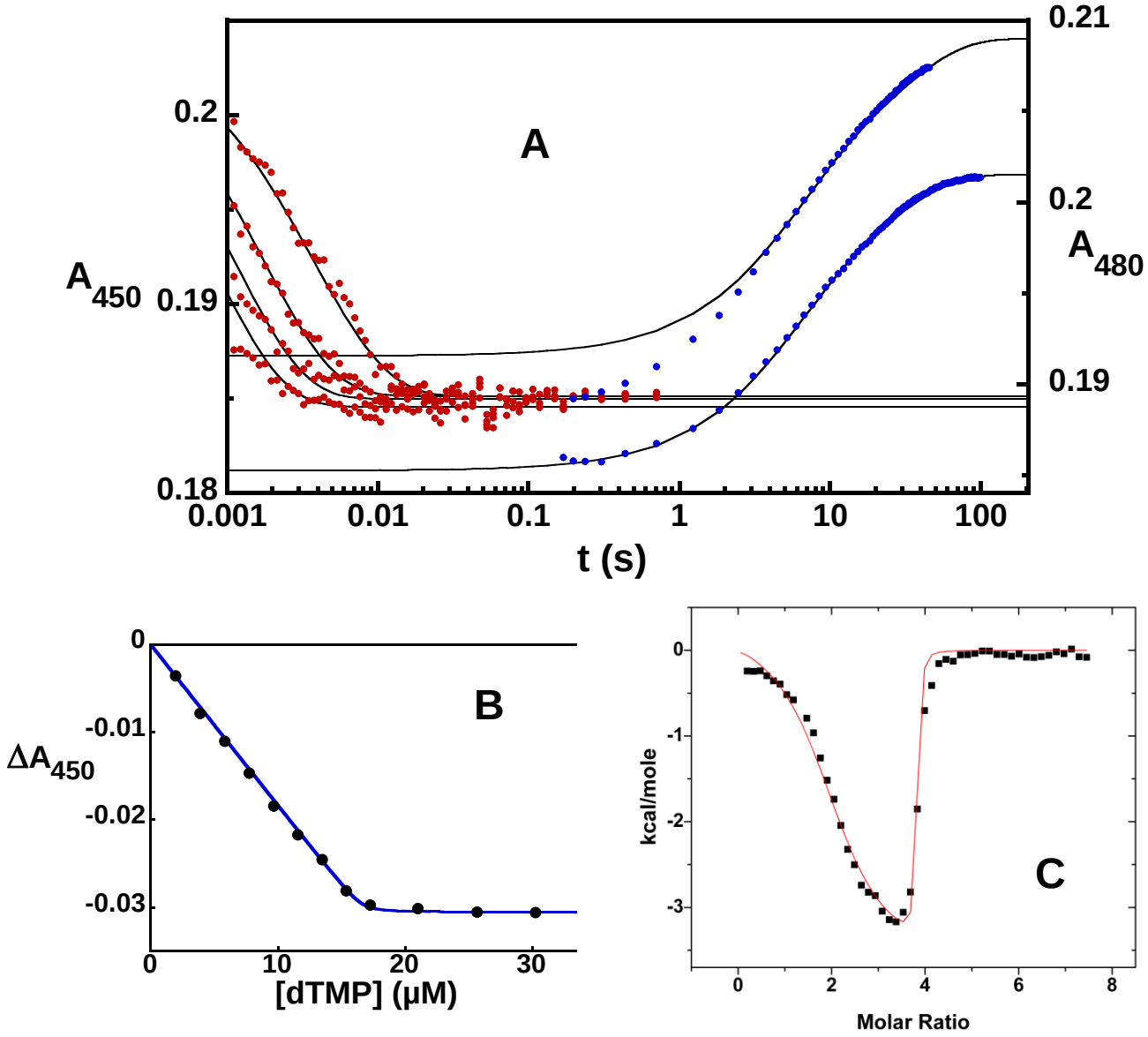

Figure 3 - 19. Global fitting of dTMP binding to oxidized TmFDTS data. (A) Stopped-flow absorbance data for dTMP binding to oxidized TmFDTS at 450 nm (red data) and dissociation of dTMP from the oxidized TmFDTS-dTMP complex by competition with dCMP (blue data) could be fit globally in Berkeley Madonna to the two independent sites model shown in Figure 3 - 17. The black lines show the best fits obtained with Berkeley Madonna. (B) The experimental absorbance titration of oxidized TmFDTS with dTMP (black data) with a simulated absorbance titration (blue line) made in Berkeley Madonna using the rate constants in Table 3 - 5. (C) The ITC titration (black data) fit using the K_d values from the global fitting and identical N-values for the two sets of binding sites (red trace).

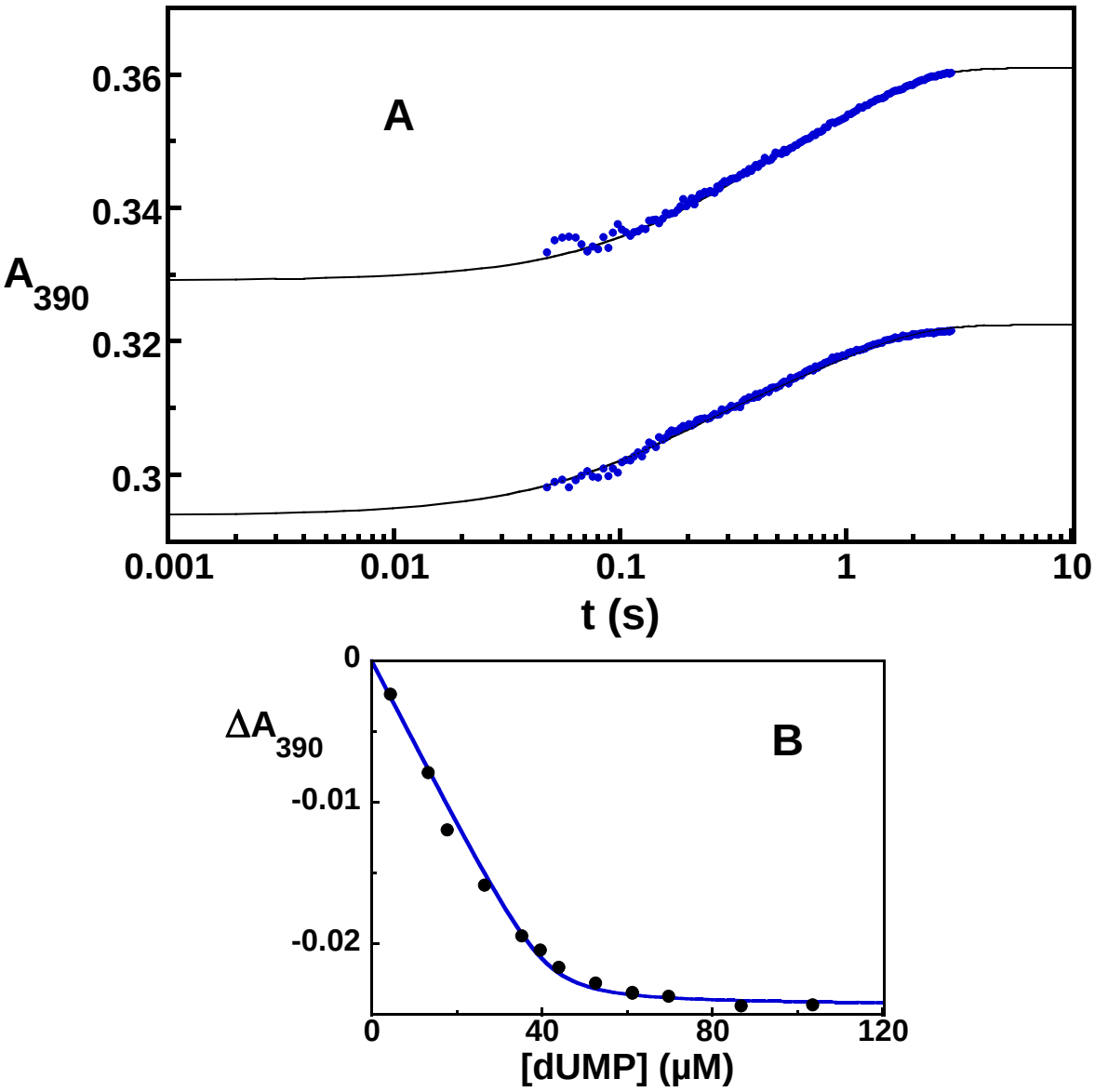

Figure 3 - 20. Global fitting of dUMP binding to reduced TmFDTS data. (A) Stopped-flow absorbance data for dUMP dissociation from the reduced TmFDTS-dUMP complex by competition with dCMP (blue data) could be fit globally in Berkeley Madonna to the two independent sites model shown in Figure 3 - 17. The k_{on} obtained from the experiments with oxidized TmFDTS was used for the global fitting of reduced TmFDTS. The black lines show the best fits obtained with Berkeley Madonna. (B) The experimental absorbance titration of reduced TmFDTS with dUMP (black data) with a simulated absorbance titration (blue line) made in Berkeley Madonna using the rate constants in Table 3 - 5.

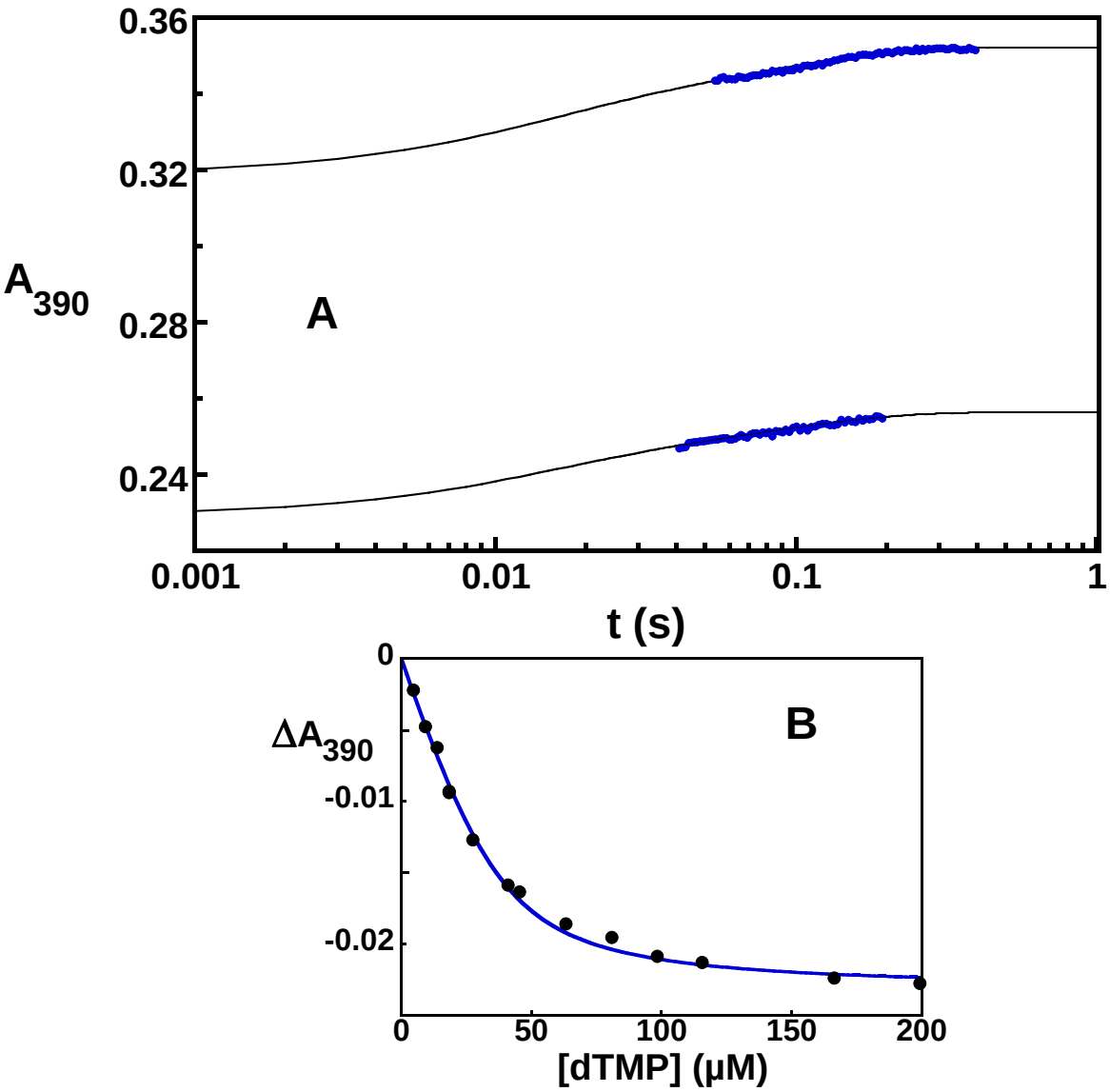

Figure 3 - 21. Global fitting of dTMP binding to reduced TmFDTS data. (A) Stopped-flow absorbance data for dTMP dissociation from the reduced TmFDTS-dTMP complex by competition with dCMP (blue data) could be fit globally in Berkeley Madonna to the two independent sites model shown in Figure 3 - 17. The data before 50 msec were omitted due to a large mixing artifact within the first 50 msec of data collection. The k_{on} obtained from the experiments with oxidized TmFDTS was used for the global fitting of reduced TmFDTS. The black lines show the best fits obtained with Berkeley Madonna. (B) The experimental absorbance titration of reduced TmFDTS with dTMP (black data) with a simulated absorbance titration (blue line) made in Berkeley Madonna using the rate constants in Table 3 - 5.

Table 3 - 5: Comparison of the Rate Constants from Global Fitting and Primary Analysis

Nucleotide	Enzyme		Experimental k_{on} ($M^{-1}s^{-1}$)	Global Fitting k_{on} ($M^{-1}s^{-1}$)	Experimental k_{off} (s^{-1})	Global Fitting k_{off} (s^{-1})
dUMP	oxidized	site A	4.4×10^6	6.4×10^6	0.009	0.008
		site B			0.032	0.043
	reduced	site A			1.2	0.8
		site B			7.1	5
dTMP	oxidized	site A	3.5×10^6	5.9×10^6	0.06	0.025
		site B			0.33	0.18
	reduced	site A			14	8
		site B			>80	>80

Additional support for the two independent sites model comes from the ITC experiments for dUMP binding to oxidized TmFDTS at low temperatures; injections of dUMP corresponding to less than half the total number of active sites initially gave off heat but then absorbed heat (Figure 3 - 5). When dUMP is first injected, TmFDTS is in excess over the concentration of dUMP; the dUMP initially binds to both sets of sites equally because they have the same k_{on}, giving rise to a single signal change (Figure 3 - 22 step 1). The difference between the K_d values of the two sets of sites (due to their different k_{off} values) then causes dUMP to dissociate from the low affinity site (step 2), producing a signal with the opposite sign of the initial binding event (making it endothermic), and to bind to the high affinity site (step 3). Since the enthalpy of dUMP binding to the low affinity site of oxidized TmFDTS is much more negative than the enthalpy of binding to the high affinity site, the re-distribution of dUMP produces an endothermic signal (steps 2 and 3). Halfway through the titration the high affinity site is completely filled with dUMP, so no redistribution from the low affinity site to the high

affinity site occurs during the second half of the titration (Figure 3 - 5). The re-distribution step would primarily be dictated by k_{off} for the low affinity site, which is very low for dUMP bound to TmFDTS. The return to baseline from the endothermic process during the ITC titration of oxidized TmFDTS with dUMP could be incorporated into the global fitting without altering the microscopic rate constants (Figure 3 – 18).

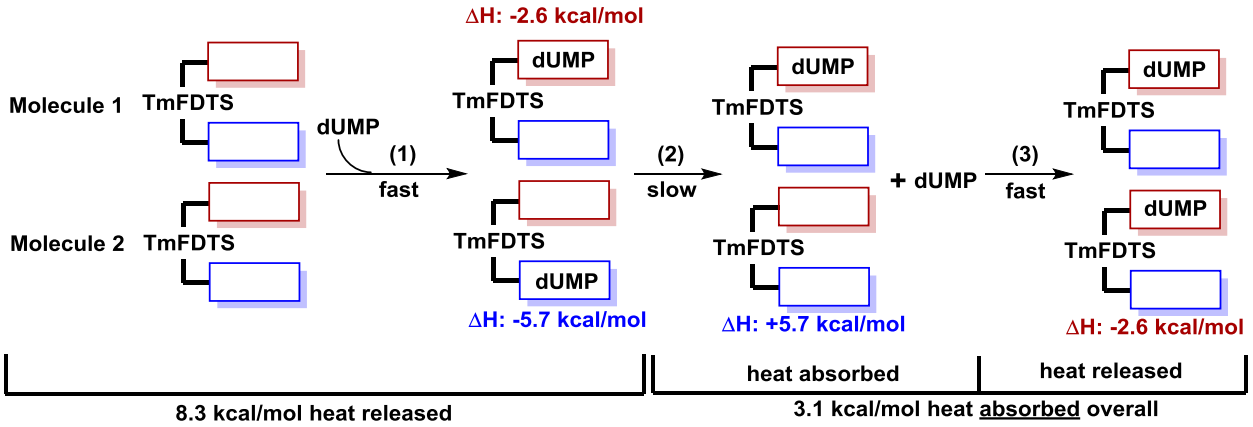

Figure 3 - 22. Mechanism causing the baseline overshoots in the ITC titrations at low temperatures. The high affinity site is shown in red and the low affinity site is shown in blue. The enthalpy values shown are for dUMP binding to oxidized TmFDTS in 0.1 M Tris-HCl pH 8 at 25°C. In the early injections of the ITC titrations, the concentration of TmFDTS is much higher than the dUMP concentration; dUMP binds to both the high affinity site and low affinity site in equal amounts since k_{on} is the same for both sites, causing 8.3 kcal/mol of heat to be released (step 1). Since there are still many unoccupied high affinity sites available to bind dUMP, the dUMP that bound to the low affinity site dissociates from the low affinity site, absorbing 5.7 kcal/mol of heat (step 2), and then binds to the unoccupied high affinity sites, releasing 2.6 kcal/mol of heat (step 3). Overall, 3.1 kcal/mol of heat is absorbed when dUMP re-equilibrates between the low and high affinity sites (steps 2 and 3). The re-equilibration step can be observed by ITC because the dissociation of dUMP from the low affinity site is much slower than the dUMP binding steps and the instrument recovery time.

Discussion

TmFDTS binds dUMP and dTMP ~200-fold less tightly when the enzyme-bound flavin is in the reduced, hydroquinone form compared to when the flavin is oxidized. The changes in nucleotide affinity with the flavin redox state are largely manifested through

changes in the dissociation rate constant (Table 3 - 5). Although we could not directly determine k_{on} for nucleotide binding to reduced TmFDTS, the changes in k_{off} between oxidized and reduced TmFDTS are similar to the changes in affinity predicted by the differences in reduction potential of free and bound TmFDTS, suggesting that k_{on} does not change with the flavin oxidation state. It is somewhat surprising that TmFDTS binds deoxynucleotides less tightly when reduced since the reduced enzyme is the form that reacts with dUMP and CH_2THF in the oxidative half-reaction. However, doing so also lowers the reduction potential of the flavin ~60 mV, which might be necessary to provide enough reducing power to reduce the dUMP-methylene intermediate in the oxidative half-reaction. Curiously, a recent study on the FDTS from *Paramecium* bursaria Chlorella virus-1 showed that the potential of the flavin in that enzyme does not change with dUMP binding,[17] indicating that changes in affinity for nucleotides with the flavin oxidation state might not apply to all FDTS enzymes. However, it is unclear if the enzyme used in that study co-purified with dTMP bound; if dTMP were present the potential likely would not change upon adding dUMP.

The very low k_{off} values provide an explanation for why TmFDTS co-purifies with dTMP. Bound dTMP could explain the discrepancies between different studies on the stimulating effects of dUMP on the reduction of FDTSs by NADPH since the study suggesting that dUMP does not affect reduction of FDTS by NADPH used the enzyme from *T. maritima*, which likely co-purified with dTMP.[18] It is unclear if FDTSs from other organisms also co-purify with dTMP. However, we have observed that FDTS from the mesophile *Campylobacter jejuni* co-purifies with dTMP in all four active sites (unpublished observation).

It is unlikely that dTMP release and dUMP binding occurs in the portion of the TmFDTS catalytic cycle when the flavin is oxidized, given the very low k_{off} values for both deoxynucleotides bound to oxidized TmFDTS. If that were the case, dTMP release during turnover would be severely rate-limiting since the rate constants for the chemistry steps in the reductive and oxidative half-reactions are much faster than the k_{off} for dTMP bound to oxidized TmFDTS reported here.[17,19] More likely, the dTMP made during the oxidative half-reaction remains bound to the enzyme until the flavin has been reduced by NADPH. Upon reducing the flavin, k_{off} for dTMP increases ~200-fold, allowing dTMP to dissociate from TmFDTS. dUMP can then bind to reduced TmFDTS to react in the oxidative half-reaction. Consistent with this idea, we have seen that dTMP stimulates the reduction of oxidized TmFDTS by NADPH to a similar degree as dUMP (unpublished observation).

TmFDTS behaves as a dimer-of-dimers with respect to nucleotide binding at temperatures below ~55°C, suggesting that there is asymmetry between the four active sites of TmFDTS at low temperatures. TmFDTS is from *T. maritima*, which normally lives at temperatures around 80°C. The dimer-of-dimers behavior of TmFDTS is a result of studying the enzyme at temperatures well below the physiologically relevant temperature of the organism. However, it is also possible that the dimer-of-dimers behavior occurs at physiological temperatures, but is only detectable at sub-physiological temperatures. It is not known if the dimer-of-dimers behavior affects other parts of the catalytic cycle of TmFDTS. Most of the previous studies on TmFDTS were done at temperatures below the 55°C threshold, so it is possible that the dimer-of-dimers behavior of TmFDTS complicated the interpretation of the data in those

studies.[11,14,18,19,27] One notable example is the lax regiochemistry in incorporating the hydride from reduced TmFDTS into dTMP during the oxidative half-reaction – at 37°C the hydride was transferred to both C6 and C7 of dTMP in roughly equal proportions whereas at 65°C the hydride was only transferred to C7 of dTMP.[14] The lax regiochemistry in hydride transfer at 37°C could therefore have been due to differences between the two sets of active sites of TmFDTS.

The origin of the dimer-of-dimers behavior of TmFDTS is currently unclear. However, an overlay of the four subunits of the deoxynucleotide-free TmFDTS structure hints at a potential reason – the isoalloxazine portion of the FADs are not well ordered and H53 exists in two different conformations in the four active sites (Figure 3 - 7A).[4] Time-resolved fluorescence spectroscopy has also shown that the active site is highly dynamic in the absence of bound deoxynucleotides.[28] The conformational flexibility of H53 and the isoalloxazine could therefore play a role in causing the asymmetry among the four active sites of TmFDTS. Supporting this idea, the two sets of sites had nearly identical K_d values in the titration of the H53A TmFDTS mutant enzyme with dUMP (Figure 3 – 7B). The active site loop (residues 89-94) could potentially be involved as well since it is completely disordered in all four active sites of the deoxynucleotide-free structure. In order for the dissociation rate constants to be different between the two sets of sites, the asymmetry should also be present in the dUMP-bound structure. However, the four subunits adopt a single conformation in the dUMP-bound structure (Figure 3 - 23).[5] Crystallization artifacts cannot be ruled out since a polyethylene glycol molecule from the crystallization solution was bound in the active sites next to H53 in

the dUMP-bound structure, which could have driven H53 to adopt a single conformation in all of the active sites.

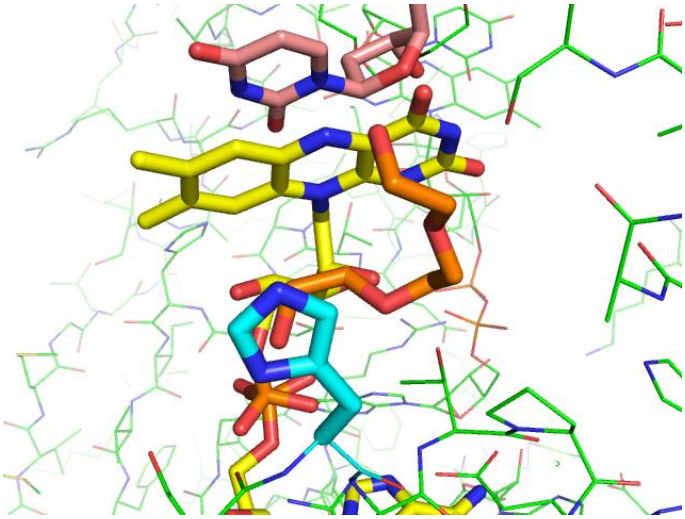

Figure 3 - 23. Active site of dUMP-bound TmFDTS (PDB code 1O26). All four subunits of the TmFDTS homotetramer – including H53 – are in the same conformation when dUMP is bound. H53 is shown in cyan, dUMP is shown in salmon, FAD is shown in yellow, and polyethylene glycol from the crystallization solution is shown in orange.

Conclusions

TmFDTS binds dUMP and dTMP less tightly when the enzyme-bound flavin is reduced than when it is oxidized, which is largely due to changes in the dissociation rate constants. As a result, we propose that the exchange of dTMP and dUMP in the catalytic cycle of TmFDTS occurs when the flavin is reduced. The TmFDTS homotetramer also acts as a dimer-of-dimers with respect to deoxynucleotide binding at low temperatures, which should be taken into consideration in all future studies on FDTSs.

References

(1) Koehn, E. M., and Kohen, A. (2010) Flavin-dependent thymidylate synthase: a novel pathway towards thymine. *Arch. Biochem. Biophys. 493*, 96–102.

(2) Mishanina, T. V, Koehn, E. M., and Kohen, A. (2012) Mechanisms and inhibition of uracil methylating enzymes. *Bioorg. Chem. 43*, 37–43.

(3) Carreras, C. W., and Santi, D. V. (1995) The catalytic mechanism and structure of thymidylate synthase. *Annu. Rev. Biochem. 64*, 721–62.

(4) Kuhn, P., Lesley, S. A., Mathews, I. I., Canaves, J. M., Brinen, L. S., Dai, X., Deacon, A. M., Elsliger, M. A., Eshaghi, S., Floyd, R., Godzik, A., Grittini, C., Grzechnik, S. K., Guda, C., Hodgson, K. O., Jaroszewski, L., Karlak, C., Klock, H. E., Koesema, E., Kovarik, J. M., Kreusch, A. T., McMullan, D., McPhillips, T. M., Miller, M. A., Miller, M., Morse, A., Moy, K., Ouyang, J., Robb, A., Rodrigues, K., Selby, T. L., Spraggon, G., Stevens, R. C., Taylor, S. S., van den Bedem, H., Velasquez, J., Vincent, J., Wang, X., West, B., Wolf, G., Wooley, J., and Wilson, I. A. (2002) Crystal structure of thy1, a thymidylate synthase complementing protein from Thermotoga maritima at 2.25 Å resolution. *Proteins 49*, 142–5.

(5) Mathews, I., Deacon, A., Canaves, J., Mcmullan, D., Lesley, S., Agarwalla, S., and Kuhn, P. (2003) Functional Analysis of Substrate and Cofactor Complex Structures of a Thymidylate Synthase-Complementing Protein. *Structure 11*, 677–90.

(6) Sampathkumar, P., Turley, S., Ulmer, J. E., Rhie, H. G., Sibley, C. H., and Hol, W. G. J. (2005) Structure of the Mycobacterium tuberculosis flavin dependent thymidylate synthase (MtbThyX) at 2.0 Å resolution. *J. Mol. Biol. 352*, 1091–104.

(7) Zhang, X., Zhang, J., Guo, G., Mao, X., Hu, Y., and Zou, Q. (2012) Crystal Structure of a Flavin-Dependent Thymidylate Synthase from Helicobacter pylori strain 26695. *Protein Pept. Lett. 19*, 1225–30.

(8) Graziani, S., Bernauer, J., Skouloubris, S., Graille, M., Zhou, C.-Z., Marchand, C., Decottignies, P., van Tilbeurgh, H., Myllykallio, H., and Liebl, U. (2006) Catalytic mechanism and structure of viral flavin-dependent thymidylate synthase ThyX. *J. Biol. Chem. 281*, 24048–57.

(9) Kan, S.-C., Liu, J.-S., Hu, H.-Y., Chang, C.-M., Lin, W.-D., Wang, W.-C., and Hsu, W.-H. (2010) Biochemical characterization of two thymidylate synthases in Corynebacterium glutamicum NCHU 87078. *Biochim. Biophys. Acta 1804*, 1751–9.

(10) Koehn, E. M., Perissinotti, L. L., Moghram, S., Prabhakar, A., Lesley, S. A., and Mathews, I. I. (2012) Folate binding site of flavin-dependent thymidylate synthase. *Proc. Natl. Acad. Sci. U. S. A. 109*, 15722–7.

(11) Mishanina, T. V, Koehn, E. M., Conrad, J. A., Palfey, B. A., Lesley, S. A., and Kohen, A. (2012) Trapping of an intermediate in the reaction catalyzed by flavin-dependent thymidylate synthase. *J. Am. Chem. Soc. 134*, 4442–8.

(12) Leduc, D., Graziani, S., Lipowski, G., Marchand, C., Le Maréchal, P., Liebl, U., and Myllykallio, H. (2004) Functional evidence for active site location of tetrameric thymidylate synthase X at the interphase of three monomers. *Proc. Natl. Acad. Sci. U. S. A. 101*, 7252–7.

(13) Gattis, S. G., and Palfey, B. A. (2005) Direct observation of the participation of flavin in product formation by thyX-encoded thymidylate synthase. *J. Am. Chem. Soc. 127*, 832–3.

(14) Koehn, E. M., Fleischmann, T., Conrad, J. A., Palfey, B. A., Lesley, S. A., Mathews, I. I., and Kohen, A. (2009) An unusual mechanism of thymidylate biosynthesis in organisms containing the thyX gene. *Nature 458*, 919–23.

(15) Wang, Z., Chernyshev, A., Koehn, E. M., Manuel, T. D., Lesley, S. A., and Kohen, A. (2009) Oxidase activity of a flavin-dependent thymidylate synthase. *FEBS J. 276*, 2801–10.

(16) Graziani, S., Xia, Y., Gurnon, J. R., Van Etten, J. L., Leduc, D., Skouloubris, S., Myllykallio, H., and Liebl, U. (2004) Functional Analysis of FAD-dependent Thymidylate Synthase ThyX from Paramecium bursaria Chlorella Virus-1. *J. Biol. Chem. 279*, 54340–7.

(17) Becker, H. F., Djaout, K., Lamarre, I., Ulmer, J. E., Schaming, D., Balland, V., Liebl, U., Myllykallio, H., and Vos, M. H. (2014) Substrate interaction dynamics and oxygen control in the active site of thymidylate synthase ThyX. *Biochem. J. 459*, 37–45.

(18) Chernyshev, A., Fleischmann, T., Koehn, E. M., Lesley, S. A., and Kohen, A. (2007) The relationships between oxidase and synthase activities of flavin dependent thymidylate synthase (FDTS). *Chem. Commun. (Camb).* 2861–3.

(19) Conrad, J. A., Ortiz-Maldonado, M., Hoppe, S. W., and Palfey, B. A. (2014) Detection of Intermediates in the Oxidative Half-Reaction of the FAD-Dependent Thymidylate Synthase from Thermotoga maritima: Carbon Transfer without Covalent Pyrimidine Activation. *Biochemistry 53*, 5199–207.

(20) Williams, C. H. J., Arscott, D. L., Matthews, R. G., Thorpe, C., and Wilkinson, K. D. (1979) Methodology Employed for Anaerobic Spectrophotometric Titrations and for Computer-Assisted Data Analysis. *Methods Enzymol. 62*, 185–98.

(21) Palfey, B. A. (2003) Time Resolved Spectral Analysis, in *Kinetic Analysis of Macromolecules* (Johnson, K. A., Ed.), pp 203–227. Oxford University Press, New York.

(22) Massey, V. (1990) A simple method for the determination of redox potentials, in *Flavins and Flavoproteins* (Curti, B., Ronchi, S., and Zanetti, G., Eds.), p 59−66. Walter de Gruyter, Berlin, Germany.

(23) Clark, W. M. (1960) Oxidation-Reduction Potentials of Organic Systems. Waverly Press, Inc., Baltimore.

(24) LiCata, V. J., and Liu, C.-C. (2011) Analysis of free energy versus temperature curves in protein folding and macromolecular interactions. *Methods Enzymol. 488*, 219–38.

(25) Todd, M. J., and Gomez, J. (2001) Enzyme kinetics determined using calorimetry: a general assay for enzyme activity? *Anal. Biochem. 296*, 179–87.

(26) Goldberg, R. N., Kishore, N., and Lennen, R. M. (2002) Thermodynamic Quantities for the Ionization Reactions of Buffers. *J. Phys. Chem. 31*, 231–370.

(27) Agrawal, N., Lesley, S. A., Kuhn, P., and Kohen, A. (2004) Mechanistic Studies of a Flavin-Dependent Thymidylate Synthase. *Biochemistry 43*, 10295–301.

(28) Laptenok, S. P., Bouzhir-Sima, L., Lambry, J.-C., Myllykallio, H., Liebl, U., and Vos, M. H. (2013) Ultrafast real-time visualization of active site flexibility of flavoenzyme thymidylate synthase ThyX. *Proc. Natl. Acad. Sci. U. S. A. 110*, 8924–9.

Chapter 4

Prior Modifications are not Required for all tRNAs to React Rapidly with tRNA-Dihydrouridine Synthase-2 from Yeast

tRNA molecules contain numerous modifications of the four encoded nucleotides that comprise all RNA. Over 100 different modifications have been identified in tRNA,[1] of which at least 25 are present in the budding yeast *Saccharomyces cerevisiae*.

Dihydrouridine is one of the most abundant tRNA modifications, occurring in nearly all organisms.[2] It is formed by the reduction of the carbon-carbon double bond of specific uridines in tRNAs by the dihydrouridine synthases (DUSs), a class of flavoenzymes (Figure 4 - 1).[3] The physiological role for dihydrouridine is still unclear. Biophysical studies have shown that dihydrouridine increases the conformational flexibility of the RNA backbone.[4] Corroborating this is the fact that species adapted to cold environments have a greater abundance of dihydrouridine whereas thermophilic organisms have much less or even none at all.[5] The amount of dihydrouridine in each class of organisms could thus optimize the flexibility of the tRNA in their respective environments.

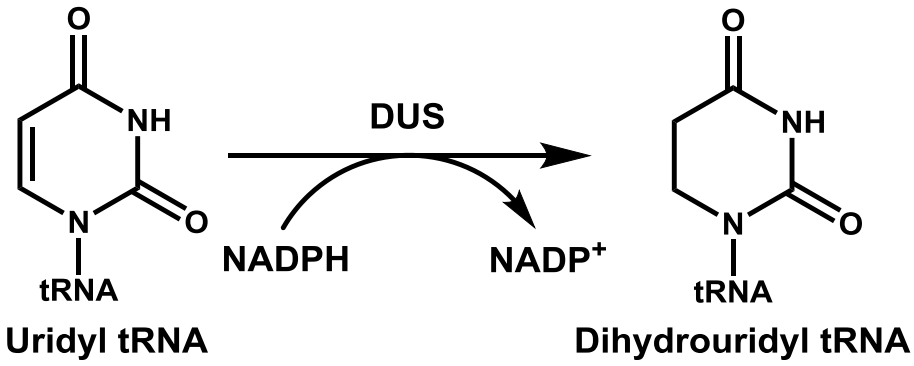

Figure 4 - 1. Reaction catalyzed by tRNA-dihydrouridine synthase.

Other studies have shown that tRNA lacking dihydrouridine in addition to other modifications degrades at a substantially increased rate.[6] The main function of dihydrouridine could therefore be to protect tRNA from degradation within the cell. It has long been known that dihydrouridine levels are increased in cancerous tissues,[7] possibly increasing the lifetimes of tRNA in cancerous cells. A recent study has shown that the human DUS2 is responsible for the increased dihydrouridine levels in pulmonary carcinogenesis, and repression of DUS2 inhibited growth of the cancerous cells.[8] DUSs might therefore be a novel target for the treatment of cancer.

Previous work has explored the kinetics of the reaction of *S. cerevisiae* DUS2 with yeast $tRNA^{Leu}$-CAA, a species of tRNA known to contain dihydrouridine modifications.[9] Intriguingly, it was found that the rate constant of the reaction of DUS2 with a synthetic, *in vitro* transcribed $tRNA^{Leu}$-CAA was far too slow to account for the level of dihydrouridine present in *S. cerevisiae* cells. However, when $tRNA^{Leu}$-CAA isolated from a yeast strain lacking DUS2 was used instead (henceforth called "mature $tRNA^{Leu}$-CAA"), the reaction was >600 fold faster. Mature $tRNA^{Leu}$-CAA in *S. cerevisiae* contains 12 other modifications in addition to dihydrouridine.[10] One possibility is that one

or more of the other modifications present in mature $tRNA^{Leu}$-CAA is needed before dihydrouridine synthesis can occur.

Here I show that yeast DUS2 is oxidized rapidly by some tRNAs devoid of modifications, indicating additional complexity in the recognition of tRNAs by DUS2. I also identify RNA elements that are important for DUS2 to react rapidly with tRNAs and show that tRNA reactivity with DUS2 is not regulated by a single modification. Unmodified $tRNA^{Leu}$-CAA reacts poorly with DUS2 because it adopts a misfolded conformation.

Experimental Procedures

Protein Expression and Purification

BL21 (DE3) cells containing the DUS2 expression plasmid were cultured and the enzyme purified as described previously.[9] The genes for pseudouridine synthase-4 (PUS4),[11] pseudouridine synthase-8 (PUS8),[12] tRNA(m^5U_{54})methyltransferase (TRM2),[13] a truncated version of tRNA(N^2,N^2G_{26})methyltransferase ((Δ1-17)TRM1),[14] tRNA(N^1G_{37})methyltransferase (TRM5)[15] from *S. cerevisiae* and the gene for tRNA(2'-O-mG_{18})methyltransferase (TrmH)[16] from *Thermus thermophilus* were cloned from their respective genomic DNAs into the pMCSG7 ligation-independent cloning expression vector.[17] The expression plasmids for PUS4, PUS8, and (Δ1-17)TRM1 were cloned into BL21(DE3)Gold competent cells whereas the expression plasmids for TRM2, TRM5, and TrmH were cloned into Rosetta2^{TM}(DE3)pLysS competent cells. All cells were grown in 1L LB + 100 mg/L ampicillin. The Rosetta2^{TM}(DE3)pLysS cultures were also grown in the presence of 34 mg/L chloramphenicol. All of the cultures, except the TrmH

cultures, were grown at 37°C until OD600 ≈ 1.0. At that point, the temperature was reduced to 28°C and each culture was induced with 0.1 mM IPTG. Four hours after induction, the cultures were harvested by centrifugation. The TrmH culture was grown at 37°C until OD600 ≈ 0.8. After that, the temperature was reduced to 20°C and the culture was induced with 0.1 mM IPTG and grown overnight (~20 hours) before harvesting. After harvesting, the cultures containing PUS4, PUS8, TrmH, or (Δ1-17)TRM1 were resuspended in 50 mM $NaPO_4$, pH 8, 300 mM NaCl, 10% glycerol (Purification Buffer A) whereas the cultures containing TRM2 or TRM5 were resuspended in 50 mM Tris-HCl, pH 7.5, 100 mM NaCl, 5 mM $MgCl_2$, 10% glycerol (Purification Buffer B). After disrupting the cells by sonication and removing the cell debris by centrifugation, the cell extracts were loaded on separate 5 mL TALON® resin columns at 4°C that were pre-equilibrated in their respective Purification Buffers. The resins were washed with the appropriate Purification Buffer with 1 M NaCl and 5 mM imidazole added. The pure proteins were eluted with the appropriate Purification Buffer + 200 mM imidazole. Purity was assessed by SDS-PAGE. The pure proteins were separately desalted into 100 mM HEPES-NaOH, pH 7.5, 100 mM NaCl, 10 mM $MgCl_2$, 1 mM DTT, 10% glycerol and stored at -80°C. The concentrations of the tRNA-modifying enzymes were estimated using the ε_{280} predicted from the amino acid sequence of the proteins.[18] The ε_{280} values used were as follows: PUS4 – 28880 $M^{-1}cm^{-1}$; PUS8 – 66420 $M^{-1}cm^{-1}$; TRM2 – 28410 $M^{-1}cm^{-1}$; (Δ1-17)TRM1 – 59210 $M^{-1}cm^{-1}$; TRM5 – 37800 $M^{-1}cm^{-1}$; TrmH – 23590 M $M^{-1}cm^{-1}$.

Construction of tRNA Plasmids

The inserts for the tRNA plasmids of $tRNA^{Asp}$, $tRNA^{Ala}$, and $tRNA^{Leu}$-CAA were each constructed by PCR using two complementary primers (Invitrogen) with a 20 bp

overlap comprising the entire tRNA gene to be transcribed with a T7 promoter upstream. The promoter-gene sequences were also flanked by an upstream and downstream EcoRI and BamHI restriction site, respectively. The original U_1-A_{72} base-pair was changed to G_1-C_{72} in the $tRNA^{Asp}$ sequence to improve the yield of full-length tRNA through *in vitro* transcription.[11] The inserts were cloned into the vector pUC118 using the aforementioned restriction sites. The *in vitro* transcription plasmid for $tRNA^{His2}$ was a gift from Jane Jackman.

In Vitro Transcription of tRNAs

The plasmid templates were linearized by digestion with BstNI (for $tRNA^{Asp}$, $tRNA^{Ala}$, and $tRNA^{Leu}$-CAA) or NsiI (for $tRNA^{His2}$). tRNAs were synthesized as run-off transcripts by *in vitro* transcription using the linearized plasmids as templates.[19] The tRNA was then purified by loading the reactions on a 5 cm x 1.5 cm I.D. DEAE-Sepharose Fast-flow column pre-equilibrated in 50 mM $NaPO_4$, pH 6.5, 150 mM NaCl, 0.2 mM EDTA. The column was washed with 50 mM $NaPO_4$, pH 6.5, 400 mM NaCl, 0.2 mM EDTA until the A_{260} reading of the eluate was 0. Pure tRNA was then eluted with 50 mM $NaPO_4$, pH 6.5, 525 mM NaCl, 0.2 mM EDTA, concentrated using 10 kDa Amicon centrifugal filter units and desalted into 100 mM HEPES-NaOH, pH 7.5, 100 mM NaCl, 10 mM $MgCl_2$, 10% glycerol using a PD-10 desalting column. Mature $tRNA^{Leu}$-CAA was purified as described previously using a resin containing an immobilized oligo with a sequence complementary to part of $tRNA^{Leu}$-CAA.[9] Prior to use, tRNAs in 100 mM HEPES-NaOH, pH 7.5, 100 mM NaCl, 10 mM $MgCl_2$ and 10 % glycerol, were heated to 65°C for 5 min, and then cooled on ice to allow proper folding.

Binding Titrations

Binding titrations were carried out in quartz fluorescence cuvettes at 4°C in 100 mM HEPES-NaOH, pH 7.5, 100 mM NaCl, 10 mM $MgCl_2$, 10% glycerol in a Shimadzu UV-2501 PC scanning spectrophotometer or a Shimadzu RF-5301PC spectrofluorimeter. 15 µM enzyme was titrated with increasing concentrations of ligand. For the fluorescence titrations, excitation was at 457 nm, and emission scanned between 480 and 600 nm, with a maximum fluorescence change at 517 nm. Plots of the signal change with ligand concentration could not be fit to a hyperbolic binding isotherm. Instead, plots were fit to Equation 1 for tight binding:

$$\Delta S = \Delta S_{max} \frac{E_0 + L_0 + K_d - \sqrt{(E_0 + L_0 + K_d)^2 - 4E_0L_0}}{2} \qquad \text{Eq. 1}$$

where ΔS is the change in absorbance or fluorescence, ΔS_{max} is the maximum change in extinction coefficient for absorbance or an arbitrary parameter in fluorescence, E_0 is the initial enzyme concentration, L_0 is the added ligand concentration and K_d is the dissociation constant.

Oxidative Half-Reaction Kinetics

Enzyme solutions were made anaerobic in glass cuvettes or tonometers by multiple cycles of evacuation followed by equilibration with purified argon. When required, DUS2 was reduced by titrating with one equivalent of dithionite. For stopped-flow experiments, tRNA solutions were made anaerobic by bubbling with purified argon. Reactions were performed at 4°C in 100 mM HEPES-NaOH, pH 7.5, 100 mM NaCl, 10 mM $MgCl_2$, 10% glycerol. The enzyme concentration for all experiments was 15 µM

after mixing. Absorbance spectra were obtained over time using a Shimadzu UV-2501PC scanning spectrophotometer for slow reactions; rapid reactions were studied using a Hi-Tech Scientific SF61DX2 stopped-flow instrument. Reaction traces were fit to sums of exponentials.

Binding Kinetics

The kinetics of unmodified $tRNA^{Asp}$ binding to $DUS2_{ox}$ were studied using a Hi-Tech Scientific SF61DX2 stopped-flow unit. Experiments were performed by mixing 15 µM $DUS2_{ox}$ with 25-400 µM unmodified $tRNA^{Asp}$ (all concentrations are after mixing) in 100 mM HEPES-NaOH, pH 7.5, 100 mM NaCl, 100 mM $MgCl_2$, 10% glycerol at 4°C. For the absorbance experiments, traces were monitored at 510 nm. For the fluorescence experiments, the observation cell was excited at 457 nm and a 500 nm cut-off filter was used for detecting the fluorescence emission.

Partial Modification of $tRNA^{Leu}$-CAA

$tRNA^{Leu}$-CAA was partially modified by incubating 100 µM unmodified $tRNA^{Leu}$-CAA with 1 µM PUS4, 1 µM PUS8, 1 µM TRM2, 1 µM TRM5, 1 µM TRM1, 1 µM TrmH, 2 mM S-adenosyl methionine, 5 mM DTT in 1 mL 100 mM HEPES-NaOH, pH 7.5, 100 mM NaCl, 10 mM $MgCl_2$, 10% glycerol at 30°C for 90 minutes. The sample was then incubated at 50°C for 30 minutes to allow for greater activity of TrmH. The reaction as then quenched by phenol-chloroform extraction followed by ethanol-precipitation. The tRNA was washed once with 70% ethanol and dissolved in 100 mM HEPES-NaOH, pH 7.5, 100 mM NaCl, 10 mM $MgCl_2$, 10% glycerol.

Electrophoresis

Electrophoresis was performed using a Bio-Rad Mini PROTEAN® 3 system at room temperature. The denaturing PAGE experiments were performed using 9% acrylamide, 1X TBE, 8 M urea gels. Native PAGE experiments were performed using 9% acrylamide, 1X TBE, 12 mM $MgCl_2$ gels. 12 mM $MgCl_2$ was also added to the 1X TBE running buffer to ensure that Mg^{2+} remained in the gels. The gels were stained using ethidium bromide.

Results

Oxidative Half-Reaction with Unmodified $tRNA^{Asp}$

I investigated the oxidative half-reaction of reduced DUS2 ($DUS2_{red}$) with unmodified yeast $tRNA^{Asp}$, which when modified contains a dihydrouridine at position 20. Intriguingly, unmodified $tRNA^{Asp}$ was reduced rapidly by $DUS2_{red}$ (Figure 4 - 2), in contrast with previous work showing that tRNA must contain other modifications in order to react rapidly with DUS2.[9] $DUS2_{red}$ was oxidized at 4°C by mixing with various concentrations of unmodified $tRNA^{Asp}$ in anaerobic stopped-flow experiments. The absorbance increases at 450 nm fit to two exponentials, with the first contributing ~90 percent of the absorbance change. The first phase was attributed to oxidation of the enzyme by tRNA. The second was attributed to a small amount of enzyme aggregation based on an increase in light-scattering at longer wavelengths that occurred with the same k_{obs} as the second exponential at 450 nm. The observed rate constant (k_{obs}) for the first exponential did not vary with $tRNA^{Asp}$ concentration, indicating a K_d much lower than 20 µM (Figure 4 - 2). The rate constant for the reaction of $DUS2_{red}$ with unmodified

tRNA^{Asp} was 0.045 ± 8 x 10^{-4} s^{-1}. This is about 3-fold slower than the rate constant obtained with mature tRNA^{Leu}-CAA (0.14 ± 0.03 s^{-1}), but is still fast enough to account for the amount of dihydrouridylated tRNA in yeast cells.[9] Modifications therefore are not universally required for rapid reactivity with DUS2.

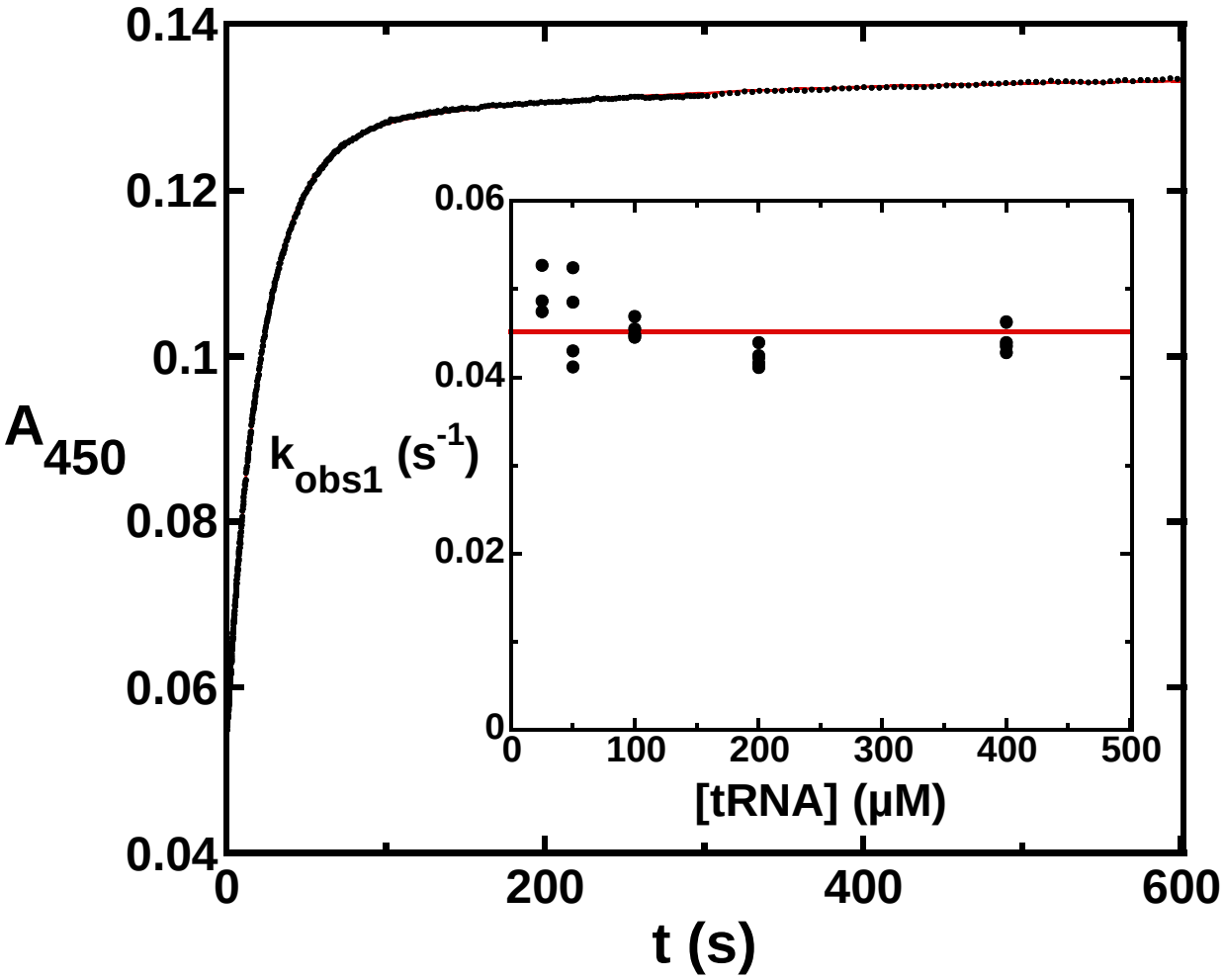

Figure 4 – 2. Oxidation of DUS2$_{red}$ by unmodified tRNA^{Asp}. Anaerobic reduced DUS2 (15 μM) was oxidized by mixing with various concentrations of unmodified tRNA^{Asp}, from 25 to 400 μM, in 100 mM HEPES-NaOH pH 7.5, 100 mM NaCl, 10 mM $MgCl_2$, 10% glycerol, 4°C in a stopped-flow spectrophotometer. The absorbance was monitored at 450 nm and traces were fit to two exponentials. The inset shows the concentration dependence of the first exponential, flavin oxidation, by unmodified tRNA^{Asp}. k_{obs1} remained constant at 0.045 s^{-1} at all tRNA concentrations used, indicating a K_d much lower than 20 μM. The second exponential was attributed to an increase in light-scattering due to the aggregation of a small population of enzyme.

Previous work has also shown that many tRNAs require Mg^{2+} for proper folding.[20,21] In an attempt to determine if DUS2 requires properly folded tRNA, the Mg^{2+} dependence of $tRNA^{Asp}$ reduction by DUS2 was investigated by performing the oxidative half-reaction in the absence of Mg^{2+} with 20 mM EDTA. The kinetics of the oxidative half-reaction without Mg^{2+} were identical to the experiments with Mg^{2+}, indicating either that DUS2 does not require properly folded tRNA for recognition or that unmodified $tRNA^{Asp}$ folds properly even without Mg^{2+}. Recent crystal structures of a DUS-tRNA complex from *Thermus thermophilus* suggest the latter since DUS in that structure makes multiple contacts with the D-, T-, and anticodon arms of a properly folded L-shaped tRNA (Figure 4 - 3).[22]

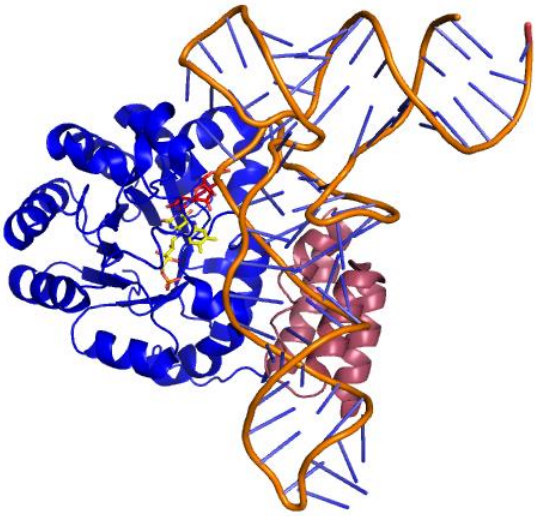

Figure 4 - 3. Structure of *T. thermophilus* DUS in complex with tRNA (PDB 3B0U). The two domains of DUS are shown in blue and pink. The tRNA is shown in orange.

DUS2 Recognizes More than Just the D-loop of tRNA

Several tRNA-modifying enzymes can recognize and modify stem-loop structures with appropriate sequences independent of the rest of the tRNA molecule.[23,24] The Mg^{2+}-dependence experiments prompted us to consider whether DUS2 recognizes the full-length tRNA transcript or solely the D-loop. To explore this possibility, the oxidative half-reaction of $DUS2_{red}$ was performed with 125 µM of a stem-loop comprised of the D-loop of $tRNA^{Asp}$ extended by the anticodon arm (Figure 4 - 4). The reaction was extremely slow, taking nearly a week to complete. The enzyme slowly aggregated over the long reaction-time – the turbidity of the sample steadily increased during the experiment – so the observed rate constant was estimated as being $1.2 \times 10^{-4} \pm 7 \times 10^{-6}$ s^{-1} using the initial rate before excessive aggregation had occurred.

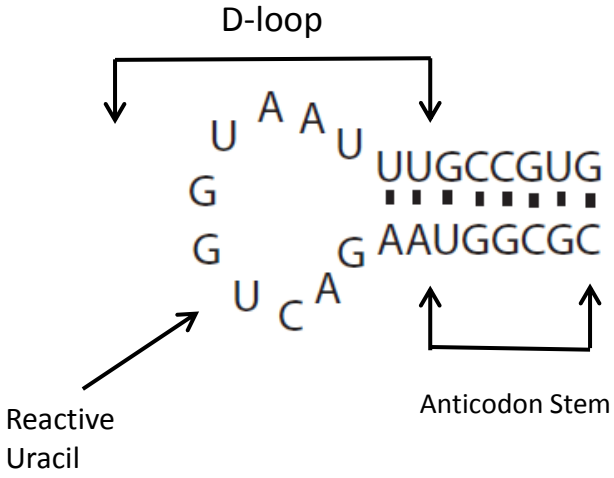

Figure 4 - 4. Stem loop consisting of the D-loop extended by the anticodon stem of unmodified $tRNA^{Asp}$. This stem-loop was a poor substrate for DUS2 in an oxidative half-reaction.

The Required Modifications for Rapid tRNA Reduction by DUS2 are not Isolated to One Region of tRNA

To determine if the essential modifications for rapid reactivity with DUS2 of $tRNA^{Leu}$-CAA are isolated to a specific region of the tRNA, chimeric tRNAs were designed with the D-loops of $tRNA^{Asp}$ and $tRNA^{Leu}$-CAA interchanged (Figure 4 - 5). If the important modifications in $tRNA^{Leu}$-CAA were isolated to regions outside of the D-loop, a chimeric tRNA containing the D-loop of $tRNA^{Leu}$-CAA and the body of $tRNA^{Asp}$ would be reduced rapidly by DUS2. Conversely, if the important modifications in $tRNA^{Leu}$-CAA were solely in the D-loop, the opposite chimeric tRNA would be reduced rapidly by DUS2. Reduction of both of these chimeric tRNAs by DUS2 was slow. The observed rate constants for tRNA reduction were 1.6 x 10^{-5} s^{-1} and 2.6 x 10^{-5} s^{-1} for the construct in Figure 4 - 5A and Figure 4 - 5B, respectively (Figure 4 - 5C).

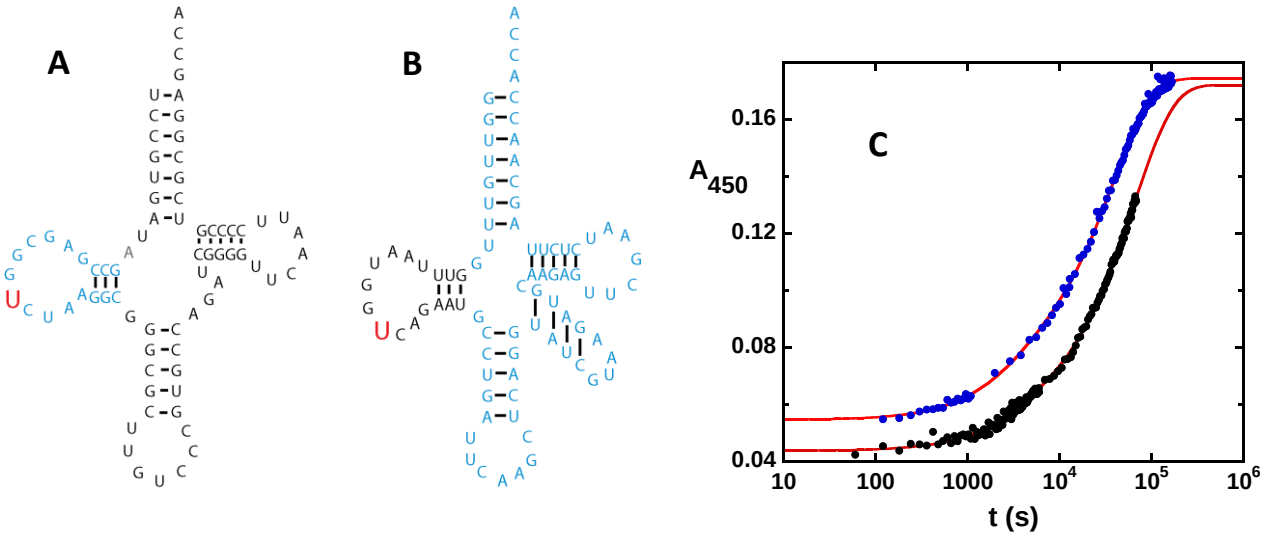

Figure 4 - 5. Cloverleaf structures and reactivity of chimeric tRNAs. (A) and (B) show the cloverleaf structures of the two chimeric tRNAs. Regions derived from $tRNA^{Asp}$ are depicted in black; regions derived from $tRNA^{Leu}$-CAA are depicted in blue. (C) Oxidative half-reactions of the tRNAs in (A) and (B) with $DUS2_{red}$. The tRNA in (A) reacted with k_{obs} of 1.6 x 10^{-5} s^{-1} (black data). The tRNA in (B) reacted with k_{obs} of 2.6 x 10^{-5} s^{-1} (blue data). Both constructs reacted poorly with DUS2.

The Reaction Rate of DUS2 is not Based on a Single Modification

The unmodified $tRNA^{Asp}$ oxidative half-reaction experiments indicate that not all tRNAs require additional modifications to react with DUS2. One possible explanation for this result is that $tRNA^{Asp}$ does not normally contain the modification that is required for $tRNA^{Leu}$-CAA to react rapidly with DUS2. Indeed, $tRNA^{Leu}$-CAA contains 7 modifications that are not found in $tRNA^{Asp}$. I sought to eliminate some of these 7 modifications as potential candidates for the modification that enhances the reactivity with DUS2 by analyzing the reactivities of additional unmodified tRNAs which contain subsets of those 7 modifications. If the important modification that enhances reactivity is normally present on a given tRNA, that tRNA should react poorly with DUS2 as an unmodified transcript. However, if a given tRNA does not normally contain the important modification, it should react rapidly with DUS2 even when unmodified. Analyzing enough tRNAs should eliminate all but one candidate modification. By examining the Transfer RNA Database,[2] $tRNA^{His2}$ and $tRNA^{Ala}$, which contain 4 and 1 of the 7 modifications, respectively (Figure 4 - 6) were chosen.

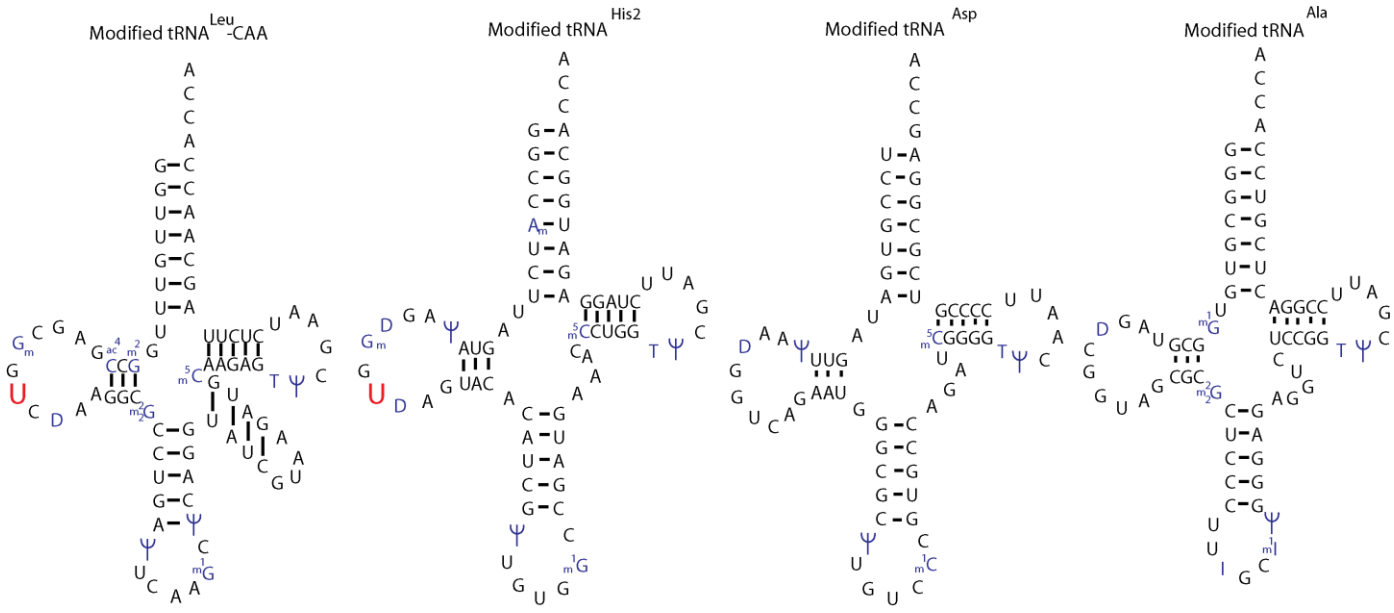

Figure 4 - 6. A comparison of the modification profiles of the four yeast tRNAs used in this study. The uridine that reacts with DUS2 is highlighted in red and the other modifications are highlighted in blue. Abbreviations used: m^2G: N^2-methylguanosine, ac^4C: N^4-acetylcytidine, Gm: 2'-O-methylguanosine, D: dihydrouridine, $m^2{}_2G$: N^2,N^2-dimethylguanosine, ψ: pseudouridine, m^5C: 5-methylcytidine, m^1G: N^1-methylguanosine, T: 5-methyluridine, Am: 2'-O-methyladenosine , I: inosine, m^1I: 1-methylinosine.

The oxidative half-reactions with these two tRNAs were monitored in a stopped-flow spectrophotometer by anaerobically mixing $DUS2_{red}$ with either unmodified $tRNA^{His2}$ or unmodified $tRNA^{Ala}$. Unmodified $tRNA^{His2}$ reacted rapidly in a single phase with an observed rate constant of 0.22 ± 0.01 s^{-1} (Figure 4 - 7A). Unmodified $tRNA^{Ala}$ also reacted rapidly with $DUS2_{red}$; traces were biphasic (Figure 4 - 7B). Similar to the reaction with unmodified $tRNA^{Asp}$, the first phase contributed the majority of the signal change and was attributed to oxidation of the flavin by unmodified $tRNA^{Ala}$. The second phase was attributed to a small amount of enzyme aggregation or multiple populations of tRNA. The rate constant for flavin oxidation of $DUS2_{red}$ by unmodified $tRNA^{Ala}$ was 0.15 ± 0.01 s^{-1}. Since unmodified $tRNA^{Ala}$ and $tRNA^{His2}$ reacted rapidly with $DUS2_{red}$, the modifications that they share with $tRNA^{Leu}$-CAA are unlikely to be the modification

required for $tRNA^{Leu}$-CAA to react rapidly with DUS2. Eliminating those modifications leaves only N^2-methylguanosine at position 10 (m^2G_{10}) and N4-acetylcytidine at position 12 (ac^4C_{12}) in $tRNA^{Leu}$-CAA as candidates.

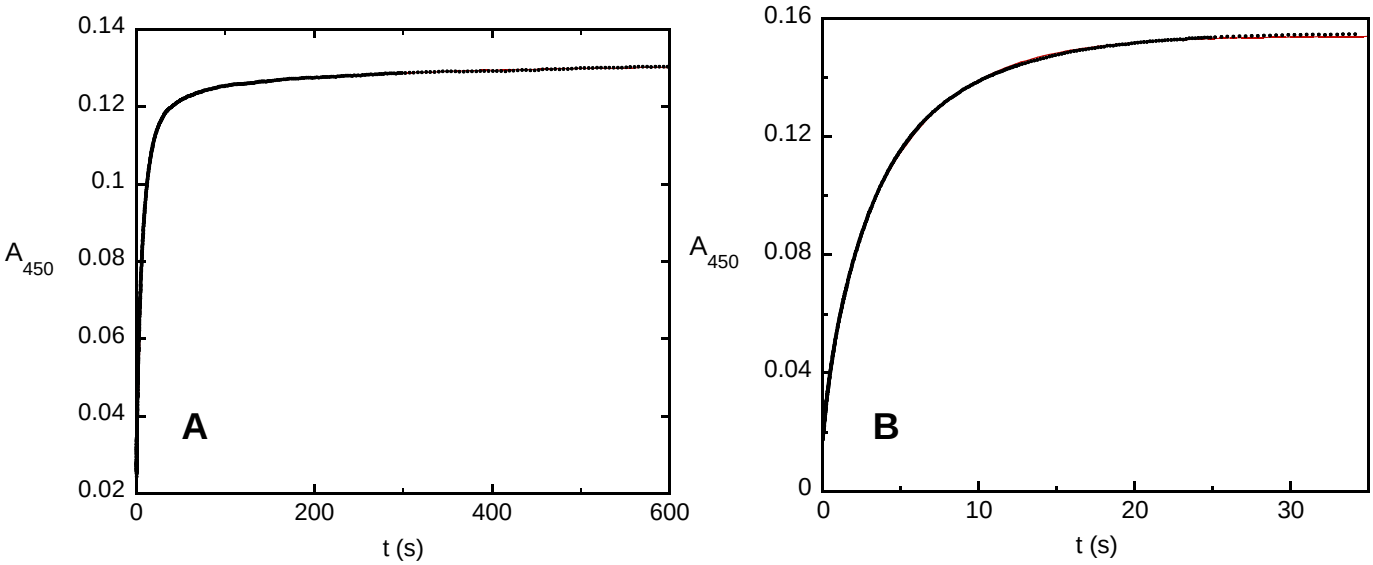

Figure 4 - 7. Oxidation of $DUS2_{red}$ by unmodified $tRNA^{Ala}$ (A) or $tRNA^{His2}$ (B). 15 µM $DUS2_{red}$ was mixed with 25-50 µM unmodified $tRNA^{Ala}$ or $tRRNA^{His2}$ after mixing in 100 mM M HEPES-NaOH pH 7.5, 100 mM NaCl, 10 mM $MgCl_2$, 10 % glycerol at 4 °C in a stopped-flow spectrophotometer. Traces at 450 nm fit to two exponentials for unmodified $tRNA^{Ala}$ and one exponential for unmodified $tRNA^{His2}$. The insets show the rate constants for flavin oxidation by the two tRNAs. The rate constants for flavin oxidation by unmodified $tRNA^{Ala}$ and unmodified $tRNA^{His2}$ were 0.15 s^{-1} and 0.22 s^{-1}, respectively, both of which are comparable to the rate constants for flavin oxidation by unmodified $tRNA^{Asp}$ and mature $tRNA^{Leu}$-CAA.

In the process of incorporating individual modifications into unmodified $tRNA^{Leu}$-CAA *in vitro* using recombinant tRNA-modifying enzymes, it was discovered that $tRNA^{Leu}$-CAA reacted rapidly with $DUS2_{red}$ if the tRNA had been pre-incubated with the enzymes that incorporate 2'-O-methylguanosine at position 18 (Gm_{18}), N^2,N^2-dimethylguanosine at position 26 ($m^2{}_2G_{26}$), pseudouridine at position 32 (ψ_{32}) and 55 (ψ_{55}), N^1-methylguanosine at position 34 (m^1G_{34}), and 5-methyluridine at position 54 (m^5U_{54}) (Figure 4 - 8). Notably absent from this partially modified $tRNA^{Leu}$-CAA are

m^2G_{10} and ac^4C_{12}, indicating that these modifications are also not required for $tRNA^{Leu}$-CAA to react rapidly with DUS2.

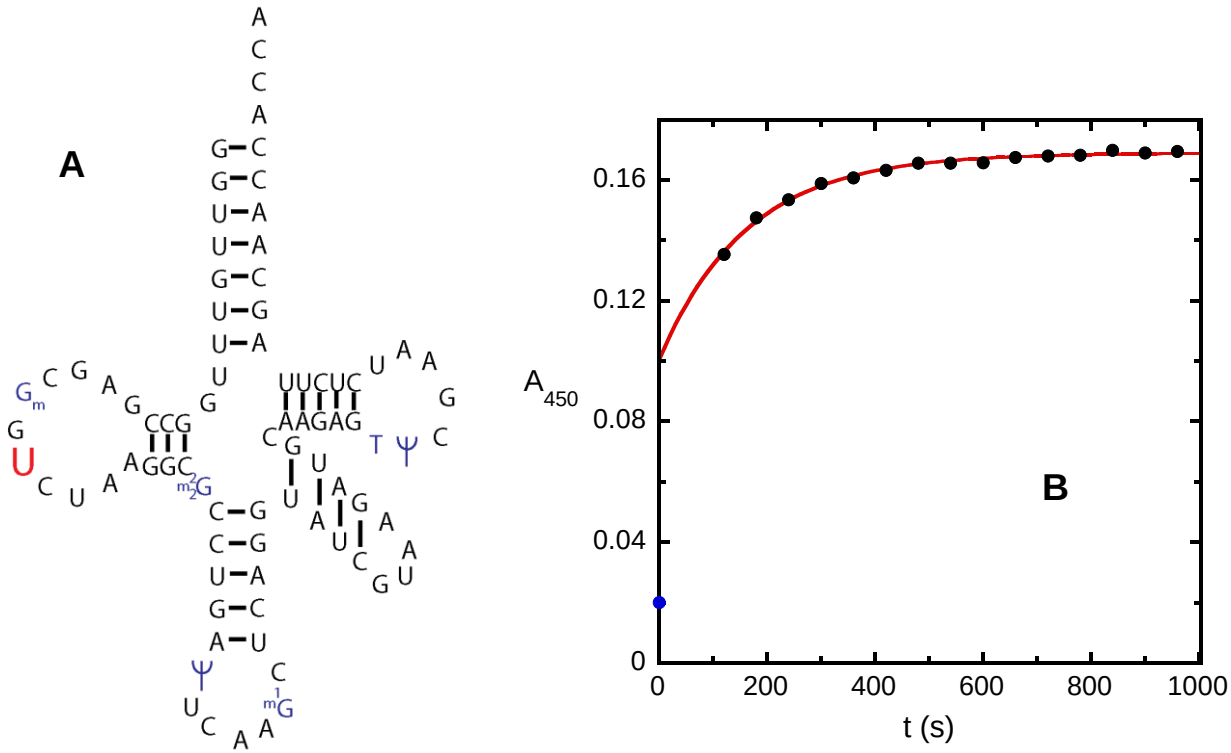

Figure 4 - 8. Oxidation of $DUS2_{red}$ by partially modified $tRNA^{Leu}$-CAA. A, cloverleaf structure of $tRNA^{Leu}$-CAA containing 6 post-transcriptional modifications incorporated *in vitro* using recombinant tRNA-modifying enzymes. B, Reaction of 15 µM $DUS2_{red}$ with 75 µM of the partially modified $tRNA^{Leu}$-CAA shown in A. The reaction was performed in 100 mM HEPES-NaOH, pH 7.5, 100 mM NaCl, 10 mM $MgCl_2$, 10 % glycerol at 4 °C using a standard scanning spectrophotometer with one minute scan intervals. Most of the flavin was oxidized after the first scan, indicating that the partially modified $tRNA^{Leu}$-CAA reacted rapidly with $DUS2_{red}$. The data fit to a single exponential with k_{obs} of 6 x 10^{-3} ± 3 x 10^{-4} s^{-1}. The fit did not extrapolate back to the initial absorbance of $DUS2_{red}$ (shown as a blue dot), indicating that at least one exponential completed prior to the first data point.

Unmodified $tRNA^{Asp}$, $tRNA^{Leu}$-CAA, $tRNA^{Ala}$, and $tRNA^{His2}$ Bind to Oxidized DUS2 with Similar Affinities

Binding of unmodified $tRNA^{Asp}$ induced a substantial change in the flavin absorbance spectrum of $DUS2_{ox}$ (Figure 4 - 9A). This spectral change can be used to track unmodified $tRNA^{Asp}$ binding in titration experiments, allowing the dissociation constant for unmodified $tRNA^{Asp}$ binding to $DUS2_{ox}$ to be determined. Unmodified $tRNA^{Asp}$ bound stoichiometrically to $DUS2_{ox}$. Fitting to Eq. 1 provided an estimate of the K_d of 1.1 ± 0.4 μM. Binding of unmodified $tRNA^{His2}$ also produced a similar change in the flavin absorbance of $DUS2_{ox}$ as binding of unmodified $tRNA^{Asp}$. Curiously, binding of unmodified $tRNA^{Leu}$-CAA, mature $tRNA^{Leu}$-CAA, or unmodified $tRNA^{Ala}$ did not produce a substantial change in the absorbance spectrum of $DUS2_{ox}$. However, binding of these tRNAs to $DUS2_{ox}$ caused significant quenching of the flavin fluorescence (Figure 4 - 9B). The affinities of unmodified $tRNA^{Leu}$-CAA, $tRNA^{Ala}$, and $tRNA^{His2}$ for $DUS2_{ox}$ were determined through fluorimetric titrations. Fitting the change in fluorescence against tRNA concentration provided estimates of 1.4 ± 0.7 μM, 1.0 ± 0.1 μM, and 1.8 ± 0.2 μM for the K_ds of binding to $DUS2_{ox}$ for $tRNA^{Leu}$-CAA, $tRNA^{Ala}$, and $tRNA^{His2}$, respectively (Figures 4 - 9C, 4 - 9D, 4 - 9E and Table 4 - 1). The affinities for the four unmodified tRNAs are similar to the affinity for mature $tRNA^{Leu}$-CAA, which had a K_d of 0.8 ± 0.5 μM.[9]

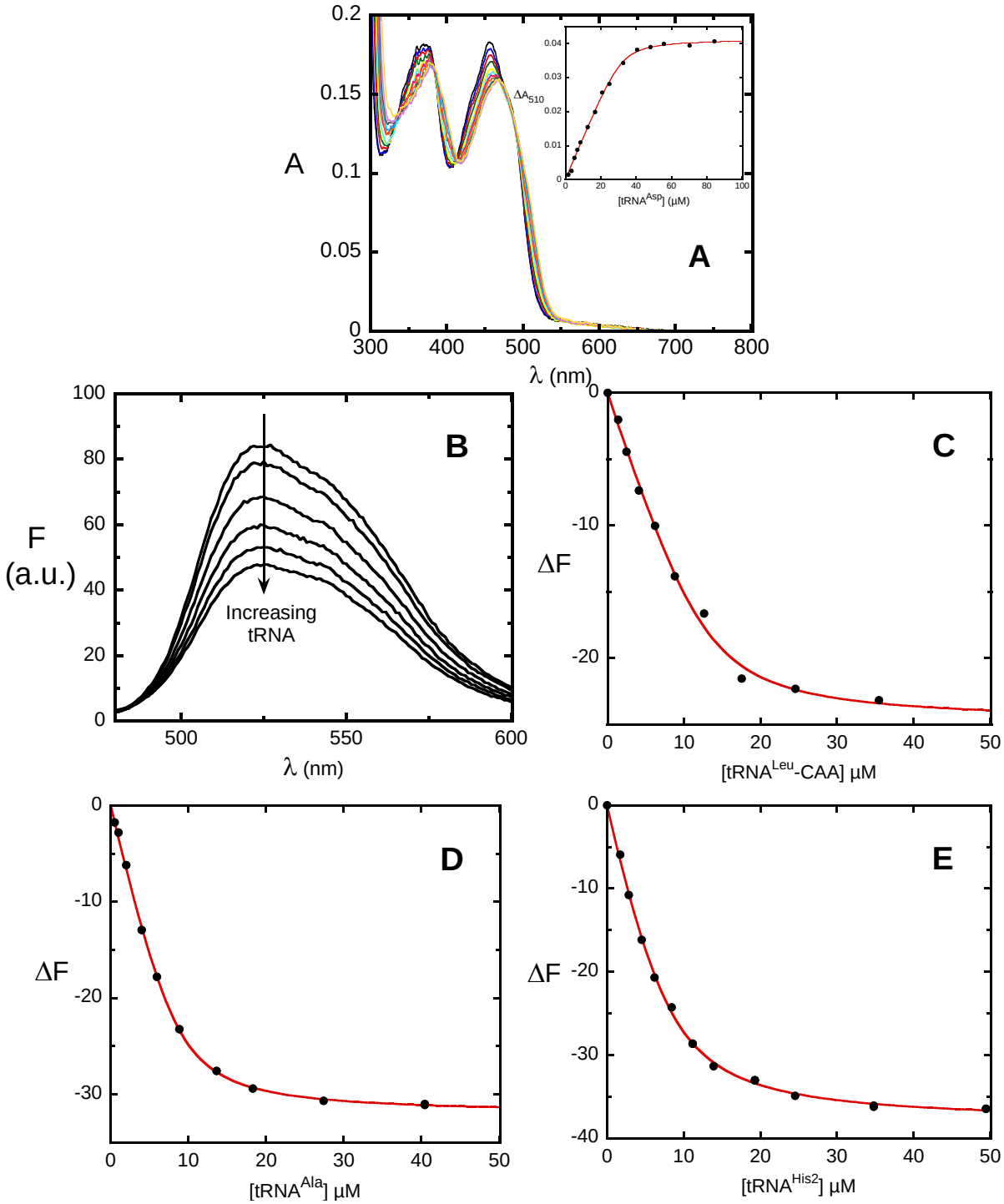

Figure 4 - 9. Titration of $DUS2_{ox}$ with unmodified tRNAs. Titrations were performed in 100 mM HEPES-NaOH, pH 7.5, 100 mM NaCl, 10 mM $MgCl_2$, 10 % glycerol at 4 °C. (A) binding of unmodified $tRNA^{Asp}$ to $DUS2_{ox}$ causes a significant change in the absorbance spectrum of the flavin. The inset shows ΔA_{510nm} against $tRNA^{Asp}$ concentration. Fitting to Eq. 1 gives a K_d of 1.1 ± 0.4 μM. (B) binding of unmodified $tRNA^{Leu}$-CAA, $tRNA^{Ala}$ or $tRNA^{His2}$ quenched the fluorescence of the flavin of $DUS2_{ox}$. (C), (D), and (E), the change in $DUS2_{ox}$ fluorescence as a function of tRNA concentration for unmodified $tRNA^{Leu}$-CAA, unmodified $tRNA^{Ala}$, and unmodified $tRNA^{His2}$, respectively. Fitting to Eq. 1 gives a K_d of 1.4 ± 0.7 μM, 1.0 ± 0.1 μM, and 1.8 ± 0.2 μM for unmodified $tRNA^{Leu}$-CAA, unmodified $tRNA^{Ala}$, and unmodified $tRNA^{His2}$, respectively.

Table 4 - 1: tRNA Binding to $DUS2_{ox}$[a]	
tRNA	K_d (μM)
Unmodified $tRNA^{Asp}$	1.1 ± 0.4
Unmodified $tRNA^{Leu}$-CAA	1.4 ± 0.7
Unmodified $tRNA^{Ala}$	1.0 ± 0.1
Unmodified $tRNA^{His2}$	1.8 ± 0.2
Mature $tRNA^{Leu}$-CAA[b]	0.8 ± 0.5

[a]0.1 M HEPES-NaOH, pH 7.5, 100 mM NaCl, 10 mM MgCl2, 10 % glycerol at 4°C. [b]Data from ref. 9

Unmodified $tRNA^{Leu}$-CAA Exists in Multiple Conformations

A native-PAGE experiment was performed to assess whether unmodified $tRNA^{Leu}$-CAA has a tertiary structure similar to mature $tRNA^{Leu}$-CAA (Figure 4 - 10). Interestingly, 1 μM unmodified $tRNA^{Leu}$-CAA refolded by heating to 65 °C then cooling on ice ran as two distinct populations on the native-PAGE, whereas unmodified $tRNA^{Asp}$, unmodified $tRNA^{Ala}$, unmodified $tRNA^{His2}$, and mature $tRNA^{Leu}$-CAA ran as a single band. The two populations were present when unmodified $tRNA^{Leu}$-CAA was refolded in the presence or absence of Mg^{2+}, indicating that Mg^{2+} does not help stabilize one conformation over the other. However, under denaturing conditions all of the tRNAs ran as a single band. Refolding the slower-running band that had been gel-purified under native conditions produced tRNA containing both populations on a native PAGE gel, indicating that the two bands are different conformations of the same molecule (Figure 4 - 11).

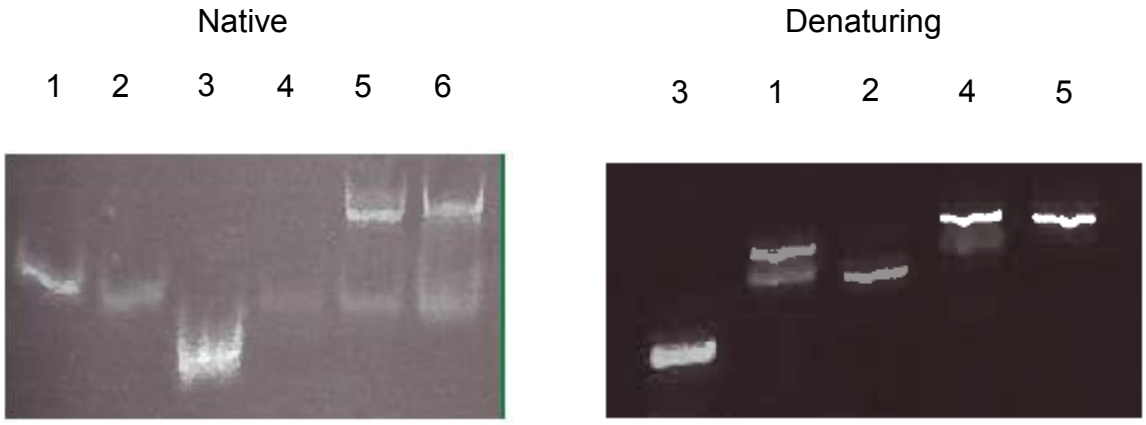

Figure 4 - 10. Native and denaturing PAGE gels of the tRNAs used in this study. tRNAs at 1 µM were refolded by heating to 65 °C for 5 minutes followed by cooling on ice in 10 mM Tris-HCl pH 8, 10 mM $MgCl_2$, 10 % glycerol. (1) Unmodified $tRNA^{Ala}$; (2) unmodified $tRNA^{Asp}$; (3) unmodified $tRNA^{His2}$; (4) mature $tRNA^{Leu}$-CAA; (5) unmodified $tRNA^{Leu}$-CAA refolded in the presence of Mg^{2+}; (6) unmodified $tRNA^{Leu}$-CAA refolded in the absence of Mg^{2+} (20 mM EDTA added). Unmodified $tRNA^{Leu}$-CAA ran as two populations on the native gel whereas the other tRNAs ran as a single population (left panel). All of the tRNAs – including unmodified $tRNA^{Leu}$-CAA – ran as a single population on the denaturing gel (right panel).

Figure 4 - 11. Native PAGE gel showing that the two conformations of unmodified $tRNA^{Leu}$-CAA can interconvert. The larger band of unmodified $tRNA^{Leu}$-CAA from the native gel in Figure 4 - 9 was gel-purified under native conditions. (1) the larger band of unmodified $tRNA^{Leu}$-CAA without refolding; (2) the larger band of unmodified $tRNA^{Leu}$-CAA refolded by heating to 65 °C for five minutes followed by cooling on ice.

The oxidative half-reaction experiments required very high concentrations of tRNA (>750 µM). Unmodified $tRNA^{Leu}$-CAA refolded at 750 µM tRNA failed to enter the gel of a native-PAGE (Figure 4 - 12A), suggesting that unmodified $tRNA^{Leu}$-CAA refolded under conditions necessary for the oxidative half-reaction experiments exists solely as a large oligomer, explaining why unmodified $tRNA^{Leu}$-CAA reacts poorly with $DUS2_{red}$. A native gel of the *in vitro* transcription reaction to produce unmodified $tRNA^{Leu}$-CAA also showed multiple populations of tRNA (Figure 4 - 12B), indicating that unmodified $tRNA^{Leu}$-CAA is not transcribed into a single conformation.

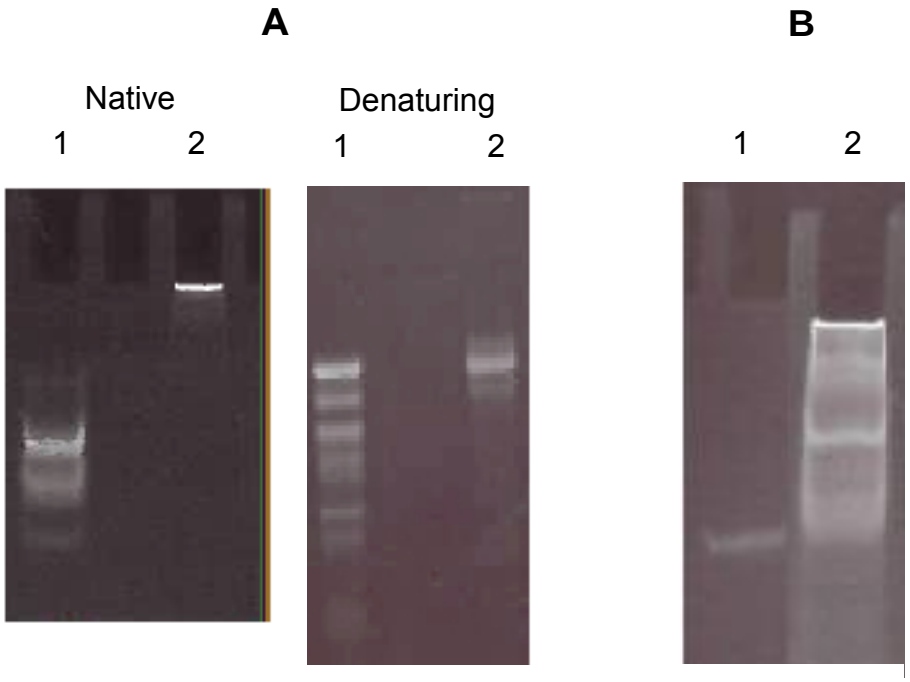

Figure 4 - 12. Unmodified $tRNA^{Leu}$-CAA does not fold correctly. (A) native and denaturing gels showing that unmodified $tRNA^{Leu}$-CAA refolded under conditions necessary for the oxidative half-reaction experiments (750 µM tRNA) is a large oligomer. (1) mature $tRNA^{Leu}$-CAA; (2) unmodified $tRNA^{Leu}$-CAA. The extra bands in the mature $tRNA^{Leu}$-CAA lane were attributed to minor degradation of the tRNA due to RNAses. (B) native gel showing that unmodified $tRNA^{Leu}$-CAA is not transcribed solely into the correct conformation during *in vitro* transcription reactions. (1) mature $tRNA^{Leu}$-CAA; (2) the *in vitro* transcription reaction to make unmodified $tRNA^{Leu}$-CAA.

Binding Kinetics of Unmodified $tRNA^{Asp}$ to $DUS2_{ox}$

Binding of unmodified $tRNA^{Asp}$ to $DUS2_{ox}$ caused a significant blue-shift in the flavin absorbance spectrum (Figure 4 - 9A). The kinetics of binding of unmodified $tRNA^{Asp}$ to $DUS2_{ox}$ was investigated by performing stopped-flow experiments, monitoring the change in flavin absorbance at 510 nm (Figure 4 - 13A). Traces fit to two exponentials. The first contributed the majority (>95%) of the signal change and was attributed to binding of unmodified $tRNA^{Asp}$ to $DUS2_{ox}$. The second, minor phase was inconsistent and attributed to minor enzyme aggregation or multiple populations of tRNA. The observed rate constant for the first exponential remained constant at 2.0 ± 0.02 s^{-1} for all $tRNA^{Asp}$ concentrations used, indicating that binding of unmodified $tRNA^{Asp}$ to $DUS2_{ox}$ does not occur in one step. If binding had occurred in a single step, the observed rate constant would increase linearly with $tRNA^{Asp}$ concentration. The invariant observed rate constant also indicates that the K_d is much less than 20 µM, which is consistent with the equilibrium titration and oxidative half-reaction experiments using $tRNA^{Asp}$.

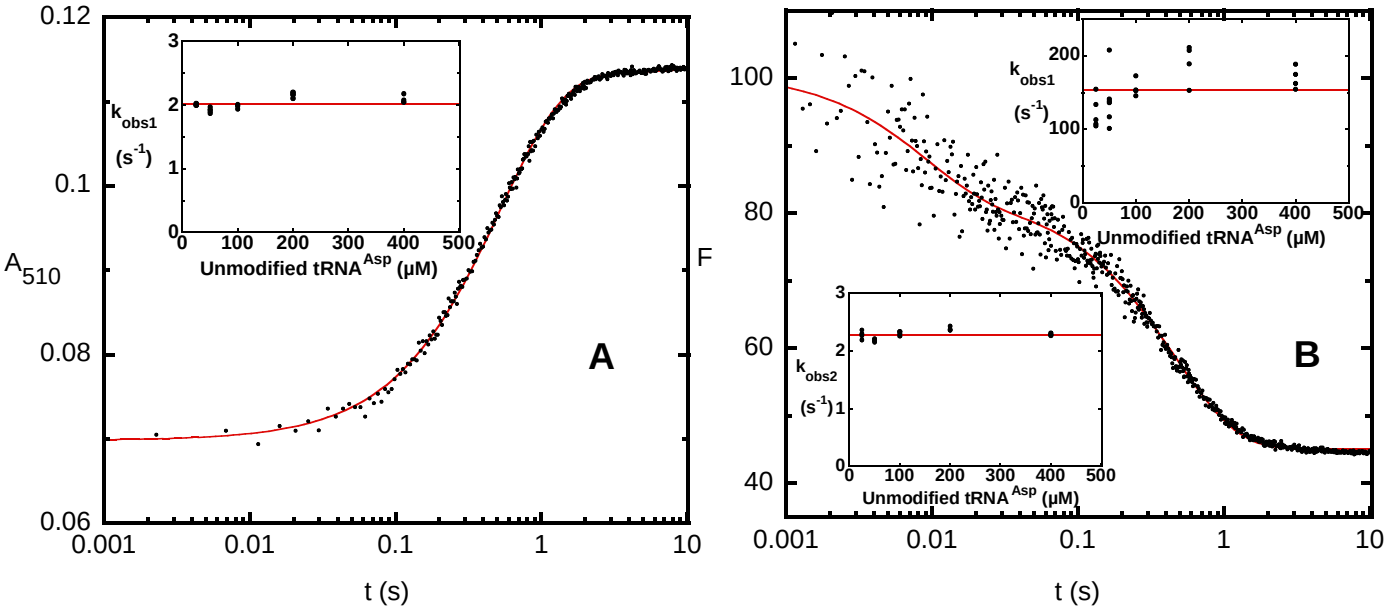

Figure 4 - 13. The kinetics of binding unmodified $tRNA^{Asp}$ to $DUS2_{ox}$. Experiments were performed in 100 mM HEPES-NaOH, pH 7.5, 100 mM NaCl, 10 mM $MgCl_2$, 10% glycerol, 4°C. The insets show the concentration dependence of the k_{obs} values for each experiment. (A) stopped-flow absorbance trace at 510 nm upon binding unmodified $tRNA^{Asp}$ to $DUS2_{ox}$. Traces fit to a single exponential with k_{obs} of 2.0 ± 0.02 s^{-1} at all tRNA concentrations. (B) stopped-flow fluorescence trace of unmodified $tRNA^{Asp}$ binding to $DUS2_{ox}$. Traces fit to two exponentials with k_{obs1} of 150 ± 31 s^{-1} and k_{obs2} of 2.3 ± 0.02 s^{-1} at all tRNA concentrations.

Binding of $tRNA^{Asp}$ to $DUS2_{ox}$ also causes a substantial quench in the fluorescence of the flavin prosthetic group of $DUS2_{ox}$. The binding reaction was monitored through stopped-flow fluorescence experiments in an attempt to characterize the initial bimolecular interaction of $tRNA^{Asp}$ binding to $DUS2_{ox}$. Flavin fluorescence was quenched in two phases (Figure 4 - 13B). The first observed rate constant appeared to remain constant at 150 ± 31 s^{-1} at all $tRNA^{Asp}$ concentrations used; however, the error for the data was relatively high for each tRNA concentration so other data fitting models cannot be excluded. The second observed rate constant remained constant at 2.3 ± 0.02 s^{-1} at all $tRNA^{Asp}$ concentrations. The second exponential likely reflects the same step detected using stopped-flow spectrophotometry. The first exponential cannot represent the initial bimolecular binding step since it does not increase linearly with

$tRNA^{Asp}$ concentration. The stopped-flow data suggest that binding of unmodified $tRNA^{Asp}$ to $DUS2_{ox}$ occurs with at least three steps (Figure 4 - 14).

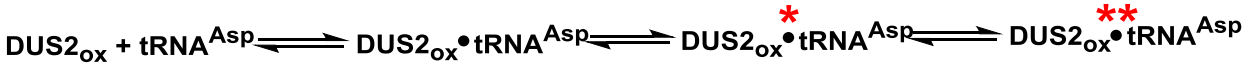

Figure 4 - 14. Proposed mechanism for unmodified $tRNA^{Asp}$ binding to oxidized DUS2.

Discussion

Some tRNAs do not require prior modifications to react rapidly with yeast DUS2 – in this study, unmodified $tRNA^{Asp}$, unmodified $tRNA^{Ala}$, and unmodified $tRNA^{His2}$ all reacted rapidly with $DUS2_{red}$. Of the tRNAs tested thus far, only $tRNA^{Leu}$-CAA requires prior modifications in order to react rapidly with DUS2, suggesting that the incorporation of tRNA modifications is not ordered for all tRNAs. It is not known which of the other yeast tRNAs also require prior modifications in order to react rapidly with DUS2. One notable difference between the cloverleaf structure of $tRNA^{Leu}$-CAA and $tRNA^{Asp}$, $tRNA^{Ala}$, and $tRNA^{His2}$ is that $tRNA^{Leu}$-CAA contains an extended variable loop (Figure 4 - 6). In yeast, the only tRNAs containing an extended variable loop are the $tRNA^{Leu}$ and $tRNA^{Ser}$ variants. The requirement for modifications might therefore be isolated to these tRNAs.

A single modification is not responsible for accelerating the reactivity of all tRNAs with DUS2. Hybrid constructs swapping the D-loops of unmodified $tRNA^{Asp}$ and unmodified $tRNA^{Leu}$-CAA both reacted poorly with $DUS2_{red}$, suggesting that modifications in both the D-loop and the body of $tRNA^{Leu}$-CAA are required for $tRNA^{Leu}$-CAA to react rapidly with DUS2; if only one modification in a particular portion of $tRNA^{Leu}$-CAA were important for reactivity with DUS2, replacing that portion with the

sequence of $tRNA^{Asp}$ should alleviate the requirement for that modification. In addition, unmodified $tRNA^{Asp}$, unmodified $tRNA^{Ala}$, and unmodified $tRNA^{His2}$ all react rapidly with $DUS2_{red}$; the modifications they share with $tRNA^{Leu}$-CAA therefore cannot be the single modification that enhances the reactivity of all tRNAs with $DUS2_{red}$. The only modifications present in $tRNA^{Leu}$-CAA that are also absent in $tRNA^{Asp}$, $tRNA^{Ala}$, or $tRNA^{His2}$ are m^2G_{10} and ac^4C_{12}. However, $tRNA^{Leu}$-CAA containing Gm_{18}, $m^2{}_2G_{26}$, ψ_{34}, m^1G_{37}, m^5U_{54}, ψ_{55} reacts rapidly with $DUS2_{red}$. Therefore, m^2G_{10} and ac^4C_{12} cannot be the single modification that enhances the reactivity of all tRNAs with $DUS2_{red}$.

Unmodified $tRNA^{Leu}$-CAA folds into multiple conformations – depending on the tRNA concentration – providing a potential explanation for the poor reactivity of unmodified $tRNA^{Leu}$-CAA with $DUS2_{red}$. At relatively low concentrations (1 μM), unmodified $tRNA^{Leu}$-CAA folds into two populations that migrate differently on a native-PAGE gel; one of the populations migrates through the native gel similar to mature $tRNA^{Leu}$-CAA whereas the other, more highly populated conformation, migrates more slowly through the gel. At concentrations used for the oxidative half-reaction experiments (750 μM), unmodified $tRNA^{Leu}$-CAA folds into a single population that is too large to enter the native gel. One possibility is that unmodified $tRNA^{Leu}$-CAA oligomerizes upon refolding, which would be consistent with the apparent dependence of the tRNA conformation on the concentration of tRNA used during refolding. $tRNA^{Leu}$-CAA wouldn't be unique with this regard, as a number of other tRNAs have been shown to form dimers.[25–27] Another possibility is that unmodified $tRNA^{Leu}$-CAA folds into a conformation that differs from the usual L-shape conformation. $tRNA^{Leu}$-CAA isolated from yeast used to be known as the "renaturable" $tRNA^{Leu}$ since it could be converted

into a misfolded conformation with an atypical secondary structure by refolding in the absence of Mg^{2+}.[28,29] Regardless, the presence of modifications in mature $tRNA^{Leu}$-CAA must help stabilize the properly folded state since only a single conformation of mature $tRNA^{Leu}$-CAA was detected by native-PAGE.

The misfolded conformation of unmodified $tRNA^{Leu}$-CAA does not have a large effect on the binding affinity of $DUS2_{ox}$ for tRNAs; the four unmodified tRNAs used in this study bind to $DUS2_{ox}$ with affinities similar to mature $tRNA^{Leu}$-CAA. This could indicate that binding of tRNAs by DUS2 is dominated by the favorable ionic interactions between the positively charged surface of DUS2 and the negatively charged phosphates of tRNA. The K_ds determined through titrations represent the apparent equilibrium constant resulting from the multiple steps that occur with tRNA binding to $DUS2_{ox}$. The kinetic data on unmodified $tRNA^{Asp}$ binding to $DUS2_{ox}$ indicates that binding of unmodified $tRNA^{Asp}$ occurs with at least three steps, one of which is only detectable by fluorescence. The steps in addition to the bimolecular step could represent conformational changes like base-flipping of the reactive uracil into the active site of DUS2, or perhaps a rearrangement of the TIM-barrel and helix-bundle domains of DUS2 to accommodate tRNA binding. It is unclear why binding of unmodified $tRNA^{Asp}$ or unmodified $tRNA^{His2}$ causes a substantial change in the absorbance spectrum of $DUS2_{ox}$ whereas binding of unmodified $tRNA^{Ala}$, unmodified $tRNA^{Leu}$-CAA, or mature $tRNA^{Leu}$-CAA do not produce a similar change in the absorbance spectrum. It does suggest, though, that the environment of the flavin is different when bound to $tRNA^{Asp}$ or $tRNA^{His2}$ compared to the other tRNAs.

One question raised by this work is how $tRNA^{Leu}$-CAA properly folds *in vivo.* $tRNA^{Leu}$-CAA would initially be transcribed without the modifications that stabilize the properly folded conformation. However, $tRNA^{Leu}$-CAA is also transcribed with an intron between the anticodon loop and the variable loop that is removed during processing. The role of the intron is currently unknown. The intron could stabilize the native conformation of $tRNA^{Leu}$-CAA, allowing some post-transcriptional modifications to be incorporated before removal of the intron. Indeed, studies in *Xenopus laevis* oocyte nuclei have shown that a number of modifications are incorporated into tRNA prior to removal of the intron.[30] Unmodified $tRNA^{Leu}$-CAA containing the intron is a poor substrate of DUS2.[9] However, DUS2 might not recognize $tRNA^{Leu}$-CAA until the intron has been removed.

Conclusions

All tRNAs do not require prior modifications in order to react rapidly with yeast DUS2, and no single modification is responsible for enhancing the reactivity of all tRNAs with DUS2. Unmodified $tRNA^{Leu}$-CAA, which is a poor substrate of DUS2, folds into different conformations depending on the tRNA concentration used during refolding. At concentrations needed for oxidative half-reaction experiments with DUS2, unmodified $tRNA^{Leu}$-CAA refolds into a large oligomer, explaining why unmodified $tRNA^{Leu}$-CAA is a poor substrate of DUS2. Multiple modifications likely must be present on $tRNA^{Leu}$-CAA for it to fold into the conformation that reacts rapidly with DUS2.

References

(1) Czerwoniec, A., Dunin-Horkawicz, S., Purta, E., Kaminska, K. H., Kasprzak, J. M., Bujnicki, J. M., Grosjean, H., and Rother, K. (2009) MODOMICS: a database of RNA modification pathways. 2008 update. *Nucleic Acids Res. 37*, D118–21.

(2) Jühling, F., Mörl, M., Hartmann, R. K., Sprinzl, M., Stadler, P. F., and Pütz, J. (2009) tRNAdb 2009: compilation of tRNA sequences and tRNA genes. *Nucleic Acids Res. 37*, D159–62.

(3) Xing, F., Martzen, M. R., and Phizicky, E. M. (2002) A conserved family of Saccharomyces cerevisiae synthases effects dihydrouridine modification of tRNA . A conserved family of Saccharomyces cerevisiae synthases effects dihydrouridine modification of tRNA. *RNA* 370–81.

(4) Dalluge, J. J., Hashizume, T., Sopchik, A. E., Mccloskey, J. A., and Davis, D. R. (1996) Conformational flexibility in RNA : the role of dihydrouridine. *Nucleic Acids Res. 24*, 1073–9.

(5) Noon, K. R., Guymon, R., Crain, P. F., Mccloskey, J. A., Thomm, M., Lim, J., and Cavicchioli, R. (2003) Influence of Temperature on tRNA Modification in Archaea : Methanococcoides burtonii (Optimum Growth Temperature [T opt], 23°C) and Stetteria hydrogenophila (T opt , 95°C). *J. Bacteriol. 185*, 5483–90.

(6) Alexandrov, A., Chernyakov, I., Gu, W., Hiley, S. L., Hughes, T. R., Grayhack, E. J., and Phizicky, E. M. (2006) Rapid tRNA decay can result from lack of nonessential modifications. *Mol. Cell 21*, 87–96.

(7) Kuchino, Y., and Borek, E. (1978) Tumour-specific phenylalanine tRNA contains two supernumerary methylated bases. *Nature 271*, 126–9.

(8) Kato, T., Daigo, Y., Hayama, S., Ishikawa, N., Yamabuki, T., Ito, T., Miyamoto, M., Kondo, S., and Nakamura, Y. (2005) A Novel Human tRNA-Dihydrouridine Synthase Involved in Pulmonary Carcinogenesis. *Cancer Res.* 4–6.

(9) Rider, L. W., Ottosen, M. B., Gattis, S. G., and Palfey, B. A. (2009) Mechanism of Dihydrouridine Synthase 2 from Yeast and the Importance of Modifications for Efficient tRNA Reduction. *J. Biol. Chem. 284*, 10324 –33.

(10) Chang, S. H., Kuo, S., Hawkins, E., and Miller, N. (1973) The Corrected Nucleotide Sequence of Yeast Leucine Transfer Ribonucleic Acid. *Biochem. Biophys. Res. Commun. 51*, 951–5.

(11) Becker, H. F., Motorin, Y., Planta, R. J., and Grosjean, H. (1997) The yeast gene YNL292w encodes a pseudouridine synthase (Pus4) catalyzing the formation of Ψ 55 in both mitochondrial and cytoplasmic tRNAs. *Yeast 25*, 4493–9.

(12) Behm-ansmant, I., Grosjean, H., Motorin, Y., Branlant, C., and I, U. H. P. N. (2004) Pseudouridylation at Position 32 of Mitochondrial and Cytoplasmic tRNAs Requires Two Distinct Enzymes in Saccharomyces cerevisiae *. *Biochemistry 279*, 52998–3006.

(13) Nordlund, M. E., Johansson, J. O. M., Von Pawel-Rammingen, U., and Byström, A. S. (2000) Identification of the TRM2 gene encoding the tRNA (m5U54) methyltransferase of Saccharomyces cerevisiae. *RNA 6*, 844–60.

(14) Liu, J., Liu, J., and Stråby, K. B. (1998) Point and deletion mutations eliminate one or both methyl group transfers catalysed by the yeast TRM1 encoded tRNA (m22G26)dimethyltransferase. *Nucleic Acids Res. 26*, 5102–8.

(15) Björk, G. R., Jacobsson, K., Nilsson, K., Johansson, M. J. O., Byström, A. S., and Persson, O. P. (2001) A primordial tRNA modification required for the evolution of life ? *EMBO J. 20*, 231–9.

(16) Ochi, A., Makabe, K., Kuwajima, K., and Hori, H. (2010) Flexible recognition of the tRNA G18 methylation target site by TrmH methyltransferase through first binding and induced fit processes. *J. Biol. Chem. 285*, 9018–29.

(17) Stols, L., Gu, M., Dieckman, L., Raffen, R., Collart, F. R., and Donnelly, M. I. (2002) A new vector for high-throughput, ligation-independent cloning encoding a tobacco etch virus protease cleavage site. *Protein Expr. Purif. 25*, 8–15.

(18) Gill, S. C., and von Hippel, P. H. (1989) Calculation of protein extinction coefficients from amino acid sequence data. *Anal. Biochem. 182*, 319–26.

(19) Easton, L. E., Shibata, Y., and Lukavsky, P. J. (2010) Rapid, nondenaturing RNA purification using weak anion-exchange fast performance liquid chromatography. *RNA 16*, 647–53.

(20) Serebrov, V., Clarke, R. J., Gross, H. J., and Kisselev, L. (2001) Mg2+-induced tRNA folding. *Biochemistry 40*, 6688–98.

(21) Yue, D., Kintanar, a, and Horowitz, J. (1994) Nucleoside modifications stabilize Mg2+ binding in Escherichia coli tRNA(Val): an imino proton NMR investigation. *Biochemistry 33*, 8905–11.

(22) Yu, F., Tanaka, Y., Yamashita, K., Suzuki, T., Nakamura, A., Hirano, N., Suzuki, T., Yao, M., and Tanaka, I. (2011) Molecular basis of dihydrouridine formation on tRNA. *Proc. Natl. Acad. Sci. U. S. A. 108*, 19593–8.

(23) Gu, X., Yu, M., Ivanetich, K. M., and Santi, D. V. (1998) Molecular recognition of tRNA by tRNA pseudouridine 55 synthase. *Biochemistry 37*, 339–43.

(24) Becker, H. F., Motorin, Y., Sissler, M., Florentz, C., and Grosjean, H. (1997) Major identity determinants for enzymatic formation of ribothymidine and pseudouridine in the T psi-loop of yeast tRNAs. *J. Mol. Biol. 274*, 505–18.

(25) Zachau, H. G. (1968) Serine Specific Transfer Ribonucleic Acids. *Eur. J. Biochem. 5*, 559–66.

(26) Loehnr, J. S., and Keller, E. B. (1968) Dimers of Alanine Transfer RNA with Acceptor Activity. *PNAS 61*, 1115–22.

(27) Curnow, A. W., and Garcia, G. A. (1994) tRNA-guanine transglycosylase from Escherichia coli: Recognition of dimeric, unmodified tRNATyr. *Biochimie 76*, 1183–91.

(28) Adams, A., Lindahl, T., and Fresco, J. R. (1967) Conformational Differences Between the Biologically Active and Inactive Forms of a transfer Ribonucleic Acid. *Biochemistry 57*, 1684–91.

(29) Kearns, D. R., Wong, Y. P., Chanp, S., and Hawkins, E. (1974) Investigation of the Structures of Native and Denatured Conformations of tRNALeu3 by High-Resolution Nuclear Magnetic Resonance. *Biochemistry 13*, 4736–46.

(30) Nishikura, K., and Derobertis, E. (1981) RNA processing in microinjected Xenopus oocytes - Sequential addition of base modifications in a spliced transfer RNA. *J. Mol. Biol. 145*, 405–20.

Chapter 5

Conclusions and Future Directions

This thesis focused on understanding the mechanism of substrate recognition and activation of two flavoenzymes involved in pyrimidine metabolism - flavin-dependent thymidylate synthase (FDTS) and tRNA-dihydrouridine synthase (DUS).

Flavin-Dependent Thymidylate Synthase

Chapter 2 focused on testing a mechanism for FDTS where dUMP is activated as a nucleophile by the electrostatically polarizing active site of the enzyme.[1] The NMR data presented in Chapter 2 show that N3 of dUMP is ionized when bound to FDTS due to a specific arginine (R174 in *T. maritima* FDTS) in the active site of the enzyme. The electrostatic polarization is so extreme that the pK_a of N3 is lowered by a still-unknown value. Therefore, I proposed an alternative mechanism for dUMP activation that explicitly includes ionization of N3 (Figure 5 - 1). Ionization of N3 of dUMP is clearly important for catalysis since the oxidative half-reaction of a R174A mutant enzyme of FDTS, which does not ionize N3 of dUMP, is ~3000-fold slower than WT.[1]

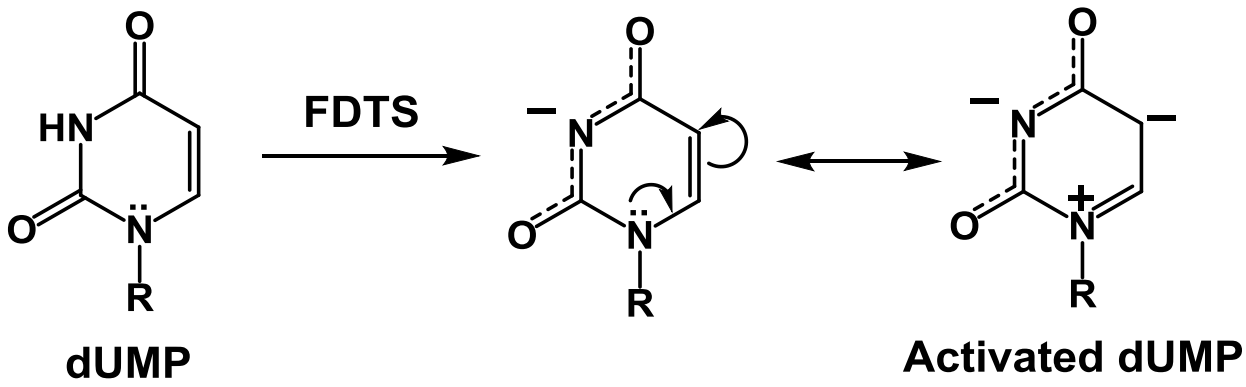

Figure 5 - 1. Activation of dUMP by FDTS. FDTS ionizes N3 of dUMP, which is proposed to enhance the contribution and reactivity of the resonance structure of dUMP with a formal negative charge on C5.

In addition to identifying that FDTS ionizes N3 of dUMP, I also presented biochemical data on substrate analogs that suggests that the phosphate of dUMP is the base that abstracts the C5 proton of the dUMP-CH_2THF bridged intermediate. dU, which lacks the phosphate, was still ionized when bound to the enzyme, but failed to promote oxidation of the flavin of reduced FDTS in the presence of CH_2THF. Likewise, dUMS – whose sulfate has a much lower pK_a than phosphate – was also unable to oxidize the flavin of reduced FDTS in the presence of CH_2THF. The crystal structures of the dU-FDTS and dUMS-FDTS complexes show that the lack of reactivity of the dUMP analogs is not due to improper positioning of the uracil in the active site of the enzyme. Presumably, dU and dUMS form the bridged intermediate with CH_2THF when reacting with FDTS, but cannot abstract the C5 proton necessary to continue to the flavin oxidation step. Notably, both ionization and acid-base chemistry by the phosphate of dUMP are not implicated in the mechanism used by classic thymidylate synthase,[2] further emphasizing the differences between FDTS and classic thymidylate synthase.

In Chapter 3 I used a battery of equilibrium and kinetic methods to monitor dUMP and dTMP binding to *Thermotoga maritima* FDTS. A number of studies have suggested that the dissociation of dTMP and association of dUMP steps occur when the flavin of FDTS is oxidized.[3,4] However, I discovered that FDTS binds deoxynucleotides with ~200-fold weaker affinity when the flavin is reduced compared to when it is oxidized, and the differences in affinity are largely due to differences in the dissociation rate constant. This finding strongly suggests that the exchange of dTMP and dUMP in the kinetic mechanism of FDTS occurs when the flavin is reduced.

I also found that there is, curiously, a temperature-dependent effect on the mechanism by which FDTS binds deoxynucleotides – below 45°C the FDTS homotetramer behaves as a dimer-of-dimers with regards to deoxynucleotide binding while at temperatures above 45°C the four subunits of FDTS bind deoxynucleotides identically. The dimer-of-dimers behavior could be active at higher temperatures as well, but is only detectable at lower temperatures. The dimer-of-dimers behavior of FDTS for deoxynucleotide binding would only be catalytically relevant with the reduced enzyme since the dTMP made at the end of the oxidative half-reaction would not have enough time to dissociate from the oxidized enzyme (due to the low k_{off} values for dTMP bound to oxidized FDTS) before reduction of the flavin by NADPH. Upon reduction of the flavin, the k_{off} values for dTMP increase ~200-fold so dTMP could quickly dissociate from one or both of the sets of sites to allow dUMP to bind and initiate the oxidative half-reaction.

Future Directions

The data I presented in Chapter 2 clearly show that dUMP is ionized in the active site of FDTS, which is important for catalysis. However, it would be beneficial to verify that C5 of dUMP is more nucleophilic in N3-ionized dUMP than in unionized dUMP. Computational methods could be used to compare the molecular orbital energies of ionized and unionized dUMP. The reactivity of dUMP could be enhanced in N3-ionized dUMP if the highest occupied molecular orbital energy more closely matches the lowest unoccupied molecular orbital energy of CH_2THF than in unionized dUMP.

It would also be interesting to determine if FDTS abstracts the N3 proton of dUMP using an active site base or if it simply binds the N3-ionized population of dUMP in solution. At pH 8, where the majority of the work on *T. maritima* FDTS has been performed, only 4.8% of the dUMP in solution would be ionized (the pK_a of N3 of dUMP is ~9.3 in water).[5] One way to address this would be to perform ITC titrations of FDTS with dUMP in different buffers that have different enthalpies of ionization. If protons are released upon binding of dUMP, the enthalpy of binding should correlate with the difference in ionization enthalpy of the different buffers. However, if an active site base abstracts the N3 proton the enthalpy of dUMP binding should be identical in all buffers. I attempted to do these experiments in Chapter 3 but the differences in binding enthalpy between buffers were not consistent with the differences in the ionization enthalpies of the buffers. The buffers could conceivably bind in the dUMP binding site, which would alter the enthalpy of binding measured by ITC; care should be taken in the future to avoid buffers that might bind in the dUMP binding site.

All chemical mechanisms proposed for FDTS include the formation of a dUMP-CH_2THF bridged intermediate at some point in the mechanism. However, such an intermediate has never been detected. In principle, dU and dUMS should stop at the bridged intermediate when reacting with FDTS. Yet, I was unable to detect the intermediate with dUMS after denaturing the enzyme, indicating that it might be unstable when removed from the active site of the enzyme. The bridged intermediate could potentially be detected while bound to the enzyme by NMR using ^{13}C-labeled dU or dUMS. Upon formation of the bridged intermediate, the C5 carbon of the uracil would go from being sp^2 hybridized to being sp^3 hybridized, which should coincide with a substantial change in the chemical shift of the C5 carbon. Therefore, the ^{13}C C5 chemical shift of dU or dUMS bound to reduced FDTS in the presence of CH_2THF (forming the bridged intermediate) should indicate the formation of the intermediate.

Another question on FDTS raised by the work presented in this thesis is the origin of the dimer-of-dimers behavior of FDTS with regards to deoxynucleotide binding at lower temperatures. The only structures of FDTS currently available are those without deoxynucleotides bound or with dUMP or its analogs bound in all four active sites of the tetramer. A structure of FDTS where half of the active sites have dUMP bound could clarify the structural differences between the two sets of binding sites. One potential clue comes from the nucleotide-free structure of FDTS – a histidine (H53 in T. maritima) is in two different conformations in the four active sites of the tetramer (Figure 5 - 2). The histidine might play a role in causing the asymmetry among the active sites of the FDTS tetramer (Chapter 3). It would also be interesting to determine if FDTS exhibits the dimer-of-dimers behavior at low temperatures in other steps of the catalytic cycle

(e.g. CH_2THF binding, flavin reduction/oxidation, etc.). It is worth noting that reduction of the flavin of dUMP-bound FDTS occurs in two phases with roughly equal amplitudes.[6]

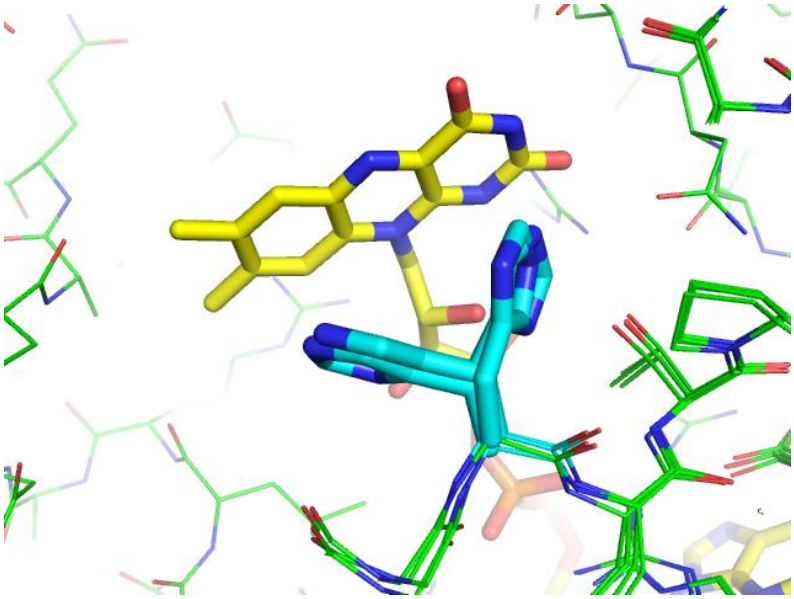

Figure 5 - 2. Overlay of the four subunits in unbound *T. maritima* FDTS (PDB code 4KQ4). Only one FAD (yellow) is shown for clarity. Histidine-53 (cyan) in the active site is in two different conformations in the four subunits of the FDTS homotetramer.

tRNA-Dihydrouridine Synthase

In Chapter 4, I examined the reactivity of several unmodified tRNAs with yeast DUS2 in oxidative half-reactions. In contrast with $tRNA^{Leu}$-CAA – which requires other modifications in order to react rapidly with DUS2[7] – $tRNA^{Asp}$, $tRNA^{Ala}$, and $tRNA^{His2}$ reacted rapidly with DUS2 as unmodified transcripts. I also presented evidence suggesting that it is unlikely that a single modification is responsible for enhancing the reactivity of $tRNA^{Leu}$-CAA with DUS2 – more likely, multiple modifications in different regions of the tRNA are necessary to enhance the reactivity of $tRNA^{Leu}$-CAA with DUS2.

Unmodified $tRNA^{Leu}$-CAA folds into an incorrect, possibly oligomeric, conformation, explaining why unmodified $tRNA^{Leu}$-CAA is such a poor substrate for DUS2. The structure of the DUS-tRNA complex from *Thermus thermophilus* shows that DUS recognizes the majority of a properly folded, L-shaped tRNA (Figure 5 - 3).[8] Given the mode of tRNA recognition in that structure, it is unlikely that DUS could recognize the correct uracil of a tRNA in a different conformation.

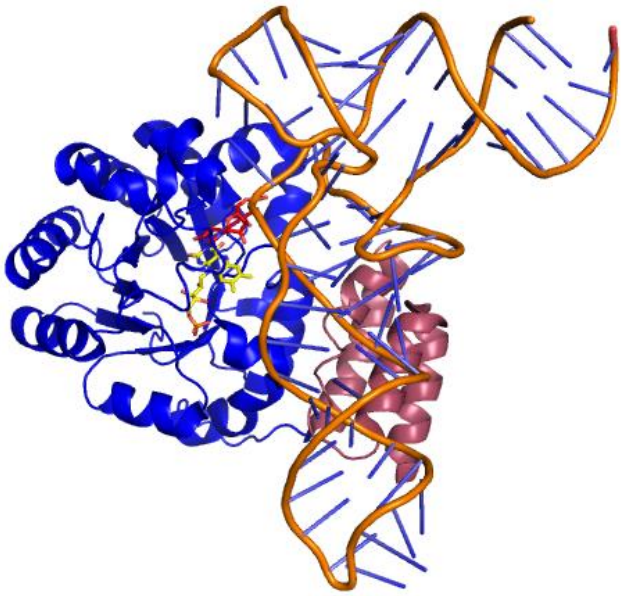

Figure 5 - 3. Structure of *T. thermophilus* DUS in complex with tRNA (PDB 3B0U). The two domains of DUS are shown in blue and pink. The tRNA is shown in orange.

Future Directions

The biggest question arising from the work presented in Chapter 4 is why $tRNA^{Leu}$-CAA requires modifications to properly fold while other tRNAs do not. This question could be addressed by assessing whether or not other unmodified tRNAs fold properly. The reactivity of each tRNA with yeast DUS2 could be used as a diagnostic of proper folding. If enough unmodified tRNAs are analyzed, patterns might develop that could indicate the features that cause certain unmodified tRNAs to misfold. While we

now know that unmodified $tRNA^{Leu}$-CAA misfolds, we still don't know the structure of the misfolded state. NMR could potentially be used to determine the secondary and tertiary structures of improperly folded unmodified $tRNA^{Leu}$-CAA, which might also shed light on why unmodified $tRNA^{Leu}$-CAA adopts the non-canonical conformation.

It is also unclear how $tRNA^{Leu}$-CAA folds properly *in vivo*. $tRNA^{Leu}$-CAA would initially be transcribed as an unmodified transcript, which would misfold. However, it is also initially transcribed with an intron that might facilitate the proper folding of $tRNA^{Leu}$-CAA, allowing some modifications to be incorporated prior to removal of the intron. It would be interesting to see if intron-containing unmodified $tRNA^{Leu}$-CAA properly folds – native PAGE could be used to initially assess whether unmodified $tRNA^{Leu}$-CAA containing the intron oligomerizes. NMR could then be used to determine if intron-containing unmodified $tRNA^{Leu}$-CAA adopts the correct secondary and tertiary structures.

References

(1) Conrad, J. A., Ortiz-Maldonado, M., Hoppe, S. W., and Palfey, B. A. (2014) Detection of Intermediates in the Oxidative Half-Reaction of the FAD-Dependent Thymidylate Synthase from Thermotoga maritima: Carbon Transfer without Covalent Pyrimidine Activation. *Biochemistry 53*, 5199–207.

(2) Carreras, C. W., and Santi, D. V. (1995) The catalytic mechanism and structure of thymidylate synthase. *Annu. Rev. Biochem. 64*, 721–62.

(3) Graziani, S., Xia, Y., Gurnon, J. R., Van Etten, J. L., Leduc, D., Skouloubris, S., Myllykallio, H., and Liebl, U. (2004) Functional Analysis of FAD-dependent Thymidylate Synthase ThyX from Paramecium bursaria Chlorella Virus-1. *J. Biol. Chem. 279*, 54340–7.

(4) Becker, H. F., Djaout, K., Lamarre, I., Ulmer, J. E., Schaming, D., Balland, V., Liebl, U., Myllykallio, H., and Vos, M. H. (2014) Substrate interaction dynamics and oxygen control in the active site of thymidylate synthase ThyX. *Biochem. J. 459*, 37–45.

(5) Aylward, N. N. (1967) Thermodynamic Constants of the Ionisation of the Acid Imino-group of Uridine 5'-Monophosphate and Poly-uridylic Acid. *J. Chem. Soc. B Phys. Org.* 401–3.

(6) Conrad, J. A. (2011) The Reactions of Flavin-Dependent Thymidylate Synthase from Thermotoga Maritima. University of Michigan.

(7) Rider, L. W., Ottosen, M. B., Gattis, S. G., and Palfey, B. A. (2009) Mechanism of Dihydrouridine Synthase 2 from Yeast and the Importance of Modifications for Efficient tRNA Reduction. *J. Biol. Chem. 284*, 10324 –33.

(8) Yu, F., Tanaka, Y., Yamashita, K., Suzuki, T., Nakamura, A., Hirano, N., Suzuki, T., Yao, M., and Tanaka, I. (2011) Molecular basis of dihydrouridine formation on tRNA. *Proc. Natl. Acad. Sci. U. S. A. 108*, 19593–8.

Appendix 1

Equations Used for Fitting ITC Data

The following is adapted from the VP-ITC MicroCalorimeter User's Manual (MicroCal, 2004, Northhampton, MA).

Single Set of Identical Sites

For a single set of binding sites

$$K = \frac{\theta}{(1-\theta)[L]} \qquad (1)$$

$$L_t = [L] + n\theta M_t \qquad (2)$$

where K is the binding constant, θ is the fraction of sites occupied by ligand L, [L] is the free concentration of ligand, L_t is the bulk concentration of ligand, n is the number of binding sites, and M_t is the bulk concentration of macromolecule in the active cell volume (V_o)

Combining equations (1) and (2) gives

$$\theta^2 - \theta\left[1 + \frac{L_t}{nM_t} + \frac{1}{nKM_t}\right] + \frac{L_t}{nM_t} = 0 \qquad (3)$$

The total heat content Q of the solution contained in V_o is

$$Q = n\theta M_t \Delta H V_o \qquad (4)$$

where ΔH is the molar heat of ligand binding. Solving equation (3) for θ and substituting into equation (4) gives

$$Q = \frac{nM_t \Delta H V_o}{2}\left[1 + \frac{L_t}{nM_t} + \frac{1}{nKM_t} - \sqrt{\left(1 + \frac{L_t}{nM_t} + \frac{1}{nKM_t}\right)^2 - \frac{4L_t}{nM_t}}\right] \qquad (5)$$

The change in heat after the ith injection {ΔQ(i)} is

$$\Delta Q(i) = Q(i) + \frac{\Delta V_i}{V_o}\left[\frac{Q(i)+Q(i-1)}{2}\right] - Q(i-1) \qquad (6)$$

where ΔV_i is the change in volume after the ith injection.

The experimental data give ΔQ(i) for each injection. Origin uses a nonlinear least-squares algorithm to provide the best-fit values for n, K, and ΔH.

Two Sets of Independent Sites

For two sets of independent binding sites

$$K_1 = \frac{\theta_1}{(1-\theta_1)[L]} \qquad K_2 = \frac{\theta_2}{(1-\theta_2)[L]} \qquad (7)$$

$$L_t = [L] + M_t(n_1\theta_1 + n_2\theta_2) \qquad (8)$$

Solving equation (7) for θ_1 and θ_2 and substituting into equation (8) gives

$$[L]^3 + p[L]^2 + q[L] + r = 0 \quad (9)$$

where

$$p = \frac{1}{K_1} + \frac{1}{K_2} + (n_1 + n_2)M_t - L_t$$

$$q = \left(\frac{n_1}{K_2} + \frac{n_2}{K_1}\right) M_t - \left(\frac{1}{K_1} + \frac{1}{K_2}\right) L_t + \frac{1}{K_1 K_2}$$

$$r = \frac{-L_t}{K_1 K_2} \quad (10)$$

Equations (9) and (10) are solved for [L] numerically in Origin by using Newton's Method to obtain n_1, n_2, K_1,and K_2 and to provide θ_1 and θ_2 from equation (7). These are then used with the total heat content Q of the solution contained in V_o

$$Q = M_t V_o (n_1 \theta_1 \Delta H_1 + n_2 \theta_2 \Delta H_2) \quad (11)$$

and the change in heat content after the ith injection

$$\Delta Q(i) = Q(i) + \frac{\Delta V_i}{V_o}\left[\frac{Q(i)+Q(i-1)}{2}\right] - Q(i-1) \quad (12)$$

using a nonlinear least-squares algorithm to provide the best-fit values for n_1, n_2, K_1, K_2, ΔH_1, and ΔH_2.

Appendix 2

Global Fitting in Berkeley Madonna

The global model that describes all of the experiments

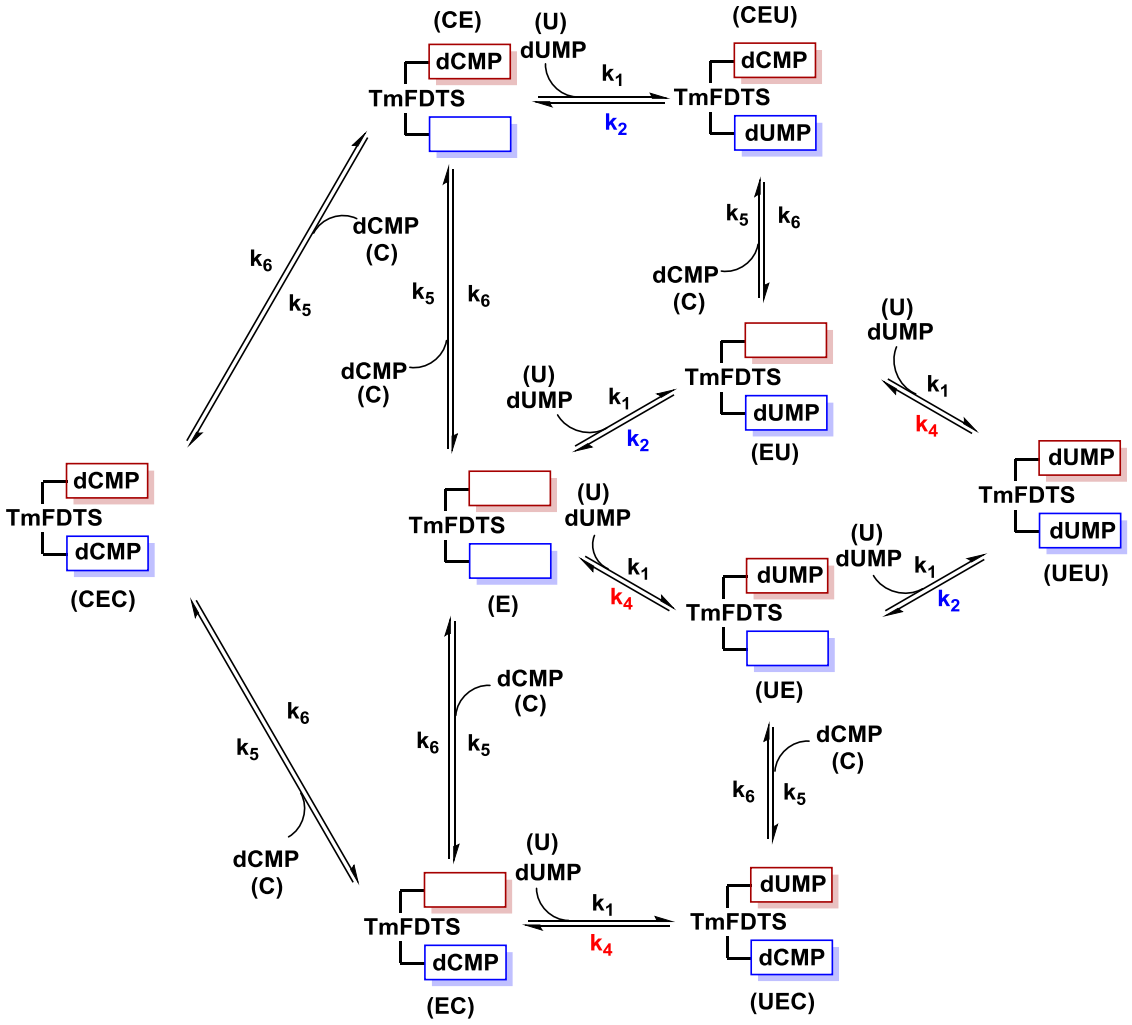

Red = high affinity site; blue = low affinity site; the term in parenthesis denotes the variable used in the differential equations.

Script Used for Global Fitting in Berkeley Madonna

```
METHOD Stiff

STARTTIME = 0

STOPTIME=600

DTMIN = 1e-6

DTMAX = 100

TOLERNACE = 1e-10

DTOUT = 0

d/dt(CEC[1..7]) = -k6*CEC[i] - k6*CEC[i] + k5*CE[i]*C[i] + k5*EC[i]*C[i]

d/dt(CE[1..7]) = -k1*CE[i]*U[i] - k6*CE[i] - k5*CE[i]*C[i] + k6*CEC[i] + k5*E[i]*C[i] +
k2*CEU[i]

d/dt(EC[1..7]) = -k1*EC[i]*U[i] - k6*EC[i] - k5*EC[i]*C[i] + k6*CEC[i] + k5*E[i]*C[i] +
k4*UEC[i]

d/dt(E[1..7]) = -k5*E[i]*C[i] - k5*E[i]*C[i] - k1*E[i]*U[i] - k1*E[i]*U[i] + k6*CE[i] + k6*EC[i] +
k2*EU[i] + k4*UE[i]

d/dt(CEU[1..7]) = -k2*CEU[i] - k6*CEU[i] + k1*CE[i]*U[i] + k5*EU[i]*C[i]

d/dt(UEC[1..7]) = -k4*UEC[i] - k6*UEC[i] + k1*EC[i]*U[i] + k5*UE[i]*C[i]

d/dt(EU[1..7]) = -k2*EU[i] - k5*EU[i]*C[i] - k1*EU[i]*U[i] + k1*E[i]*U[i] + k6*CEU[i] +
k4*UEU[i]

d/dt(UE[1..7]) = -k4*UE[i] - k5*UE[i]*C[i] - k1*UE[i]*U[i] + k1*E[i]*U[i] + k6*UEC[i] +
k2*UEU[i]
```

d/dt(UEU[1..7]) = -k4*UEU[i] - k2*UEU[i] + k1*EU[i]*U[i] + k1*UE[i]*U[i]

d/dt(U[1..7]) = -k1*CE[i]*U[i] + k2*CEU[i] - k1*EC[i]*U[i] + k4*UEC[i] - k1*E[i]*U[i] +

k2*EU[i] - k1*E[i]*U[i] + k4*UE[i] - k1*EU[i]*U[i] + k4*UEU[i] - k1*UE[i]*U[i] + k2*UEU[i]

d/dt(C[1..7]) = -k5*CE[i]*C[i] + k6*CEC[i] - k5*EC[i]*C[i] + k6*CEC[i] - k5*E[i]*C[i] +

k6*CE[i] - k5*E[i]*C[i] + k6*EC[i] - k5*EU[i]*C[i] + k6*CEU[i] - k5*UE[i]*C[i] + k6*UEC[i]

{Experiments 1 through 4 correspond to 50 - 200 µM dUMP binding to free TmFDTS}

init E[1..4] = Et

Et = 8.33e-6

init CEC[1..4] = 0

init CE[1..4] = 0

init EC[1..4] = 0

init CEU[1..4] = 0

init UEC[1..4] = 0

init EU[1..4] = 0

init UE[1..4] = 0

init UEU[1..4] = 0

init U[1] = U1

init U[2] = U2

init U[3] = U3

init U[4] = U4

U1 = 5e-5

U2 = 10e-5

U3 = 15e-5

U4 = 20e-5

init C[1..4] = 0

{Experiments 5 and 6 correspond to competition experiments where the TmFDTS-dUMP complex was competed with 0.1 M or 0.2 M dCMP}

init E[5..6] = 0

init CE[5..6] = 0

init EC[5..6] = 0

init CEU[5..6] = 0

init UEC[5..6] = 0

init EU[5..6] = 0

init UE[5..6] = 0

init UEU[5..6] = UEUt

UEUt = 10.42e-6

init U[5] = U5

init U[6] = U6

U5 = 0

U6 = 0

init C[5] = C5

init C[6] = C6

C5 = 0.1

C6 = 0.2

{Experiment 7 corresponds to the return to baseline of the endothermic event, Figure 3 - 8, detected by ITC}

init E[7] = Et7

Et7 = 0.936e-4

init CEC[7] = 0

init CE[7] = 0

init EC[7] = 0

init CEU[7] = 0

init UEC[7] = 0

init EU[7] = 0

init UE[7] = 0

init UEU[7] = 0

init C[7] = 0

init U[7] = U7

U7 = 0.936e-4

k1 = 6.4e6

k2 = 0.043

k4 = 0.0086

k5 = 1e6

k6 = 7.17

A1 = A[1]

A2 = A[2]

A3 = A[3]

A4 = A[4]

A5 = A[5]

A6 = A[6]

A7 = A[7]

{Different extinction coefficients were used for the binding and competition experiments because the experiments were monitored at different wavelengths - 450 nm for dUMP binding and 390 nm for competition of the TmFDTS-dUMP complex with dCMP}

A[1..4] = os[i] + Ecec1*CEC[i] + Ece1*CE[i] + Eec1*EC[i] + Ee1*E[i] + Eceu1*CEU[i] + Euec1*UEC[i] + Eeu1*EU[i] + Eue1*UE[i] + Eueu1*UEU[i]

Ee1 = 24125

Eeu1 = 23054

Eue1 = 23054

Eueu1 = 21983

Ecec1 = 23000

Ece1 = 23000

Eec1 = 23000

Eceu1 = 23000

Euec1 = 23000

A[5..6] = os[i] + Ecec5*CEC[i] + Ece5*CE[i] + Eec5*EC[i] + Ee5*E[i] + Eceu5*CEU[i] + Euec5*UEC[i] + Eeu5*EU[i] + Eue5*UE[i] + Eueu5*UEU[i]

Ee5 = 20000

Eeu5 = 20000

Eue5 = 20000

Eueu5 = 22050

Ecec5 = 19902

Ece5 = 20000

Eec5 = 20000

Eceu5 = 20976

Euec5 = 20976

{Experiment 7 corresponds to the return to baseline of the endothermic event, Figure 3 - 8, detected by ITC}

A[7] = os[i] + Ecec7*CEC[i] + Ece7*CE[i] + Eec7*EC[i] + Ee7*E[i] + Eceu7*CEU[i] + Euec7*UEC[i] + Eeu7*EU[i] + Eue7*UE[i] + Eueu7*UEU[i]

Ee7 = 0

Eeu7 = 50000

Eue7 = -20000

Eueu7 = 22800

Ecec7 = 20000

Ece7 = 20000

Eec7 = 20000

Eceu7 = 20000

Euec7 = 20000

os[1] = os1

os[2] = os2

os[3] = os3

os[4] = os4

os[5] = os5

os[6] = os6

os[7] = os7

os1 = 0

os2 = -3.478e-5

os3 = -1.41e-4

os4 = -5.456e-4

os5 = 0

os6 = 0.0150869

os7 = 0

Appendix 3

Flavin-Mediated Dual Oxidation Controls an Enzymatic Favorskii-Type Rearrangement

This published study (Teufel, R.*, Miyanaga, A.*, Michaudel, Q.*, Stull, F.*, Louie, G., Noel, J. P., Baran, P. S., Palfey, B., Moore, B.S. *Nature*, 2013, 503, 552-556), for which I am a co-first author, was conducted alongside the work presented in this thesis. The Supporting Information can be found at

http://www.nature.com/nature/journal/v503/n7477/extref/nature12643-s1.pdf

*Contributed equally to the work.

The antibiotic enterocin (compound **1**, Figure A - 1) is produced by various streptomycete bacteria[1] and contains a unique tricyclic caged core. Nearly 40 years ago, isotope labeling studies suggested the involvement of a rare oxidative Favorskii-type rearrangement during its biosynthesis.[2] More recently, the discovery, expression, and biochemical analyses of the *Streptomyces maritimus* enterocin biosynthetic gene cluster including *in vitro* reconstitution of the metabolic pathway showed further involvement of the type II polyketide synthase EncABC and the NADPH-dependent reductase, EncD[1,3,4] (Figure A - 1). Although type II polyketide synthase pathways typically yield polycyclic aromatic products such as the antibiotic tetracycline and the anticancer agent doxorubicin,[5] aromatic polyketides called wailupemycins are formed

only as minor products of the enterocin biosynthetic pathway.[1] Remarkably, the FAD-dependent “favorskiiase” EncM proved to be singly responsible for interruption of the more typical polycyclic aromatization of the poly(β-carbonyl) chain to direct generation of the rearranged desmethyl-5-deoxyenterocin (**2**).[3,6] Until now, detailed mechanistic studies of EncM have been hampered by the inherently high reactivity of the proposed EncM substrate, a putative acyl carrier protein (ACP)-bound C7,O4-dihydrooctaketide intermediate (EncC-octaketide) (**3**). To overcome this experimental limitation we employed synthetic substrate analogs (for synthesis see Supplementary Information), including the untethered C7,O4-dihydrotetraketide (**4**, Figure A - 1), for structure-function analyses of recombinant EncM.

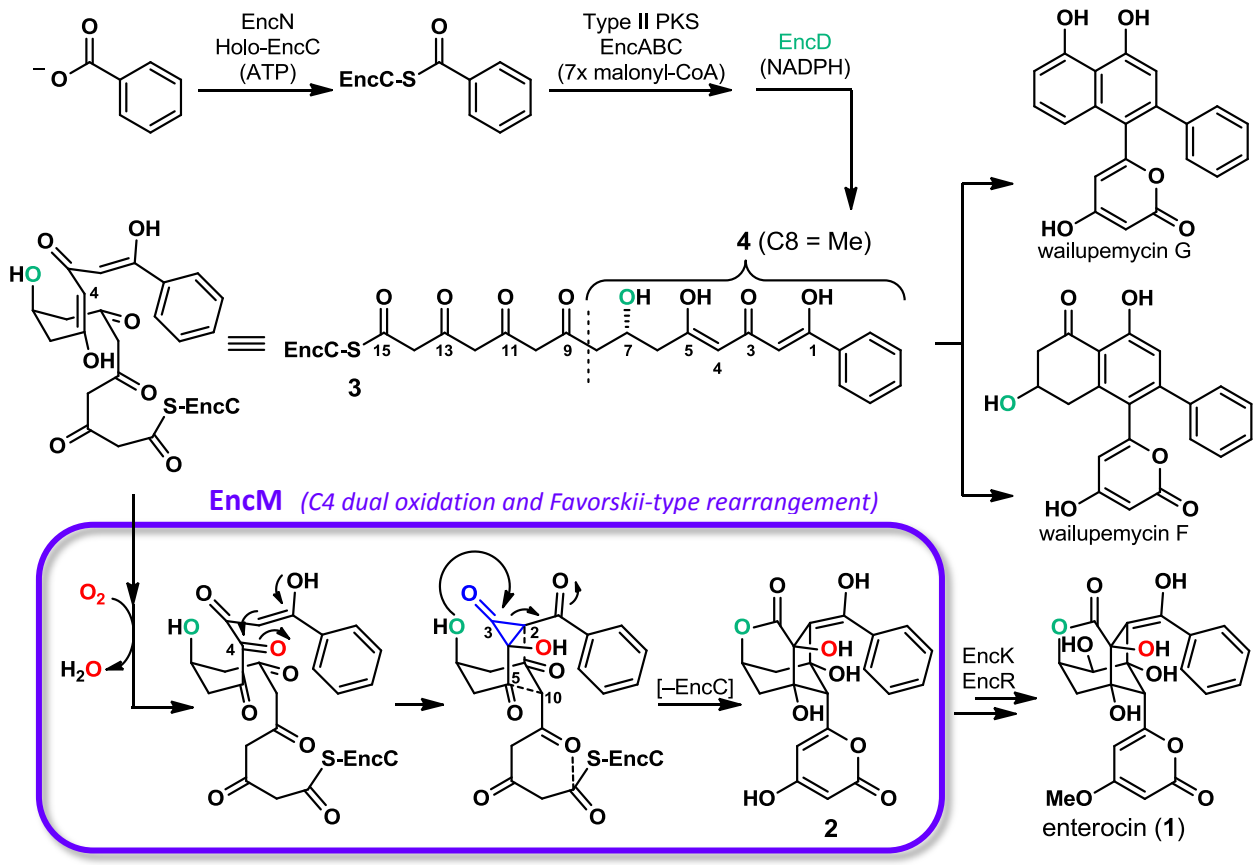

Figure A - 1. Overview of the *Streptomyces maritimus* enterocin biosynthetic pathway and proposed EncM catalysis. The ACP EncC is primed with benzoate by ligase EncN, followed by seven iterative type II polyketide synthase (EncAB)-catalysed elongation steps by decarboxylative Claisen condensations with malonyl-CoA. The ketoreductase EncD probably forms the (R)-7-hydroxyl group during elongation. The linear ((R)-C7,O4-dihydrooctaketide (**3**) can cyclize to various wailupemycins (for example G and F), whereas in the presence of EncM it is preferentially converted into desmethyl-5-deoxyenteroxin (**2**). Final pathway steps leading to enterocin (**1**) are catalyzed by EncR and EncK. EncM catalysis (blue box) involves dual oxidation at C4 (see Figure A - 3b) and a Favorskii-type rearrangement, followed by aldol condensations and heterocycle formation (dashed lines). Functional studies of EncM were conducted with the substrate analogue 4.

Several crystal structures of FAD-bound EncM were determined at resolutions up to 1.8 Å by molecular replacement against 6-hydroxy-D-nicotine oxidase (6HDNO) from *Arthrobacter nicotinivorans*[7] (Figure A - 1, Supplementary Table 1). Structurally, EncM shows greater architectural similarity to flavin dehydrogenases than to oxygenases such as 6HDNO (33% sequence identity for 444 equivalent amino acid residues, 2.2 Å root-mean-square-deviation (rmsd) for Cα-atoms, Z-score = 46.4), glucooligosaccharide oxidase[8] (31% sequence identity for 415 equivalent residues, 2.3 Å rmsd) and aclacinomycin oxidoreductase[9] (37% sequence identity for 316 equivalent residues, 2.5 Å rmsd). In contrast to these monomeric dehydrogenases, EncM exists as a homodimer in crystal form and in solution (Figure A - 2a, Supplementary Fig. 1). The monomeric subunits of the homodimer show structural similarity (0.19 Å rmsd for Cα atoms), and each contains distinct domains for substrate binding (residues 211-418) and FAD-binding (residues 2-210 and 419-461). The FAD-binding domain sequesters the ADP-ribosyl of the flavin cofactor, and the reactive isoalloxazine core resides at the interface between the substrate and cofactor domains (Figures A - 2a, b). As previously observed in 6HDNO, the flavin is covalently linked to EncM via the C8-methyl group of the isoalloxazine ring system and a histidine residue (His78) (Figure A - 2b).

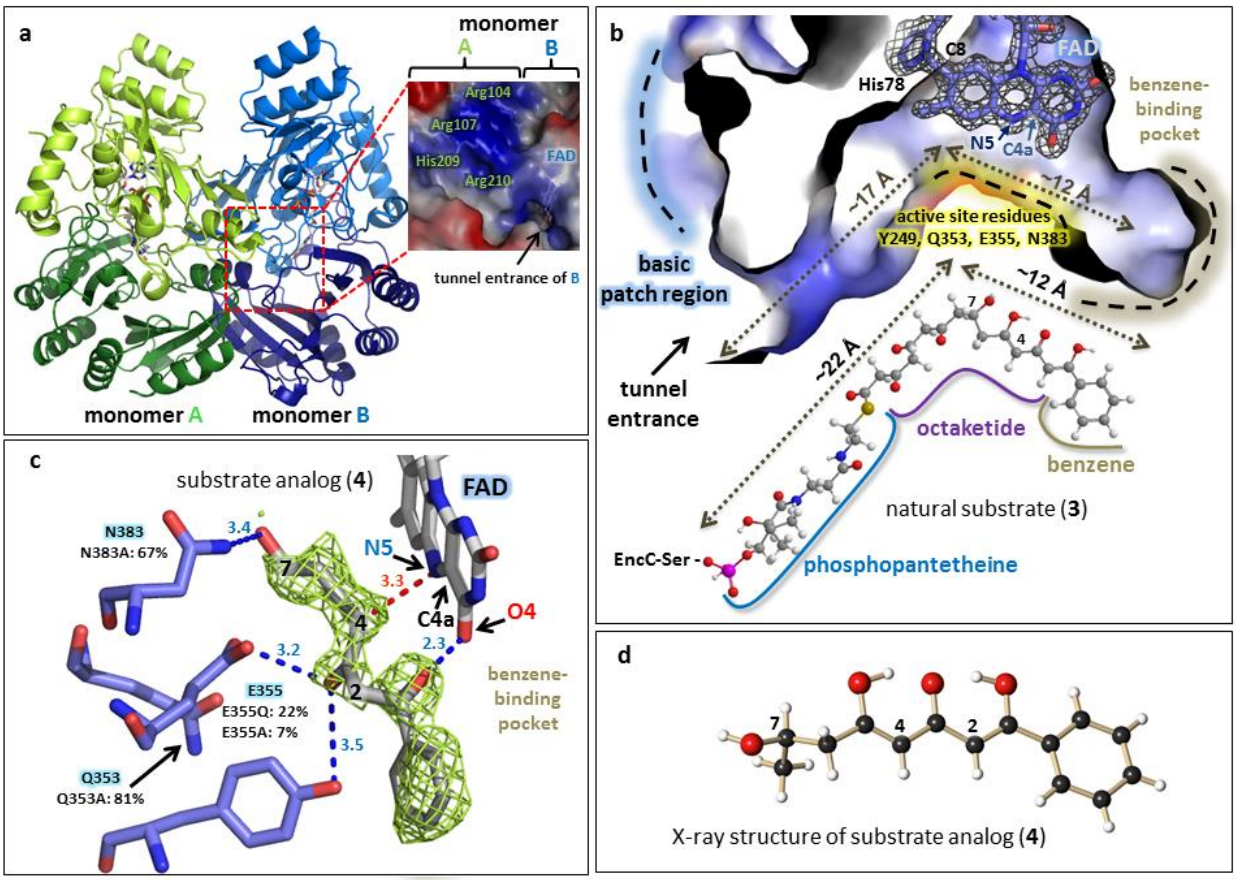

Figure A - 2. Crystal structure of EncM. (a) Homodimeric EncM shown as a ribbon diagram (with flavin cofactors as colour-coded stick model). Monomeric subunits are coloured in green and blue, with darker shades of each highlighting the substrate-binding domains and lighter shades emphasizing the flavin-binding domains. The basic patch abutting the active-site tunnel entrance (dashed red box) is magnified (blue and red colours indicate positive and negative charges, respectively). (b) Sliced-away interior view of the EncM substrate tunnel, showing a covalent link between His78 and FAD (shown is the SIGMAA-weighted $2F_o - F_c$ electron density map contoured at 2.0σ). The natural substrate **3** is shown below. Approximate lengths of the tunnel and substrate are indicated. (c) SIGMAA-weighted $F_o - F_c$ difference map of EncM co-crystallized with **4** calculated with the ligand omitted, contoured at 2.0σ around modelled **4**. Hydrogen-bonding interactions are indicated by blue dashed lines. The red dashed line shows the sitance (in Å) from the site of oxidation to the reactive N5 of FAD. Normalized activities of active site mutants are shown (native EncM = 100%). (d) X-ray structure of the chemically synthesized substrate analogue **4**.

Structure comparisons with homologous flavin-dependent enzymes emphasized the unusually elongated L-shaped EncM ligand-binding tunnel that extends about 30 Å from the surface to a hydrophobic pocket at its base. This orthogonally arranged two-room tunnel is complementary to the shapes of the ACP-derived phosphopantetheine

arm, the octaketide chain and the terminal benzene moiety of **3** (Figure A - 2b, Supplementary Fig. 2). The entrance of the tunnel of EncM sits near the dimer interface and adjacent to a surface-exposed basic patch formed by a few positively charged residues, including Arg107 and Arg210, from the dyad related monomer (Figure A - 2a). This positively charged region of EncM is complementary to the decidedly negative surface area of ACPs,[10] which is indicative that EncC[1] presents elongated polyketide intermediates to EncM through protein-protein interactions to limit deleterious side reactions of the highly reactive poly(β-carbonyl) chain. Support for the close association of EncM and EncC was obtained by protein-protein computational docking simulation using an EncC homology model (Supplementary Fig. 3). Moreover, disruption of the positive surface area of the EncM dimer with the EncM-R210E mutant resulted in about 40% of the relative activity of native EncM (Supplementary Fig. 4).

To explore the interaction of EncM with the polyketide reactant, we co-crystallized the enzyme with substrate analogues harbouring the benzene moiety of **3** (Supplementary Table 1). The resulting SIGMAA-weighted F_o-F_c electron-density difference maps clearly indicated mimetic binding to the active site, although elevated B-factors and incomplete occupancy (for example roughly 33 $Å^2$ and 0.8, respectively for substrate **4**) caused slightly disordered electron densities (Figure A - 2c, Supplementary Fig. 5). Binding occurred with little overall structural perturbation to the EncM polypeptide backbone (e.g., 0.14 Å rmsd for **4**) and no significant backbone or side-chain displacements in the binding region. The terminal benzene group sits at the hydrophobic end of a long tunnel and forms aromatic-aromatic interactions with Tyr150 and Trp152 and van der Waals interactions with Leu357. It is likely that the enol at C1

engages in hydrogen bonding with O4 of the flavin (2.3 Å), whereas the C3 ketone twists away from the flavin and may accept a hydrogen bond from the side chain of Glu355 (3.2 Å) and possibly from Tyr249 (3.5 Å). Mutagenesis of these residues confirmed their importance for EncM activity (Figure A - 2c). In particular, the putative C7-hydroxyl group of **4** resides at the elbow of the L-shaped two-room tunnel and ostensibly serves as the pivot point in the natural substrate **3**. The mutually orthogonal sections of the EncM ligand-binding pocket separate the C1–C6 triketide head from the C8–C15 pantothenate-linked tetraketide tail to uncouple the reactivity of the entire C1-C16 poly(β-carbonyl) chain. This chemical and structural disconnection prevents kinetically facile but unwanted cyclization-aromatization reactions, and instead favours the EncM-mediated oxidative Favorskii-type rearrangement (Figure A - 2b).

We propose that EncM performs a dual oxidation of **3** at C4 to effectively convert a 1,3-diketone to a 1,2,3-triketone. In this mechanistic model, C4 is now set up to undergo a facile electrophilic cyclization with C2 to trigger the proposed Favorskii-like rearrangement (Figure A - 1). Typical flavin oxygenases are initially reduced with NAD(P)H to enable capture of O_2 by reduced flavin (Fl_{red}), generating the flavin-C4a-peroxide oxygenating species.[11] EncM, however, lacks an NAD(P)H binding domain and functions in the absence of a flavin reductase,[3] raising questions surrounding the oxidative mechanism of EncM.

To gain further insight into the EncM chemical mechanism, we analysed the *in vitro* reaction of EncM with either racemic or enantiomerically pure **4** by reversed-phase high-performance liquid chromatography (HPLC) and ultraviolet-visible spectroscopy. We found that **4** was converted in the absence of NAD(P)H into diastereomeric products

5 and **5'** without detectable intermediates (Figure A - 3a). Through comprehensive NMR and mass spectrometric analyses together with chemical synthesis (see Supplementary Information), we identified **5** and **5'** as ring-opened derivatives of the expected enterocin-like lactone **6** (Figure A - 3b). Circular dichroism experiments proved that the configuration of **4** is maintained during the transformation (see Supplementary Information). We reasoned that a facile hydrolytic retro-Claisen ring cleavage[12,13] of **6** occurs after an oxidative Favorskii-type rearrangement and lactonization (Figure A-3b, step VII) that is probably responsible for the racemization of C4. This proposed reaction was further substantiated by the observation that glycerol also effectuates the ring opening to form **7** and **7'** (Figure A - 3a, Supplementary Figs 6, 7). During actual enterocin biosynthesis this reaction is probably prevented through aldol condensations with the remainder of the ketide chain (Figure A - 1). Notably, the C1 and C5 deoxo-substrate analogs **8** and **9**, respectively, were not transformed by EncM, while the dehydroxy-substrate **10** (see Figure A - 3d or Supplementary Fig. 5 for compound structures) was converted into multiple unstable products that were not further characterized. This series of structure-activity relationships revealed that the triketone motif (C1–C6) is essential for catalysis and suggested that the C7-hydroxyl is critical for spatial and temporal control of the EncM catalysed reaction.

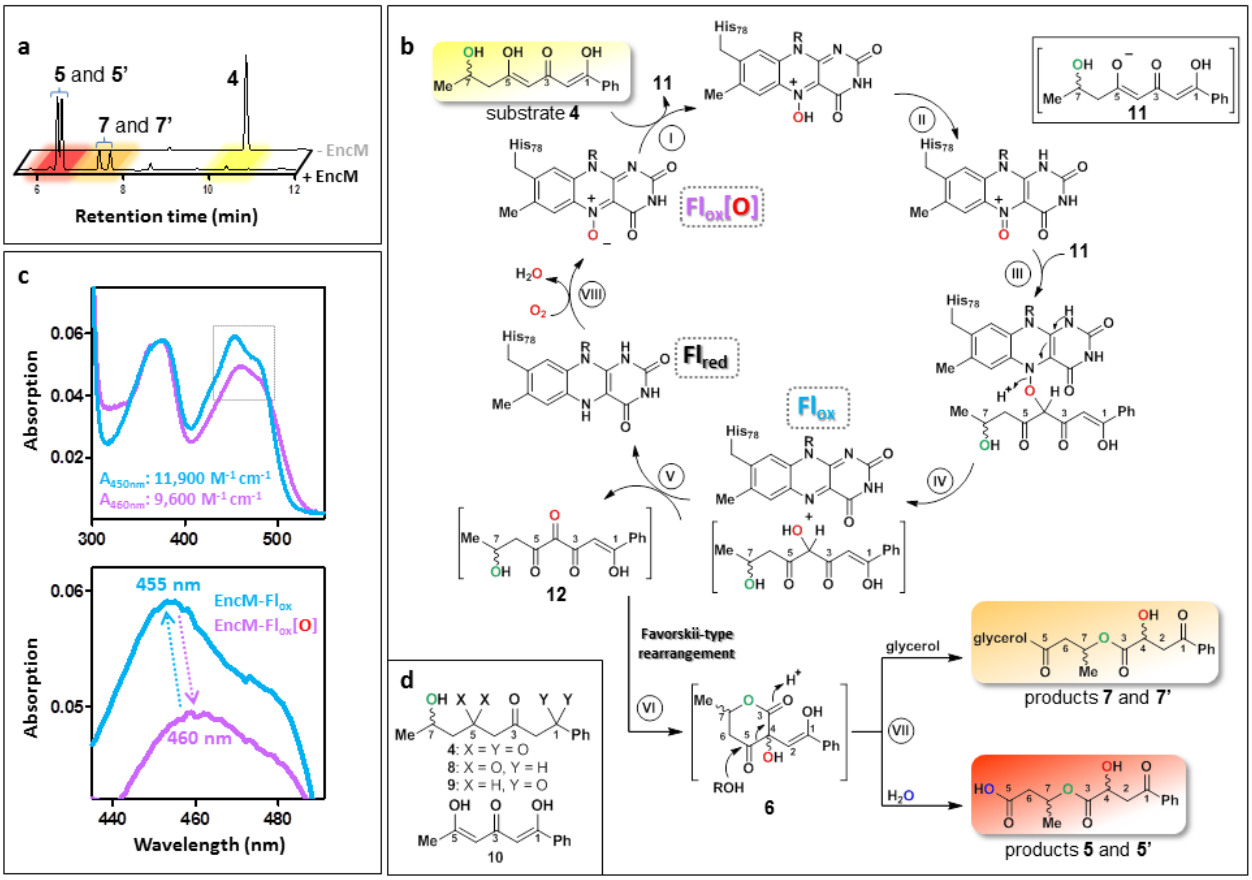

Figure A - 3. Proposed EncM mechanism and spectral features of the flavin cofactor catalytic states. (a) Reversed-phase HPLC analysis (absorption detection at 254 nm) of enzymatic assays showing substrate analogue **4** (upper lane; control assay without EncM) and diastereomeric product pairs **5/5'** and **7/7'** (lower lane; after incubation with EncM). The colour code refers to b. Products **7/7'** were observed only in the presence of glycerol (here 20% v/v). No intermediates could be detected. (b) Proposed catalytic mechanism of EncM involving substrate oxygenation by means of a flavin-N5-oxoammonium species. The resultant electrophilic C4-ketone of 12 triggers the Favorskii-type rearrangement and lactone formation (see Figure A - 1 for the detailed analogous reactions during the natural biosynthesis of enterocin), while the formed Fl_{red} reacts with O_2 and restores the N5-oxide. The stepwise dual oxidation is supported by anaerobic single-turnover experiments (Supplementary Fig. 16). The C7-hydroxyl group is shown in green, and oxygen atoms derived from O_2 and H_2O are colour-coded red and blue, respectively. Roman numerals indicate reaction steps as discussed in the main text. (c) Ultraviolet-visible spectra of the oxidized flavin of EncM as isolated ($Fl_{ox}[O]$, catalytically active, purple curve) and after multiple substrate turnovers (Fl_{ox}, catalytically inactive, blue curve). Molar absorption coefficients were ε_{450} = 11,900 $M^{-1}cm^{-1}$ for EncM-Fl_{ox} and ε_{460} = 9,600 $M^{-1}cm^{-1}$ for EncM-$Fl_{ox}[O]$. (d) Compounds used for structure-activity relationship analyses.

The monooxygenase activity of EncM was evaluated by following the incorporation of oxygen atoms from $^{18}O_2$ into **5**/**5'** and **7**/**7'** at C4. In contrast, isotope labeling from $H_2{}^{18}O$ was only associated with the non-enzymatic retro-Claisen cleavage of **6** to **5**/**5'** (Supplementary Figs 8 and 9). These measurements suggest that lactone formation during enterocin biosynthesis is controlled by the C7-hydroxyl group by means of direct intramolecular attack (Figure A - 1). Further support for this biosynthetic model came from the structure analysis of the EncM ligand-binding tunnel that can only accommodate the (*R*)-enantiomer of **3** (Supplementary Fig. 10), which is consistent with the observed retention of the C4-hydroxyl configuration in the final product enterocin (Figure A - 1).

EncM became inactivated after several turnovers (Supplementary Fig. 11). Moreover, the oxidized flavin cofactor of inactivated EncM (EncM-Fl_{ox}) showed distinct, stable changes in the ultraviolet-visible spectrum (Figure A - 3c). We speculated that these spectral perturbations are caused by the loss of an oxygenating species maintained in the enzyme's active state. This species, "EncM-Fl_{ox}[O]", is largely restored at the end of each catalytic cycle (Figure A - 3b), thereby providing an explanation for the innate monooxygenase activity of EncM in the absence of exogenous reductants. We excluded the participation of active-site residues in harbouring this oxidant using site-directed mutagenesis and by showing that denatured EncM retained the Fl_{ox}[O] spectrum (Supplementary Fig. 12). We therefore focused on the flavin cofactor as the carrier of the oxidizing species. On the basis of the spectral features of EncM-Fl_{ox}[O], we ruled out a conventional C4a-peroxide.[14,15] Moreover, Fl_{ox}[O] is extraordinarily stable

(no detectable decay for more than 7 d at 4°C) and thus is vastly longer lived than even the most stable flavin-C4a-peroxides described so far ($t_{1/2}$ of ≤30 min at 4°C[16,17]).

To further test the possible intermediacy and catalytic role of EncM-Fl_{ox}[O], we reduced the flavin cofactor anaerobically and showed that only flavin reoxidation with molecular oxygen restored the EncM-Fl_{ox}[O] species. In contrast, anoxic chemical reoxidation generated catalytically inactive EncM-Fl_{ox} (Supplementary Fig. 13a). Notably, EncM reoxidized with $^{18}O_2$ formed EncM-Fl_{ox}[^{18}O], which converted **4** to [^{18}O]**5**/**5'** with 1:1 stoichiometry of Fl_{ox}[^{18}O] to [^{18}O]**5**/**5'** (Supplementary Fig. 13b). The collective structure-function analyses reported here currently support the catalytic use of a unique flavin-oxygenating species that is consistent with a flavin-N5-oxide. This chemical species was introduced over 30 years ago as a possible intermediate in flavin monooxygenases[18,19] before the conventional C4a-peroxide model was accepted experimentally. Crucially, spectrophotometric comparison of chemically synthesized flavin-N5-oxide and EncM-Fl_{ox}[O] revealed many of the same spectral features,[20] and both can be chemically converted to oxidized flavin (Supplementary Fig. 12). Moreover, consistent with an N-oxide, EncM-Fl_{ox}[O] required four electrons per flavin cofactor to complete reduction in dithionite titrations, whereas EncM-Fl_{ox} required only two (Supplementary Fig. 14). We could not observe this flavin modification crystallographically (see Figure A - 2b), presumably as a result of X-radiation-induced reduction[21] of the flavin-N5-oxide, which is highly prone to reduction.[20]

We propose that during EncM catalysis, the N5-oxide is first protonated by the hydroxyl proton of the C5-enol of substrate **4** (Figure A - 3b, step I). Despite the generally low basicity of N-oxides, the proton transfer is probably enabled by the high

acidity of the C5 enol and its appropriate positioning 3.3 Å from the N5 atom of the flavin (Figure A-2c). After protonation, tautomerization of the N5-hydroxylamine would lead to the electrophilic oxoammonium (step II). Subsequent oxygenation of substrate enolate **11** by the oxoammonium species may then occur via one of several possible routes (Supplementary Fig. 15), yielding Fl_{ox} and a C4-hydroxylated intermediate (steps III and IV). Fl_{ox}-mediated dehydrogenation of the introduced alcohol group then produces the C4-ketone **12** and Fl_{red} (step V). Anaerobic single turnover experiments with **4** support this reaction sequence (Supplementary Fig. 16). Finally, **12** would undergo the Favorskii-type rearrangement (step VI) and *retro*-Claisen transformation (step VII) to yield the observed products **5**/**5'** or **7**/**7'**, while the reduced cofactor Fl_{red} reacts with O_2 to regenerate EncM-Fl_{ox}[O] and thus prime the enzyme for the next catalytic cycle (step VIII). However, alternative mechanisms are also plausible (Supplementary Fig. 17). This extraordinary flavin cofactor-mediated dual oxidation vaguely resembles the role of flavins in the scarce "internal monooxygenases" (EC 1.13.12) that also use their substrate as an electron donor.[22]

Here we provide the first in-depth investigation of an enzymatic oxidation-induced Favorskii-type rearrangement. The exceptionally reactive poly(β-carbonyl) substrate requires EncM to direct the reaction along a defined mechanistic trajectory by sequestration of reactants from bulk solvent, spatial separation of reactive functional groups, rapid "one-step" generation of a new electrophilic centre, and expulsion of solvent from the active site to prevent retro-Claisen ring cleavage. The discovery that EncM uses a stable flavin-N5-oxide for oxygenation rather than the universally accepted flavin peroxide suggests that this species may have been overlooked in the flavin

biochemical literature. Further studies are underway to explore the factors that govern enzymatic formation of the flavin-N5-oxide. In short, the archetypal dual oxidase EncM employs unexpected oxidative flavin biochemistry for the NAD(P)H-independent processing of extremely reactive polyketides.

Methods Summary

Amino-terminal octahistidine-tagged EncM from *S. maritimus* was produced heterologously in *Escherichia coli* BL21 (DE3) and purified by means of Ni^{2+}-affinity chromatography. For crystallization, the EncM His-tag was removed and the protein further purified by ResourceQ anion-exchange chromatography. Substrate analogues and flavin-N5-oxide were acquired through chemical synthesis. Site-directed mutagenesis was conducted with the QuikChange site-directed mutagenesis kit (Stratagene), using self-constructed primers.

The activities of wild-type EncM and EncM-R210E were assayed using the fully reconstituted enzyme set as previously reported[6]. Other EncM assays were conducted at 22°C, pH 7.5 using HEPES-Na^+ buffer, 150-300 mM NaCl and at least 10 % (v/v) glycerol. Products were separated and purified by reverse-phase HPLC with optical detection at 254 nm using a Sync Polar RP column with an ammonium acetate-buffered (pH 5.0) acetonitrile gradient. A 6230 Accurate-Mass TOF-MS system (Agilent) was used for mass spectrometry measurements. NMR spectra were recorded on Bruker DRX-600 and AMX-400 instruments. Ultraviolet-visible spectra were conducted with a Cary 50 UV-Vis spectrophotometer (Agilent). A Perkins-Elmer 341 polarimeter and an

Aviv circular dichroism spectrometer were used for optical rotation and circular dichroism spectroscopy measurements, respectively.

Crystals of EncM were grown from a 1:1 mixture of protein solution (5 mg/ml in 10 mM TES-Na^+ (pH 7.7) and 10% (v/v) glycerol) and a reservoir solution (2 mM DTT, 0.1 M HEPES-Na^+ pH 7.5, 0.2 M calcium acetate, 20% PEG3350) using hanging-drop vapour diffusion method at 4 °C. For co-crystallization the enzyme was incubated with the substrate mimic (2 mM) before being mixed with the reservoir solution. The crystals were stored in 25% (v/v) glycerol until X-ray data collection at the Advanced Light Source (Berkeley, CA, USA). The initial phases were determined by molecular replacement with 6HDNO (PDB code 2BVG) as a search model.

References

(1) Piel, J., Hertweck, C., Shipley, P. R., Hunt, D. M., Newman, M. S., and Moore, B. S. (2000) Cloning, sequencing and analysis of the enterocin biosynthesis gene cluster from the marine isolate “Streptomyces maritimus”: evidence for the derailment of an aromatic polyketide synthase. *Chem. Biol. 7*, 943–55.

(2) Seto, H., Sato, T., Urano, S., Uzawa, J., and Yonehara, H. (1976) Utilization of 13C-13C Coupling in Structural and Biosynthetic Studies. VII The Structure and Biosynthesis of Vulgamycin. *Tetrahedron Lett. 17*, 4367–4370.

(3) Cheng, Q., Xiang, L., Izumikawa, M., Meluzzi, D., and Moore, B. S. (2007) Enzymatic total synthesis of enterocin polyketides. *Nat. Chem. Biol. 3*, 557–8.

(4) Hertweck, C., Xiang, L., Kalaitzis, J. A., Cheng, Q., Palzer, M., and Moore, B. S. (2004) Context-Dependent Behavior of the Enterocin Iterative Polyketide Synthase : A New Model for Ketoreduction. *Chem. Biol. 11*, 461–468.

(5) Hertweck, C., Luzhetskyy, A., Rebets, Y., and Bechthold, A. (2007) Type II polyketide synthases: gaining a deeper insight into enzymatic teamwork. *Nat. Prod. Rep. 24*, 162–90.

(6) Xiang, L., Kalaitzis, J. A., and Moore, B. S. (2004) EncM, a versatile enterocin biosynthetic enzyme involved in Favorskii oxidative rearrangement, aldol condensation, and heterocycle-forming reactions. *Proc. Natl. Acad. Sci. U. S. A. 101*, 15609–14.

(7) Koetter, J. W. A., and Schulz, G. E. (2005) Crystal structure of 6-hydroxy-D-nicotine oxidase from Arthrobacter nicotinovorans. *J. Mol. Biol. 352*, 418–28.

(8) Huang, C.-H., Lai, W.-L., Lee, M.-H., Chen, C.-J., Vasella, A., Tsai, Y.-C., and Liaw, S.-H. (2005) Crystal structure of glucooligosaccharide oxidase from Acremonium strictum: a novel flavinylation of 6-S-cysteinyl, 8alpha-N1-histidyl FAD. *J. Biol. Chem. 280*, 38831–8.

(9) Alexeev, I., Sultana, A., Mäntsälä, P., Niemi, J., and Schneider, G. (2007) Aclacinomycin oxidoreductase (AknOx) from the biosynthetic pathway of the antibiotic aclacinomycin is an unusual flavoenzyme with a dual active site. *Proc. Natl. Acad. Sci. U. S. A. 104*, 6170–5.

(10) Crosby, J., and Crump, M. P. (2012) The structural role of the carrier protein--active controller or passive carrier. *Nat. Prod. Rep. 29*, 1111–37.

(11) Palfey, B. A., and McDonald, C. Af. (2010) Control of catalysis in flavin-dependent monooxygenases. *Arch. Biochem. Biophys. 493*, 26–36.

(12) Baumann, K., Bacher, M., Damont, A., and Steck, A. (2004) Selective transformation of ascomycin into 11-epi-ascomycin. *Tetrahedron Lett. 45*, 549–551.

(13) Takikawa, H., Takada, A., Hikita, K., and Suzuki, K. (2008) Formation of alpha-hydroxy-beta-diketones through hydroxylation of isoxazolium salts: stereoselective approach to angular cis-diols in polycyclic systems. *Angew. Chem. Int. Ed. Engl. 47*, 7446–9.

(14) Entsch, B., Ballou, D. P., and Massey, V. (1976) Flavin-Oxygen Derivatives Involved in Hydroxylation by p-Hydroxybenzoate Hydroxylase. *J. Biol. Chem. 251*, 2550–2563.

(15) Entsch, B., and Ballou, D. P. (1989) Purification, properties, and oxygen reactivity of p-hydroxybenzoate hydroxylase from Pseudomonas aeruginosa. *Biochim. Biophys. Acta 999*, 313–22.

(16) Thotsaporn, K., Chenprakhon, P., Sucharitakul, J., Mattevi, A., and Chaiyen, P. (2011) Stabilization of C4a-hydroperoxyflavin in a two-component flavin-dependent monooxygenase is achieved through interactions at flavin N5 and C4a atoms. *J. Biol. Chem. 286*, 28170–80.

(17) Valton, J., Mathevon, C., Fontecave, M., Nivière, V., and Ballou, D. P. (2008) Mechanism and regulation of the Two-component FMN-dependent monooxygenase ActVA-ActVB from Streptomyces coelicolor. *J. Biol. Chem. 283*, 10287–96.

(18) Rastetter, W. H., Gadek, T. R., Tane, J. P., and Frost, J. W. (1979) Oxidations and Oxygen Transfers Effected by a Flavin N(5)-Oxide. A Model for Flavin-Dependent Monooxygenases. *J. Am. Chem. Soc. 101*, 2228–2231.

(19) Orf, H. W., and Dolphin, D. (1974) Oxaziridines as possible intermediates in flavin monooxygenases. *Proc. Natl. Acad. Sci. U. S. A. 71*, 2646–50.

(20) Walsh, C., Fisher, J., Spencer, R., Graham, D. W., Ashton, W. T., Brown, J. E., Brown, R. D., and Rogers, E. F. (1978) Chemical and enzymatic properties of riboflavin analogues. *Biochemistry 17*, 1942–51.

(21) Garman, E. F., and Owen, R. L. (2006) Cryocooling and radiation damage in macromolecular crystallography. *Acta Crystallogr. D. Biol. Crystallogr. 62*, 32–47.

(22) Van Berkel, W. J. H., Kamerbeek, N. M., and Fraaije, M. W. (2006) Flavoprotein monooxygenases, a diverse class of oxidative biocatalysts. *J. Biotechnol. 124*, 670–89.